Characterisation of the contribution of the kinase and RNase activities of Ire1α to activation of apoptotic JNK signalling

WATSON, JAMIE,NICHOLAS

Characterisation of the contribution of the kinase and RNase activities of Ire1α to activation of apoptotic JNK signalling

Jamie Nicholas Watson

This thesis is submitted as part of the requirements for the award of

Degree of Doctor of Philosophy

School of Biological and Biomedical Sciences

Durham University

August 2016

ABSTRACT

The unfolded protein response (UPR) is a highly conserved mechanism by which all eukaryotes respond to endoplasmic reticulum (ER) stress. In higher eukaryotes this response is mediated by three ER transmembrane stress sensors: activating transcription factor 6 (ATF6α/β), PKR-like ER kinase (PERK) and inositol requiring 1 (IRE1 α/β). IRE1 is the most highly conserved of the three ER stress sensors and is also the only sensor to mediated UPR signalling via two different enzymatic domains.

It is currently believed that during prolonged ER stress, the RNase domain of IRE1α provides cytoprotection via *XBP1* splicing, whilst the kinase domain initiates proapoptotic JNK signalling via interaction with the adaptor protein TRAF2. However, characterising how these domains contribute to cell fate decisions is complicated by the fact that traditional models use ER stress mimetic drugs, which activate all three branches of the UPR and thus make it difficult to attribute downstream events to individual effectors. Therefore, the aim of the research presented in this thesis was to produce a model that allowed isolated activation of IRE1α in order to determine the contribution of its kinase and RNase activities to proapoptotic JNK signalling, without input from other upstream effectors.

Using the Fv2E-IRE1α system, the data presented in this thesis provides novel insight into the mechanism by which IRE1α instigates proapoptotic JNK signalling by suggesting that a functional kinase domain is not required for IRE1α to interact with TRAF2 and that endoribonuclease function may be required for downstream JNK activation in humans. Furthermore, evidence is also provided to suggest that, whilst kinase activity is not required for interaction with TRAF2, it is required for downstream JNK activation. This gives rise to the possibility that, contrary to current knowledge, the IRE1α kinase domain has the capacity to phosphorylate proteins other than IRE1α.

TABLE OF CONTENTS

LIST OF TABLES

Chapter 1

No tables

Chapter 2

Chapter 3

Chapter 4

No tables

Chapter 5

No tables

Chapter 6

LIST OF FIGURES

Chapter 1

Chapter 2

No Figures

Chapter 3

No Figures

Chapter 4

Chapter 5

Chapter 6 and Appendices

LIST OF ABBREVIATIONS

1NM-PP1	1-tert-butyl-3-naphthalen-1-ylmethyl-1H219pyrazolo[3,4-d]pyrimidin-4-ylemine
AIP1	Actin interacting protein 1
ANOVA	Analysis of variance
ASK1	Apoptosis signal-regulating kinase 1
ATF	Activating transcription factor
ATF-2	Activating transcription factor 2
ATP	Adenosine triphosphate
BAK	Bcl-2 antagonist/killer
BAR	Bifunctional apoptosis regulator
BAX	Bcl-2-associated X protein
Bcl-2	B-cell lymphoma 2
BI-1	Bax inhibitor 1
BIM	Bcl-2 interacting mediator of cell death
BiP	Binding immunoglobulin protein
BSA	Bovine serum albumin
bZIP	Basic leucine zipper
CBF	Core binding factor
CHOP	C/EBP homologous protein
cIAP	Cellular inhibitor of apoptosis
cLD	Core luminal domain
CMV	Cytomegalovirus
Co-IP	Co-immunoprecipitation
COP	Coat protein
CSSR	Core sensing region
dATP	Deoxyadenosine triphosphate
dCTP	Deoxycytidine triphosphate
DEPC	Diethylpyrocarbonate
dGTP	Deoxyguanosine triphosphate
DMEM	Dulbecco's modified eagle medium
DMSO	Dimethyl sulfoxide
DNA	Deoxyribonucleic acid
dNTP	Deoxynucleoside triphosphate
DTT	Dithiothreitol
dTTP	Deoxythymidine triphosphate
EDTA	Ethylenediaminetetraacetic acid
eIF2α	Eukaryotic initiation factor-2 α
ELK1	ETS domain-containing protein-1

ER	Endoplasmic reticulum
ERAD	Endoplasmic reticulum-associated degradation
ERK	Extracellular regulated kinases
ERSE	Endoplasmic reticulum stress response element
FBS	Fetal bovine serum
GADD	Growth arrest and DNA damage-inducible
GAPDH	Glyceraldehyde 3-phosphate dehydrogenase
GCN	General control nonderepressible
GlcNAc	N-acetylglucosamine
GLS	Golgi localization sequence
GPT	GlcNAC phosphotransferase
GRP	Glucose-regulated protein
GTP	Guanosine triphosphate
HAC1	H3/H4 histone acetyltransferase/transcription cofactor
HEK	Human embryonic kidney
HeLa	Henrietta Lacks
HRI	Heme-regulated eIF2α kinase
HRP	Horseradish peroxidase
HSF	Heat shock factor
IgG	Immunoglobulin G
IkBα	Inhibitor of kappa B
IKK	Inhibitor of kappa B complex kinase
IP	Immunoprecipitation
IRAK2	Interleukin-1 receptor-associated kinase-like 2
IRE1	Inositol-requiring 1
IRF	Interferon-regulatory factor
JIK	JNK inhibitory kinase
JNK	c-Jun N-terminal kinase
KAR2	Karyogamy 2
KEAP1	Kelch-like ECH-associated protein 1
MAP	Mitogen-activated protein
MAPK	Mitogen-activated protein kinase
MAPKKK	Mitogen-activated protein kinase kinase kinase
MEF	Mouse embryonic fibroblast
MEK	MAP Kinase/ERK Kinase
MEKK	MAP Kinase/ERK Kinase Kinase
MHC	Major histocompatibility complex
miRNA	Micro ribonucleic acid

MKK	Mitogen-Activated Protein Kinase Kinase
MOPS	3-(N-morpholino)propanesulfonic acid
mRNA	Messenger ribonucleic acid
mTORC	Mammalian target of rapamycin complex 1
MTT	3-[4,5-dimethylthiazol-2-yl]-2,5-diphenyltetrazolium bromide; thiazolyl blue
MUC2	Mucin 2
NCK	Non-catalytic region of tyrosine kinase adaptor protein
NFAT	Nuclear factor of activated T cells
NF-Y	Nuclear transcription factor Y
NF-κB	Nuclear factor kappa-light-chain-enhancer of activated B cells
NLS	Nuclear localisation signal
NMIIB	Non-muscle myosin heavy chain IIB
NP-40	Nonidet P-40
NRF2	Nuclear factor-erythroid-derived 2 (NF-E2)-related factor 2
ORF	Open reading frame
PARP-1	Poly ADP ribose polymerase-1
PBS	Phosphate-buffered saline
PC12	Pheochromocytoma 12
PCR	Polymerase chain reaction
PDI	Protein disulphide isomerase
PDIA6	Protein disulphide isomerise-associated 6
p-eIF2α	Phosphorylated eukaryotic initiation factor-2 α
PERK	Protein kinase R-like endoplasmic reticulum kinase
PH	Pleckstrin homology
PI	Phosphatidylinositol
p-JNK	Phosphorylated c-Jun N-terminal kinases
PKA	Protein kinase A
PKR	Double-stranded RNA-dependent protein kinase
PP1c	Protein phosphatase 1c
PUMA	p53 upregulated modulator of apoptosis
PVDF	Polyvinylidene difluoride
RelA	REL-associated
RIDD	Regulated IRE1-dependent decay
RIPA	Radio-immunoprecipitation assay
RNA	Ribonucleic acid
ROS	reactive oxygen species
RT-PCR	Reverse transcription polymerase chain react
S1P	Site-1 protease

S2P	Site-2 protease
SDS	Sodium dodecyl sulphate
SDS-PAGE	Sodium dodecyl sulphate polyacrylamide gel electrophoresis
SERCA	Sarco/endoplasmic reticulum $Ca2^{+}$-ATPase
SH-2	Src-homology-2
ShRNA	Small hairpin ribonucleic acid
SiRNA	Small interfering ribonucleic acid
SP1	Specificity protein 1
STAT3	Signal transducer and activator of transcription 3
SubAB	Subtilase cytotoxin AB
TBE	Tris/Borate/EDTA
TBST	Tris-buffered saline Tween 20
TFIID	Transcription Factor II D
Tg	Thapsigargin
Tm	Tunicamycin
TM	Transmembrane
TNF	Tumour necrosis factor
TRAF2	TNF receptor-associated factor 2
TRB3	Tribbles homolog 3
TREB5	Tax-responsive element-binding protein
T-REx	Tetracycline-regulated mammalian expression
Tris	Tris(hydroxymethyl) methylamine
TXNIP	Thioredoxin interacting protein
uORF	Upstream open reading frame
UPR	Unfolded protein response
UPRE	Unfolded protein response element
WT	Wild-type
XBP1	X-box binding protein 1

DECLARATION

I confirm that this thesis is my own work and that it contains no material previously submitted for a degree in this or any other institute. All data are my own other than those represented in the following figures: 1.1, 1.2, 1.3, 1.4, 1.5, 1.6, 1.7 and 6.3. It will also be stipulated in the text where research is not my individual contribution.

STATEMENT OF COPYRIGHT

ACKNOWLEDGEMENTS

First and foremost I want to thank my supervisor; Dr Martin Schröder. His extensive knowledge and tireless work ethic are a true inspiration and it is impossible to overstate how much his support and guidance have contributed to the completion of this project. Thank you for persevering with me; you have been an excellent mentor.

Secondly I would like to give thanks to all the past and present members of the Schröder lab. Your experience and support have been invaluable in helping me bridge the considerable gap between being an undergraduate student and postgraduate researcher. However, of those members, special thanks must go to Max Brown, who is genuinely one of the best human beings you could ever meet. Always willing to go above and beyond when asked for help, Max also provides a seemingly endless supply of humility and humour. Debunking fervent opinions, submitting unfortunate typos and creating cringe-worthy, yet extremely catchy, buffer-based parodies; working with you has been an absolute hoot! I must also give thanks to the BBSRC for part-funding this project.

I am also extremely grateful to my friends and family, who always ensure that I have everything I could ever need in order to achieve success. Mum and Dad, I cannot truly express how invaluable your tireless support has been, not only during this project, but throughout my entire life. Gabby, you have expertly taken on the role of older sibling (despite being 4 years younger) and it was probably the genuine threat of you completing your PhD thesis before I completed mine that drove my across the finishing line.

Finally, I must give thanks to my late grandfather, who unfortunately will not get to see the completion of my PhD. However, I will forever be indebted to him for providing the finances to allow me to embark upon this project and for always leading by example when reminding me that you don’t get owt for nowt.

1 Introduction

Proteins are essential to every process within the field of cell biology; providing structure, controlling chemical reactions and allowing communication between cells and tissues. Precise tertiary and quaternary structures allow proteins to exert strict control over processes such as immunity, development, transport and even their own creation and degradation (Lodish, 2008). Therefore, it is unsurprising that the production of proteins is a highly regulated process which, if done incorrectly, can be fatal to the organism in question (Ellisdon and Bottomley, 2004). The main site for the maturation and folding of secretory and membrane proteins within the cell is the endoplasmic reticulum, which provides a compartmentalised folding environment that houses the molecular chaperones and enzymes that regulate protein folding. However, there are many factors that can cause the perturbation of protein folding within the ER and these factors cause the accumulation of toxic unfolded protein species (Araki and Nagata, 2011). Therefore, there is a highly conserved mechanism by which the cell tries to alleviate stress caused by unfolded proteins and this is known as the unfolded protein response (UPR). Owing to their essential function, many diseases stem from aberrant protein production and this means that the endoplasmic reticulum and, more specifically, the unfolded protein response have been found to be central to the pathology of these diseases. Consequently, understanding the UPR is becoming increasingly pertinent to therapeutic treatments for diseases ranging from cancer to type 2 diabetes (Salvadó et al., 2015). However, studying stress signalling pathways is difficult owing to the fact that there are huge amounts of cross-talk and fine margins between cell fate decisions that determine if a cell should attempt to adapt to a particular insult or undergo apoptosis in order to protect surrounding cells (Hetz, 2012, Chaudhari et al., 2014). As a result, systems that can isolate cell signalling pathways are extremely useful when trying to understand the pathology of diseases and it is for this reason that my thesis concerns itself with the creation of a system that can isolate and characterise the signalling transduced by inositol requiring 1 alpha (IRE1α), a transmembrane, bifunctional enzyme that is central to cell fate decisions during the unfolded protein response (Jiang et al., 2015, Mori et al., 1993, Tirasophon et al., 1998).

This introductory section will outline the role of the endoplasmic reticulum; current understanding of how the unfolded protein response determines cell fate and how it can be both initiated by, and contribute to, a plethora of human diseases. It will then review current models for studying the unfolded response before detailing how this project aims to

contribute current understanding of the UPR and the development of therapies to diseases such as type 2 diabetes.

1.1 The Endoplasmic Reticulum

The endoplasmic reticulum (ER) is a large organelle composed of a complex network of flattened sac-like and tubular structures that is responsible for the synthesis and maturation of transmembrane and secretory proteins (Palade, 1956). The ER also serves as a site of lipid biosynthesis and as a cellular calcium storage unit in higher eukaryotes. However, with regard to the generation of new membrane and secretory proteins, the functions of the ER involve folding, quality control and exporting newly synthesised proteins, so that they can be transported to their correct intra- or extracellular locations (Palade, 1975). In order for the ER to carry out these roles, tight homeostatic regulation is required to ensure optimal folding capacity. As a result of this, any disruption of ER homeostasis causes the accumulation of misfolded proteins, a situation that rapidly becomes terminal for the cell if not remedied. Therefore, all eukaryotic organisms, from yeast to mammals, have a strongly conserved 'unfolded protein response' (UPR) that attempts to either alleviate stress or destroy cells with aberrant ER function. The function of the ER during normal conditions has been extensively reviewed (Araki and Nagata, 2011, Noack et al., 2014, Smith et al., 2011, Rutkevich and Williams, 2011) and therefore the next section will discuss current knowledge of the ER during conditions of stress, rather than presenting information that does not directly impact upon the focus of this thesis.

1.2 Endoplasmic Reticulum Stress and the Unfolded Protein Response

1.2.1 Causes of ER stress

The maturation and folding of proteins is a complex process and requires a well-regulated set of conditions to work efficiently. Therefore, it is unsurprising that there are a wide variety of factors that can offset ER homeostasis and perturb protein production. Glucose deprivation (Logue et al., 2013), hypoxia (Thuerauf et al., 2006), excessive demand for *de novo* protein synthesis, disturbances of the redox environment within the ER (Fedoroff, 2006) and changes in pH, Ca^{2+} concentration, or temperature (Gorlach et al., 2006) can all reduce the capacity of the ER to correctly fold proteins and inevitably result in the accumulation of misfolded proteins within the ER lumen. This accumulation of misfolded proteins is what constitutes ER stress and when this occurs the cell instigates a highly conserved defence mechanism known as the unfolded protein response.

1.2.2 The unfolded protein response

First proposed by Kozutsumi in 1988, the unfolded protein response (UPR) is described as an adaptive mechanism to increase the protein folding capacity, as well as to decrease the unfolded protein load, of the ER (Kozutsumi et al., 1988). This is achieved by increasing the production of chaperones and proteins that aid protein folding, decreasing the load of proteins in the ER via translational attenuation and increasing the rate at which misfolded proteins are degraded via endoplasmic reticulum-associated protein degradation (ERAD) (Schroder, 2008). This increased folding capacity is also associated with a visible expansion of the ER in yeast (Bernales et al., 2006). However, if ER stress is prolonged and cannot be resolved, the UPR can also instigate cell death in order to protect surrounding cells and tissues (Walter and Ron, 2011).

In higher eukaryotes the endoplasmic reticulum possesses at least three transmembrane ER stress sensors, which respond to the accumulation of misfolded proteins within the ER by initiating the unfolded protein response. These sensors are: activating transcription factor 6 (ATF6α/β), PKR-like ER kinase (PERK) and inositol requiring 1 (IRE1 α/β). Each of these proteins initiates slightly different aspects of the UPR, with all three being able to enhance survival or initiate cell death (Wu et al., 2014). All three ER stress sensors are ER transmembrane proteins with ER luminal sensor domains and cytoplasmic effector domains. Their ability to detect misfolded proteins is, at least in part, believed to revolve around the ER chaperone 'binding immunoglobulin protein' (BiP), which under non-stressed conditions binds to their luminal domains and prevents their activation. However, upon the accumulation of misfolded proteins, BiP dissociates to aid the protein folding effort allowing the luminal domains of the three stress sensors to mediate their activation (Lee, 2005). Upon release from BiP, ATF6 undergoes proteolytic cleavage that allows its N-terminal cytosolic domain to translocate to the nucleus, where it acts as a transcription factor for UPR genes that encode proteins involved in enhancing protein folding within the ER. However, in addition to the protective function of increasing the folding capacity of the ER, ATF6 can also stimulate cell death via the activation of C/EBP homologous protein (CHOP) (Haze et al., 1999).

PERK and IRE1α share significant homology between their luminal domains, so much so that they have been shown to be interchangeable (Liu et al., 2000) and, in addition to being regulated by BiP, it is also believed that they bind directly to misfolded proteins as well (Cui et al., 2011, Credle et al., 2005, Gardner and Walter, 2011, Kohno, 2007). Upon

activation PERK and IRE1α both form dimers/oligomers and undergo autophosphorylation. PERK then phosphorylates eukaryotic initiation factor 2 α (eIF2) in order to initiate its contribution to protective UPR signalling, which is the attenuation of protein translation in order to reduce ER client protein load. However, like ATF6, PERK can also initiate apoptosis via upregulation of CHOP (Harding et al., 2000b).

IRE1 is the most conserved ER stress sentinel and is also the most complex as a result of having dual enzymatic functions. In yeast, only the endoribonuclease domain of IRE1 contributes to the UPR, where it offers cytoprotection through the unconventional splicing of H3/H4 histone acetyltransferase/transcription cofactor (*HAC1*) mRNA, resulting in the translation of the potent UPR transcription factor Hac1 (Shamu and Walter, 1996, Mori et al., 1993) However, in higher eukaryotes the kinase domain of IRE1α also contributes to UPR signalling via interaction with the scaffolding protein TRAF2. This interaction can result in either protective (Brown et al., 2016) or apoptotic (Urano et al., 2000b) signalling depending on the intensity and duration of the stress. This duality makes IRE1α particularly attractive when it comes to designing therapeutic treatments for UPR-related diseases as manipulation of IRE1α could allow control over cell fate (Jiang et al., 2015).

The process of characterising the unfolded protein response has been found to be extremely complicated because there is a large amount of cross-talk between the three branches of the UPR and all three ER stress sensors can contribute to the opposing processes of adaptation and apoptosis. Therefore, if the UPR is to be harnessed as a tool for combating diseases that centre around aberrant protein production, of which there are many, elucidating the individual contribution of each ER stress sensor and the pathways it initiates is going to be essential. As such, our current knowledge of the three known ER stress sentinels will be detailed below before explaining how this project aims to further our understanding of IRE1α and its contribution to the UPR.

1.2.3 ATF6

Activating transcription factor 6 (ATF6) was first identified by *Yoshida et al.* whilst trying to find *cis*-acting elements and transactivators responsible for the activation of UPR specific genes (Yoshida et al., 1998). Through analysis of the promoter regions of human glucose-regulated protein 78 (GRP78/BiP), glucose-regulated protein 94 (GRP94) and calreticulin, genes that are upregulated during ER stress, the authors identified a consensus sequence of CCAAT-N_9-CCACG, which they termed the ER stress response element (ERSE). This sequence was shown to be necessary and sufficient for the induction of UPR

inducible ER chaperones and, through use of a yeast one-hybrid screen, human cDNA encoding a basic leucine zipper (bZIP) protein was identified as a putative ERSE-binding protein. This protein, named ATF6, was found to enhance the transcription of UPR genes in an ERSE-dependent manner when overexpressed in Henrietta Lacks (HeLa) cells.

It is now known that ATF6 is a type II transmembrane glycoprotein that spans the ER membrane as a result of a hydrophobic domain in the middle of its structure. The C-terminus of ATF6 resides in the ER lumen, whilst the bZIP containing the N-terminus faces into the cytoplasm. When exogenously expressed, wild type ATF6 and N-terminal deletion mutants localise to the ER membrane. Conversely, mutants representing the cytoplasmic N-terminus of ATF6 translocate to the nucleus, resulting in the activation of UPR genes such as GRP78/BiP (Haze et al., 1999). The mechanism by which ATF6 is able to sense ER stress is believed to revolve around BiP, which controls ATF6 activity in the ER by binding to specific sites on the luminal domain of ATF6 in order to inhibit its translocation to the Golgi, which is essential to ATF6 signalling. However, during ER stress, it is proposed that BiP dissociates from ATF6 revealing two Golgi localisation signals (GLSs). This hypothesis is supported by the fact that BiP overexpression slows the translocation of ATF6 to the Golgi and ATF6 mutants lacking their BiP binding domain, whilst retaining their GLSs, exhibit constitutive translocation to the Golgi (Shen et al., 2002). Once activated by the dissociation of BiP, ATF6 translocates to the Golgi, potentially in association with coat protein complex II (COPII) vesicles (Schindler and Schekman, 2009). However, whilst the exact method of translocation is still being disputed, it has been shown that translocation is dependent on the 272 amino acid luminal domain of ATF6, which is both necessary and sufficient for the translocation of ATF6 from the ER to the Golgi, as shown by the fact that the luminal domain of ATF6 is sufficient to sense ER stress and causes translocation to the Golgi when fused to another ER transmembrane protein (LZIP) (Chen et al., 2002).

Upon reaching the Golgi, ATF6 undergoes proteolytic cleavage through interaction with *cis/medial* Golgi resident protein site-1 protease (S1P), which targets RxxL and asparagines/proline motifs on ATF6 (Ye et al., 2000). This cleavage event occurs at site in the luminal domain of ATF6 known as the CD1 region (amino acids (aa) 468-500) and is required for a second cleavage event mediated by site-2 protease (S2P). This second cleavage event occurs near the junction of the cytoplasmic and luminal domains of ATF6, named the CD2 region (aa 550-640) and is essential for UPR signalling, as it allows the cytoplasmic bZIP domain of ATF6 to translocate to the nucleus and bind to the ERSE. It

was initially believed that this sequential cleavage of ATF6 was the result of compartmentalisation of the two protease enzymes, however, experiments showing that S2P can cleave shortened versions of the ATF6 luminal domain have led to the belief that S1P cleavage is required to produce a substrate of optimal size for S2P. It is now proposed that without the action of SP1, the bulky luminal domain of uncleaved ATF6 prevents the catalytic centre of SP2 from accessing the substrate cleavage sites within the CD2 region of ATF6 and thus inhibits ATF6 activation and subsequent translocation to the nucleus (Shen and Prywes, 2004).

Upon translocation to the nucleus, ATF6 upregulates UPR target genes in an ERSE-dependent manner, as shown by the fact that mutations in the ERSE sequence (Yoshida et al., 1998) or the use of a dominant negative ATF6 inhibits expression of these genes during ER stress (Wang et al., 2000). However, whilst it was initially thought that ATF6 bound the entire ERSE sequence, it has since been shown that it actually binds to the CCACG motif of the CCAAT-N_9-CCACG ERSE element. Furthermore, this binding will only occur if NF-Y (CBF) is bound to the upstream CCAAT sequence (Yoshida et al., 2000). In this respect, it would appear that the mammalian ERSE element shares an homologous structure with the UPR element in yeast, which can be bound by three different transcription factors; Hac1p (Mori et al., 1992), general control protein 4 (Gcn4p) (Patil et al., 2004) and heat shock factor 1(Hsf1p) (Yamamoto et al., 2005), in order to control the magnitude of the transcriptional response. Like in yeast, it would appear that basal transcription of UPR genes is controlled by one transcription factor (NF-Y) whilst ATF6 and XBP1 binding can amplify transcription during times of stress (Yoshida et al., 2000).

Having identified ATF6 as a key component in the unfolded protein response and elucidated the method by which it transmits signals from the ER to the nucleus, many groups have endeavoured to determine the genes that reside under the transcriptional control of ATF6. A genome wide search for ATF6 target genes in mice identified 30 direct targets, 40% of which were ER quality control proteins and 20% were ER proteins, whilst the rest had unknown functions (Adachi et al., 2008, Wu et al., 2007, Yamamoto et al., 2007). Most research into ATF6 target genes are concurrent with this analysis and there is a general consensus that the majority of ATF6 signalling is protective and involved in increasing the capacity of the ER to fold proteins by upregulating the translation of foldases and chaperones (Okada et al., 2002) such as protein disulphide isomerise-associated 6 (PDIA6) (Vekich et al., 2012). However, there are a few notable examples of genes that suggest ATF6 may have a broader role to play within the UPR. For example, it

is well documented that ATF6 activates CHOP (GADD153) (Fawcett et al., 1999), a transcription factor heavily involved in apoptotic signalling during ER stress (see section 1.2.5) and *XBP1*, which is the primary target of the IRE1α endoribonuclease domain (Yoshida et al., 2000). Other, less well documented roles for ATF6 during ER stress include the upregulation of lipid biosynthesis during ER expansion (Bommiasamy et al., 2009) and the regulation of micro-RNAs (miRNAs), which are emerging as interesting candidates for fine-tuning many signalling pathways (Belmont et al., 2012).

Finally, one report has proposed that ATF6 may also be involved in the upregulation of NF-κB signalling (Yamazaki et al., 2009) and the authors suggest this because the use of an endoribonuclease-deficient mutant of IRE1α did not reduce NF-κB signalling during ER stress. However, the endoribonuclease domain of IRE1α has been shown to be dispensable for interaction with TRAF2 (Urano et al., 2000b), which is the mechanism by which IRE1α instigates NF-κB signalling (Hu et al., 2006). This, combined with the fact that there is a substantial amount of literature to suggest that PERK (Deng et al., 2004) and IRE1α (Kaneko et al., 2003) are able to compensate for one another in order to instigate NF-κB signalling, means that it is more likely that NF-κB is regulated by a combination or PERK and IRE1α (Tam et al., 2012).

1.2.4 PERK

Through phosphorylation of eukaryotic initiation factor 2 alpha (eIF2α), PERK contributes to the protective function of the UPR by inducing translational arrest, whilst PERK signalling can also push cells towards apoptosis via activating transcription factor 4 (ATF4)/CHOP. Furthermore, PERK has been instigated in influencing the cell cycle (Raven and Koromilas, 2008, Brewer and Diehl, 2000, Hamanaka et al., 2005), autophagy (Kouroku et al., 2007, Avivar-Valderas et al., 2011) and survival during hypoxia (Koumenis et al., 2002).

PERK was originally discovered by *Shi et al.* whilst screening for kinases capable of phosphorylating eIF2α and, a year later, *Harding et al.* identified PERK as being the kinase responsible for instigating the attenuation of protein synthesis during ER stress (Harding et al., 1999, Shi et al., 1998, Hayes et al., 1999). Prior to the work of these groups, three protein kinases; general control non-derepressible 2 (Gcn2) (Ramirez et al., 1991) double-stranded RNA-dependent protein kinase (PKR) (Srivastava et al., 1995) and heme-regulated eIF2α kinase (HRI) (Chen and London, 1995) had previously been identified as eIF2α kinases. PKR had initially been thought to be responsible for the translational arrest

observed during ER stress as a result of being shown to have a role in mediating translational arrest during Ca^{2+} release from the ER (Srivastava et al., 1995, Prostko et al., 1995). However, the level of translational arrest in cells that had PKR knocked-out was similar to that of WT cells during ER stress (Harding et al., 1999). Therefore, it had to be assumed that there was another eIF2α kinase responsible for initiating translational attenuation during ER stress. In order to identify this protein, a hybridisation probe was used to isolate cDNA encoding a murine protein with a kinase domain similar to PKR and HRI. This protein was 1,114 residues long and shared N-terminal homology with mammalian IRE1α and a C-terminal domain that was 40% identical to PKR. A C-terminal Myc-tag was then used to determine that this new protein co-localises with ribophorin, an ER membrane marker. This, combined with the similarity to PKR, lead the authors to name this new protein PERK (PKR-like ER kinase). PERK was found to phosphorylate eIF2α on serine 51 *in vitro* and treatment of translation-competent reticulocyte lysates with bacterially expressed PERK lead to a profound inhibition of mRNA translation. PERK was also found to undergo autophosphorylation *in vivo* and inhibition of autophosphorylation, via mutation of lysine 618 to alanine, abolished the ability of PERK to phosphorylate eIF2α or inhibit translation. Finally, the kinase activity of PERK was observed to be initiated by the accumulation of proteins in mouse embryonic fibroblasts (MEFs), suggesting that the attenuation of protein synthesis observed *in vitro* may also be replicated *in vivo*. All of these data combined lead the authors to propose that PERK is an ER membrane spanning protein that initiates translational arrest during ER stress by first phosphorylating itself and then eIF2α (Harding et al., 1999, Shi et al., 1998).

In higher eukaryotes PERK is an ER transmembrane protein whose N-terminal domain resides in the ER lumen and C-terminal catalytic domain resides in the cytoplasm. The current model for PERK signalling is that during times of little or no ER stress, PERK dimers are held inactive as a result of BiP binding to their luminal N-terminal domains (Bertolotti et al., 2000a). However, owing to data showing that PERK and IRE1α share significant luminal domain homology, it is proposed that during ER stress, BiP dissociates from PERK, allowing unfolded proteins to bind multiple PERK dimers via MHC-like grooves formed by their luminal domains (Credle et al., 2005). This binding event is believed to result in the clustering of PERK dimers in a back-to-back formation, resulting in the flexible activation loop of one PERK dimer being close enough to interact with the catalytic domain of another PERK dimer for transphosphorylation to occur (Cui et al., 2011). Resolving the structure of PERK kinase domains to 2.8 Å revealed that this phosphorylation occurs on threonine 980 and stabilises both the activation loop and helix

αG in the C-terminal lobe, which is where eIF2α, the primary substrate of PERK, binds. Consequently, transphosphorylation activates the PERK dimer by stabilising both the activation loop and the eIF2α binding site in the C-lobe (Cui et al., 2011) (see Figure 1.1). Therefore PERK, like ATF6, is subject to control by the ER chaperone BiP. However, unlike ATF6, PERK also binds directly to unfolded proteins within the ER lumen to transduce ER stress.

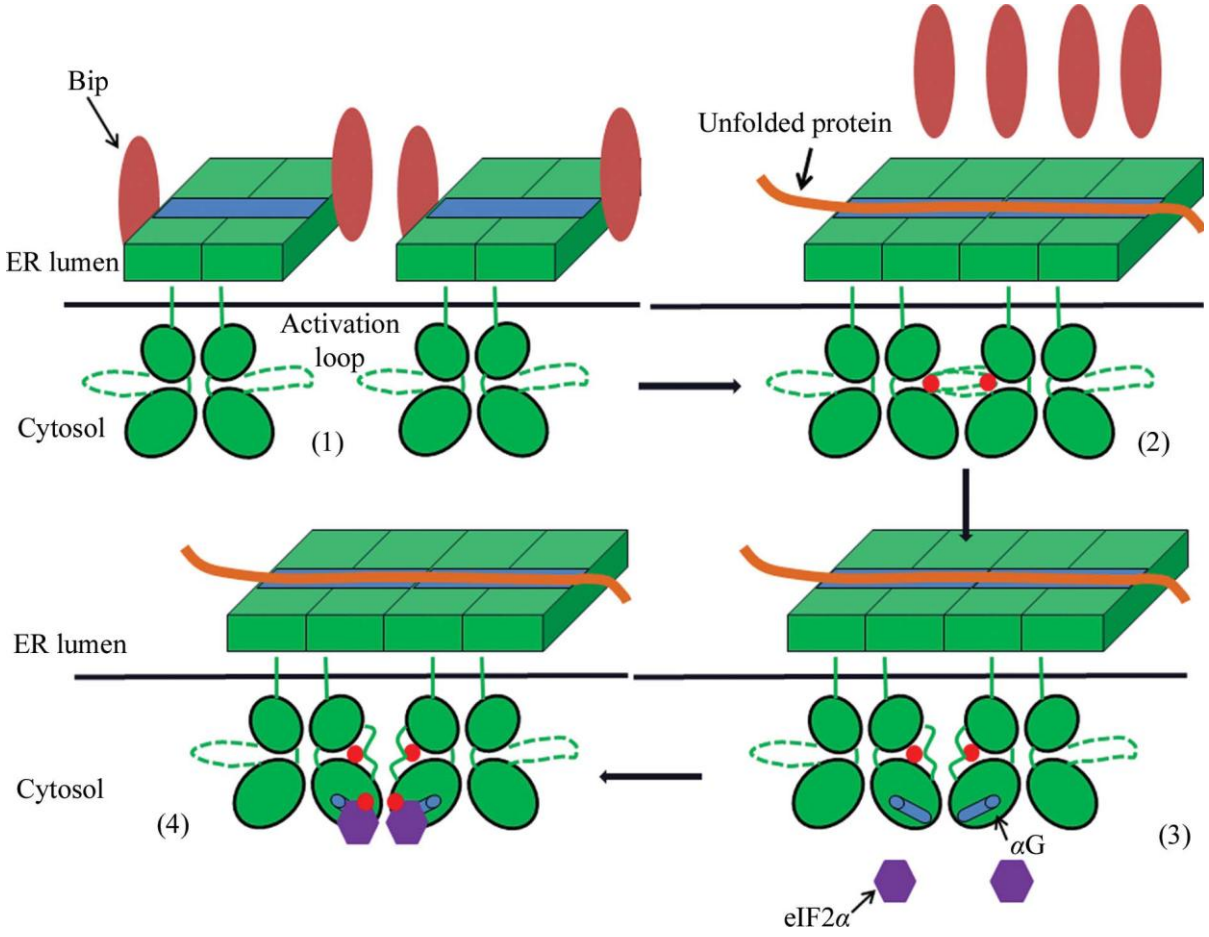

Figure 1.1 – A diagram taken from (Cui et al., 2011) depicting the activation of PERK during ER stress.

There are some other factors that are believed to influence PERK signalling in addition to BiP and unfolded proteins. Firstly, $p58^{IPK}$ a heat shock protein 40 (Hsp40) family member with an ERSE promoter, has been shown to localise to the ER membrane and decrease eIF2α phosphorylation during ER stress, giving rise to the possibility that IRE1α and ATF6 may be able to modulate PERK signalling (Yan et al., 2002). The ability to influence the activity of individual branches of the UPR is something that is of great interest when studying ER stress-related diseases and many groups are working on small chemical inhibitors that could have effects similar to $p58^{IPK}$ by inhibiting the kinase domain of

PERK (Pytel et al., 2014). In addition to factors that inhibit PERK, there are also reports that there may be additional factors that activate PERK signalling. For example, it has been shown that protein translation is attenuated during hypoxia in a PERK dependent manner, whilst *perk*$^{-/-}$ MEFs exhibit lower survival rates during hypoxia than their wild type counterparts (Koumenis et al., 2002).

PERK initiates translational arrest via phosphorylation of eIF2α on serine 51, resulting in eIF2α having a much higher affinity for eIF2B. As a result, eIF2B becomes sequestered by phosphorylated eIF2α during PERK signalling. This prevents eIF2B from carrying out its role as a guanine nucleotide exchange factor, which in turn rapidly depletes the cell of eIF2α-GTP. eIF2α –GTP is essential for the formation of the ternary complex that contains the initiator methionine (Met-tRNAi) during translation and, without this, protein translation rapidly grinds to a halt (Wek et al., 2006). This is beneficial during ER stress because it reduces client protein load within the ER lumen and, therefore, increases the probability that ER homeostasis will be restored. PERK and eIF2α are completely dependent on one another for the initiation of translation during ER stress, as inhibition of either of these proteins prevents translational attenuation. This is shown by the fact that replacement of wild type eIF2α with a mutant that cannot be phosphorylated, eIF2α^{S51A}, completely abrogates PERK signalling (Jiang et al., 2003, Scheuner et al., 2001), whilst *perk*$^{-/-}$ MEFs fail to phosphorylate eIF2α and, as a result, their ability to survive ER stress is significantly impaired (Koumenis et al., 2002). Therefore, PERK and eIF2α are interdependent in activating translational attenuation, which is a vital protective measure instigated during ER stress, as shown by the fact that cycloheximide (which inhibits protein synthesis), increases survivability in *perk*$^{-/-}$ MEF during ER stress (Harding et al., 2000b).

Interestingly, whilst the major role of PERK during ER stress is the reduction of protein synthesis, there are some proteins that not only escape the effects of eIF2α-mediated translational arrest, but are actually upregulated as a result of eIF2α phosphorylation. It is believed that this selective upregulation of some proteins during translational arrest has evolved from the ‘general control response’ of yeasts to amino acid deprivation, whereby the majority of protein synthesis is arrested, but proteins involved in amino acid biosynthesis are upregulated (Hinnebusch, 1994). The best documented example of this in higher eukaryotes is the upregulation is activating transcription factor-4 (ATF4) translation during ER stress, which occurs in a PERK-dependent manner and results in the upregulation of genes involved in amino acid import and resistance to ER stress (Harding

et al., 2003). This apparently counterintuitive upregulation of ATF4 during PERK-mediated translational arrest would appear to be the result of two upstream open reading frames (uORFs) in the 5' leader of *ATF4* mRNA, as replacement of these open reading frames with AUA (instead of the AUG start codon) abolished the positive regulation of ATF4 during translational arrest (Harding et al., 2000a). It is proposed that the reason behind the selective upregulation of ATF4 by PERK is that *ATF4* mRNA retains association with the small ribosomal subunit after the translation of its uORF1, whilst the 60 S ribosomal subunit dissociates, in a fashion similar to *GCN4* mRNA in yeast (Grant et al., 1995). Under non-stressed conditions, where eIF2-GTP coupled Met-$tRNA_i$ is plentiful, the small ribosomal subunits quickly acquire the eIF2 ternary complex, allowing the 43 S preinitiation complex to form upstream of uORF2. This means that translation is reinitiated at uORF2, which is inhibitory to ATF6 as its reading frame overlaps the *ATF4* coding region. Therefore, under non-stressed conditions ribosomes dissociate at the end of uORF2 and fail to translate *ATF4*. However, during ER stress, eIF2α phosphorylation results in a reduction in eIF2-GTP levels and this in turn means that the formation of the eIF2 ternary complex takes longer and the 40S subunit will have moved beyond the uORF2 before association with the 60S subunit. This means that translation will be reinitiated at the *ATF4* coding region initiation codon, allowing elevation in the level of ATF4 protein (see Figure 1.2). In support of this model, it has been found that increasing the distance between uORF1 and uORF2 reduces ATF4 translation (Vattem and Wek, 2004). Furthermore, mutating uORF1 or increasing the distance between uORF1 and uORF2 inhibits *ATF4* translation, assumedly because the former causes translation to start at uORF2 and the latter results in there being sufficient time in between uORFs for the tertiary complex to reform before reaching uORF2 (Vattem and Wek, 2004). Several other proteins have been reported to be upregulated in a similar manner during PERK-induced translational arrest. For example, cationic amino acid transporter 1 and cellular inhibitor of apoptosis proteins (cIAP1 and cIAP2) have also been identified as proteins that are upregulated by PERK as a result of uORFs in the 5' region of their mRNA (Fernandez et al., 2002, Hamanaka et al., 2009). However, ATF4 is regarded as the most important mediator of PERK signalling as a result of its role as a transcription factor for a selection of UPR genes.

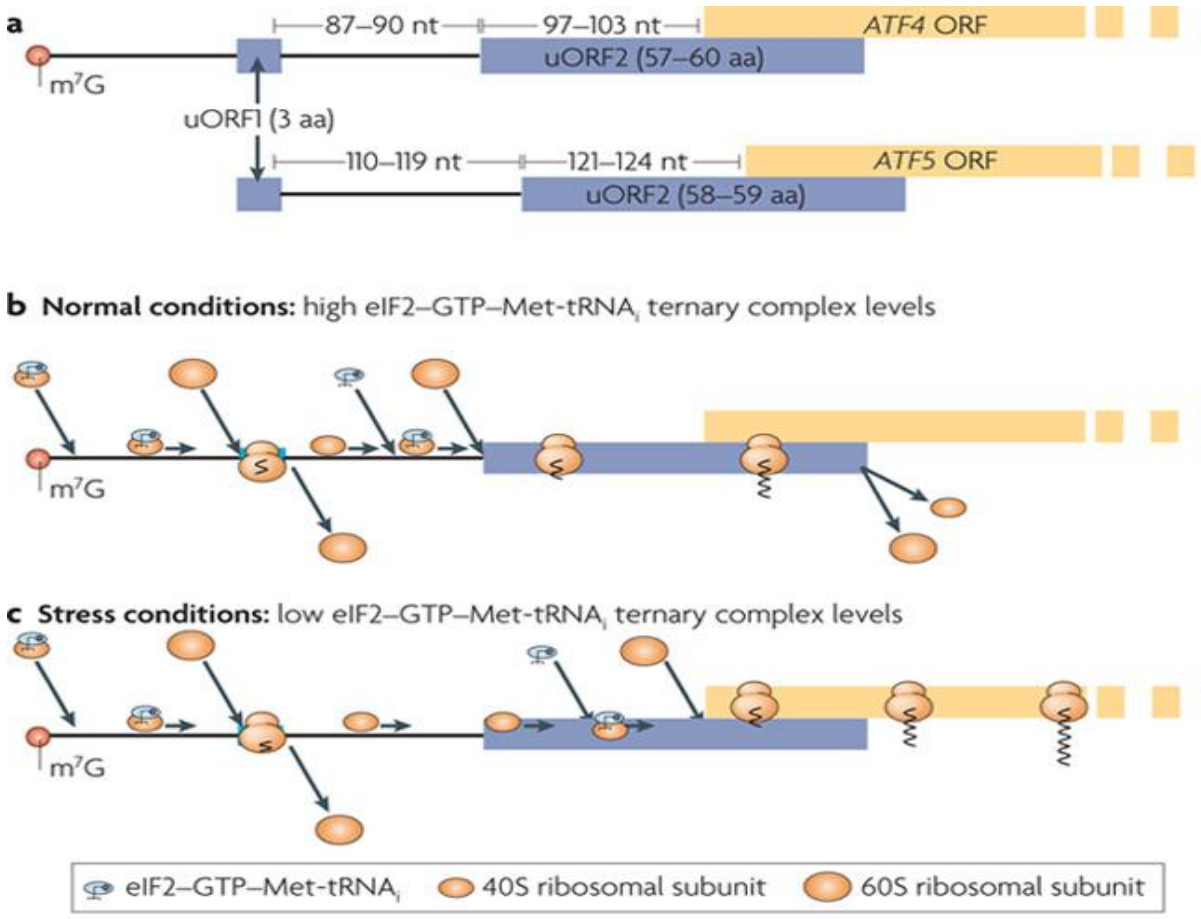

Figure 1.2 – A diagram taken from (Jackson et al., 2010) that depicts how attenuation of translation during ER stress causes the upregulation of *ATF4* mRNA translation.

1.2.5 CHOP (C/EBP homologous protein)

The main target of ATF4 during PERK signalling is the bZIP transcriptional regulator C/EBP homologous protein (CHOP/GADD153) (Averous et al., 2004), which is upregulated when either ATF6 or ATF4 bind to its promoter (Fawcett et al., 1999). Therefore, CHOP is upregulated during ER stress by both ATF6 and PERK, with ATF6 binding directly to the ERSE promoter and PERK-induced ATF4 binding to the C/EBP-ATF composite site (Ma et al., 2002).

CHOP is widely regarded as the major transcription factor responsible for driving cells towards cell death when ER stress becomes so severe that adaptation is no longer an option. There are numerous reports of apoptotic genes that are upregulated by CHOP during conditions of ER stress including death receptor 5, which induces cell death via activation of caspase-3, Bax (Yamaguchi and Wang, 2004) and Tribbles homolog 3 (TRB3), which is activated by collaborative binding between ATF4 and CHOP to response

elements in its promoter (Ohoka et al., 2005). Furthermore, there are numerous studies to show that the deletion of CHOP causes enhanced survival during ER stress. For example, *chop*$^{-/-}$ mice exhibit significantly less cell death after intraperitoneal injection of tunicamycin than either *CHOP*$^{-/+}$ or *CHOP*$^{+/+}$ mice (Zinszner et al., 1998) and, even more interestingly in the context of ER stress and type 2 diabetes, insulin resistant *chop* $^{-/-}$ mice exhibit improved β-cell survival and glycemic control in addition to increased expression of UPR and oxidative stress response genes (Song et al., 2008).

However, the CHOP target that has been studied the most by those investigating ER stress is growth arrest and DNA damage inducible 34 (GADD34), which was initially identified by screening a library of retroviruses for clones that inhibit a CHOP-GFP reporter (Novoa et al., 2001). GADD34 has been shown to be upregulated by both CHOP (Marciniak et al., 2004) and ATF4, with the latter binding a highly conserved stretch 20 bp upstream of the TATA box (-67 bp to -60 bp in the mouse *GADD34* promoter and -58 bp to -51 bp in the human *GADD34* promoter). Once translated, GADD34 activates the catalytic subunit of protein phosphatase 1 (PP1c), a type 1 protein serine/threonine phosphatase that dephosphorylates eIF2α (Connor et al., 2001). Dephosphorylation of eIF2α results in increased protein synthesis and the downregulation of both ATF4 and CHOP (Novoa et al., 2003). Therefore, there is some dispute as to whether GADD34 acts to protect against ER stress or promote cell death. On the one hand, it could be that GADD34 is responsible for turning off apoptotic signalling through inhibition of AFT4/CHOP and restoring translation in the aftermath of an ER stress insult (Ma and Hendershot, 2003). However, it could also be argued that removing the translational block is a sign that the cell has stopped trying to adapt and is increasing the translational load upon the ER in order to increase the rate of apoptosis. This is supported by research showing that there is a reduction in high molecular weight protein complexes and greater resistance to ER-stress in *chop*$^{-/-}$ mice and GADD34 mutant cells (Marciniak et al., 2004). Overall, given that CHOP signalling occurs at the onset of ER stress (rather than as the stress is alleviated) and the fact that the majority of CHOP target genes amplify apoptotic signalling, it seems more likely that GADD34 functions as a mediator of apoptosis.

Another protein that has been reported as being part of the PERK signalling pathway is nuclear factor erythroid 2–related factor 2 (NRF2), which is a bZIP transcription factor that regulates the expression of antioxidant proteins in order to protect against oxidative stress. Usually sequestered in the cytoplasm via association with kelch-like ECH-associated protein 1 (KEAP1), phosphorylation by PERK causes NRF2 to dissociate from KEAP1

and translocate to the nucleus. In addition to this, cells harbouring a targeted deletion of NRF2 exhibit a greater susceptibility to ER stress induced cell death, suggesting that PERK-NRF2 signalling forms part of a protective signalling response (Cullinan et al., 2003).

1.3 IRE1

1.3.1 Discovery

Inositol requiring 1 (IRE1) is the most highly conserved ER stress sensor in the UPR and is expressed in all eukaryotes from yeasts through to plants and mammals (Tirasophon et al., 1998, Wang et al., 1998). As with many highly conserved proteins, IRE1 (or Ire1p in the case of its yeast orthologue) was first cloned and sequenced in yeast, during genetic complementation of a *myo*-inositol auxotrophic mutant (Nikawa and Yamashita, 1992). However, in this instance the primary role of Ire1p was believed to be inositol prototrophy and it was not until a year later that its role in detecting and providing protection against ER stress was elucidated (Mori et al., 1993). Whilst screening for *S. cerevisiae* mutants that were unable to activate transcription of *KAR2* and *PDI1*, which encode the ER chaperones BiP and protein disulphide isomerase respectively, it was discovered that cells lacking the *IRE1* gene were not only unable to activate these genes, but they also exhibited a significant decrease in viability when treated with tunicamycin (Cox et al., 1993). Upon further analysis it was determined that the protein encoded by the *IRE1* gene was a membrane bound serine/threonine kinase, whose glycosylated N-terminus is located inside the ER lumen and whose cytoplasmic C-terminus was positioned in the cytoplasm. It was also determined that the C-terminus carries the aforementioned protein kinase activity, which is essential for signal transduction from the ER to the nucleus (Mori et al., 1993).

Human IRE1α was identified by screening a human fetal liver cDNA library with degenerate oligonucleotide primers that had been designed against an amino acid sequence that is specific to the kinase domains of both *S. cerevisiae* and *C. elegans* IRE1 (Tirasophon et al., 1998). This resulted in the isolation of cDNA encoding a type 1 transmembrane Ser/Thr protein kinase that displayed intrinsic autophosphorylation activity and also contained a domain homologous to RNase L. However, whilst human IRE1α shares a highly conserved cytoplasmic domain with its yeast counterpart (so much so that it is able to cleave *HAC1* mRNA), the luminal domain of human IRE1α has significantly diverged from its predecessor.

1.3.2 Isoforms

In simple eukaryotes there is just one gene encoding a single isoform of IRE1. However, in mammalian cells there are two genes encoding two distinct isoforms of the protein, which are referred to as IRE1α and IRE1β. The kinase domains of these proteins both share strong homology with Ire1p in *S. cerevisiae* and *C. elegans* and were both discovered whilst searching cDNA libraries for what was originally thought to be a single homologue of Ire1p. IRE1α (Tirasophon et al., 1998) was found to be ubiquitously expressed in mammalian cells and its deletion results in developmental defects and embryonic death in mice after 12.5 d gestation (Zhang et al., 2005). The reason for this appears to be that the deletion of IRE1α results in a reduction in vascular endothelial growth factor-A and severe dysfunction of the labyrinth, which is a highly developed tissue of blood vessels in the placenta (Iwawaki et al., 2009).

IRE1β (Wang et al., 1998), on the other hand, is solely expressed in the gastrointestinal tract and, unlike their *ire1α*$^{-/-}$ counterparts, *ire1β*$^{-/-}$ knockout mice appear to be phenotypically normal barring hypersensitivity to experimental colitis (Bertolotti et al., 2001). However, whilst the removal of IRE1β is not lethal, it is far from redundant. For example, IRE1β is required to maintain ER homeostasis in goblet cells by optimising the level of their major secretory product MUC2, a task which IRE1α is unable to do (Tsuru et al., 2013), and whilst it may not have a role in the development of mice, it has been postulated that it is required for mesoderm formation in *Xenopus* embryos (Yuan et al., 2008). Therefore, whilst IRE1α and IRE1β are both localised to the ER-membrane and share a significant amount of structural homology, it is clear that their divergent evolution has resulted in surprisingly disparate roles within organisms. This is believed to be a result of structural differences between the RNase domains conferring alternate substrate specificities upon the two IRE1 isoforms. For example, whilst both IRE1α and IRE1β are capable of splicing the traditional target of the endoribonuclease domain, X-box binding protein 1 (*XBP1)* mRNA, IRE1α is significantly more efficient at doing so. IRE1β on the other hand, has a much higher specificity for 28S ribosomal RNA (Imagawa et al., 2008) (Iwawaki et al., 2001) and this, coupled with evidence suggesting that IRE1β can cleave several ER-located mRNAs that are not targeted by IRE1α (Nakamura et al., 2011, Iqbal et al., 2008), may suggest that IRE1β has evolved to aid IRE1α in combating ER-stress by contributing the attenuation of translation in cells with a high demand for secretory proteins, such as those in the gastrointestinal tract.

1.3.3 Detecting ER stress

The mechanism by which IRE1α detects ER stress was initially through to be regulated by BiP (Bertolotti et al., 2000b). However, more recent studies have suggested that direct binding to unfolded proteins within the ER lumen could be responsible for the activation of IRE1α (Credle et al., 2005). Therefore, this section will review the evidence from both models and aim to present the most likely method of activation for IRE1α.

1.3.3.1 BiP

Binding immunoglobulin protein (BiP) is primarily an ER chaperone and it is upregulated during cytoprotective UPR signalling in order to aid with protein folding (Kohno et al., 1993). However, it also widely believed that BiP plays a role in the regulation of the ER stress response (Bertolotti et al., 2000b). The theory that BiP is responsible for the ability of IRE1α to sense ER stress was based upon findings that in unstressed cells the luminal domain of IRE1α forms stable complexes with BiP, but upon treatment with thapsigargin or dithiothreitol (ER stress mimetic drugs), BiP disassociated from the luminal domain of IRE1α resulting in the formation of high molecular mass complexes of activated IRE1α. Therefore, it was argued that BiP inhibits IRE1α until misfolded proteins stimulate the dissociation of BiP from their luminal domains, an idea further supported by results showing that that overexpression of BiP attenuates IRE1α signalling (Bertolotti et al., 2000b). However, in this instance it is unclear whether the increased BiP expression prevents the detection of ER stress by IRE1α or reduces the amount of stress, and therefore UPR activation, by reducing the amount of misfolded proteins within the ER. Additional evidence for the BiP binding model was presented by *Liu et al.* (Liu et al., 2000) who showed that Ire1p could be constitutively activated in *S. cerevisiae* by replacing its luminal domain with a functional leucine zipper dimerisation motif. Seeing as it is extremely unlikely that a non-specific bZIP motif would be able to bind to a theoretical ER stress ligand, this indicated that dimerisation is both required and sufficient for activation of UPR signalling. Therefore, it seemed more likely that Ire1p is controlled via negative regulation by a molecule such as BiP, which dissociated during ER stress, than a positive regulatory model whereby an ER stress ligand causes dimerisation by binding to the luminal domain of Ire1p. The authors also demonstrated that the luminal domains of IRE1 and PERK are interchangeable, by replacing the luminal domain of Ire1p with that of *Caenorhabditis elegans* PERK to produce a protein that could rescue UPR signalling in *ire1*Δ *S. cerevisiae* cells. This showed that the luminal domains of PERK and IRE1 share structural and functional aspects that have been conserved throughout evolution and suggests that any

ligand that is capable of initiating ER stress directly would bind and activate both PERK and IRE1.

Determining the crystal structure of enzymes often gives the best insight into their activation as it can reveal structural changes that occur upon their activation. Therefore, several groups have studied various domains of IRE1 using X-ray crystallography in order to try and determine the mechanism by which it is activated. Upon studying the luminal domain of human IRE1α via this method, *Zhou et al.* were able to identify a dimerisation interface, stabilised by hydrogen bonds and hydrophobic interactions, which resulted in the creation of a major histocompatibility complex (MHC)-like groove at the interface between the IRE1α monomers (Zhou et al., 2006). However, whilst this groove would normally indicate protein binding, the authors concluded that it appeared to be too narrow for protein binding and cited the fact that the purified IRE1α luminal domains formed high affinity dimers *in vitro* as evidence that the BiP model was more likely than the binding of misfolded proteins (Zhou et al., 2006). Further support of the BiP regulatory model was also supplied by the finding that mammalian cells expressing an IRE1α mutant with a low affinity for BiP showed a significant increase in activation even without ER stress (Oikawa et al., 2009).

1.3.3.2 Unfolded proteins

The evidence that direct interaction with unfolded proteins could be the cause of IRE1α activation was also proposed as a result of studying the crystalline structure of the protein and, more specifically, the MHC-like groove at the interface of IRE1α monomers. However, in this instance, the authors used the formation of the conserved MHC-like region within the luminal domain of Ire1 to argue that Ire1 was activated by direct binding to unfolded proteins (Credle et al., 2005). As a result, *Credle et al.* used their findings to propose that this MHC-like domain (termed the core luminal domain or cLD) directly binds unfolded proteins and, in doing so, changes the quaternary association of the Ire1 monomers in the ER membrane (see Figure 1.3). This progressed to the proposition that these conformational changes in the ER lumen were responsible for positioning the cytosolic Ire1 kinase domains optimally for the autophosphorylation event that is essential to initiate the UPR. *Credle et al.* cited their findings that mutations of residues within the cLD reduced the response of Ire1 to ER stress as evidence to support this model (Credle et al., 2005).

Additional evidence supporting the protein binding model of IRE1α activation has been provided in the form of work showing that the cLD of yeast Ire1 binds to unfolded proteins

in vivo and dimerises when binding peptides composed mainly of basic and hydrophobic amino acids *in vitro*. Furthermore, mutating certain residues within cLD of Ire1 inhibited peptide binding, perhaps providing the mechanism by which the mutation of cLD residues inhibited the ability of Ire1 to respond to ER stress during Credle's investigation (Credle et al., 2005). These results would suggest that Ire1 senses ER stress by directly binding to misfolded proteins in the ER lumen (Gardner and Walter, 2011) and have been used as evidence against the BiP model of activation. Gardner and Walter also state that the sequence of the cLD is conserved between yeast and humans and propose that, whilst the MHC groove formed by mammalian IRE1α dimers is too narrow in the absence of peptide binding, interaction with misfolded proteins would cause a conformational switch so that the hIRE1α MHC-like groove assumes and "open" conformation. This conformation would be like the one exhibited in yeast and the authors propose that it would be this open formation that is required for oligomerisation and activation of hIRE1α.

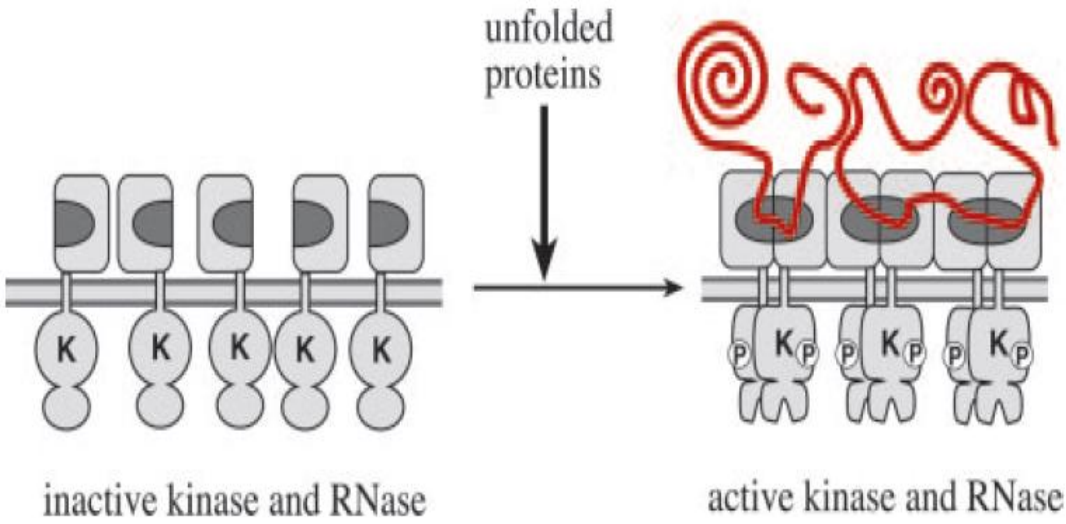

Figure 1.3 –Diagrammatic representation of Ire1 activation via the binding of unfolded proteins to its luminal domain, taken from (Credle et al., 2005)

1.3.3.3 The 'two step' model

With evidence supporting both BiP and misfolded proteins being responsible for initiating IRE1α signalling, many groups started investigating the possibility that it could be a combination of the two models that results in IRE1α activation rather than it being one or the other. One group that supports the idea of both BiP and unfolded proteins being integral for IRE1α signalling propose a 'two step' model of activation. According to *Kimata et al*. (Kimata et al., 2007), the first step in this process would be dissociation of BiP, which would cause IRE1 cluster formation. Then, once IRE1 clusters had formed, misfolded proteins would be able to bind to the core sensing region (CSSR) of the luminal domain of Ire1 in a manner that orients the cytosolic effector domains of Ire1 in a conformation conducive to signal transduction (Kimata et al., 2007). However, Pincus suggests that the role of BiP is not as significant as this and that BiP is not responsible for IRE1α dimerisation (Pincus et al., 2010). Building upon findings that the deletion of the BiP binding domain of Ire1 does not result in constitutive activation (Kimata et al., 2004), Pincus argues that Ire1 is in a dynamic equilibrium with BiP and unfolded proteins. In this model BiP dissociation would merely yield monomeric Ire1, rather than triggering oligomerisation. Monomeric Ire1 would then either bind to misfolded proteins, allowing oligomerisation and activation, or re-associate with BiP (Pincus et al., 2010).

Thus, it would appear that both BiP and misfolded proteins are likely to contribute to the activation of IRE1α, with the 'two step' model appearing to be the most probable version of events. Data showing that the deletion of the BiP binding domain of Ire1 does not result in constitutive activity, combined with the fact that mutating residues in the cLD of Ire1 inhibit protein binding and activation, suggest that misfolded proteins play a significant role in activating IRE1α signalling. However, the MHC-like domain required for protein binding is generally believed to require pre-formed IRE1α dimers and therefore a model whereby BiP dissociation allows dimerisation, followed by protein binding causing a conformational change that results in autophosphorylation and activation, currently appears to be the most likely scenario (see Figure 1.4).

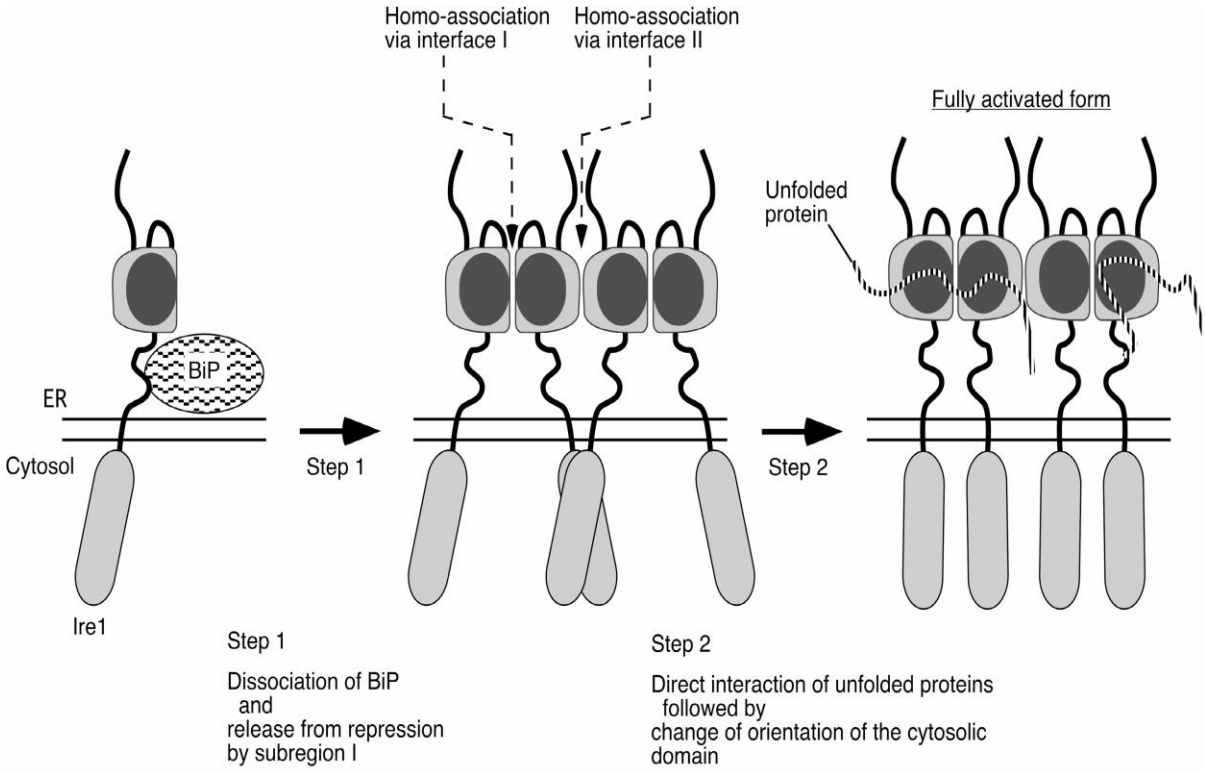

Figure 1.4 –Diagrammatic representation of the "two step" model of Ire1 activation during ER stress, taken from (Kimata et al., 2007).

1.3.3.4 Lipids

Whilst detecting the accumulation of unfolded proteins remains the major role of IRE1α, there have been a few studies to suggest that IRE1α can also detect, and react to, abnormalities in lipid homeostasis as well. The first group to propose this idea found that an Ire1p mutant, whose ability to bind misfolded proteins has been weakened by a mutation in its luminal domain, could still be activated by depletion of inositol or deletion of genes involved in lipid homeostasis. In addition to this, an Ire1p mutant that had its luminal domain exchanged for a bZIP luminal domain was found to cluster just as efficiently as wild-type (WT) Ire1p under inositol depletion, despite being less efficient when stimulated by tunicamycin treatment (Promlek et al., 2011). These findings were then further supported by research indicating that IRE1α and PERK are activated by increased lipid saturation in a transmembrane domain dependent manner in MEFs (Volmer et al., 2013). The emergence of data supporting this novel method of IRE1α activation reveals the potential for an interesting new layer to its regulation of ER homeostasis. However, more evidence will be needed in order to consider regulation of membrane lipid composition as a significant instigator of UPR signalling.

1.3.4 Activation

During ER stress IRE1α monomers dimerise/oligomerise and *trans*-autophosphorylate one another in order to activate UPR signalling (Shamu and Walter, 1996). Interestingly, the activity of the endoribonuclease domain of IRE1 is dependent on the functionality of its kinase domain (Tirasophon et al., 2000), making it similar to RNase L, which forms homodimers upon activation (Dong and Silverman, 1995) and requires the presence of ATP for optimal RNA cleavage (Dong et al., 1994). However, whilst a functional kinase domain is essential for endogenous IRE1α signalling, autophosphorylation is not actually required for endoribonuclease activity. This was shown by *Papa et al.* through use of a mutant Ire1p protein in which leucine 745 had been replaced with alanine (Papa et al., 2003). This enlarges the ATP binding pocket of the $Ire1p^{L745A}$ kinase domain and prevents ATP binding. However, treatment with the ATP competitive drug 1- (1, 1-dimethylethyl)- 3-(1-naphthalenylmethyl)- 1H-pyrazolo[3, 4-d]pyrimidin-4-amine (1NM-PP1) restores endoribonuclease activity, in a phosphorylation-independent manner, suggesting that a conformational change initiated by ATP binding is responsible for activating Ire1p signalling, rather than the phosphorylation event itself (Papa et al., 2003).

Elucidating the roles of dimerisation and the kinase domain in the activation of IRE1α signalling has been significantly advanced by the ability to study the crystalline structure of IRE1α, which has ultimately allowed the creation of a model to describe how activation may occur during ER stress. Various studies have revealed that, upon ER stress, the luminal domains of Ire1p monomers dimerise, and possibly oligomerise, resulting in the cytoplasmic domains being brought together in a face-to-face orientation (Korennykh et al., 2009). This conformation is proposed to position the C-termini of the Ire1 monomers in close enough proximity for *trans*-autophosphorylation to occur. The binding of ATP during this autophosphorylation event is proposed to causes a conformational change that switches the catalytic domains from a face-to-face orientation to the back-to-back orientation assumed by active IRE1α. However, it must be noted that the only evidence for this conformation change thus far has been obtained via crystal structures, which may not be representative of the situation *in vivo*. Therefore, biochemical data will need to be obtained in order to determine the exact mechanism by which activation of endoribonuclease activity occurs.

It has also been reported that auto-phosphorylation is the stimulus for the switch to a back-to-back configuration (Ali et al., 2011). However, this would make autophosphorylation essential to endoribonuclease activity which, as is shown by the L745A mutant, it is not.

Therefore, nucleotide binding stimulating the back-to-back organisation currently seems the more likely scenario. What is agreed among various reports is that the back-to-back configuration of Ire1p cytosolic domains brings two endoribonuclease domains together to form a cleft (termed the KEN domain) that will act as the catalytically active site for *XBP1* splicing (Lee et al., 2008a) (see Figure 1.5).

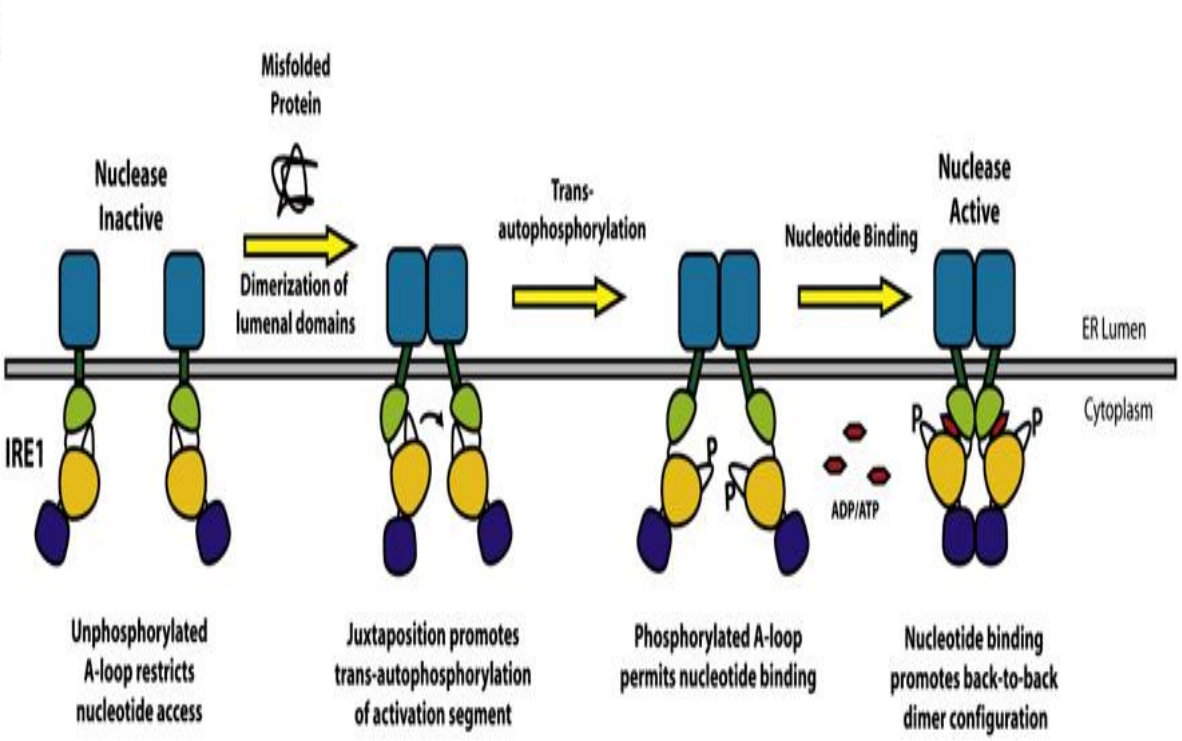

Figure 1.5 – A diagram taken from (Lee et al., 2008a) depicting the activation of the Ire1p endoribonuclease domain in response to misfolded proteins.

1.3.5 Signalling via the IRE1 endoribonuclease domain

The splicing of *HAC1* by Ire1p in yeast is a process that has been highly conserved throughout evolution (Calfon et al., 2002). However, it took a significant time after the discovery of *XBP1* to realise that it was the *HAC1* homologue and that IRE1α was responsible for mediating the unconventional splicing required for the production of active XBP1. In yeast, Ire1p signalling is mediated solely through the endoribonuclease domain, which cleaves *HAC1* mRNA in order to control the transcription of UPR genes. However, in higher eukaryotes IRE1α signalling is far more complex and is mediated by both the endoribonuclease domain and the kinase domain. Therefore, this section will assess the downstream signalling targets of IRE1α endoribonuclease activity, whilst the next section will deal with the inflammatory signalling mediated by the kinase domain.

1.3.5.1 XBP1

Hac1, the yeast homologue of XBP1, was initially identified as a basic-leucine zipper transcription factor that binds to the UPR-element of UPR genes and whose transcription is regulated by splicing of its mRNA. This combined with the fact that Hac1 was only found in UPR activated cells, suggested that it played a key role in modifying the unfolded protein response in yeast (Cox and Walter, 1996, Mori et al., 2000). The splicing of *HAC1* mRNA was found to be carried out by Ire1p which, in combination with tRNA ligase, was able to cleave *HAC1* mRNA at two junctions to produce an alternate version of the mRNA (*HAC1(i*)) *in vitro*. This provided the first evidence that Ire1p is a bifunctional enzyme, acting as both a kinase and an endoribonuclease (Sidrauski and Walter, 1997).

The mechanism by which Hac1 protein is produced is particularly interesting because, whilst *HAC1* mRNA is transcribed during times where there is little ER stress, *HAC1* mRNA is only translated during ER stress. The reason behind this is that, prior to ER stress, *HAC1* mRNA resides in the cytoplasm in a stable association with polyribosomes, but it is not translated because translation is blocked by a base-pairing interaction between the intron and the 5' untranslated region (see Figure 1.6). However, upon the occurrence of ER stress *HAC1* mRNA is recruited to active Ire1p via a conserved bipartite element (BE) targeting unit in the 3' untranslated region (Aragon et al., 2009) and the inhibitory intron is removed via splicing carried out by the Ire1p endoribonuclease domain. Therefore, the reason why unspliced *HAC1* is not translated is because translation is stalled until ER stress activates the endoribonuclease activity of Ire1p, allowing splicing of the mRNA to produce a template for the active transcription factor Hac1(i) (Ruegsegger et al., 2001). Splicing of *HAC1* mRNA during ER stress results in the C-terminus of the *HAC1* mRNA being replaced with an exon encoding 18 amino acids. These 18 amino acids function as a potent activation domain, thus explaining why protein translated from unspliced *HAC1 in vitro* is unable to induce the UPR (Mori et al., 2000).

The discovery of the mammalian orthologue of Hac1 occurred whilst carrying out yeast one-hybrid screen for proteins that bound to the human endoplasmic reticulum stress element (ERSE). This resulted in the identification of a bZIP protein named X-box protein binding 1 (XBP1/TREB5) (Yoshida et al., 1998). However, after finding that over-expressing XBP1 had little effect on the promoter activities of various ER chaperone genes (Yoshida et al., 2000), it was discounted until it was discovered that endogenous XBP1 from ER stressed HeLa cells appeared at a different molecular weight than *in vitro* translated XBP1 (Mori et al., 2000). This finding indicated that *XBP1* mRNA is spliced

during ER stress to give a different protein product. RT-PCR confirmed that 26 nucleotides were removed from *XBP1* mRNA during thapsigargin induced ER stress and that this splicing event caused a frame shift that resulted in the replacement of the C-terminus of XBP1. Pulse-chase labelling showed that there was essentially no difference in stability between the protein translated from unspliced *XBP1* mRNA (*XBP1u*) and protein translated from spliced *XBP1* mRNA (*XBP1s*), with both exhibiting half-lives of about an hour. However, there was a marked difference in the ability of the two proteins to act as transcriptional activators because, whilst both versions of the protein contain the N-terminal DNA binding domain, the C-terminus of XBP1(s) also possesses a potent activation domain that that XBP1(u) lacks. Thus, mammalian XBP1 exhibits a mechanism of activation that would appear to have been conserved from yeast (Calfon et al., 2002, Shen et al., 2001).

IRE1α was first identified as the endoribonuclease responsible for cleaving *XBP1* mRNA in higher eukaryotes via a co-overexpression assay in which overexpression of both IRE1α and *XBP1* mRNA lead to significant increases in XBP1(s), whilst overexpression of *XBP1* alone only resulted in elevated XBP1(u). This, combined with data showing that point mutations on *XBP1* mRNA abolished XBP1(s) when overexpressed with IRE1α, provided strong evidence that IRE1α specifically cleaves *XBP1* mRNA and that IRE1α/XBP1 signalling has been conserved from Ire1p/Hac1 signalling in yeast (Yoshida et al., 2001). In addition to this, it was also shown that IRE1α is essential to *XBP1* splicing in response to ER stress as an IRE1α$^{\Delta C}$ mutant exhibited a strong dominant negative effect on XBP1(s) production in response to thapsigargin. This was further supported by the fact that *ire1α*$^{-/-}$ MEFs are unable to fully activate normal UPR transcriptional program owing to a deficiency in *XBP1* splicing and the production of XBP1(s) protein (Lee et al., 2002).

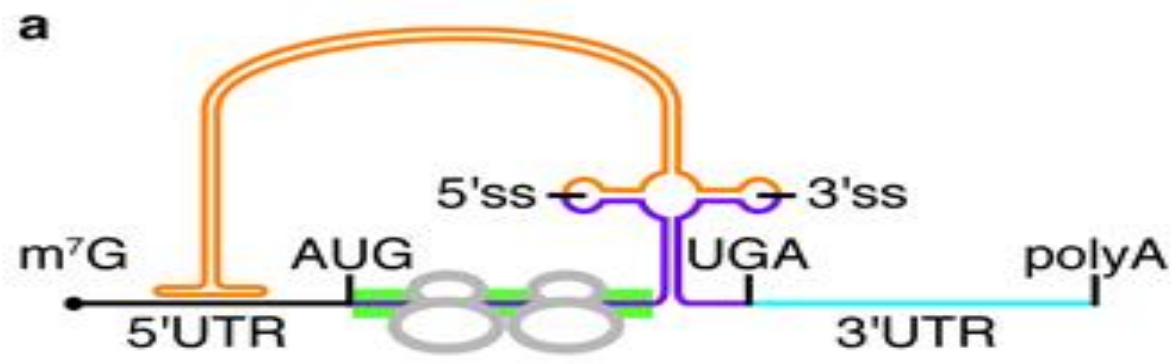

Figure 1.6 – A diagram depicting the structure of *HAC1* mRNA taken from (Aragon et al., 2009).
The orange section represents the intron that inhibits translation, which is removed by unconventional splicing mediated by Ire1p.

The mechanism by which IRE1α cleaves *XBP1* is non-conventional (Uemura et al., 2009) and ligation is mediated by tRNA ligase in order to produce the mRNA template for active XBP1 protein (Jurkin et al., 2014). Once produced XBP1 protein translocates to the nucleus where it binds to the UPR response elements (UPRE) in order to upregulate a wide variety of UPR genes. In this respect XBP1 and ATF6 have very similar roles and their inter-connection is enhanced further by the fact that XBP1 has an ESRE element in its promoter, allowing ATF6 to upregulate its translation. However, XBP1 is regarded as being the more powerful of the two transcription factors because, whilst the UPRE (TGACGTGG/A) forms part of ESRE in mammalian cells, it can also exist in genes that do not have an ESRE promoter. Therefore, whilst XBP1 can act as a promoter to genes under the control of ATF6, ATF6 cannot exert an effect on all of the genes controlled by XBP1. This means that there is a subset of genes that are entirely dependent on the activity of XBP1 (Lee et al., 2003) (Acosta-Alvear et al., 2007). As a result of this, it has been proposed that ATF6 exists to instigate a rapid response to ER-stress (as it does not need to be translated), but XBP1 becomes predominant during prolonged stress as it can up-regulate itself, via the UPRE in its own promoter, unlike ATF6 (Yoshida et al., 1998, Yoshida et al., 2001).

1.3.5.2 Regulated inositol-requiring 1 dependent decay (RIDD)

In addition to its primary role of splicing *XBP1* mRNA, the endoribonuclease domain of IRE1α has been shown to cleave other mRNAs in a manner that destabilises them and targets them for degradation. This process, known as regulated inositol-requiring 1 dependent decay (RIDD), adds another level to the control of IRE1α mediated UPR signalling. The idea that IRE1α is capable of cleaving mRNAs other than *XBP1* was first proposed after the observation that IRE1α forms complexes with a variety of different RNAs *in vivo* and that the frequency of these associations increases during ER stress (Bertolotti and Ron, 2001). In addition to this, the length of these RNAs was found to be shorter when isolated from ER stressed cells than from their unstressed counterparts. Finally, association of IRE1α and these RNA species was abolished when using IRE1α mutants with defective endoribonuclease domains, leading to the conclusion that IRE1α was splicing these RNAs (Bertolotti and Ron, 2001). These initial findings by Bertolotti and Ron were followed by evidence that IRE1α independently mediates the rapid degradation of a specific subset of ER-localised mRNAs via endonucleolytic cleavage in *Drosophila* (Hollien and Weissman, 2006) and murine cells (Hollien et al., 2009). Interestingly, some of the mRNAs targeted by mammalian IRE1α encoded ER chaperones,

giving the first indication that unlike *XBP1* splicing, RIDD has the potential to induce apoptosis (Han et al., 2009). With growing evidence to suggest that IRE1α is capable of splicing mRNA targets via RIDD, the question was posed as to whether *XBP1* splicing and RIDD occur via the same mechanism or whether they occur independently to one another. In order to determine this, analysis of two crystalline structures of yeast Ire1p binding mRNA was carried out to identify the essential residues for the endoribonuclease action of Ire1p. The result of this study was that H1061 and Y1043 were shown to be essential for transition state stabilisation, whilst N1057 and R1056 were required for the co-ordination of the scissile phosphate (Korennykh et al., 2011). Therefore the authors propose that, as each Ire1p monomer possesses these residues, Ire1p monomers would be capable of carrying out endonucleolytic cleavage independently. However, it was also suggested that individual monomers would not be able to cleave *XBP1* owing to the fact that the creation of the stem loop docking domain, essential for interaction with *XBP1*, occurs during the dimerisation of two Ire1p monomers. This lead to the conclusion that, whilst it is unlikely that all of the components of the Ire1p dimer/oligomer are involved in *XBP1* splicing, the formation of the dimer/oligomer results in the formation of a domain that is essential for *XBP1* splicing. However, if RIDD substrates do not contain a stem loop structure similar to that of *XBP1*, then dimerisation/oligomerisation would not be required, giving rise to the potential for a slightly different mechanism for RIDD substrates than that used for *XBP1* (Korennykh et al., 2011). The hypothesis that mRNAs targeted by RIDD may be processed differently from *XBP1* mRNA is further supported by research showing that residues essential for the catalysis of *XBP1* cleavage are not required for the endolytic cleavage of RIDD substrates. *Tam et al.* (Tam et al., 2014) found that whilst the H1061 residue in yeast Ire1p (involved in the catalysis of splicing) is essential for the splicing of both *HAC1* and RIDD substrates, the mutation of the R1039 residue (required for *HAC1* binding) did not affect ability of Ire1p to cleave RIDD substrates. This, combined with the fact that RIDD substrates do not compete with *HAC1* during *in vitro* RNase reactions, was used to suggest that whilst both *XBP1* and RIDD substrates share a catalytic site that includes the H1061 residue, the binding sites for *XBP1*/*HAC1* and RIDD substrates may differ, (Tam et al., 2014).

Interestingly, *Schizosaccharomyces pombe* lack a Hac1/XBP1 ortholog and, in this organism, Ire1p cleaves a select group of ER-localised mRNAs instead, perhaps supporting the idea that RIDD and *XBP1* splicing can occur independently. Whilst investigating the mRNAs that are cleaved by Ire1p in *S. pombe* it was found that all of them were destabilised and swiftly degraded with the exception of BiP mRNA, which is stabilised by

the truncation of its 3' UTR. Therefore, in *S. pombe*, it would appear that RIDD serves a function in promoting cell survival by increasing folding capacity (upregulating BiP) and reducing the folding burden on the ER (by down regulating other proteins) (Kimmig et al., 2012). However, in contrast to this, the majority of RIDD targets that have been identified in higher eukaryotes appear to be associated with instigating cell death, with mRNAs involved in lipogenesis, protein folding, and lipoprotein metabolism all being targeted for degradation (So et al., 2012). Furthermore, in addition to inhibiting the translation of proteins involved in restoring ER homeostasis, RIDD has also been shown to upregulate proteins involved in apoptotic signalling by degrading microRNAs that would otherwise have prevented their translation. For example, RIDD has been shown to initiate the rapid decay of miRNAs-17, -34a, -96 and -125b, which usually repress caspase-2 translation. The fact that miRNA-17 has been targeted is of particular interest because it results in the stabilisation of thioredoxin interacting protein (TXNIP) mRNA and consequently the upregulation of TXNIP protein. TXNIP protein causes elevations in caspase-1 cleavage and interleukin 1β secretion, promoting sterile inflammation and programmed cell death in response to IRE1α signalling during ER stress (Lerner et al., 2012). Therefore, it would appear that the upregulation of protein synthesis via RIDD also has an apoptotic signalling effect (Upton et al., 2012).

With such a wide variety of RNA substrates now being determined, efforts have been made to try to elucidate how IRE1α determines which mRNAs to degrade. To this end an exon microarray analysis has been used to isolate IRE1α endoribonuclease substrates. This revealed that a consensus sequence of CUGCAG, when accompanied by a stem-loop structure, is essential for IRE1α-mediated cleavage (Oikawa et al., 2010). However, the need for a stem-loop structure would obviously conflict with the model whereby RIDD occurs separately to *XBP1* splicing based on stem-loop docking (Korennykh et al., 2011) (Tam et al., 2014). Therefore, it is clear that more work needs to be done to determine how IRE1α identifies targets for RIDD and the mechanism by which RIDD actually occurs, although there is sufficient evidence to indicate that RIDD is an important part of the UPR and provides yet another way in which IRE1α can either act to protect cells or target them for death during ER stress.

1.3.6 Signalling via the IRE1α kinase domain

In yeast, Ire1p is the sole mediator of the UPR and, whilst the kinase domain of Ire1p is essential for enabling the activation of endoribonuclease function, no other functions for the kinase domain have been found. However, in metazoans, the UPR is far more complicated with PERK and ATF6 contributing to IRE1α signalling to form a complex, inter-related signalling cascade. This situation is then complicated further by the fact that IRE1α appears to initiate two distinct responses to ER stress rather than the singular linear response exhibited in yeast. In metazoans, IRE1α retains its ability to activate a protective transcriptional program via *XBP1* splicing, whilst also having the potential to mediate inflammatory signalling via its kinase domain (Urano et al., 2000a, Nishitoh et al., 2002, Brown et al., 2016).

The complexity of ER signalling in metazoans means that untangling the protective signalling from apoptotic signalling is difficult, especially when individual stress sensors are capable of inducing both protection and cell death. Therefore, this section of the introduction will establish what is already known about IRE1α apoptotic signalling, before presenting my work on a novel model that allows the specific study of IRE1α signalling and characterisation of the its downstream effectors in isolation. This is important because isolating the exact mechanics behind IRE1α signalling would allow the development of therapeutic treatments targeted at inhibiting apoptosis in disease models such as insulin resistance and type 2 diabetes.

1.3.6.1 TRAF2/JNK

Tumour necrosis factor receptor associated factor 2 (TRAF2) is a member of the TRAF family of intracellular adaptor proteins, which mediate the formation of signalling complexes that link upstream receptors to downstream effector enzymes (Wajant et al., 2001). All members of the TRAF family contain a TRAF domain that is composed of an N-terminal coiled-coil region (TRAF-N) and a C-terminal β-sandwich (TRAF-C) (Ha et al., 2009). TRAF2 also possesses an N-terminal ring finger domain accompanied by five zinc fingers (Ostuni et al., 2010), which enables TRAF2 to act as a ubiquitin ligase in the presence of sphingosine-1-phosphate (Alvarez et al., 2010). The TRAF domain of TRAF proteins is responsible for forming protein-protein interactions, including TRAF protein oligomerisation, whilst minor structural differences in the β-sandwich structure of the TRAF-C domain are believed to give the individual members of the TRAF family specificity for their target receptors (Chung et al., 2007). TRAF proteins are then believed

to interact with effectors via either their TRAF-N domains or N-terminal ring finger domains depending on the effector in question (Takeuchi et al., 1996). Downstream TRAF signalling pathways mediated by these effectors usually result in the activation of nuclear factor kappa-light-chain-enhancer of activated B cells (NF-κBs), mitogen activated protein kinases (MAPKs) or interferon-regulatory factors (IRFs) (Ostuni et al., 2010).

Prior to the identification of the IRE1α-TRAF2 signalling pathway, it had been noted that ER stress induced JNK signalling (Davis, 2000). However, up until the ground breaking paper published by *Urano et al* (Urano et al., 2000b), the mechanism by which ER stress induced JNK signalling was unknown. This was changed when Urano *et al.* showed that overexpression of IRE1α, or IRE1β, resulted in the activation of JNK and that this activation was dependent upon the kinase domain of IRE1α/β specifically. Overexpression of IRE1 is well documented for inducing ER stress (Tirasophon et al., 1998, Iwawaki et al., 2001, Wang et al., 1998) and the authors found that overexpression of both wild type IRE1β and IRE1α endoribonuclease deficient mutant ($IRE1\beta^{\Delta EN}$) caused elevations in the amount of active JNK. However, a kinase deficient mutant ($IRE1\beta^{K536A}$) was unable to cause activation of JNK signalling, even after being overexpressed at much higher levels. In addition to this, $ire1\alpha^{-/-}$ mice failed to activate JNK when ER stress was induced via 1 h thapsigargin treatment, but were still able to respond to UV-light induced JNK signalling as efficiently as their wild type counterparts. These data combined provide strong evidence that IRE1α/β is responsible for mediating JNK signalling during ER stress.

Having shown that IRE1α is responsible for stimulating JNK synthesis, the authors began a search for proteins that could be involved in IRE1α mediated JNK signalling. To achieve this, a yeast two hybrid screen using the cytosolic domain of IRE1β as bait was carried out, returning 24 possible candidates. One of the 24 proteins that interacted with IRE1β was TRAF2, which bound to the COOH-terminus of IRE1β via its TRAF domain. To show that TRAF2 was capable of interacting with IRE1β *in vivo*, a co-immunoprecipitation reaction between IRE1β and TRAF2 was carried out in human embryonic kidney 293T (HEK293T) cells and revealed that TRAF2 binds to wild type IRE1β. It was also found that this interaction still takes place when using an endoribonuclease deficient mutant of IRE1β ($IRE1\beta^{\Delta EN}$), but was inhibited when using the kinase deficient $IRE1\beta^{K536A}$. Therefore, the authors were able to show that not only do TRAF2 and IRE1β interact in mammalian cells, but this interaction occurs in an IRE1β kinase domain-dependent manner in the same way as JNK depends on the IRE1β kinase for its activation. To prove that TRAF2 is essential for IRE1α/β-JNK signalling during ER stress, a dominant negative TRAF2 mutant (that

lacks its NH_2-terminal signalling domain) was also expressed and caused reduced JNK activation via IRE1β (Urano et al., 2000b).

Finally, seeing as IRE1β is not widely expressed, *Urano et al.* investigated whether IRE1α could be isolated during a co-immunoprecipitation with TRAF2, which was isolated from AR42J cells with antiserum against the NH_2-terminal of the protein. They found that IRE1α did interact with TRAF2, but only if the AR42J cells were subjected to ER stress. Therefore, the work of *Urano et al.* (Urano et al., 2000b) not only identified that the kinase domain of IRE1β is capable of initiating a stress signalling cascade, in a manner that is independent of endoribonuclease function, but also that this signalling results in the activation of JNK via direct interaction with the adaptor protein TRAF2.

The idea that TRAF2 binds to IRE1α in order to initiate the construction of a signalling scaffold is one that has been pursued by many groups trying to elucidate how signalling is mediated via the IRE1α kinase domain. Using the idea of a scaffold as the basis for the signalling pathway, various proteins have been suggested as holding the key to mediating JNK activation and perhaps one of the most convincing candidates comes in the form of apoptosis signal-regulating kinase 1 (ASK1). ASK1 has been shown to be essential for IRE1α-TRAF2-JNK signalling during ER stress caused by accumulation of poly-glutamine (polyQ) repeats. During this research it was shown that ASK1 interacts with TRAF2 in an ER stress dependent manner and that ASK1 also co-immunoprecipitates with IRE1α in a TRAF2 and ER stress dependent manner. This suggests that ER stress causes the formation of an IRE1α-TRAF2-ASK1 protein complex which, the authors propose, results in the phosphorylation, and subsequent activation, of ASK1, which is observed during thapsigargin induced ER stress (Tobiume et al., 2002, Nishitoh et al., 2002). Following the identification of the IRE1α-TRAF2-ASK1 complex, the authors were able to show that thapsigargin treatment and IRE1α overexpression resulted in JNK activation in *ask1*$^{+/+}$ MEFs, whereas in *ask1*$^{-/-}$ MEFs JNK activation was abolished. Furthermore, reconstituting *ask1*$^{-/-}$ MEFs with exogenously expressed ASK1 restored ER stress-induced JNK signalling. Finally, the authors provided evidence to show that the induction of ER stress by thapsigargin, tunicamycin and dithiothreitol resulted in cell death in *ASK1*$^{+/+}$ MEFs and that this cell death was significantly reduced in *ask1*$^{-/-}$ MEFs (Nishitoh et al., 2002). This combined with their previous findings that TRAF2 activates JNK via ASK1 during TNFα signalling suggests a model whereby ER stress causes cell death via a pathway that sees IRE1α and TRAF2 activate ASK1, which in turn activates JNK via MAP kinase/ERK kinase 4/7 (MEK4/7) (Nishitoh et al., 1998) (Weston and Davis, 2002).

Therefore, as a result of the work by *Urano et al.* (Urano et al., 2000b) and *Nishitoh et al.*(Nishitoh et al., 2002), the current model for JNK activation during ER stress works as follows: ER stress causes the activation of IRE1α, which then dimerises and autophosphorylates itself. Active IRE1α then recruits the adaptor protein TRAF2 to its kinase domain via the C-terminus of TRAF2 (presumably via interaction with the TRAF domain). TRAF2 subsequently forms multimers by recruiting other TRAF2 molecules to the scaffold, causing the clustering of their TRAF2 N-ring domains. The N-termini of these TRAF2 proteins recruit ASK1 (also known as mitogen-activated kinase kinase kinase 5) proteins which, upon clustering, are in close enough proximity to undergo *trans*-autophosphorylation and become active kinases (Fujino et al., 2007). Once activated, it is proposed that ASK1 phosphorylates and activates MEK4 and, in turn, MEK4 phosphorylates and activates JNK (Ichijo et al., 1997).

It has also been reported that TRAF2 can recruit MAP kinase/ERK kinase kinase 1 (MEKK1) to signalling scaffolds, which situates the MEKK1 proteins in close enough proximity for autophosphorylation to occur (Baud et al., 1999). Once phosphorylated MEKK1 becomes an active kinase capable of instigating JNK signalling via phosphorylation and activation of MAP kinase/ERK kinase 4/7 (MEK4/7) (Weston and Davis, 2002). Therefore, this provides an alternative pathway by which the IRE1α-TRAF2 signalling scaffold could activate JNK, should it be that ASK1-mediated activation of JNK is specific to neurones (Nishitoh et al., 2002).

There has been some dispute as to how JNK mediates cell death once it has been activated during IRE1α signalling. This is largely because JNK is a signalling molecule that is activated as part of a plethora of signalling pathways and can instigate many more (Weston and Davis, 2002, Bogoyevitch and Kobe, 2006). It has been shown that JNK is activated by the dual phosphorylation of a Thr-Pro-Tyr motif by MKK4 (Cuenda, 2000) and MKK7 (Tournier et al., 1997) and, downstream of this activation, it has been reported that JNK modulates a multitude of proteins involved in promoting either cell survival (Molton et al., 2005, Lamb et al., 2003, Svensson et al., 2011, Yu et al., 2004) or apoptosis (Huang et al., 2014, Jung et al., 2014, Zhang et al., 2001, Nishitoh et al., 2002).

Various data have shown that JNK can regulate a wide number for transcriptions factors involved in inflammatory signalling including; c-jun (Ip and Davis, 1998), activating transcription factor 2 (ATF2), ETS domain-containing protein (ELK1) (Yang et al., 1998), p53 (Fuchs et al., 1998), nuclear factor of activated T cells 4 (NFAT4) (Chow et al., 1997), nuclear factor of activated T cells cytoplasmic 1 (NFATc1) (Ortega-Perez et al., 2005),

signal transducer and activator of transcription 3 (STAT3) (Lim and Cao, 1999) and heat shock factor 1 (HSF1) (Park and Liu, 2001), many of which have also been linked with being both pro-survival and promoting cell death. Furthermore, in addition to regulating transcription factors, JNK has been shown to regulate adaptor proteins (Aguirre et al., 2002, Kelkar et al., 2000), ubiquitin ligases (Gallagher et al., 2006), mitochondrial proteins (Deng et al., 2001, Kim et al., 2006) and members of the cytoskeleton (Huang et al., 2003, Chang et al., 2003). Therefore, given the wide range of proteins that JNK modulates, and the seemingly counterintuitive ability to signal for both cell survival and cell death, the task of elucidating the role JNK has to play within ER stress is complex and, thus far, incomplete. However, there is a growing consensus that there are two phases of JNK activation during ER stress. There first, an early and transient anti-apoptotic phase (Brown et al., 2016), and the second, a late pro-apoptotic phase (Nishitoh et al., 2002, Urano et al., 2000b). Thus, JNK signalling can be both pro-survival and pro-apoptotic depending on the stress and its duration.

However, whilst the exact mechanism for JNK mediated apoptosis is yet to be deciphered, the current model IRE1α-JNK-stimulated cell death is based on a pathway whereby JNK activates Bcl-2 interacting mediator of cell death (Bim), a member of the BH3-only subgroup of B cell lymphoma 2 (Bcl2) family of proteins. JNK is proposed to activate Bim via phosphorylation on threonine 56, which has been shown to disrupt the association of Bim with dynein and myosin V motor complexes and to increase apoptosis. This apoptosis is believed to be the result of free Bim protein activating BCL-2-associated X protein (Bax) and/or BCL-2 antagonist or killer (Bak) (Lei and Davis, 2003). Bax and Bak then translocate to mitochondria where they permeabilise the mitochondrial outer membrane and stimulate the release of proteins from the mitochondrial intermembrane space into the cytosol (Antignani and Youle, 2006). The proteins that are released during this process, such as cytochrome *c*, stimulate cell death by promoting the activation of caspases (Zou et al., 1999). These caspases then orchestrate cell death via proteolysis of structural and regulatory proteins within the cell (Parsons and Green, 2010).

1.3.6.2 TRAF2/NF-κB

The NF-κB family of transcription factors has also been reported to be one of the mediators of the inflammatory signalling that is instigated as a consequence of ER stress (Pahl and Baeuerle, 1995). NF-κB signalling is mediated by a family of dimer forming transcription factors that include RelA (p65), p50, p52, RelB, and c-Rel. RelA (p65)/p50 is the most common form in mammalian cells and is usually held inactive in the cytoplasm in a complex with IκBα, which masks the nuclear localisation signal (NLS) of NF-κB. Activation of NF-κB is often the result of phosphorylation of IκBα by IκB kinase (IKK), which results in the poly-ubiquitination and subsequent proteasomal degradation of IκBα (DiDonato et al., 1996). This exposes the NLS of NF-κB, allowing it to translocate to the nucleus and activate transcription of its target genes by binding to consensus κB promoter sites (Gilmore, 2006).

Initially, there was some dispute as to how NF-κB was activated during ER stress, with both PERK and IRE1α being postulated as the ER stress sensor responsible for its activation. The argument for PERK-eIF2α signalling was first proposed as a result of data that showed NF-κB activation in response to treatment with thapsigargin or tunicamycin was reduced in *perk*$^{-/-}$ MEFs or cells that expressed a mutant eIF2α that cannot be phosphorylated (eIF2α^{S51A}) (Jiang et al., 2003). These data were further supported by findings demonstrating that activation of PERK is sufficient for the upregulation of NF-κB signalling. This evidence was provided through the use of Fv2E-PERK, a fusion of the cytoplasmic kinase domain of PERK to an artificial Fv2E domain that can be dimerised via the addition of the chemical AP20187, to investigate the role of PERK in NF-κB activation (Deng et al., 2004). As this dimerisation event results in the activation of Fv2E-PERK in a manner that does not induce ER stress, the authors were confident that any downstream signalling was the direct result of PERK signalling. Using this method *Deng et al.* were able to show that induction of Fv2E-PERK increased NF-κB signalling. Interestingly, it was also found that, whilst NF-κB signalling increased as a result of a reduction of IκBα, the level of phosphorylated IκBα was not increased. This indicated that, unlike in normal models of NF-κB signalling, IκBα protein levels were not decreased as a result of phosphorylation. Instead, pulse chase experiments revealed that IκBα has a shorter half-life than NF-κB, leading the authors to propose that the translational arrest instigated by PERK signalling was responsible for the activation of NF-κB, as it causes a depletion of new IκBα capable of sequestering NF-κB (Deng et al., 2004). This finding supported prior research indicating that UV light treatment induces NF-κB activation via attenuation of

IκBα synthesis (Wu et al., 2004). However, whilst the work of Deng *et al.* provides strong evidence that PERK can instigate NF-κB activation without IRE1α or ATF6 signalling, their work does not support their claim that PERK is sufficient *and* necessary for NF-κB activation because there were no experiments to prove that IRE1α/ATF6 do not cause elevations in NF-κB signalling as well. Therefore, only the former is true, which is important when considering the evidence supporting an IRE1α based model of activation.

The argument that IRE1α is responsible for NF-κB signalling during ER stress was born from evidence showing that NF-κB is induced by thapsigargin and tunicamycin treatments and that this activation was inhibited by both dominant negative IRE1α and dominant negative TRAF2 (Kaneko et al., 2003). This hypothesis was further strengthened by data showing that IKK forms a complex with TRAF2 and IRE1α during ER stress. Furthermore, NF-κB activation was shown to be impaired in IRE1α knockdown cells and *ire1α*$^{-/-}$ MEFs (Hu et al., 2006).

Therefore, with data supporting both PERK and IRE1α being able to induce NF-κB signalling during ER stress it was eventually proposed that both proteins could in fact induce the activation of NF-κB. *Tam et al.* (Tam et al., 2012) were the first group to investigate NF-κB signalling whilst accounting for both PERK and IRE1α and they concluded that PERK is essential for optimal NF-κB activation as the level of PERK induced translational repression is proportional to increase in NF-κB signalling during thapsigargin or DTT-induced ER stress. However, the extent to which PERK can activate NF-κB is regulated by IKK, which in turn appears to be governed by IRE1α (Hu et al., 2006). This theory is supported by the fact that IRE1α and IKKβ expression helped restore NF-κB activation in *ire1α*$^{-/-}$ cells and that this restoration occurs in an IRE1α kinase domain dependent manner. Interestingly, neither JNK nor the endoribonuclease function of IRE1α have been found to influence NF-κB signalling. However, TRAF2 was found to be required for NF-κB activation (Tam et al., 2012). This suggests that IKK activation is instigated via the IRE1α-TRAF2 branch of IRE1α signalling and compliments the theory that IKK interacts directly with the IRE1α-TRAF2 complex (Hu et al., 2006).

Based on the evidence, it is reasonable to assume that NF-κB signalling involves both PERK and IRE1α, which activate NF-κB in two disparate ways. PERK induces the activation of NF-κB target genes by instigating translational repression through the phosphorylation of eIF2α. This causes a depletion of inhibitory IκBα, which has a far shorter half-life than NF-κB, resulting in an increased pool of non-sequestered NF-κB. IRE1α on the other hand, recruits TRAF2 and IKK to a signalling complex which results in

the phosphorylation and activation of IKK. IKK then phosphorylates IκBα, targeting it for polyubiquitination, and subsequent degradation by the proteasome, causing an increase in free NF-κB. Therefore, either PERK or IRE1α can instigate NF-κB signalling during ER stress, but both are required for optimal activation of NF-κB target genes (see Figure 1.7).

The final of result of NF-κB signalling during ER stress is once again unclear because NF-κB, like JNK, has many activators, many targets and can support both prosurvival and proapoptotic outcomes. However, it is currently believed that ER stress induced NF-κB signalling results in the activation of caspase-8 via upregulation of TNFα signalling (Hu et al., 2006).

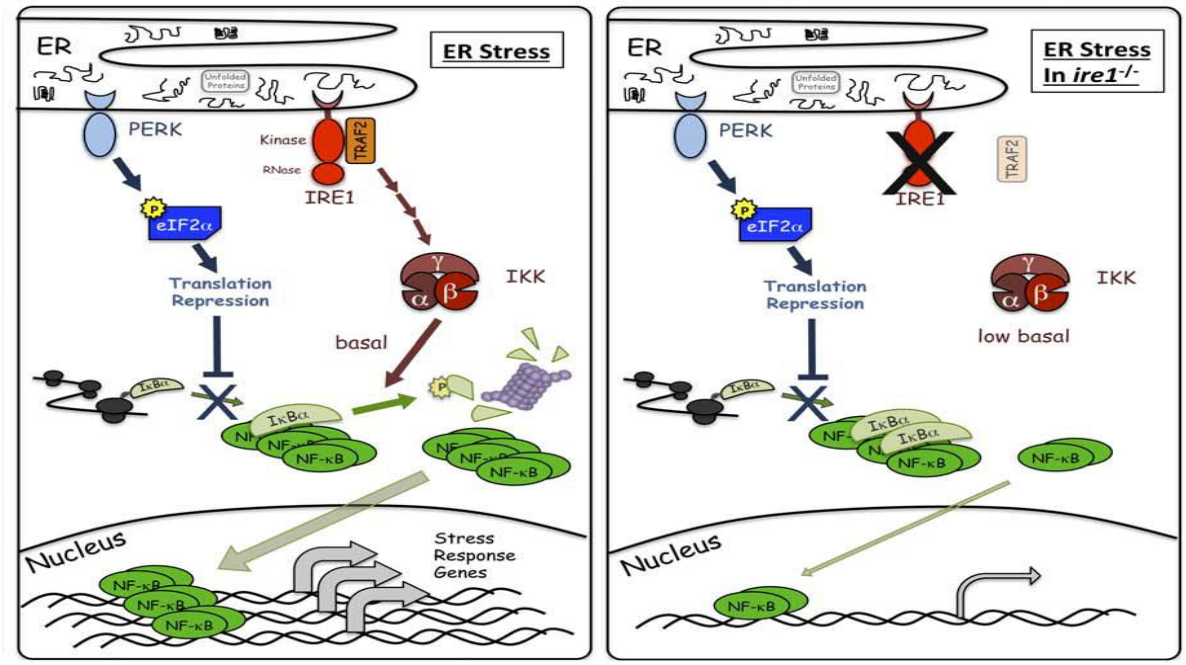

Figure 1.7 – A diagram adapted from (Tam et al., 2012) depicting the contributions of both PERK and IRE1α during ER stress.

1.3.7 The IRE1α signalling scaffold

The IRE1α signalling pathways that have been discussed up until this point are regarded by the majority as the best representation of this branch of the UPR, even if the exact interactions and mechanisms of activation/inhibition are yet to be elucidated. However, in addition to the well-known modulators and downstream targets of IRE1α, many papers report the existence of proteins that are involved in IRE1α signalling, resulting in a plethora of potential mediators of the IRE1α cascade. In most cases these are one off reports from specific cell lines; however, in the interests of exploring all avenues when trying to elucidate how IRE1α mediates cytoprotection and cell death, these findings will be reviewed here.

The B cell lymphoma 2 (Bcl-2) family of proteins are involved in a wide range pathways that regulate cell fate and have already been discussed as likely candidates for mediating cell death downstream of IRE1α. However, there have also been several reports to suggest that members of the Bcl-2 family regulate IRE1α itself (Urra et al., 2013). Bcl-2-associated X protein (BAX) is one member of the Bcl-2 family that has been reported to influence IRE1α. Double knockout of Bax and Bak (another member of the Bcl-2 family) in mice has been shown to result in extensive tissue damage and decreased expression of XBP1 as a result of treatment with tunicamycin. ER-stressed double knock out cells showed deficient IRE1α signalling and, having shown that Bax can be isolated in complex with IRE1α, the authors proposed that BAX forms a complex with the cytosolic domain of IRE1α that is essential for IRE1α activation (Hetz et al., 2006). Building on this theory there is also data to suggest that bifunctional apoptosis regulator (BAR) acts to elevate *XBP1* splicing during ER stress. BAR is an ER-associated RING-type E3 ligase that promotes the proteasomal degradation of Bax-inhibitor 1 (BI-1) (Rong et al., 2011) and in doing so alleviates the inhibition of *XBP1* splicing that is observed when BI-1 is over expressed in fly and mouse models (Lisbona et al., 2009). This would fit in with the work of *Hetz et al.* as the degradation of BI-1 by BAR would relieve BAX form the inhibitory effects of BI-1.

In addition to work studying Bax, BIM and PUMA have been identified as another set of Bcl-2 family members that could be involved in the regulation of IRE1α signalling. In this instance, data showing that BIM/PUMA double knock-out cells fail to maintain *XBP1* mRNA splicing during prolonged ER stress has been used to suggest that they interact with IRE1α to prevent early inactivation (Rodriguez et al., 2012). It seems plausible that the association of proteins such as BIM/PUMA could prevent dissociation of IRE1α

monomers and therefore prolong IRE1α signalling by keeping IRE1α dimers/oligomers together. However, it seems strange to suggest that proapoptotic factors such as BIM and PUMA would do this to promote cell survival through *XBP1* splicing. Instead, it would make more sense that prolonging the ER stress signal would push cells towards apoptosis via prolonged signalling through the IRE1α-TRAF2 branch. Therefore, future efforts assessing this area of IRE1α signalling may benefit from doing so in the context of cell death, rather than protection via *XBP1* splicing.

In addition to Bcl-2 family members, a variety of other proteins that have also been implicated in modulating IRE1α signalling during ER stress. Hsp72 (PC12 cells) (Gupta et al., 2010), mTORC1 (Pfaffenbach et al., 2010) (rat liver explants), and PKA (murine hepatocytes) (Mao et al., 2011), have all be identified as proteins that are required for efficient *XBP1* splicing and upregulation of XBP1 target genes, whilst non-muscle myosin heavy chain IIB (NMIIB) has been reported as a protein required for successful IRE1α-*XBP1* signalling in mammalian and *C. elegans* cells. However, the role of NMIIB is slightly different to the aforementioned proteins as the authors believe it is required mechanistically for the aggregation of IRE1α rather than activating it through direct binding or altering its phosphorylation status (He et al., 2012).

Proposed protagonists of the IRE1α signalling pathway have not been limited to proteins that affect upregulation or inhibition of IRE1α signalling, as shown by the fact that there are also reports of non-canonical downstream targets as well. An example of this can be found in interleukin-1 receptor associated kinase 2 (IRAK2), which has been identified as a protein that is regulated by IRE1α and which may also influence IRE1α signalling in a positive feedback loop-type mechanism. The authors found that IRAK2 is induced during ER stress in an IRE1α-XBP1 dependent manner. In addition to this, IRAK2 shRNA knock down in PPCI (cancer) cells blunted *XBP1* splicing and JNK phosphorylation suggesting a possible positive feedback loop between IRAK2 and IRE1α (Benosman et al., 2013). Another protein that has being identified as a potential target of IRE1α signalling is Nck. The authors propose a model whereby activation of IRE1α results in a conformational change of IRE1α cytosolic domains that leads to the release of IRE1α bound non-catalytic region of tyrosine kinase adaptor protein (Nck) and subsequent activation of mitogen-activated protein kinase 3 (MAPK3) (Nguyen et al., 2004).

Continuing on the theme of MAPK signalling cascades, other papers have focused on proteins that may interact with IRE1α to modulate its activation of JNK, which is perhaps unsurprising as JNK is widely regarded to be the main instigator of IRE1α-mediated cell

death (Urano et al., 2000b). The first of the papers reporting on modulators of the IRE1α-JNK signalling pathway builds on the idea presented by *Nishitoh et al.* that ASK1 plays an essential role in the stimulation of JNK signalling during ER stress (Nishitoh et al., 2002). Here, the authors propose that the aptly named ASK1 interacting protein 1 (AIP1) also binds to the IRE1α-TRAF2 signalling scaffold (Luo et al., 2008). The evidence supporting the involvement of AIP1 is that *aip1*$^{-/-}$ MEF cells and mice show dramatic reductions in ER stress-induced JNK activation and cell apoptosis. Furthermore, JNK signalling and cell death can be partly restored in these models via reconstitution of WT AIP1. Furthermore, ER stress was shown to induce the formation of an AIP1-IRE1α complex via the pleckstrin homology (PH) domain of AIP1. Therefore, evidence of direct interaction, combined with the fact that AIP1 knockout specifically blunts the IRE1α-JNK, but not the PERK-CHOP, axis of ER stress signalling, suggests that AIP1 may be an essential component of the IRE1α apoptotic signalling pathway (Luo et al., 2008). Another protein that has been proposed to join the IRE1α signalling cascade in order to instigate JNK signalling is tumour necrosis factor receptor 1 (TNFR1). In this paper it was shown that TNFR1 interacts with IRE1α in a TRAF2 independent manner during ER stress and that this interaction was essential for JNK signalling. This was evidenced by the fact that *tnfr1*$^{-/-}$ MEFs are defective in ER stress induced JNK signalling, but this effect could be reversed via reconstitution of TNFR1 expression. The activation of JNK by IRE1α over-expression was also abolished in *tnfr1*$^{-/-}$ cells. These data provide fairly strong evidence to support the involvement of TNFR1 in mediating IRE1α-JNK signalling during ER stress, although the role of TNFR1 remains a mystery because inhibition of TNF binding to TNRF1 did not abolish ER stress mediated JNK elevations (Yang et al., 2006b).

Finally, JNK inhibitory kinase (JIK) has been suggested to influence the activation of JNK during IRE1α-TRAF2 signalling, although bizarrely the authors argue that this inhibitory kinase is required for JNK activation (Yoneda et al., 2001). The evidence for the involvement of JIK, presented by the authors, is that JIK was found to be associated with both IRE1α and TRAF2 in a two-hybrid system and was shown to directly impact upon JNK signalling through both overexpression, which elevated JNK signalling, and the use of a catalytically inactive JIK mutant, which inhibited JNK signalling. In addition to this, phosphorylated TRAF2 was seen to increase along with phosphorylated JNK when JIK was overexpressed (Yoneda et al., 2001). Overall these data seem incongruous to other research that suggests that JIK inhibits, rather than instigates, JNK signalling (Tassi et al., 1999). However, the possibility that TRAF2 requires phosphorylation in order to transduce

ER stress signalling is one that is important when discussing the results obtained using the Fv2e-IRE1α system (Chapter 5).

The wide variety of proteins that have been shown to precipitate with, and modulate, the action of IRE1α have made the idea of a IRE1α-TRAF2 signalling scaffold or 'UPRosome' gain significant popularity in recent years (Woehlbier and Hetz, 2011) and, the fact that the proteins involved seem to vary in a cell line-dependent manner, suggests that the components of the UPRosome are tissue specific. However, TRAF2 is a consistent presence, and would seem to be the anchor of the scaffold, whilst the initiation of apoptosis via JNK and NF-κB inflammatory signalling is widely considered to be the end goal of IRE1α kinase domain signalling during prolonged ER stress. However, the proteins and mechanisms involved during the intermediary steps remain elusive (Hetz and Glimcher, 2009) and identifying them is difficult given the apparently tissue-specific nature of IRE1α signalling and cross-talk between various stress signalling pathways. Therefore, a model that could isolate IRE1α signalling in various cell types, and allow characterisation of the proteins that interact with it, would be particularly useful and this is the target of the research reported in this thesis.

1.4 Current Models for Studying the UPR

1.4.1 Chemical inducers of ER stress

In order to study the unfolded protein response, research groups use a variety of chemical agents to perturb ER homeostasis and induce ER stress. These 'ER stress mimetic drugs' include thapsigargin, tunicamycin, subtilase cytotoxin, dithiothreitol, brefeldin A and bortezomib. Thapsigargin (Tg) exerts its effects by inhibiting the action of sarco/endoplasmic reticulum Ca^{2+} ATPase (SERCA) pumps in the ER membrane (Thastrup et al., 1990) , preventing them from pumping calcium from the cytosol into the ER lumen. This depletes the ER of Ca^{2+}, which is required for the function of many ER chaperones and therefore rapidly induces the formation of misfolded protein aggregates. Tunicamycin (Tm) promotes ER stress by blocking the *N*-linked glycosylation of newly translated proteins via the inhibition of GlcNAc phosphotransferase (GPT) (Stevens et al., 1982) and, therefore, tunicamycin treatment also induces the rapid accumulation of misfolded protein species within the ER (Kaufman, 1999). Subtilase cytotoxin (SubAB) is an AB_5 toxin produced by Shiga toxigenic *Escherichia coli* bacteria (Fan et al., 2000). It selectively degrades BiP which (Paton et al., 2006), as discussed in section 1.3.3.2, is an essential ER chaperone and also has a role in modulating the activity of IRE1α, PERK and

ATF6. Therefore, treatment with SubAB causes the accumulation of protein aggregates and the activation of the ER stress sensors which, at least in part, use BiP depletion as an indicator of ER stress (Wolfson et al., 2008). Dithiothreitol (DTT) is a small-molecule reducing reagent that is used to reduce the disulphide bonds that hold proteins together and also to prevent the formation of any prospective disulphide bonds. Therefore, DTT is another chemical agent that increases the concentration of unfolded protein within the ER. Brefeldin A instigates ER stress indirectly by inhibiting the formation of COPI-mediated transport vessels and therefore prevents the transport of proteins from the ER to the Golgi. Finally, bortezomib is a drug that acts as a proteasome inhibitor, preventing the degradation of misfolded proteins, which increases their concentration within the ER and thus instigates ER stress (Hill et al., 2009).

All of the methods described above are capable of inducing ER stress and are therefore useful in studying the UPR. However, they also possess fairly broad modes of action and thus provide a fairly crude way of investigating UPR signalling pathways. One of the major issues with studying stress signalling pathways is that there is a lot of cross-talk and drugs that affect calcium homeostasis, proteasome function and vesicular transport are going to cause global problems within the cell and trigger a multitude of stress signalling pathways. Therefore, whilst it is possible to confirm that drugs such as thapsigargin and brefeldin A activate the UPR, when trying to determine if downstream targets such as JNK or NF-κB are activated by ER stress or other, off-target, stress signalling cascades, the picture becomes far more difficult to elucidate. Even using drugs such as SubAB, which specifically target the ER, can be viewed as too general when trying to elucidate the intricacies of UPR signalling because there are three ER stress sensors in higher eukaryotes, all of which can signal for either protection or apoptosis (as discussed in section 1.2). This is a particularly pertinent issue when trying to find therapeutic strategies to deal with diseases such as cancer or type 2 diabetes that require the selection of either apoptotic or protective UPR signalling, rather than just switching the UPR on or off. Therefore, whilst generic ER stress mimetic drugs serve to provide a broad picture of how the UPR works, experimental systems that allow the specific activation of individual branches of the UPR are required to provide the meticulous detail that is needed to fine tune the UPR into a tool for combating disease.

1.4.2 The Fv2E system

The Fv2E system used during this project differs from ER stress mimetic drugs because it allows the specific activation of IRE1α without the induction of ER stress. This is achieved by the fusion of the cytoplasmic effector domain of IRE1α with a polypeptide containing two FK506 binding domains (Fv2E). The result is a soluble, cytoplasmic Fv2E-IRE1α protein that can be dimerised via the addition of a synthetic small organic molecule, AP20187. The Fv2E domain has a high affinity for AP20187 and, as each Fv2E monomer contains two FK506 domains, Fv2E acts as a bivalent ligand that can be engaged by two additional Fv2E domains, allowing dimerisation/oligomerisation. Therefore, AP20187 allows activation of IRE1α that is entirely independent of ER stress, which gives the system a powerful advantage over ER stress mimetic drugs (Lu et al., 2004a) (Spencer et al., 1993). The Fv2E system has been used successfully to study PERK signalling (Deng et al., 2004), however, its application when studying IRE1α has, thus far, been limited to one paper. This paper reported the use of an IRE1α-FK506 fusion protein (F_v-IREN-HA) to investigate if dimerisation of IRE1α was sufficient for *XBP1* splicing in the absence of ER stress (Back et al., 2006). However, the authors observed no significant increase in spliced *XBP1* when cells expressing F_v-IREN-HA were treated with AP20187. Therefore, the 2-fold increase in *XBP1* splicing that occurred in cells transfected with F_v-IREN-HA is more likely to have been the result of splicing carried out by endogenous IRE1α in response to ER stress caused by the over expression of F_v-IREN-HA protein, rather than dimerisation caused by AP20187. As such, the main focus of this project has been to produce a system that can specifically activate IRE1α, through use of AP20187, in order to elucidate the mechanisms by which it controls cell fate without cross-talk from the other pathways that are normally activated during ER-stress.

1.4.3 Mutational analysis

Point mutations can be useful for assessing the contribution of individual motifs to the function of a protein within a signalling cascade, potentially providing the kind of in-depth understanding required to design therapeutic drugs that are able to exert influence over specific members of these pathways. As a result of this, there have been a vast number of IRE1α, PERK and ATF6 mutants created whilst attempting to elucidate the nuances of the UPR. Therefore, this section will only deal with the IRE1α mutants that have been used in this study.

The point mutants used during this study target either the kinase domain or the endoribonuclease domain of IRE1α. However, in order to comprehend the effects of these mutations it is first important to understand the mechanics by which these domains function in the wild-type protein. Protein kinases carry out the transfer of a phosphate group from an ATP molecule to a tyrosine or serine/threonine residue on the protein that is being targeted by the kinase domain. This process usually requires the presence of a divalent metal ion, such as Mg^{2+} and, except in rare circumstances, protein kinases will be specific for either tyrosine or serine/threonine residues. Kinase domains are present in 2% of eukaryotic genes and consist of several highly conserved motifs within a 200-250 amino acid core. Therefore, the process by which kinases are able to catalyse the transfer of the γ-phosphate of ATP to their target protein(s) is well understood, allowing the manipulation of this process via point mutations. IRE1α is a serine/threonine kinase and kinase activity is instigated by the transfer of a phosphate group from ATP to serine residues on the activation loop of the IRE1α kinase domain. This causes a conformational change whereby the activation loop folds into connection with positively charged residues within the RD pocket. The active IRE1α kinase is then able to recognise phosphorylatable residues on target proteins via conserved motifs around the activation site. Therefore, by altering amino acids within the core 200-250 of the kinase domain, it has been possible to create a series of mutants that lack kinase activity. These mutants are outline below.

1.4.3.1 D711A

The kinase domain of human IRE1α relies on a conserved Asp-Phe-Gly motif for the function of its magnesium binding loop, which in turn is required to mediate the chelation of a magnesium ion. Mg^{2+} chelation is essential in order to position the phosphates of ATP correctly for cleavage to occur (Hubbard et al., 1998) and mutating residues within the Asp-Phe-Gly motif have been shown to reduce kinase activity to 4% in yeast (Mori et al., 1993). However, whilst the transfer of phosphates is almost entirely abolished, nucleotide binding assays suggest that nucleotide binding can still occur and this means that endoribonuclease activity is still possible (Chawla et al., 2011). Therefore, mutations in the magnesium binding loop are useful because they can create kinase inactive, endoribonuclease active IRE1 mutants (Chawla et al., 2011). This is exhibited by the $IRE1\alpha^{D711A}$ mutant, which has its conserved DFG motif disrupted by substituting aspartate 711 with alanine but, despite this, is still capable of restoring ~60% of *XBP1* splicing activity in $ire1\alpha^{-/-}$ MEFs (Sutcliffe, 2012).

1.4.3.2 I642G

Another residue that has been used to study the function of IRE1α is isoleucine 642, which exists as part of the β5 sheet that forms the domain that accepts the adenine of ATP (Bishop et al., 2000). Replacing this isoleucine with glycine enlarges the ATP binding pocket, significantly reducing the affinity of $Ire1^{I642G}$ for ATP, creating a kinase and endoribonuclease impaired mutant. However, enlarged analogues of ATP such as 1NM-PP1 are capable of binding to this modified pocket and, whilst they do not restore kinase activity (as there are no phosphates that can be transferred), their binding is sufficient to restore endoribonuclease activity (Papa et al., 2003). This was used to great effect in *Papa et al.* (Papa et al., 2003), who used this as evidence to show that nucleotide binding is responsible for the conformational change that imbues Ire1p with endoribonuclease activity, as opposed to the phosphorylation event that follows ATP binding in wild type Ire1p. Therefore, this mutant has the potential to provide insight into IRE1α function because, being 'analogue sensitive', it allows endoribonuclease activity to be switched on and off. However, it must be noted that whilst 1NM-PP1 treatment has been shown to restore endoribonuclease in yeast, it failed to do so in MEFs (Sutcliffe, 2012).

1.4.3.3 K599A/K599R

$IRE1\alpha^{K599A}$ is a mutant that sees the positively charged amino acid lysine 599 substituted with a neutral alanine. In wild-type IRE1α, lysine 599 resides in the β3 helix of the kinase domain and is believed to orientate the α and β phosphates of the ATP molecule, thus having an important role in mediating phosphotransfer. Disruption of this residue by switching it to an uncharged alanine is believed to produce a kinase and endoribonuclease deficient IRE1α protein (Iwawaki et al., 2001). Indeed, unlike the D711A mutant, expression of K599A in *ire1α*$^{-/-}$ MEFs fails to restore *XBP1* splicing (Zhou et al., 2006). Another mutation centred around lysine 599 is the $IRE1^{K599R}$ mutant, which conserves the positive charge of lysine by substitution with arginine. In yeast this has been reported to reduce both endoribonuclease and kinase activity without instigating complete loss of function (Mori et al., 1993) (Shamu and Walter, 1996).

1.4.3.4 K907A

Lysine 907 is located in the RNase domain of IRE1α and when this lysine is replaced by an alanine, IRE1α is no longer able to cleave *XBP1* mRNA. However, whilst the IRE1α^{K907A} mutant lacks endoribonuclease activity, it has been shown that IRE1α^{K907A} is capable of phosphorylating the kinase deficient IRE1α^{K599A}, suggesting that the K907A mutation leaves kinase function intact. This makes the K907A mutant useful, as it provides an IRE1α protein that retains kinase activity, whilst lacking endoribonuclease activity (Tirasophon et al., 2000).

1.5 Aims and objectives

1) Prior work has reported that signalling via the IRE1α-JNK pathway is initiated by an upstream interaction between IRE1α and TRAF2 (Urano et al., 2000b, Brown et al., 2016). However, it is yet to be determined if this interaction is direct or whether it requires bridging proteins. Therefore, the first aim of this thesis will be to determine if the interaction between IRE1α and TRAF2 is direct or indirect. This will be achieved via the use of co-immunoprecipitation assays between TRAF2 and the cytosolic portion of IRE1α, which have both been transcribed and translated *in vitro*, in order to elucidate if a direct interaction can be isolated.

2) Whilst it is agreed that IRE1α mediates cell fate decisions via interaction with TRAF2 (Urano et al., 2000b, Brown et al., 2016), little is known about the mechanism by which this occurs. This is likely to be because it is difficult to study the impact of a single protein when most models used to study ER stress involve drugs that initiate multiple signalling cascades (Thastrup et al., 1990, Stevens et al., 1982). Therefore, the final aim of this thesis is to produce a model whereby IRE1α signalling can be characterised in isolation so that a greater understanding of the mechanism by which it interacts with TRAF2, and subsequently induces JNK signalling, can be obtained. Furthermore, the final results chapter will also attempt to enhance our understanding of the mechanism by which human IRE1α splices *XBP1* mRNA, as most of our knowledge on this topic has been obtained in yeast (Lee et al., 2008a). These goals will be achieved via the use of cells that express a chemically inducible IRE1α chimera, the downstream targets of which will be analysed via co-immunoprecipitation and Western blotting. SiRNA knockdown of TRAF2 and cell lines expressing IRE1α mutants will then be used to gather further information regarding the mechanisms by which IRE1α signals through both its kinase and RNase domains.

2 Materials

2.1 Chemicals and Solutions

2.1.1 De-ionised/MilliQ/Sterile Water

Unless stated otherwise, water was produced by a MilliQ water purifier. The de-ionised water from this machine had a resistivity of less than 18 Ω-cm; total organic content of less than 10 parts per billion; less than 10 bacterial colony forming units/ml; and less than 0.03 endotoxin/ml.

2.2 Solutions for DNA Work

Table 2.1 - Solutions for DNA work

Solution	Supplier	Product Number
6x DNA loading dye	Thermo Scientific, Paisley, PA4 9RF	R0611
GeneRuler DNA Ladder	Thermo Scientific, Paisley, PA4 9RF	SM0331

2.3 Solutions for RNA Work

All equipment used for RNA work was either baked to remove RNases or purchased clean.

Table 2.2 - Reagents for RNA work

Solution	Supplier	Product Number
1 kbp DNA Ladder	Promega, Southampton, SO16 7NS	G5711
5 x First Strand Buffer	Invitrogen, Paisley, PA4 9RF	Y02321
5 x Green GoTaq Flexi Buffer	Promega, Southampton, SO16 7NS	M5001
Oligo(dT)15	Promega, Southampton, SO16 7NS	C110A

Table 2.3 - Solutions for RNA work

Solution	Composition
2 mM RNase-free dNTPs in 1 mM Tris-HCl (pH 8.0)	910 µl H_2O 10 µl 100 mM Tris·HCl (pH 8.0) 20 µl 100 mM dATP 20 µl 100 mM dCTP 20 µl 100 mM dGTP 20 µl 100 mM dTTP
6 x RNA sample loading buffer	63 g glycerol 250 mg bromophenol blue 10 ml 100mM Na_3PO_4 (pH 7.0) Add DEPC-H_2O to 100ml Add 100 µl DEPC treated H_2O
Diethylpyrocarbonate (DEPC)-H_2O	1 ml DEPC per 1 l of H_2O.

2.4 Solutions for Protein Work

Table 2.4 - Reagents for Protein work

Reagent	Supplier	Product Number
[35S] Methionine (1,000Ci/mmol at 10mCi/ml)	Hartmann Analytic, Braunschweig, Germany	ARS-0104A
[γ-32P]ATP (3,000Ci/mmol at 10mCi/ml)	Hartmann Analytic, Braunschweig, Germany	SRP-301
20 x MOPS Running Buffer	Invitrogen, Paisley, PA4 9RF	NP0001
Complete Mini Protease Inhibitor cocktail Tablets	Roche, Hertfordshire, AL7 1TW	11836153001
Decon	Decon Laboratories Ltd., Hove BN3 3LY	00188082
PageRuler Prestained Protein Ladder	Thermo Scientific, Paisley, PA4 9RF	26619
PhosSTOP	Roche, Hertfordshire, AL7 1TW	04906845001
Protein A-Agarose Beads	Santa Cruz Biotechnology, Heidelberg, Germany	sc-2001

S-protein Agarose	Novagen, Hertfordshire WD18 8YH	69704
Western Blot Stripping Buffer	Thermo Scientific, Paisley, PA4 9RF	21059

Table 2.5 - Solutions for protein work

Solution	Composition
6 x SDS-PAGE Sample Buffer	Per 10 ml H_2O: 3.5 ml 1M tris·HCl 3.78 g glycerol 1 g SDS 500 µl 10 g/l bromophenol blue 200 µl β-mercaptoethanol
High salt buffer	800 mM KCl 20 mM HEPES (pH 7.9) 1.5 mM $MgCl_2$ 0.5 mM DTT 0.2 mM EDTA 25% glycerol (v/v) 1% NP-40 (w/v)
IP-Buffer	150 mM NaCl 50 mM Tris pH (7.5) 1 mM EDTA 0.1% (w/v) NP-40 0.05% (w/v) SDS
Low Salt Buffer	20 mM HEPES (pH 7.9) 1.5 mM $MgCl_2$ 20 mM KCl 0.5 mM DTT 0.2 mM EDTA 25% glycerol (v/v)

RIPA Buffer	50 mM Tris·HCl, pH 8.0 150 mM NaCl 1% (v/v) Triton X-100 0.5% (w/v) sodium deoxycholate 0.1% (w/v) SDS
Sucrose Buffer	0.32 M Sucrose 10 mM Tris HCl pH 8.0 3 mM $CaCl_2$ 2 mM MgOAc 1 mM DTT 0.1 mM EDTA 0.5% (w/v) NP-40

2.5 Tissue Culture

All chemicals used for cell culture were filter-sterilised and only opened under sterile conditions in a laminar flow cabinet that had been cleaned with 70% (v/v) ethanol. Filter sterilisation was carried out using a 0.2 μm sterile filter and syringe.

Table 2.6 - Reagents for tissue culture

Name	Supplier	Product Number
0.25% Trypsin-EDTA	Sigma-Aldrich, Gillingham, SP8 4XT	T4049-100ML
200 mM L-glutamine	Sigma-Aldrich, Gillingham, SP8 4XT	G7513
AP20187 (B/B homodimerizer) 0.5mM	Clontech, Saint-Germain-en-Laye, France	635060
Blasticidin S hydrochloride	Melford, Ipswich, IP7 7LE	B1105
DMEM (high glucose without L-glutamine and without sodium pyruvate)	Biosera, Uckfield, TN22 1QQ	LM-D1108/500
DMEM (high glucose, no glutamine, no phenol red)	Life Technologies, Paisley, PA4 9RF	31053-028
DMSO	Sigma-Aldrich, Gillingham, SP8 4XT	D5879-100ML
Dulbecco's phosphate buffered saline (PBS)	Biosera, Uckfield, TN22 1QQ	LM-S2041-1000
Fetal bovine serum (FBS)	Biosera, Uckfield, TN22 1QQ	FB-1090/500
Fetal bovine serum (Tetracycline free)	Biosera, Uckfield, TN22 1QQ	FB-1275T/500
Hygromycin B, *Streptomyces* sp.	Millipore, Watford, WD18 8YH	400042

INTERFERin®	Polyplus Transfection, Illkirch-Graffenstaden, France	409-10
MTT (3-[4,5-dimethylthiazol-2-yl]-2,5-diphenyltetrazolium bromide; thiazolyl blue)	Sigma-Aldrich, Gillingham, SP8 4XT	M5655
Nonidet P-40	Fluka, Gillingham, SP8 4XT	74385
Precept disinfection tablets	Medisave, Weymouth, Dorset, DT3 5FA	PSW50
SP600125	Enzo Life Sciences, Exeter, EX2 4DG	BML-EI305-0010
Tetracycline	Sigma-Aldrich, Gillingham, SP8 4XT	T7660
Thapsigargin	Calbiochem, Watford, WD18 8YH	586005-1MG
Trypan blue solution 0.4% (w/v)	Sigma-Aldrich, Gillingham, SP8 4XT	T8154
Tunicamycin	Calbiochem, Watford, WD18 8YH	645380

Table 2.7 - Solutions for tissue culture

Solution	Composition
0.5 mg/ml MTT (3-[4,5-dimethylthiazol-2-yl]-2,5-diphenyltetrazolium bromide; thiazolyl blue)	Per 1 ml H_2O: 0.5 mg MTT
10 mg/ml tunicamycin (stock solution)	10 mg tunicamycin dissolved in 1 ml DMSO (used at 0.1-2.0 μg/ml)
100 mM thapsigargin (stock solution)	1 mg thapsigargin, dissolved in 1 ml of DMSO and then diluted into 15 ml DMSO (used at 500 nM-1 μM)
20 mM SP600125 (stock solution)	4.4 mg SP600125 dissolved in 1ml DMSO
Precept	2 x 5g precept tablets (purchased from Advanced Sterilisation Products) dissolved in 500ml H_2O

2.6 Enzymes

Table 2.8 - Enzymes

Name	Supplier
200U/µl Superscript III reverse transcriptase	Purchased from Invitrogen (#1000782)
5U/µl GoTaq HotStart Polymerase	Purchased from Promega (#M5001)
T4 DNA ligase	Purchased from Promega (#C1263A)

2.7 Oligonucleotides

Table 2.9 - Oligodeoxynucleotide primers

Code	Purpose	Sequence
H8289	Human *XBP1* Forward	GAGTTAAGACAGCGCTTGGG
H8290	Human *XBP1* Reverse	ACTGGGTCCAAGTTGTCCAG

Table 2.10 - siRNA oligonucleotides

Species	Gene	Sequence (sense strand)
H. sapiens	*TRAF2*	CACUCAGAGUGGGAGCACAdTdT

2.8 Plasmids

Table 2.11 - Plasmids

Name	Source
pcDNA5/FRT/TO-Fv2E-C'IRE1α	Dr. David Cox & Dr. Martin Schröder, Durham University
pcDNA5/FRT/TO-Fv2E-D711A,I642G-C'IRE1α	Dr. David Cox & Dr. Martin Schröder, Durham University
pcDNA5/FRT/TO-Fv2E-D711A-C'IRE1α	Dr. David Cox & Dr. Martin Schröder, Durham University
pcDNA5/FRT/TO-Fv2E-K599A-C'IRE1α	Dr. David Cox & Dr. Martin Schröder, Durham University
pcDNA5/FRT/TO-Fv2E-K599R-C'IRE1α	Dr. David Cox & Dr. Martin Schröder, Durham University
pCITE4a(+)-IRE1α^{496}-his	Dr. David Cox & Dr. Martin Schröder, Durham University
pCITE4a(+)-IRE1α^{555}-his	Dr. David Cox & Dr. Martin Schröder, Durham University
pCITE4a(+)-S-tag-TRAF2	Dr. David Cox & Dr. Martin Schröder, Durham University

2.9 Antibodies

Table 2.12 - Antibodies for Western blotting and co-immunoprecipitation

Name	Type	Host	Supplier	Catalogue Number	Batch Number
Anti-tubulin	Primary	Rat	Abcam, Cambridge, CB4 0FL	Ab6160	Unknown
Anti-HA	Primary	Rabbit	Sigma-Aldrich, Gillingham, SP8 4XT	H6908	015M4868V
eIF2α	Primary	Rabbit	Santa Cruz Biotechnology , Heidelberg, Germany	sc-11386	G1309
GAPDH	Primary	Mouse	Sigma-Aldrich, Gillingham, SP8 4XT	G8795	092M4820V
Goat anti-rabbit IgG-Dy-Light 488	Secondary	Goat	Santa Cruz Biotechnology , Heidelberg, Germany	sc-2028	B2607
Goat anti-rat IgG H&L (HRP)	Secondary	Goat	Abcam, Cambridge, CB4 0FL	Ab97057	Unknown
His-tag (rabbit polyclonal)	Primary	Rabbit	Cell signalling, Leiden, The Netherlands	2365X	2
Horse anti-mouse IgG Dy-Light 594	Secondary	Horse	Vectorlabs, Peterborough, PE2 6XS	DI-2594-1.5	Unknown
IRE1α	Primary	Rabbit	Cell signalling, Leiden, The Netherlands	3294S	7
Lamin A (Jol4)	Primary	Mouse	Professor Chris Hutchinson, Durham University, DH1 3LE	N/A	Unknown

Mouse IgG	Primary	Mouse	Santa Cruz Biotechnology , Heidelberg, Germany	D1712	Unknown
PARP	Primary	Rabbit	Cell signalling, Leiden, The Netherlands	9542S	17
Phospho-eIF2α (Ser51)	Primary	Rabbit	Cell signalling, Leiden, The Netherlands	9721S	10
Phospho-IRE1α (pS724)	Primary	Rabbit	Epitomics, Cambridge, CB4 0FL	3881-1	Y1010408
Phospho-SAPK/JNK (Thr183/Tyr185)	Primary	Rabbit	Cell signalling, Leiden, The Netherlands	4668S	9
SAPK/JNK Rabbit mAb	Primary	Rabbit	Cell signalling, Leiden, The Netherlands	9258	9
TRAF2 (F-2)	Primary	Mouse	Santa Cruz Biotechnology , Heidelberg, Germany	Sc-136999	H0709

2.10 Chemically Competent *Escherichia coli* Cells

Table 2.13 - Chemically competent *E. coli* cells

Name	Source
XL10-GOLD (Tet^R Δ(mcrA)183 Δ(mcrCB-hsdSMR-mrr)173 endA1 supE44 thi-1 recA1 gyrA96 relA1 lac Hte [F' proAB $lacI^qZ\Delta M15$ Tn10(Tet^R) Amy Cam^R])	Dr. Martin Schröder, Durham University

2.11 Cell Lines

All cell lines were cryopreserved in 90% FBS, 10% DMSO.

Table 2.14 - Cell lines

Cell Line	Source/Reference	Culture Medium
3T3-F442A	Professor Chris Hutchinson, Durham University	DMEM, 10% FBS, 2 mM L-glutamine
Flp-In T-REx HEK293 Cells	Life Technologies	DMEM, 10% FBS, 2 mM L-glutamine +100 µg/ml zeocin + 15 µg/ml blasticidin
Flp-In T-REx HEK293 with Fv2E-IRE1α (D711A) stably integrated	Dr. David Cox, Durham University	DMEM, 10% FBS, 2 mM L-glutamine + 15 µg/ml blasticidin + 100 µg/ml hygromycin B
Flp-In T-REx HEK293 with Fv2E-IRE1α (D711A/I642G) stably integrated	Dr. David Cox, Durham University	DMEM, 10% FBS, 2 mM L-glutamine + 15 µg/ml blasticidin + 100 µg/ml hygromycin B
Flp-In T-REx HEK293 with Fv2E-IRE1α (K599A)stably integrated	Dr. David Cox, Durham University	DMEM, 10% FBS, 2 mM L-glutamine + 15 µg/ml blasticidin + 100 µg/ml hygromycin B
Flp-In T-REx HEK293 with Fv2E-IRE1α (K599R) stably integrated	Dr. David Cox, Durham University	DMEM, 10% FBS, 2 mM L-glutamine + 15 µg/ml blasticidin + 100 µg/ml hygromycin B
MEF (WT) ire1α$^{-/-}$ rescued with IRE1α flag tagged	Dr David Ron, University of Cambridge	DMEM high glucose, 10%FBS, 2 mM L-glutamine

2.12 Commercially Available Kits

Table 2.15 - Commercially Available Kits

Name	Source	Product Code
DC Protein Assay Reagents Package	Bio-Rad	500-0116
EZ-RNA Total RNA Isolation Kit	Biological industries	20-400-100
First Strand cDNA Synthesis Kit	Invitrogen	11904-018
GenElute™ Gel Extraction Kit	Sigma-Aldrich	NA1111-1KT
GenElute™ HP Plasmid Midiprep Kit	Sigma-Aldrich	NA0200-1KT
GenElute™ PCR Clean-Up	Sigma-Aldrich	NA1020
Gel Shift Assay System	Promega	E3300
JetPRIME® DNA Transfection Kit	Polyplus Transfection	114-15
MagZ™ Protein Purification System	Promega	V8830
Pierce ECL Plus (ECL2) Western Blotting Substrate	Thermoscientific	32132
Pierce ECL Western Blotting Substrate	Thermoscientific	32109
TnT® Quick Coupled Transcription/Translation Systems	Promega	L1170

2.13 Sterilisation of equipment

Solutions and glassware were autoclaved at 121°C for 20 min and 1 atmosphere. Tissue culture waste was autoclaved as 121°C for 50 min and 1 atmosphere before being disposed of.

3 Methods

3.1 Bacterial Culture

All work with *E. coli* was carried out beneath a Bunsen burner flame on a bench that had been sterilised with 70% (v/v) ethanol. The orifices of any tubes, flasks or bottles that were opened during bacterial culture were flamed using the Bunsen burner before and after use.

3.1.1 Making LB-Broth

Lennox LB-broth was dissolved at 20 g/l in de-ionised H_2O using a magnetic stirrer before being autoclaved to sterilise. If necessary, antibiotics were added under the flame of a Bunsen burner once the medium had cooled.

3.1.2 Making LB-Agar Plates

Lennox LB-agar was dissolved at 35 g/l in de-ionised H_2O and mixed using a magnetic stirrer before being autoclaved to sterilise. After sterilisation ~20 ml of agar was poured into as many Petri dishes as required. If the addition of antibiotics was necessary they were added before pouring, once the agar had cooled below 40^{o}C.

3.1.3 Storage of *E. coli* Stocks

1 ml of *E. coli* culture (see 3.1.5 for details of how E. coli cultures were produced) was gently mixed with 1 ml of 30% (v/v) glycerol before being flash-frozen in liquid nitrogen and stored at −80 ^{o}C.

3.1.4 Revival of frozen *E. coli* Cultures

A portion of the frozen cell suspension (~10-20 μl) was removed using a sterile pipette tip and transferred onto an LB-agar plate that contained the appropriate concentration of antibiotics to select for the desired bacterial colonies. Upon melting the stock solution was streaked across the plate using a flamed inoculation loop and incubated at 37 ^{o}C overnight.

3.1.5 Growth of *E. coli* Cultures

4 ml LB-broth containing the appropriate concentration of antibiotics to select for the desired bacteria were inoculated with cells from a single *E. coli* colony. The *E. coli* were incubated at 37 ^{o}C with shaking at 225 – 250 rpm overnight. The cells were collected by centrifugation at 12,000 g for 1 min at room temperature and washed three times with 1 ml of LB-broth. The pellets were resuspended in LB broth and diluted 1:100 into LB-broth containing the appropriate concentration of antibiotics. Cultures were incubated at 37 ^{o}C with shaking at 225 – 250 rpm overnight.

3.1.6 Production of Frozen *E. coli* Stocks

1 ml of 30% (v/v) glycerol was mixed with 1 ml of a fresh overnight culture (see 3.1.5 for details of how E. coli cultures were produced) in a 2 ml cryovial and flash-frozen in liquid nitrogen before storage at −80 °C.

3.1.7 Chemical transformation of *E. coli* (Chung et al., 1989)

Controls: For each transformation made, there was a negative and a positive control. In the negative control, cells were mock-transformed with 5 µl of 1x TE buffer (pH 8.0). In the positive control cells were transformed with a plasmid which has been previously tested and whose transformation efficiency was known.

XL10-Gold competent *E. coli* cells were placed on ice and allowed to thaw. Whilst the cells were thawing, up to 5µl of DNA was added to 13 ml culture tubes and placed on ice. 100 µl of XL-10 Gold cells were added to the DNA, pipetting slowly to avoid the production of bubbles/over-agitation of the cells. The DNA and cells were mixed briefly by gently flipping the tubes before being incubated on ice for 30 min. After incubation the cells were heat-shocked for 42 s in a 42^{o}C water bath. The cells were incubated on ice for 2 min before being transferred to culture tubes containing 1 ml of LB-broth using wide orifice pipette tips. The cells were incubated for 1 h at 37 ^{o}C with shaking at 250 rpm. 100 µl of the competent cell suspensions were plated onto LB agar plates containing appropriate antibiotics. Cells were harvested from the remaining 900 µl by centrifugation at 12,000 g for 1 min at room temperature. The cells were resuspended in 100 µl of LB-medium before being plated onto LB agar plates containing appropriate antibiotics. These plates were incubated at 37 ^{o}C for 16 h before individual colonies were selected to be grown for use in DNA extraction protocols or frozen stock production.

3.2 Protocols for the preparation/use of DNA

3.2.1 Plasmid DNA miniprep from *E. coli* (Birnboim and Doly, 1979)

1.5 ml of saturated overnight *E. coli* culture was transferred into a 1.5 ml microcentrifuge tube. The *E. coli* were collected by centrifugation at room temperature for 1 min at 14,000 g before the supernatant was aspirated. Centrifugation for a further 1 min at 14,000 g and any excess medium was removed. 100 µl of 50 mM D-Glucose, 25 mM Tris·HCl (pH 8.0), 10 mM EDTA were added to the cells, which were resuspended by vortexing before being incubated for 5 min at room temperature. 200 µl of 0.2M NaOH, 1% (w/v) SDS were added and the tubes were inverted 4-6 times before being incubated on ice for 5 min. After incubation, 150 µl of ice-cold 5 M KOAc (pH 4.8) were added and the tubes were inverted 4-6 times before a 5 min incubation on ice. The lysates were centrifuged for 3 min at 14,000 g and 4 ^{o}C before being transferred to fresh microcentrifuge tubes. 800µl EtOH were added and the solution was mixed by inverting 2-3 times before the samples were incubated at room temperature for 2 min. The samples were centrifuged for 1 min at 14,000 g and room temperature before the supernatant was aspirated. 1 ml of EtOH was added before centrifugation for 1 min at 14,000 g and room temperature. The supernatant was once again discarded and the tubes were centrifuged for 10-15 s at 14,000 g at room temperature before any remaining liquid was removed. Following this, the pellets were air dried for 15 min at room temperature before the addition of 30 µl of 1x TE buffer (pH 8.0), 0.3 mg/ml RNase A. The pellets were incubated at 4 ^{o}C until they had dissolved (~0.5-1 h) at which point the plasmid DNA was either stored short term at 4 ^{o}C or long term at −20 ^{o}C.

3.2.2 Plasmid DNA midiprep from *E. coli* (Sigma-Aldrich)

Plasmid DNA midipreps were carried out using Sigma's GenElute^{TM} HP Plasmid Midiprep Kit (See Table 2.15 "Commercially Available Kits"), which provided the following instruments and solutions: *Resuspension/RNase A solution, Lysis solution, Neutralization solution, Binding solution, Filter syringe, GeneElute HP midiprep Binding column, Collection tube, Column preparation solution, Wash solution 1, Wash solution 2,* and *Elution solution*.

A single colony was used to inoculate 4 ml of LB-Broth containing the appropriate antibiotics (as described in 3.1.5). This culture was incubated at 37 ^{o}C for 8 h whilst shaking at 250 rpm. 100 µl of culture were transferred to a 50 ml falcon tube and diluted 1:500 in 50 ml of LB-broth, containing the appropriate antibiotics, before being incubated

at 37 ^{o}C for 16 h whilst shaking at 250 rpm. The *E. coli* were collected by centrifugation at 5,000 g for 10 min and the supernatants were discarded. The pellets were re-suspended in 4 ml of the r*esuspension/RNase A solution* via vortexing. 4 ml of *lysis Solution* were added and the contents of the tubes were mixed by gently inverting eight times before being incubated at room temperature for 4 min. The lysates were neutralised by the addition of 4 ml of chilled *neutralization solution* and gently inverted six times. After this, 3 ml of *binding solution* were added to the lysates and the tubes were inverted twice before immediately pouring into the barrel of a *filter syringe*. Following this the lysates were incubated for 5 min at room temperature whilst a *GeneElute HP midiprep binding column* was prepared for use. This was achieved through the addition of 4 ml of c*olumn preparation solution* before centrifugation at 3,000 g for 2 min. The eluate was discarded from the *collection tube* and the half of the cell lysate was expelled from the *filter syringe* into the *GeneElute HP midiprep binding column*. The column was centrifuged at 3,000 g for 2 min before the eluent was discarded. This process was repeated for the other half of the cell lysate. 4 ml of *wash solution 1* were added to the binding column and centrifuged at 3,000 g for 2 min. The eluent was discarded and the process was repeated with *wash solution 2*. The binding column was transferred to a fresh collection tube before the addition of 1 ml of *elution Solution*. The column was centrifuged at 3,000 g for 5 min to collect the plasmid DNA. The DNA was either used immediately, stored short term at 4 ^{o}C or stored long term at −80 ^{o}C.

3.2.3 Concentration of DNA via ethanol precipitation

3 M NaOAc (pH 5.2) was added to 1.5 ml microcentrifuge tubes containing DNA samples at a ratio of 1:10 and mixed by inverting the tubes 2-3 times. This was followed by the addition of EtOH at a volume equal to 2.5 times that of the DNA and NaAc mixture. This mixture was mixed by inverting the tubes 2-3 times and stored at 4^{o}C overnight. After overnight incubation the samples were centrifuged at 13,000 g for 20 min at 4^{o}C to pellet the DNA, the supernatants were discarded. 500 µl of 70% (v/v) EtOH were added to the pellets before centrifugation at 13,000 g for 20 min at 4^{o}C and disposal of the supernatant. The pellets were resuspended in 30µl of sterile, de-ionised H_2O before being stored at 4 ^{o}C (short term) or - 20^{o}C (long term).

3.2.4 DNA Agarose Gel Electrophoresis (Meyers et al., 1976)

0.3-3.0 g of electrophoresis-grade agarose were placed into an Erlenmeyer flask along with 30-150 ml of TAE buffer, with the volumes of TAE and weight of agarose being dependent on the desired size and percentage of the final gel. The DNA samples were mixed with 6x DNA loading dye and added to the wells alongside a *GeneRuler* DNA ladder. The gel was run at 100 V and the DNA was visualized at 312 nm, 0.120 J/cm^2 using a UV transilluminator.

3.2.5 Restriction Enzyme Digestion

Restriction enzyme digests were performed according to the protocols recommended by the manufacturer. If cleanup was required after the enzymatic digest, the product was either purified with a GenElute™ PCR Clean-Up Kit or the reaction was run on an agarose gel and isolated using a GenElute™ Gel Extraction Kit.

For diagnostic digests 20 µl reactions were set up as follows:

1 µg plasmid DNA
x µl (restriction enzyme buffer)
y µl (restriction enzyme 1)
z µl (restriction enzyme 2) (if required)
2 µl BSA
Sterile, de-ionised H_2O to 20 µl

The samples were incubated at 37 ^oC for 2 h before the DNA was separated via gel electrophoresis. The gel was imaged on a UV transilluminator, at a wave length of 312 nm and energy density of 0.120 J/cm^2, to confirm whether the digest had worked.

3.2.6 DNA Ligation with T4 DNA Ligase

The following components were combined in a 100 µl PCR tube:

33-50 ng of vector DNA
Insert DNA at a 1:1 or 1:3 molar ratio
1µl of T4 DNA ligase buffer
0.5 µl of T4 DNA ligase
Sterile, de-ionised H_2O to 10 µl

The samples were incubated at 16 ^{o}C overnight, after which they were ready for use in the transformation of *E. coli* (see 3.1.7 'Chemical Transformation of *E. coli*').

3.2.7 Sequencing

Sanger sequencing was performed by Source BioScience (Nottingham, NG8 6PX).

3.3 Mammalian Cell Culture (Davis, 2002)

All cells were incubated at 37 °C with 5% (v/v) CO_2 at 95% humidity. Appropriate antibiotics were added to the medium when using stably transfected cell lines. All work was done in a laminar flow cabinet and all equipment, including the flow hood, was sterilised with 70% (v/v) ethanol before use.

3.3.1 Cryopreservation

Cells were grown to 95% confluency. The medium was aspirated and cells were washed with 10 ml of phosphate buffered saline (PBS). The cells were treated with 0.25% trypsin-EDTA for 30 s before being incubated for 2 min at 37 °C with 5% (v/v) CO_2 at 95% humidity. The cells were resuspended in 1 ml of 90% (v/v) FBS, 10% (v/v) DMSO for every stock vial that was to be produced (for cells grown in a 175 cm^3 flask, eight vials were produced). 1 ml of the cell suspension was aliquoted to individual cryovials before being transferred to a 'CoolCell®', which ensured the gradual freezing at the rate of −1 ^{o}C/min. The 'CoolCell®' was and stored at −80 ^{o}C for 24 h before the cryovials were transferred to a −150 ^{o}C freezer or liquid nitrogen tank for long term storage.

3.3.2 Revival of Frozen Cells

Cryovials were removed from the −150 ^{o}C freezer and placed in a 37 ^{o}C water bath until the cell suspension started to thaw. The vials were wiped with 70% EtOH before the addition of 1 ml of pre-warmed medium (see Table 2.14 'Cell Lines'). The medium was slowly pipetted up and down until the cells were fully suspended and added to a culture flask containing 9 ml of pre-warmed medium before being incubated at 37 °C with 5% (v/v) CO_2 at 95% humidity. If antibiotics were required for they were added 24 h after revival.

3.3.3 Passaging Cells

Upon reaching >90% confluency the growth medium was discarded and the cells were gently washed with 10 ml of PBS. The cells were detached from the flask via treatment with 0.25% Trypsin-EDTA for 30 s before being incubated for 2 min at 37°C with 5% (v/v) CO_2 at 95% humidity. Based on desired confluency, a predetermined volume of the appropriate growth medium (see table 2.14 'Cell Lines'), which had been pre-heated to 37 ^{o}C was added to the cells. The cell suspension was pipetted up and down to ensure even distribution before being transferred to a new flask. Additional fresh medium was introduced to give a final volume of 10 ml for 75 cm^2 flasks or 25 ml for 125 cm^2 flasks. Appropriate antibiotics were added as required for stable cell lines (see Table 2.14 'Cell Lines') and the cells were incubated at 37 °C with 5% (v/v) CO_2 at 95% humidity.

3.3.4 Cell Counting with a Haemocytometer

Cells were detached and resuspended in the appropriate medium as described above. A 100 µl sample of the cell suspension was aliquoted into a sterile 1.5 ml microcentrifuge tube and mixed in a 1:1 ratio with 0.4% (v/v) trypan blue in 0.9% (w/v) NaCl by gently pipetting up and down four times. The haemocytometer was cleaned using 70% (v/v) ethanol and the cover slip was attached using a few droplets of water from a 10 ml pipette. ~ 10 µl of the cell suspension was loaded underneath the cover slip using the loading groove and left to settle for 2 min. The counting grids were visualised at a 100x magnification and the cells within a square of area 0.04 mm^2 were counted on both of the counting grids so that the average number of cells per ml of medium could be calculated using the following formula:

$$\text{Cells/ml} = 2 \times \text{average count per square} \times \text{dilution factor} \times 10^4$$

3.3.5 Induction of Fv2E-IRE1α in Flp-In T-REx HEK293 Cells

Preparation of tetracycline stock solution: 10 ml of a 10 mg/ml tetracycline solution were produced (see Table 2.7 'Solutions for tissue culture') and stored in opaque microcentrifuge tubes at −20 ^{o}C.

Induction of Fv2E-IRE1α in Flp-In T-REx HEK293 Cells: ~3.5 million cells were seeded in 10 ml of DMEM, 10% FBS, 2 mM L-glutamine onto 100x20 mm tissue culture dishes and incubated at 37 °C with 5% (v/v) CO_2 at 95% humidity overnight. 10 µl of freshly made 1 mg/ml tetracycline solution were added to the cells to give a final concentration of 1 µg/ml tetracycline. The dishes were gently swirled to homogenise the solution before being incubated at 37 °C with 5% (v/v) CO_2 at 95% humidity for the duration of the time course.

3.3.6 Induction of IRE1α signalling in Flp-In T-REx HEK293 Cells

Fv2E-IRE1α signalling was induced by the addition of AP20187 (see Table 2.7) at a concentration of 200 nM. After addition of AP20187 the dishes were gently swirled to homogenise the solution before being incubated at 37 °C with 5% (v/v) CO_2 at 95% humidity for the duration of the time course.

3.3.7 Treatment Flp-In T-REx HEK293 Cells with SP600125

SP600125 (see Table 2.6) was administered at a concentration of 20 µM at the same time, and in the same manner, as both AP20187 and tetracycline before the cells were returned to being incubated at 37 °C with 5% (v/v) CO_2 at 95% humidity for the remainder of the time course.

3.3.8 SiRNA Transfection of Flp-In T-REx HEK293 Cells (Polyplus-Transfection Inc.)

~1.75 million cells were seeded in 10 ml of DMEM, 10% FBS, 2 mM L-glutamine onto 100x20 mm tissue culture dishes and incubated at 37 °C with 5% (v/v) CO_2 at 95% humidity overnight. The following morning 500 µl of DMEM, 10% FBS, 2 mM L-glutamine, 40 µl of INTERFERin^{TM} and siRNA duplexes (at a concentration of either 10 nM or 20 nM) were mixed per sample and immediately vortexed for 10 s to create siRNA stock solutions, which were incubated for 12 min at room temperature. Whilst the siRNA

stock solutions were incubating, the cells were retrieved from the incubator and the old medium was replaced with fresh medium. After the 12 min incubation period had elapsed, 500 µl of the appropriate siRNA stock solution were added to each sample. The dishes were gently swirled to homogenise the contents and incubated at 37 °C with 5% (v/v) CO_2 at 95% humidity for 24 h. At this point the cells were ready for treatment with tetracycline and AP20187, as described above.

3.3.9 Transient Transfection of Flp-In T-REx HEK293 Cells (Polyplus-Transfection Inc.)

Transient transfection of Flp-In T-REx HEK293 cells was carried out using Polyplus Transfection's jetPRIME® DNA transfection kit, which provided the following reagents: *jetPRIME® buffer* and *jetPRIME® reagent*.

~500,000 cells were seeded in 2 ml of DMEM, 10% FBS, 2mM L-glutamine into the wells of 6-well tissue culture plates and incubated at 37 °C with 5% (v/v) CO2 at 95% humidity overnight. The following day plasmid DNA was diluted in jetPRIME ® buffer at a ratio of 1 µg:100 µl so that each well was transfected with a total of 2 µg of DNA. The DNA/buffer mix was vortexed for 10 s before being collected by centrifugation. For each well, 4 µl of jetPRIME® reagent were added to the DNA/buffer mix before being vortexed and centrifuged. The DNA/buffer/reagent mix was incubated for 10 min at room temperature before being added to the cells. After transfection the cells were incubated at 37 °C with 5% (v/v) CO_2 at 95% humidity for the desired time period before being treated with tetracycline (see section 3.3.5) and/or AP20187 (see section 3.3.6). At the end of the time course the cells were harvested for analysis via either Western Blotting (See section 3.5.12) or *XBP1* splicing (see section 3.4).

3.3.10 MTT Assay for Cell Viability (Mosmann, 1983)

To assess the number of living cells post-treatment an MTT colourimetric assay was used. ~7,500 cells were seeded into the cavities of a 96 well tissue culture plate in 100 µl of medium. After the desired treatments had concluded, the medium was aspirated and replaced with fresh DMEM medium that lacked phenol red, but contained 0.5 mg/ml MTT. The cells were incubated at 37 °C with 5% (v/v) CO_2 at 95% humidity for 3 h. The medium was aspirated and replaced with 150 µl of 4 mM HCl, 0.1% (v/v) nonidet P-40 in isopropanol. The plates were covered with aluminium foil and shaken for 15 min on an orbital shaker at room temperature to dissolve the MTT crystals. Once this was done the

absorbance was read at 590 nm (test wavelength) and 690 nm (reference wavelength) using 'SpectraMax 190 absorbance microplate reader'. The reading at the reference wavelength was subtracted from the reading at the test wavelength in order to negate the effects of precipitated proteins and/or cellular debris.

3.4 RNA Protocols

3.4.1 RNA isolation from Mammalian Cells (GeneFlow)

RNA was harvested using an EZ-RNA Total RNA Isolation Kit (see Table 2.15 'Commercially Available Kits'), which provided the following solutions: *denaturing solution* and *extraction solution*.

The cells being harvested were placed on ice and washed three times with 2 ml of ice cold PBS before being incubated on ice for 5 min in 500 µl of *denaturing solution*. During this incubation the dishes were gently shaken by hand to help detach the cells. The cells were transferred to RNase-free 1.5 ml microcentrifuge tubes and incubated at room temperature for 5 min before the addition of 500 µl of *extraction solution*. The lysates were vortexed for 15 s before being incubated for a further 10 min at room temperature. The lysates were centrifuged at 12,000 g for 15 min at 4^{o}C before the supernatants were transferred to fresh RNase-free 1.5 ml microcentrifuge tubes. 500 µl of isopropanol were added to the supernatants, which were incubated at room temperature for 10 min and at 4^{o}C overnight to allow the RNA to precipitate from the aqueous phase.

After overnight incubation the samples were centrifuged at 12,000 g for 15 min at 4^{o}C to pellet the RNA. The supernatants were discarded and the pellets were washed with 1 ml of 75% ethanol before being centrifuged at 12,000 g for 15 min at 4^{o}C. The ethanol was removed and the pellets were allowed to dry for 15 min at room temperature. The pellets were dissolved in 15-30 µl of diethylpyrocarbonate (DEPC)-treated water and the samples were either stored at −80 ^{o}C or quantified and separated via gel electrophoresis.

3.4.2 RNA Quantitation (Warburg, 1945)

2 µl of RNA were diluted 1 in 50 with DEPC-treated water before being added to the cavities of a 96 well microtiter plate. Each sample was produced in duplicate and a DEPC water blank was used as a control. The concentration and purity of the RNA was determined using a spectrophotometer (OD at 260nm, OD260/OD280 ratio) and concentrations confirmed by intensity of bands visible by RNA gel electrophoresis. Concentration was calculated using the following formula:

$$40 \times A260 \times 50 = \text{concentration } (mg/ml^{-1})$$

3.4.3 cDNA production from RNA (Invitrogen)

cDNA was reverse transcribed from RNA using a '*First strand cDNA synthesis kit'* (see Table 2.15 'Commercially Available Kits'). The following reactions were set up on ice:

1 µl of oligo$(dT)_{15}$
Up to 5 µg of RNA dissolved in DEPC-treated water
1 µl of 10 mM RNase-free dNTPs in 1 mM Tris-HCl pH 8.0
DEPC-treated water until the total volume of the reaction mixture equals 13 µl

The samples were centrifuged for ~3 s to collect the reagents before being heated to 65 °C for 5 min in a thermocycler and then cooled on ice to 4°C.

The following components were added:

4 µl of 5x first strand buffer
1 µl of 0.1 M DTT
1 µl of 40 U/µl RNAsein
1 µl of 200 U/µl Superscript III reverse transcriptase

The samples were centrifuged for ~3 s to collect the reagents together before being incubated at 50 °C for 60 min and then 70 °C for 15 min in a thermocycler in order to inactivate the reverse transcriptase.

3.4.4 Reverse transcription (RT)-PCR Assays for *XBP1* splicing (Invitrogen)

The following reaction mixture was set up on ice with the primers being added last to minimise primer-dimer formation.

10 µl 5x Green GoTaq Flexi Buffer
3 µl 25 mM $MgCl_2$
5 µl 2 mM dNTPs in 1 mM Tris-HCl pH 8.0
5 µl forward primer at 10 µM
5 µl reverse primer at 10 µM
0.5 µl of 5 U/µl Promega GoTaq HotStart Polymerase
2.5 µl cDNA reaction (See 'cDNA production from RNA')
Sterile H_20 to 50µl

The reagents were collected by centrifugation and PCR was carried out in a thermocycler, as detailed below:

Table 3.1 – Conditions for *XBP1* PCR

Step	Temperature (^oC)	Time (s)	Number of cycles
Initial Denaturation	94.0	120	1
Denaturation Annealing Extension	94.0 59.0 72.0	60 60 30	35
Final Extension	72.0	300	1
Hold	4.0	∞	N/A

Samples were collected via centrifugation for ~3 s and placed on ice before being run on a 2% agarose gel at 100 V and visualised under UV light of 312 nm, 0.120 J/cm^2 (See 3.2.4 'DNA agarose gel electrophoresis').

3.5 Protein protocols

3.5.1 *In vitro* Transcription and Translation of Plasmid DNA (Promega)

In vitro transcription and translation reactions were carried out using Promega's '*TnT® Quick Coupled Transcription/Translation*' kit. The reactions were set up as follows:

40 µl *TnT quick master mix* (provided as part of the kit)
1 µg plasmid DNA
2 µl [^{35}S] Methionine (1,000 Ci/mmol at 10 mCi/ml)
Sterile, de-ionised H_2O until total volume of reaction mixture equals 50 µl

The samples were incubated at 30 ^{o}C for 60 min.

3.5.2 MagZ Purification of IRE1α (Promega)

IRE1α that had been produced via *in vitro* transcription and translation (see above) was purified using Promega's 'MagZ™ Protein Purification System' (see Table 2.15'commercially available kits') as described below.

100 µl of "*MagZ™ Binding/Wash Buffer*" were added to 50 µl of the TNT® reaction (see 3.5.1) and mixed by slowly pipetting the solution up and down. This solution was added to *MagZ™ Binding Particles* before being incubated for 15 min at 4^{o}C whilst rotating at 8 rpm. The samples were placed on a magnetic stand for approximately 15 s to capture the *MagZ™ binding particles* before the supernatant was discarded. The beads were subjected to four washes in 200 µl of MagZ™ *binding/wash buffer*. 100 µl of *MagZ™ elution buffer* were added to the binding particles, which were resuspended by slowly pipetting them up and down. The tubes were placed in the magnetic stand for ~15 s, before the supernatants, which contained the target protein, were transferred to fresh 1.5 ml microcentrifuge tubes.

3.5.3 Kinase Assay

When obtaining proteins for the kinase assay, the MagZ™ purification system (see above) was used up until the 'washing' stage. At this point the beads were washed 3 times in 200 µl of 1x protein kinase buffer instead of '*MagZ™ binding/wash buffer*'. After the supernatant from the last wash had been discarded the beads were resuspended in 30 µl of 1x kinase buffer, 50 µM ATP. The beads were incubated at 37 ^{o}C for 30 min before the supernatant was discarded and replaced with 30 µl of 6x SDS-PAGE sample buffer. The samples were boiled at 100 ^{o}C for 5 min before being collected via centrifugation. The

samples were separated via gel electrophoresis (section 3.5.9) and analysed via Western blotting (section 3.5.12) with phospho-specific antibodies.

3.5.4 Protein isolation from mammalian cell lines

One '*PhosSTOP* phosphatase inhibitor' and one '*Complete mini protease inhibitor cocktail* tablet' were added per 10 ml of ice-cold RIPA buffer. It was necessary to do this on the day of protein isolation as the inhibitors are only stable for 24 h once dissolved.

The cells were placed on ice and the medium was aspirated and discarded. The cells were washed three times in 2 ml of ice-cold PBS before the addition 300 µl of ice-cold RIPA buffer. The cells were scraped in order to detach them from the bottom of the dish. The dishes were left at an angle of ~45^{o} for 5 min on ice to ensure all of the cells had been collected before being transferred to a 1.5 ml microcentrifuge tube and incubated for 10 min on ice to allow lysis to occur. The protein lysates were centrifuged at 16,000 g for 10 min at 4 ^{o}C to pellet the cell debris and the supernatants were transferred to fresh 1.5 ml microcentrifuge tubes. If being analysed via Western blotting (section 3.5.12), 20-30 µg of protein were combined with 6x SDS-PAGE loading buffer and denatured at 100 ^{o}C for 5 min before being separated by gel electrophoresis (section 3.5.9).

3.5.5 Collection of Separate Nuclear and Cytosolic Protein Fractions

Before protein isolation phosphatase and protease inhibitors were added to the RIPA buffer as described in section 3.5.4.

Obtaining Cytosolic Proteins: The cells were washed three times in 5 ml of PBS before the addition of 100 µl of ice-cold sucrose buffer per 10^7 cells. The cells were scraped to detach them from the bottom of the dish and left at a ~45^{o} angle for 5 min on ice to ensure they were collected in the sucrose buffer and that lysis of the outer cell membranes could occur. The cells were transferred to a 1.5 ml microcentrifuge tube and centrifuged at 5,000 g for 5 min. The supernatants, which contained the cytosolic proteins, were removed and stored on ice.

Obtaining Nuclear Proteins: The pellets obtained from the centrifugation were washed in 500 µl of ice cold sucrose buffer (without NP-40) by gently pipetting up and down before centrifugation for 5 min at 5,000 g. The buffer was aspirated and replaced with 30 µl of low salt buffer per 10^7 cells and the pellets were gently re-suspended by slowly pipetting them up and down. Once the pellet had been re-suspended, an equal volume of high salt

buffer was slowly added whilst mixing with the pipette tip. The samples were rotated slowly for 40 min at 4 ^{o}C to allow complete lysis of the nuclei. The lysates were centrifuged at 14,000 g for 5 min at 4 ^{o}C and the supernatants, which contained the nuclear proteins, were transferred to fresh 1.5 ml microcentrifuge tubes.

3.5.6 Protein Quantification (Bio-Rad)

To produce a standard curve by which the unknown samples could be compared, protein standards were created by dissolving BSA in RIPA buffer to produce a concentration range. Quantification of protein samples was carried out using Bio-Rad's *DC Protein Assay* kit, which provided the following reagents: *Bio-Rad Solution A, Bio-Rad Solution S* and *Bio-Rad Solution B.*

Protein lysates were diluted 1 in 5 with water and 5 µl of these samples were aliquoted into the cavities of a 96 well microtiter plate alongside the protein standards and a blank. Each sample was tested in duplicate so that an average value could be obtained. A solution containing *Bio-Rad Solution A* and *Bio-Rad Solution S* at a ratio of 50:1 was produced and 25 µl were added to each well. 200 µl *Bio-Rad Solution B* were added to each sample and the plate was incubated at room temperature for 15 min whilst shaking on an orbital shaker. The absorbance was read at 750 nm and protein concentrations were calculated against the standard curve using '*SoftMaxPro*' software.

3.5.7 Immunoprecipitation

3.5.7.1 Proteins isolated from Flp-In T-REx HEK293 cells

Before protein isolation phosphatase and protease inhibitors were added to the RIPA buffer as described in section 3.5.4.

Pre-clearing: 20 µl of Protein A-agarose beads were centrifuged at 800 g for 2 min. The supernatant was removed and the beads were re-suspended in 100 µl of RIPA buffer before being centrifuged at 800 g for 2 min. The supernatant was discarded and 250 µg of protein in 200 µl of RIPA buffer, plus 0.8 µg of rabbit IgG, were added to the beads. These samples were incubated at 4 ^{o}C for 1 h whilst rotating at 8 rmp. The samples were centrifuged at 800 g for 2 min before the supernatants were transferred to fresh 1.5ml microcentrifuge tubes.

Antibodies specific to the protein that was being used as the 'bait' during the assay were added to the samples and incubated overnight at 4 ^{o}C rotating at 8 rpm. The amount of

antibodies used for individual assays is detailed in the results. 20 µl of protein A-agarose beads were added to the protein lysates and incubated for 1 h at 4 °C whilst rotating at 8 rpm. The samples were centrifuged at 800 g for 2 min before the supernatants were discarded. The beads were washed three times in 500 µl RIPA buffer + 0.1% NP-40. 500µl RIPA buffer were added to the beads and centrifuged at 800 g for 2 min before the buffer was discarded. The beads were centrifuged a final time for 2 min at 800 g and any residual buffer was removed. 30 µl of 6x SDS-PAGE sample buffer were added to the beads, which were heated at either 100 °C for 5 min or 70 °C for 10 min. After this, the samples were collected via centrifugation for ~15 s. From this point on the proteins were separated via gel electrophoresis (section 3.5.9) and analysis via Western blotting (3.5.12).

3.5.7.2 Proteins obtained via *in vitro* transcription and translation

The following reactions were set up:

20 µl TnT master mix post-*in vitro* transcription and translation of desired protein (section 3.5.1)
200 µl of IP-Buffer
8 µl of either his-tag antibody or S-tag agarose.

The samples were incubated at 4 °C overnight in an overhead rotator at 8 rpm. 50 µl of protein A-agarose beads were added to samples containing his-tag antibodies using wide orifice pipette tips and all samples were then incubated at 4 °C for 1 h whilst rotating at 8 rpm. The beads were collected via centrifugation for 2 min at 800 g and 4 °C and the supernatants discarded and replaced with 500 µl of IP-Buffer. Samples were centrifuged for 2 min at 4 °C and 800 g before the IP buffer was discarded. 500 µl of IP-buffer without NP-40 were added to the beads and centrifuged for 2 min at 800 g and 4 °C. The buffer was discarded and 15 µl of 6x SDS-PAGE sample buffer were added to the beads before they were incubated at 100 °C for 5 min.

3.5.8 Gel Shift Assay (Promega)

This protocol was carried out using Promega's '*Gel Shift Assay System*' which provided the following reagents: *NF-κB oligonucleotide, T4 polynucleotide kinase 10x buffer, Gel shift binding 5x buffer, HeLa nuclear extract, unlabelled NF-κB consensus oligonucleotides, SP1 consensus oligonucleotides, unlabelled noncompetitor oligonucleotides, TFIID consensus oligo* and *T4 polynucleotide kinase*.

Before the gel shift assay was conducted the oligonucleotide probes were labelled via incubation with 1 µl of [γ-^{32}P]ATP (3,000 Ci/mmol at 10 mCi/ml) and 1 µl T4 Polynucleotide Kinase at 37 ^{o}C for 10 min. After incubation the reaction was stopped via the addition 1 µl of 0.5 M EDTA and this was followed by the addition of 89 µl of TE buffer. During this incubation period the samples to be analysed via gel shift assay were set up as follows:

5 µg of protein from nuclear lysates
2 µl G*el shift binding 5X buffer*
Nuclease-free water until total volume of reaction mixture was 9 µl

In addition to the test samples, positive controls were set up using 2 µl *HeLa nuclear extract* in place of 5 µg of protein from nuclear cell lysates, whilst negative controls contained only the buffer and nuclease-free water. When calibrating the assay, 1 µl of either an unlabelled competitor or unlabelled non-competitor oligonucleotide probe were added to additional control samples. 1 µl of the appropriate ^{32}P-labelled consensus probe was added to each sample before incubation at room temperature for 20 min. 1 µl of gel loading 10x buffer was added and the samples were separated via electrophoresis (see below).

3.5.9 Gel Electrophoresis (Wood, 1993)

3.5.9.1 Proteins obtained from mammalian cells

Proteins being used directly after harvesting (section 3.5.4) or co-immunoprecipitation (section 3.5.7.1) were loaded onto a *20% Criterion™ TGX™ gel* in 1x SDS-PAGE running buffer. 8 µl of a suitable protein ladder were also loaded so as to indicate the molecular weights of any proteins detected during Western blotting. A voltage of 240 V was applied until the bromophenol blue dye front had eluted from the gel, which took ~50 min. At this point proteins were ready for semi-dry transfer (section 3.5.11).

Samples obtained from the gel shift assay (section 3.5.8) were loaded onto a NOVEX® 6% DNA retardation gel in 0.5x TBE buffer. A voltage of 250 V was applied until the bromophenol blue dye front and travelled ¾ of the way down the gel, which took ~20 min. The gel was prepared for phosphorimaging (section 3.5.10).

3.5.9.2 Proteins obtained via *in vitro* transcription and translation

Proteins were separated on 4-12% Bis-Tris gels via electrophoresis in 1x MOPS running buffer. A voltage of 200 V was applied until the bromophenol blue dye front had eluted from the gel, which took ~2 h. The protein samples were visualised via phosphorimaging (see below).

3.5.10 Phosphorimaging (Voytas and Ke, 2001)

After electrophoresis, the gel was washed in H_2O before being dried overnight. The gel was transferred to an exposure cassette along with a '*storage phosphor screen*' and incubated at room temperature for 24 h. The storage phosphor screen was imaged using a phosphorimager.

3.5.11 Semi-Dry Transfer of Protein

Preparation: The gel from which the protein was being transferred was measured and one piece of PVDF membrane plus eight pieces of laboratory filter paper were cut a few millimetres larger than the area of the gel so as to allow complete coverage of the gel. The PVDF membrane was soaked in methanol at room temperature for 5 min before being washed in 1x semi-dry buffer for 5 min at the same temperature. The eight pieces of laboratory filter paper were soaked in 1x Semi-Dry Buffer for 5 min at room temperature.

The SDS-PAGE gel (section 3.5.9.1) was placed in 1x semi-dry transfer buffer for 2 min at room temperature with gentle shaking.

Semi-Dry Transfer: Four pieces of laboratory filter paper were stacked on the semi-dry transfer apparatus and rolled flat to remove air bubbles. The PVDF membrane was placed on top of the filter paper and the SDS-PAGE gel on top of the PVDF membrane. After this, the remaining four pieces of laboratory filter paper were placed on top of SDS-PAGE gel and the whole stack was rolled to remove air bubbles. The semi-dry transfer apparatus was used to apply an amperage of 2 mA/cm^2 for 1 h.

To confirm that the transfer had been successful, the membrane was washed in 1x TBST buffer and incubated in 0.5% (w/v) Ponceau S, 1% (v/v) HOAc for 5 min at room temperature in order to visualise the protein bands. Once protein transfer had been confirmed, the PVDF membrane was de-stained by washing for 12 min in distilled H_2O.

3.5.12 Western blotting (Towbin et al., 1979)

PVDF membranes were blocked by submersion in ~25 ml of 1x TBST + 5% (w/v) skimmed dried milk powder for 1 h at room temperature on an orbital shaker at ~50-60 rpm. After blocking, the membranes were washed in ~25 ml of 1x TBST at room temperature. 1x TBST + 5% (w/v) skimmed dried milk powder or 5% (w/v) bovine serum albumin, containing the appropriate concentration of primary antibody, were added to the membranes, which were incubated on a roller mixer at 4 ^oC overnight. The membranes were again washed in ~25 ml of 1x TBST to remove any unbound antibodies before being incubated in 1x TBST + 5% (w/v) skimmed dried milk powder, containing the appropriate concentration of secondary antibody, on rollers for either 1 h at room temperature or 4^oC overnight. After incubation the membranes were washed in ~25 ml of 1x TBST to remove any unbound secondary antibodies.

The concentration of antibodies commonly used during Western blotting, and the solutions used whilst incubating them with the PVDF membrane, are outlined in the table on the next page. Any antibodies that were not used as described in the following table will be mentioned as they appear in the results.

Table 3.2 – Antibody dilutions used during Western Blotting

Antibody	Type	Dilution	Solution
Anti-HA	Primary	1:1000	1x TBST + 5% (w/v) skimmed dried milk powder
eIF2α	Primary	1:1000	1x TBST + 5% (w/v) skimmed dried milk powder
GAPDH	Primary	1:5000	1x TBST + 5% (w/v) skimmed dried milk powder
Goat anti-Rabbit	Secondary	1:20000	1x TBST + 5% (w/v) skimmed dried milk powder
Horse anti-mouse	Secondary	1:20000	1x TBST + 5% (w/v) skimmed dried milk powder
IRE1α	Primary	1:1000	1x TBST + 5% (w/v) skimmed dried milk powder
Mouse IgG	Secondary	1:20000	1x TBST + 5% (w/v) skimmed dried milk powder
PARP-1	Primary	1:1000	1x TBST + 5% (w/v) skimmed dried milk powder
Phospho-eIF2α (Ser51)	Primary	1:1000	1x TBST + 5% (w/v) BSA
Phospho-IRE1α (pS724)	Primary	1:1000	1x TBST + 5% (w/v) BSA
Phospho-SAPK/JNK (Thr183/Tyr185)	Primary	1:1000	1x TBST + 5% (w/v) BSA
TRAF2 (F-2)	Primary	1:100	1x TBST + 5% (w/v) skimmed dried milk powder

3.5.13 Visualisation and Imaging

Western blots were visualised using Pierce's ECL Western blotting kits (See Table 2.15 'Commercially Available Kits'). Depending on the protein that was being investigated, a solution of ECL or ECL2 was prepared according to the manufacturer's protocols. Once prepared the solution was incubated in a foil-wrapped 15 ml tube at room temperature for 5 min. The solution was spread evenly over the PVDF membrane and incubated in the dark for 5 min. The membranes were transferred to an X-ray cassette and incubated with a '*CL-XPosure*^{TM} *film*' for a time period between 30 s and 12 h depending on the protein being investigated. The film was developed to produce the final image of the Western blot.

3.5.14 Membrane Stripping

In the instance that multiple proteins of similar sizes were being examined it was possible to strip the original antibodies off the PVDF membrane and re-probe it for a different protein. This was done by submerging the membrane in '*stripping buffer*' (purchased from Thermo Scientific, see table 2.5) and shaking at 50-60 rpm for 15 min at room temperature. The stripping buffer was removed and the membrane was washed three times in ~25 ml of 1x TBST. At this point the membrane could be re-blocked and immunoblotted as described in section 3.5.12.

4 *In vitro* isolation of the IRE1α-TRAF2 interaction

4.1 Rationale

The first known interaction in the IRE1α kinase domain-mediated signalling cascade is with the adaptor protein TRAF2 (Urano et al., 2000b). However, other than knowing that the TRAF domain of TRAF2 and the cytoplasmic domain of IRE1α are required for this interaction to occur, little else is known about the initial instigation of IRE1α signalling via this pathway. Therefore, it was decided that the first part of this investigation should concern itself with characterising the IRE1α-TRAF2 interaction. In order to do this, IRE1α and TRAF2 would be transcribed and translated *in vitro* and then co- immunoprecipitation (co-IP) analysis would be carried out to discern if the interaction could occur in isolation. If this were possible then it would indicate that no other proteins were required for the interaction to occur and provide a system where point mutations could be introduced to IRE1α to see if the interaction can be disrupted. The ultimate goal of this would be to identify residues that could be targeted to disrupt the interaction with TRAF2 without affecting kinase activity. However, this process was complicated by the fact that full length membrane proteins very rarely fold correctly *in vitro* owing to their hydrophobic transmembrane domains and, as a result, it was decided that experiments would be carried out with cytoplasmic truncations of IRE1α. This would avoid the issue of transmembrane domain folding, whilst retaining the cytosolic domain, which has been reported to be responsible for the interaction with TRAF2 (Urano et al., 2000b). This strategy would also have the potential to isolate the regions of the IRE1α cytoplasmic domain that are required for the interaction with TRAF2 should results be obtained indicating that certain truncations were capable of binding TRAF2 whilst others were not.

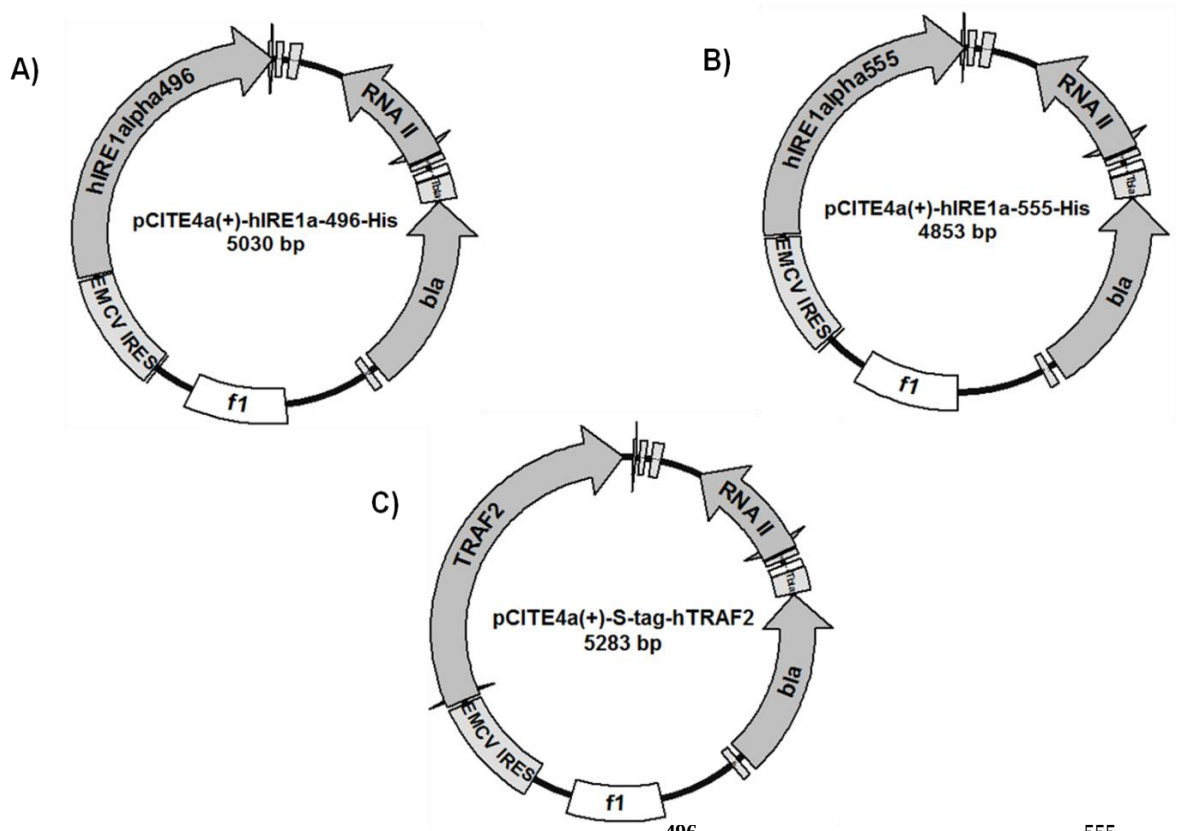

Figure 4.1-Plasmid maps for pCITE4a(+)-IRE1α^{496}-his (A), pCITE4a(+)-IRE1α^{555}-his (B) and pCITE4a(+)-S-tag-TRAF2 (C).

The lab already possessed plasmids encoding two his-tagged IRE1α truncations; IRE1α^{555} and IRE1α^{496}, and an S-tagged TRAF2 protein, which could be used to investigate if it were possible to observe the IRE1α-TRAF2 interaction in vitro. The plasmids containing these genes are shown in Figure 4.1 and the locations of the IRE1α truncations are shown in Figure 4.2. The IRE1α proteins were deemed suitable for use as both possess the serine threonine kinase domain and the RNase domain of IRE1α, but exclude the transmembrane domain. They also exclude a series of poly-glutamine repeats located between the transmembrane domain and the kinase domain, which is important as poly-glutamine repeats are also liable to cause problems with protein folding (Kakizuka, 1998).

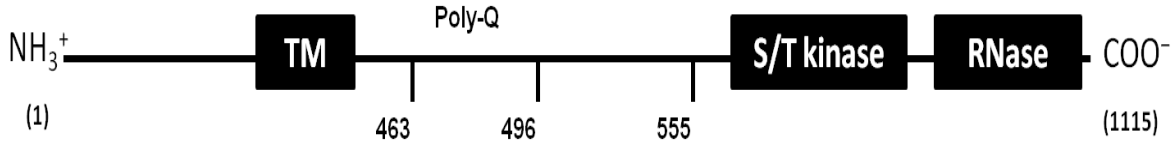

Figure 4.2 - A schematic of the domains of full length IRE1α.

Transmembrane (TM) domain folding can be problematic in vitro, and for this reason truncations of the IRE1α protein were used. The locations of these truncations are indicated by the numbers below the IRE1α domain map. The "Poly-Q" label refers to a series of glutamine residues, which are well documented to cause problems with protein folding (Kakizuka, 1998).

4.2 Results

4.2.1 No interaction detected between IRE1α^{555} and TRAF2 *in vitro*

In order to investigate whether the shortest IRE1α truncation contained the motif required to interact with TRAF2, S-tagged TRAF2 and his-tagged IRE1α^{555} proteins were transcribed and translated from 1 μg of their respective plasmid DNAs and labelled with [^{35}S]-L-methionine *in vitro*, as described in Chapter 3.5. The two proteins were pulled-down via incubation with either S protein agarose beads or an anti-his-tag antibody before 40 % of the *in vitro* translation reactions were run on an SDS-PAGE gel. The proteins were then visualised using a phosphorimager to detect the presence of [^{35}S]-L-methionine (Figure 4.3, lanes 1-3). IRE1α^{555} appeared at 50 kDa and TRAF2 appeared at 57 kDa, with the data from the input controls showing that both proteins were synthesised at roughly equal amounts (Figure 4.3, lanes 1 and 2), even when they were co-translated in the same reaction (lane 3). Both proteins were then pulled-down using solely the S protein agarose or the anti-his tag antibody. These experiments showed that both the anti-his tag antibody and the S protein agarose successfully pull-down his-tagged IRE1α^{555} (lane 4) and S-tagged TRAF2 (lane 7) respectively and that there was no detectable cross-reactivity between the antibodies and the opposing target protein (lanes 5 and 8). However, when both proteins were incubated together, and precipitated with either S protein agarose or the anti-his tag antibody, no co-precipitation was observed (Figure 4.2, lanes 6 and 9). These data therefore suggest that IRE1α^{555} and TRAF2 do not interact *in vitro*.

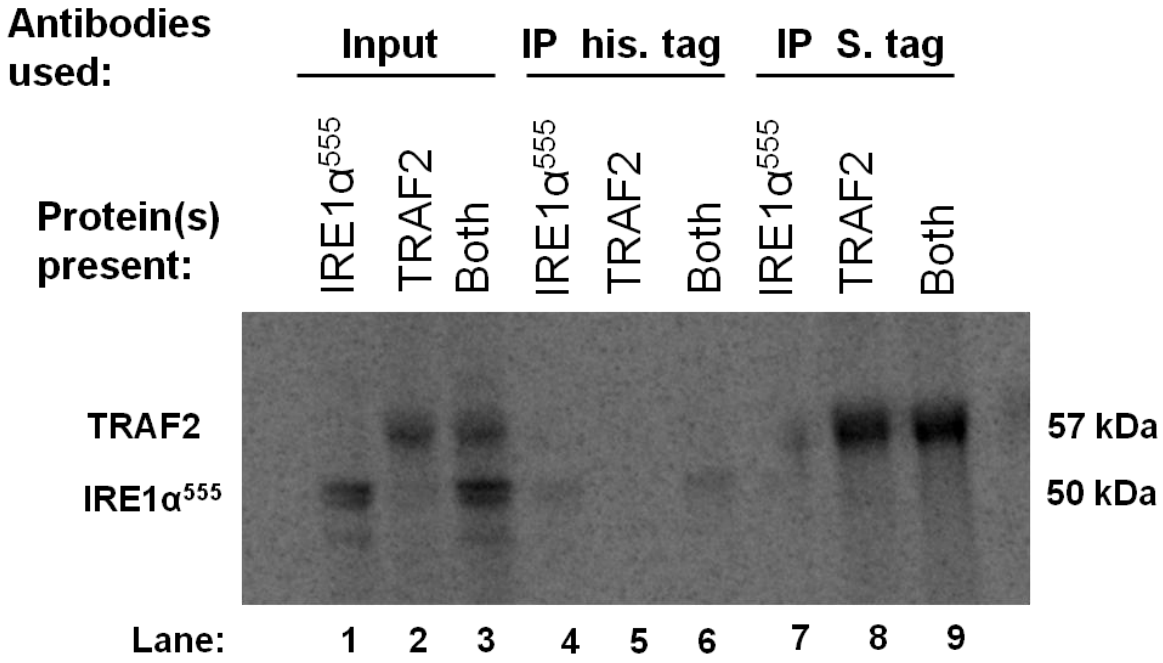

Figure 4.3 –No interaction was detected between IRE1α^{555} and TRAF2 *in vitro*.
The IRE1α^{555} and TRAF2 proteins were obtained via transcription and translation of plasmid DNA. Input samples (lanes 1-3) contained antibodies against the proteins that were present in the sample, whilst the other samples were either treated with a His-tag antibody or S-protein agarose as indicated. For each antibody three samples were tested, one containing IRE1α^{555}, one containing TRAF2 and one containing both proteins.

4.2.2 No interaction detected between IRE1α^{555} and TRAF2 *in vitro*

4.2.2.1 The molecular weights of IRE1α^{469} and TRAF2 are too similar for individual bands to be resolved

The predicted molecular weight of IRE1α^{469} is 56 kDa (Figure 4.1), whilst the predicted molecular weight of TRAF2 is 57 kDa. This had the potential to be problematic because it is unlikely that proteins this similar in size can be resolved via SDS PAGE. Therefore, it was first investigated whether it would be possible to distinguish between TRAF2 and IRE1α^{469} using the same method as was used to obtain the results in section 4.1.2, or whether an alternative solution needed to be found. To do this, S-tagged TRAF2 and his-tagged IRE1α^{469} proteins were translated from 1 μg of their respective plasmid DNAs *in vitro* and labelled with [^{35}S]-L-methionine as described in Chapter 3.5. The two proteins were pulled-down via incubation with either S protein agarose beads or an anti-his-tag antibody before 40 % of the *in vitro* translation reactions were directly run on an SDS-PAGE gel. The proteins were then visualised using a phosphor imager (Figure 4.4).

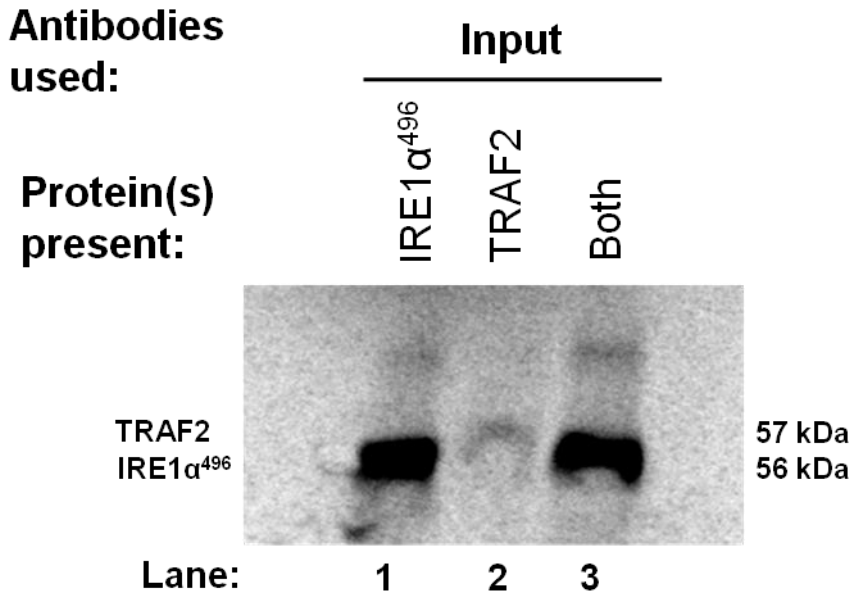

Figure 4.4 - The molecular weights of IRE1α^{469} and TRAF2 are too similar for individual bands to be resolved
IRE1α^{496} and TRAF2 proteins were obtained via transcription and translation of plasmid DNA. A co-IP assay was then carried out using antibodies as indicated.

Figure 4.3 confirmed that both IRE1α^{496} (lane 1) and TRAF2 (lane 2) appear very close to one another. This combined with the fact that the bands vary significantly in intensity, meant that it was impossible to distinguish between them when they were combined (lane 3). It is unknown why the band intensity varied to such an extent but, given that the experiment was carried out in the same way as in section 4.2.1 (which produced a clearly detectable TRAF2 band) and the same quantity of each reaction mixture was loaded in each well of the gel, it could be that there was an issue with the *in vitro* transcription and translation of TRAF2 in this instance. Repeating this experiment would have allowed further insight into the cause of the issue, however, this was not a priority as the experiment has served its purpose in proving that the bands appear too closely together and therefore an alternative approach would need to be taken when using IRE1α^{496}.

4.2.2.2 No interaction detected between IRE1α^{496} and TRAF2

To distinguish between the 56 kDa IRE1α^{496} protein and the 57 kDa TRAF2 protein a combination of non-radiolabelled and radiolabelled proteins were used. Both TRAF2 and IRE1α^{496} were transcribed and translated from 1 µg of their respective plasmid DNAs using either [^{35}S]-methionine or normal methionine (section 3.5). This was done because the phosphorimager only detects radiolabelled proteins and therefore it would be possible to distinguish between TRAF2 and IRE1α^{469} based on whether they had been produced using [^{35}S] methionine or not (see Figure 4.5). This method therefore allowed the use of

non-radiolabelled IRE1α^{496} as 'bait' in the co-immunoprecipitation reaction, whilst a band would only appear should radiolabelled TRAF2 bind to it, as depicted in Figure 4.5. In order to determine of an interaction had occurred between IRE1α^{496} and TRAF2, 40% of the *in vitro* translation reactions were run directly on an SDS-PAGE gel and imaged using a phosphorimager (Figure 4.6).

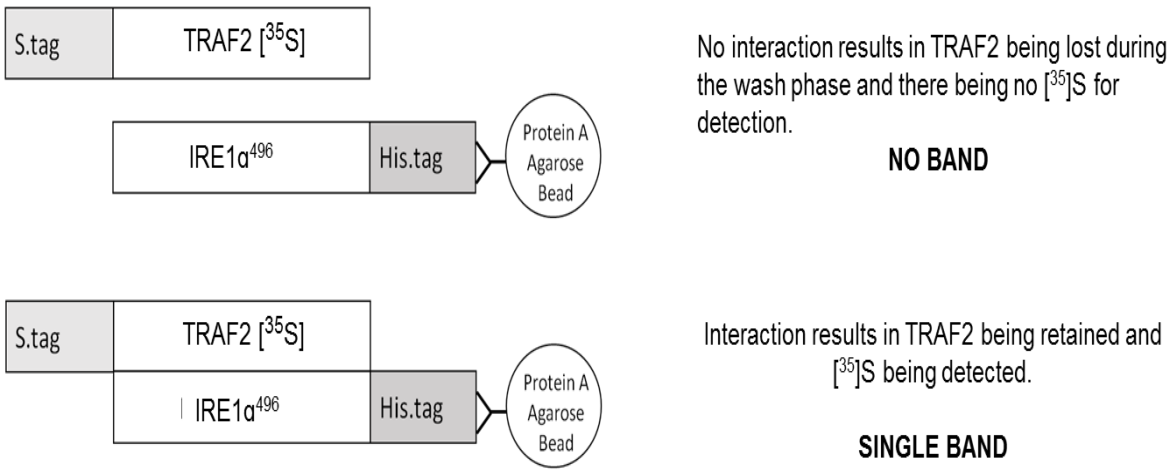

Figure 4.5 – Diagrammatic representation of the potential interaction between radiolabelled TRAF2 and non-radiolabelled IRE1α^{496}.

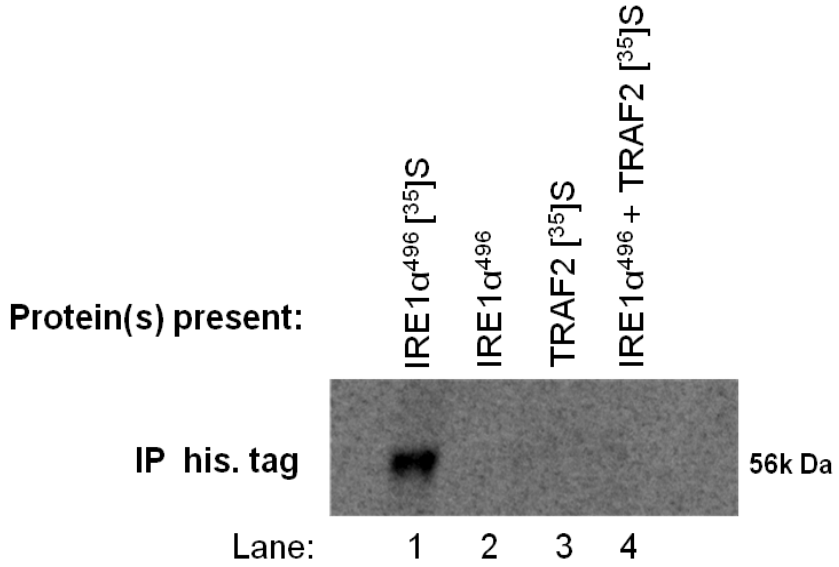

Figure 4.6 – No interaction detected between IRE1α^{496} and TRAF2 *in vitro*.
IRE1α^{496} and TRAF2 proteins were obtained via transcription and translation of plasmid DNA using either [^{35}S] -methionine or unlabelled methionine. All samples were incubated with his-tag antibodies during the co-immunoprecipitation stage in order to retain IRE1α^{496}. However, only proteins that had been produced using radiolabelled methionine ([^{35}S]) were visualised during phosphor imaging.

Lane 1 of Figure 4.5 was loaded with a sample containing [^{35}S]-methionine-labelled IRE1α^{496} and a band was detected at 56 kDa, confirming that the his-tag antibody was capable of pulling down IRE1α^{496} and that there was sufficient protein for detection by the phosphorimager. Lane 2 contained non-labelled IRE1α^{496} and no band was detected, which confirmed that without the presence of a radiolabel, proteins will not be detected. Lane 3 contained [^{35}S]-methionine labelled TRAF2 and no band appeared, confirming that the his-tag antibody is specific and will not pull down TRAF2 alone. Lane 4 contains non-labelled IRE1α^{496} and [^{35}S]-methionine-labelled TRAF2 and, if there had been an interaction between the two proteins, it would be expected that a band would have appeared in this lane. However, without a control to prove that TRAF2 had been successfully transcribed and translated, the only conclusion that can be drawn is that, in this individual experiment, there was no interaction detected between IRE1α^{496} and TRAF2.

4.2.3 IRE1α^{496} retains its kinase activity, but no evidence of autophosphorylation by IRE1α^{555} was detected

The data from sections 4.2.1 and 4.2.2 suggest that neither IRE1α^{555} nor IRE1α^{496} interact with TRAF2 *in vitro* and therefore it was logical to try and discern why this might be the case. As mentioned earlier, full length IRE1α will not fold correctly *in vitro* and this was the reason for using truncated forms of the protein as opposed to the full length version. Current understanding of IRE1α signalling dictates that a functional kinase domain is required for its interaction with TRAF2 (Urano et al., 2000b) and, given that truncated versions of IRE1α were being used, it was logical to question whether loss of kinase function was the reason behind the failed interaction with TRAF2. Given that the only known target of IRE1α kinase activity is itself (Tirasophon et al., 1998), it was decided that a kinase assay should be used to determine whether IRE1α^{555} or IRE1α^{496} are capable of autophosphorylation. Obviously if the truncated proteins were capable of autophosphorylation then it could be assumed that kinase function was intact and there was another reason for their inability to interact with TRAF2. However, if autophosphorylation did not occur, it could be argued that a lack of a functional kinase domain was the reason for their failure to interact. Although subsequent data (see Chapter 5) suggest that, contrary to current understanding (Urano et al., 2000b), kinase activity is not required for interaction between IRE1α and TRAF2.

The proteins analysed during the kinase assay were transcribed and translated using the same methodology as described in sections 4.2.1 and 4.2.2 and were subsequently isolated

from the *TnT*® mixture by using a *MagZ™ Purification system* (section 3.5.3), which utilises magnetic beads that bind to the his-tag of the IRE1α proteins. The proteins were then incubated in 1x Kinase Buffer, 50 μM ATP (Table 2.7), before being separated by SDS PAGE and analysed via Western blotting (Figure 4.7).

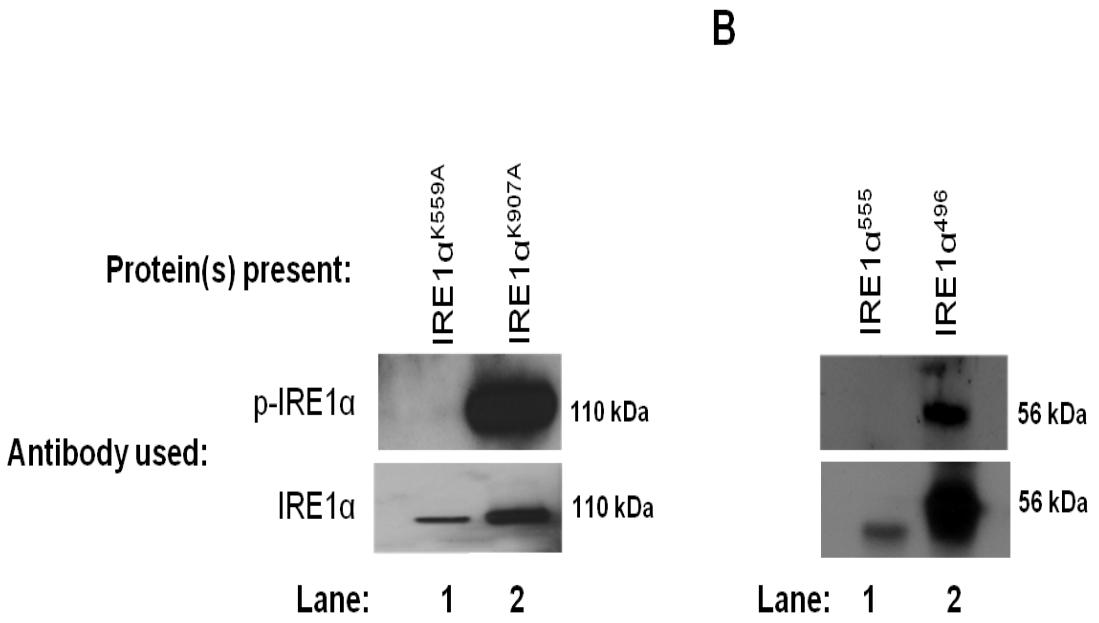

Figure 4.7 – IRE1α^{496} retains kinase activity whilst phospo-IRE1α^{555} was not be detected.
All proteins were transcribed and translated from plasmid DNA using a kit from Promega. IRE1α^{K559A} was used as a negative control for kinase activity whilst IRE1α^{K907} was used as a positive control. Antibodies against IRE1α and phospho-IRE1α were used as indicated and detected via Western blotting. Panel A shows the detection of phospho-IRE1α and total IRE1α when using the positive and negative controls, whilst panel B shows the detection of phospho-IRE1α and total IRE1α when using the IRE1α truncations being investigated.

During Western blotting all of the samples were first probed using a phospho-specific IRE1α antibody that detects phosphorylation on serine 724. The blots were then stripped and probed with an antibody against IRE1α. Lane 1 of Figure 4.7 was loaded with IRE1α^{K599A}, a kinase deficient mutant owing to the replacement of lysine 599, which is essential for the positioning of the α and β phosphates of ATP and therefore inhibits phosphotransfer (Iwawaki et al., 2001). As expected, when probing for IRE1α, a band representing IRE1α^{K599A} appeared at 110 kDa, but when using an antibody that targets the phosphorylated version of IRE1α no band was detected. In Lane 2, a sample containing IRE1α^{K907A} was used as a positive control because this mutant (see introduction section 1.4.3.4) has been shown to retain kinase activity (Tirasophon et al., 2000) and a his-tagged version of the protein was already available in the lab. Once again, a band appeared when Western blotting for IRE1α, but this time a band also appeared when using the phospho-specific antibody. Therefore lanes 1 and 2 indicate that the phospho-IRE1α antibody was

able to distinguish between the phosphorylated form of IRE1α and the non-phosphorylated form.

Lane 3 was loaded with the shorter IRE1α^{555} construct and, whilst a band representing the non-phosphorylated version of the protein appeared, there was no band observed when using the phospho-IRE1α antibody. This result suggests that IRE1α^{555} is incapable of phosphorylating itself. Lane 4 was loaded with IRE1α^{496} and bands appeared at ~110 kDa when using both the IRE1α antibody and the phospho-IRE1α antibody. This would therefore suggest that IRE1α^{496} is capable of autophosphorylation, unlike its shorter counterpart. However, it must be noted that there are uneven amounts of protein in lanes 3 and 4, with there being 5 times more IRE1α^{496} present than IRE1α^{555}. Thus, it could be argued that if there were equivalent levels of IRE1α^{555}, a phosphorylated version of the protein may have been detected. However, variations in the amount of protein in a protocol that involves transcription, translation, immunoprecipitation and various wash stages are inevitable and this is discussed (section 4.3) as an area that will need to be addressed before any concrete deductions can be made about the activity of IRE1α^{555} and IRE1α^{496}.

4.3 Discussion

In an attempt to determine if the interaction between IRE1α and TRAF2 is direct, or requires bridging proteins, co-immunoprecipitation assays were carried out using truncated versions of IRE1α and full length TRAF2 *in vitro*. The truncated proteins IRE1α^{555} and IRE1α^{496} were selected for use as they include the cytosolic effector domains, but exclude the transmembrane domain and a series of poly-glutamine repeats, which are present in the full length protein and would have increased the likelihood of misfolding in vitro.

The data obtained from the co-immunoprecipitation assays suggest that neither IRE1α^{555} nor IRE1α^{496} are capable of interacting with TRAF2 *in vitro* and therefore that the residues necessary for the interaction with TRAF2 may lie closer to the transmembrane domain or bridging proteins may be required. However, it must be noted that there were several reliability issues that will need to be resolved in order to draw reliable conclusions from the data presented in this chapter and these will be discussed below.

The image produced in Figure 4.3 shows detection of IRE1α^{555} at 50 kDa and TRAF2 at 57 kDa and, whilst the amount of protein retained whilst using IRE1α^{555} as bait are too faint to draw conclusions (lanes 4-6), there are clear bands whilst using TRAF2 as bait (lanes 7-9). Therefore lanes 7-9, combined with the control, would suggest that TRAF2 and IRE1α^{555}

do not interact *in vitro*. However, the inability to detect IRE1α^{555} using the his-tag antibody (lanes 4-6) raises questions regarding the ability of this assay to reliably synthesise, retain and detect target proteins. Therefore, whilst the data presented in Figure 4.3 may suggest that there is no interaction between IRE1α^{555} and TRAF2 *in vitro*, without the repeats, no significant conclusions can be drawn.

Fluctuations in protein retention during this assay are difficult to avoid owing to variation in the amount of transcription and translation and the amount of protein that may be lost during the large number of wash stages (Chapter 3.5). For this reason, whilst Figure 4.6 suggests that IRE1α^{496}, like IRE1α^{555}, does not interact with TRAF2, this result could also have occurred because the amount of TRAF2 protein was below detectable limits. Thus, a TRAF2 loading control should have been included in order to provide confirmation that TRAF2 was present. Therefore, whilst the work carried out with TRAF2 and IRE1α^{555}/IRE1α^{496} may indicate that there is no interaction between the two proteins *in vitro*, further repeats and, in the case of IRE1α^{496}, appropriate controls will need to be included to allow this conclusion to be drawn.

There are various reasons why the IRE1α truncations and TRAF2 may not interact *in vitro* and one of these could have been that the IRE1α truncations were unable to undergo phosphorylation which, prior to the work with Fv2E-IRE1α^{D771A} (Chapter 5), was believed to be essential for the interaction between IRE1α and TRAF2 to occur (Urano et al., 2000b). This hypothesis was the impetus behind the kinase assay carried out in Figure 4.7 and the data collected imply that IRE1α^{496} is capable of autophosphorylation, whilst IRE1α^{555} is not. However, it is important to note that there was five times as much IRE1α^{496} present as there was IREα1^{555}, which weakens this conclusion. This issue is further compounded by the fact that detection using X-ray film follows a sigmoidal pattern rather than a linear one. Therefore, if the band for total IRE1α^{496} is saturated, which it appears to be, there could be significantly more than 5 times the amount of IRE1α^{496} when compared to IRE1α^{555}. As a result of this, there would need to be more repeats carried out in order to obtain blots that have comparable amount of both proteins for any legitimate conclusions to be drawn. However, in a protocol that involves transcription, translation, immunoprecipitation, multiple wash phases and no opportunity to quantify the amount of protein before gel loading (methods section 3.7), it is difficult to see how this could have been achieved consistently. Therefore, an alternative method of quantifying the amount of protein, such as using a digital SLR camera instead of X-ray film (Khoury et al., 2010), may be the best course of action.

Ultimately, whilst the evidence provided in this chapter suggests that there is no interaction between IRE1α and TRAF2 *in vitro*, there can be no significant conclusions drawn without doing further work to improve the controls and the reproducibility of the data. Furthermore, based on the data presented in Chapter 5, it would appear that kinase activity is not a prerequisite for interaction between TRAF2 and IRE1α, which would make any further work on the kinase activity of IRE1α^{496} and IRE1α^{555} obsolete in the context of this thesis. Therefore, future work would be better directed at investigating if the inability of the IRE1α truncations to interact with TRAF2 is down to them lacking the motif required to do so or the absence of an essential bridging protein, which might not be present *in vitro*. The former could be achieved by producing longer truncations of IRE1α but, as discussed in Section 4.1, there would be concerns that these proteins would fold incorrectly *in vitro* owing to the inclusion of a section of poly-glutamine repeats (Bates, 2005) (Figure 4.2). Alternatively, future work could be directed at carrying out *in vivo* co-IPs (as described in section 3.5.7.1) in order to identify proteins involved in the IRE1α-TRAF2 signalling scaffold and then these proteins could be targeted with siRNAs to elucidate if they are necessary for the interaction between TRAF2 and IRE1α.

5 Isolation and characterisation of the IRE1α- signalling cascade *in vivo*

5.1 Rationale

IRE1α is a bifunctional enzyme that mediates both protective and apoptotic UPR signalling via its endoribonuclease and kinase domains (Chen and Brandizzi, 2013, Sano and Reed, 2013). Protective IRE1α signalling is mediated via its endoribonuclease domain, which carries out the unconventional splicing of *XBP1* mRNA, a pathway that has been fairly well characterised because genes under the influence of XBP1 can be identified via ERSE elements in their promoters (Acosta-Alvear et al., 2007). However, apoptotic signalling via the kinase domain has proved far more difficult to elucidate owing to the fact that there is a significant amount of crosstalk between ER stress sensors and, as the intensity of the stress increases, other stress pathways as well. For example, JNK and NF-κB have both been indicated as playing important roles in IRE1α signalling, but they are also the target of many other pathways and can be involved in proliferation or cell death (Weston and Davis, 2007, Gilmore, 2006). Another layer of complexity is then added by the fact that current research suggests that IRE1α signalling via its kinase domain involves the creation of a multi-protein complex or "UPRosome", with a wide plethora of proteins having been reported as being involved (Woehlbier and Hetz, 2011). This poses a significant problem when trying to elucidate and understand the signalling pathways induced by the IRE1α kinase domain as, without being able to study IRE1α in isolation, it is extremely difficult to know which downstream effects have been caused by IRE1α and which have been caused by other effectors.

Owing to the complexity of stress signalling during the initiation of the UPR, a system that would allow the activation of the IRE1α signalling cascade in isolation of other pathways would be useful, yet no such system currently exists. Therefore, ER stress mimetic drugs have been used to study IRE1α signalling up until this point. However, this is not ideal because interfering with essential processes such as Ca^{2+} homeostasis (thapsigargin) and vesicular trafficking (brefeldin A) are bound to activate a number of stress signalling cascades, making it difficult to deduce whether the activation of downstream targets such as JNK is the result of IRE1α signalling or another upstream effector. Even drugs such as tunicamycin, which more specifically targets protein folding, will activate all three UPR signalling cascades rather than just IRE1α. Therefore, this project aims to fill the current

niche in models for studying the UPR by producing and characterising a system that will allow the specific activation of IRE1α *in vivo*.

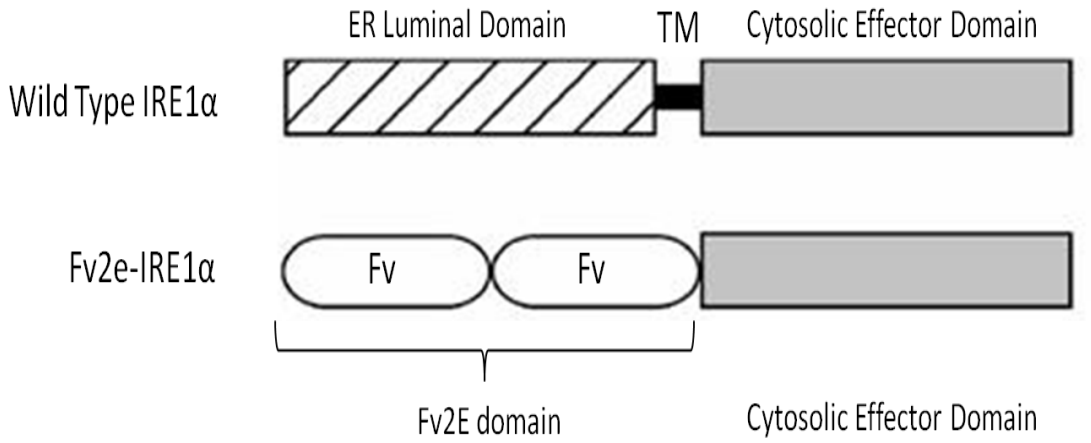

Figure 5.1 – Diagrammatic comparison of the structure of wild type IRE1α and Fv2E- IRE1α.

The need to be able to study UPR signalling pathways in isolation has been recognised by other groups and several of them have managed to take advantage of a model that allows the uncoupling of PERK signalling from general ER stress by attaching the cytosolic effector domain of PERK to an Fv2E domain (Lin et al., 2009, Lu et al., 2004b). As discussed in the introduction (section 1.4.2), the Fv2E domain forms homodimers/oligomers upon treatment with AP20187 and this has been shown to successfully activate the PERK signalling cascade without inducing UPR signalling by either IRE1α or ATF6 (Deng et al., 2004). Therefore, it was decided that this technology could be applied to IRE1α in order to characterise its signalling. Stable cell lines expressing a fusion protein of the IRE1α cytosolic effector domain attached to an Fv2E domains (see Figure 6.1) were already available to the lab having been created by Dr. David Cox. The HEK293 cells that were produced express a tetracycline-inducible HA-tagged version of Fv2E-IRE1α and were created using Invitrogen's Flp-In™ system. This system enables the stable integration of two plasmids into the genome of Flp-In™ HEK293 cells (Invitrogen). The first plasmid pcDNA6/TR contains genes for tetracycline repressor protein (tetR) and blastacidine resistance, whilst the second plasmid pcDNA5/FRT contains a gene for hygromycin resistance and the gene of interest, in this instance Fv2E-IRE1α, which is under the control of a CMV promoter and two tetracycline operators (CMV/TetO_2) (Figure 6.2).

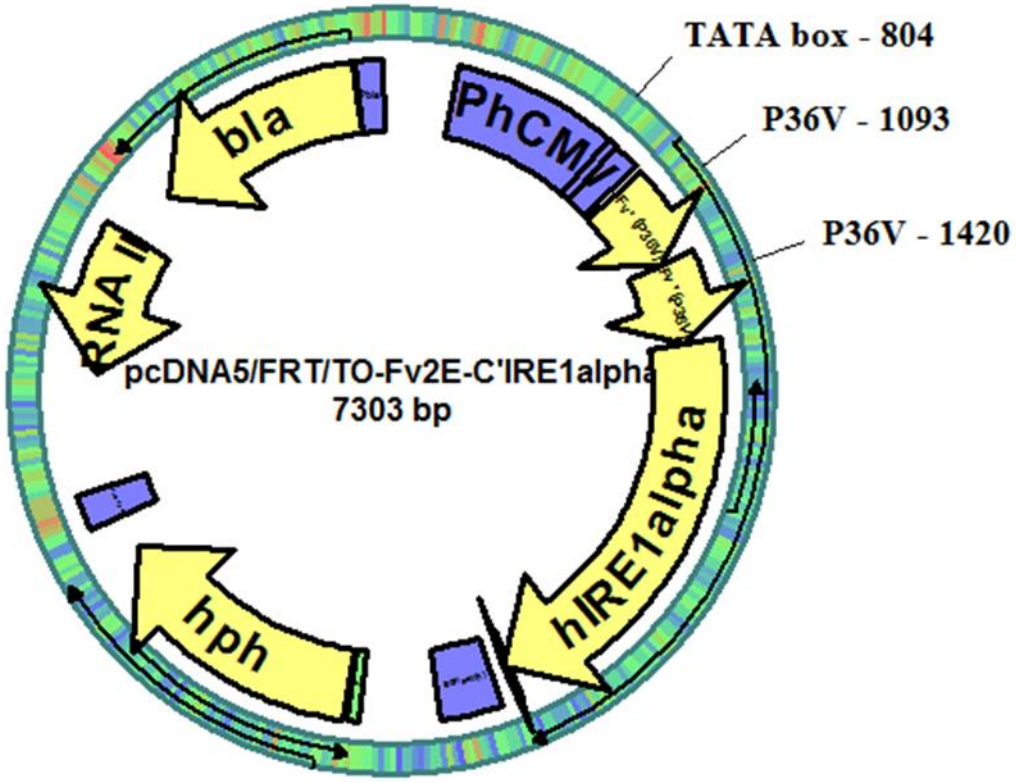

Figure 5.2 - Plasmid map of pcDNA5/FRT/TO-Fv2E-IRE1α. The plasmid contains the Fv2E-IRE1α gene in a vector competent for transfer to a stable cell line using the FRT site.

Therefore the final product, Flp-In T-REx HEK293 Fv2E-IRE1α cells, can be selected for via the use of a combination of blasticidin and hygromycin and allows control over Fv2E-IRE1α expression via addition of tetracycline to the growth medium. This control is possible because the cells constitutively express tetR protein which, in the absence of tetracycline, forms homodimers that bind with high affinity to tetracycline operators, blocking the transcription any genes that possess them. However, the addition of tetracycline lifts this translational repression by binding to tetR homodimers and causing a conformational change that results in their dissociation from the tetracycline operator (Yao et al., 1998, Hillen and Berens, 1994) (Figure 6.3). Therefore, because the Fv2E-IRE1α gene contains two tetracycline operators, the expression of Fv2E-IRE1α can be controlled via the use of tetracycline.

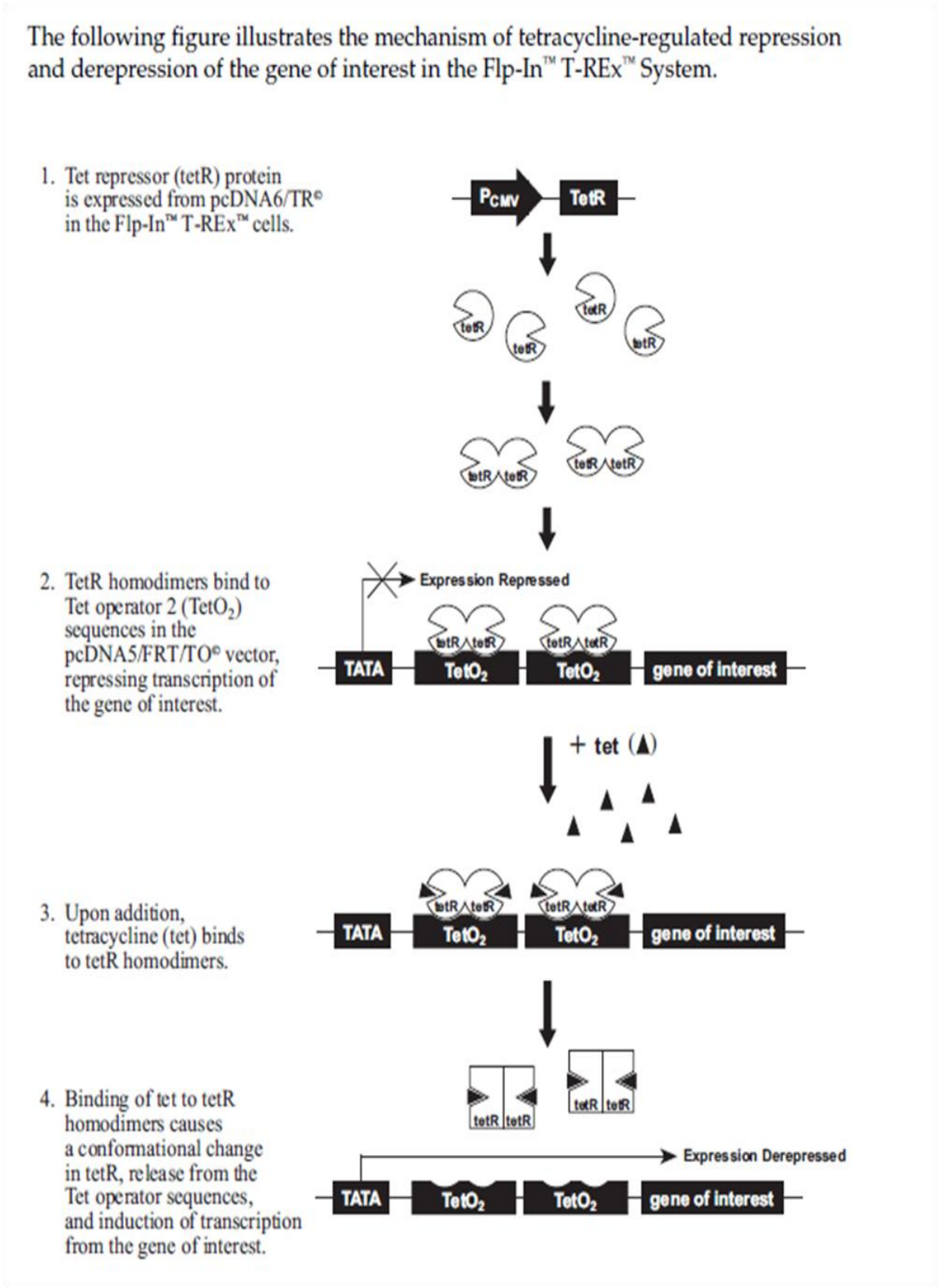

Figure 5.3 – Diagrammatic representation of how tetracycline repression is mediated in T-REx HEK293 Fv2E-IRE1α cells.

This was obtained from the instruction manual of Invitrogen's Flp-InTM system.

Thus, through use of cells that exhibit inducible expression of an HA–tagged Fv2E-IRE1α protein, the experiments in this section aim to achieve the following:

1. Design a co-immunoprecipitation assay that can be used to isolate Fv2E-IRE1α and TRAF2.
2. Determine if interaction between IRE1α and TRAF2 suffices to cause apoptotic cell death.
3. Confirm that Fv2E-IRE1α is capable of splicing *XBP1* in order to elucidate a direct mechanism for cell death rather than one that arises indirectly from a lack of protective XBP1 signalling.
4. Determine whether IRE1α RNase activity is required for the interaction with TRAF2 and subsequent downstream JNK signalling.

5.2 Results

5.2.1 Dimerised Fv2E-IRE1α co-immunoprecipitates with TRAF2

In order to show that the interaction between IRE1α and TRAF2 is sufficient to cause cell death, it was first essential to show that Fv2E-IRE1α forms a complex with TRAF2 *in vivo*. It was decided that the best way to confirm this would be to attempt to isolate the complex using a co-immunoprecipitation (co-IP) assay with Fv2E-IRE1α acting as 'bait' for TRAF2. However, before this could be done, it was necessary to confirm that Fv2E-IRE1α could be reliably induced using tetracycline and that it could be successfully isolated during the co-IP assay.

5.2.1.1 Fv2E-IRE1α can be induced with tetracycline and isolated using antibodies against its HA tag

To prove that Fv2E-IRE1α protein could be successfully induced and isolated, an initial co-IP experiment was carried out using Flp-In T-REx HEK293 Fv2E-IRE1α cells that had been treated for 24 h with 1 μg/ml tetracycline or an equal volume of 100% ethanol (the vehicle used to deliver the tetracycline) prior to harvesting (section 3.5.4). In order to determine the best method of isolating the Fv2E-IRE1α protein, individual samples were combined with primary antibodies raised against IRE1α (at a 1:50 dilution), HA-tags (at a 1:200 dilution) or Fv2E domains (at a dilution of 1:50) during a co-IP assay, as described

in section 3.5.7.1. The proteins retained from the co-IP assay were then separated via gel electrophoresis (section 3.5.9) and visualised via Western blotting with antibodies against IRE1α (1:1000) and TRAF2 (1:100) (section 3.5.12).

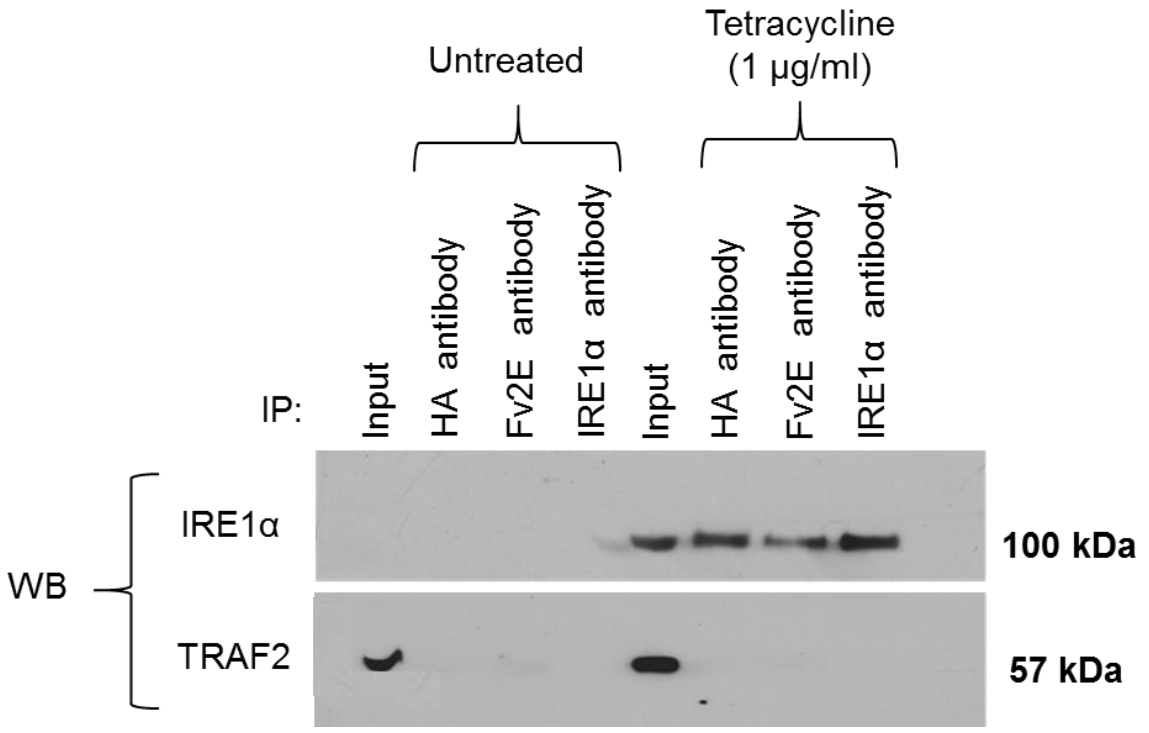

Figure 5.4 – Co-immunoprecipitation of Fv2E-IRE1α and TRAF2 with antibodies against the Fv2E domain, IRE1alpha, and the HA-epitope.
Flp-In T-REx HEK293 Fv2E-IRE1α cell lysates were treated with 1 µg/ml tetracycline or an equal volume of EtOH (vehicle) for 24 h. Cell lysates were then obtained co-immunoprecipitation assays were carried out using a variety of different antibodies to isolate Fv2E-IRE1α. 'Input' samples contained whole cell lysates as positive controls.

As can be seen in Figure 5.4 there are no detectable IRE1α bands present in any of the samples that have not been treated with tetracycline. This result suggested that the tetracycline inducible Fv2E-IRE1α construct is working and negligible amounts of Fv2E-IRE1α protein were produced in the absence of tetracycline induction. In contrast to the untreated samples, the samples that were obtained from cells that had been treated with tetracycline produced bands representing Fv2E-IRE1α in the input lane, which contained whole cell lysates, and all 3 of the samples that had been subject to the co-immunoprecipitation assay. This not only confirmed that the Fv2E-IRE1α could be successfully induced with tetracycline, but also that it could be isolated using antibodies against IRE1α, the HA tag or the Fv2E domain.

On the bottom half of Figure 5.4 it is clear to see that bands representing TRAF2 appeared in both "input" lanes, but none of the co-IP samples. The absence of TRAF2 in the co-IP

samples supports the work of Urano et al (Urano et al., 2000b) who state that only active, dimerised IRE1α can interact with TRAF2. This would also appear to be true of the Fv2E system because, whilst the Fv2E-IRE1α protein was present, it should only dimerise, and become active, in the presence of AP20187 (Spencer et al., 1993, Lu et al., 2004a), and therefore the lack of TRAF2 in these samples would be expected. Thus, given the results obtained in Figure 5.4, it can be concluded that that detectable levels of Fv2E-IRE1α production are only induced in the presence of tetracycline and that when the protein is produced it can be isolated via co-immunoprecipitation using antibodies against IRE1α, the HA-tag or the Fv2E domain.

5.2.1.2 TRAF2 secondary antibodies do not detect rabbit IgG chains

When planning the co-IP experiments it was noted that TRAF2 and the heavy IgG chains of antibodies have very similar molecular weights, with the mass of TRAF2 being 57 kDa and the mass of heavy IgG chains being 55 kDa. This was something that had the potential to be problematic when carrying out co-immunoprecipitation (co-IP) assays because the antibodies used to isolate proteins during the co-IP are retained in the samples during Western blotting. Under normal circumstances this is not a concern because the heavy IgG chains will be separated from the target protein during gel electrophoresis owing to their different sizes. However, with TRAF2 and heavy IgG chains differing by just 2 kDa, it is unlikely that gel electrophoresis would be able to reliably resolve the two proteins. In an attempt to avoid this problem it was decided that rabbit primary antibodies would be used to isolate Fv2E-IRE1α during the co-IP and mouse primary antibodies would be used to visualise TRAF2 during Western blotting. This had the potential to prevent any issues in distinguishing between TRAF2 and the heavy IgG chains because the mouse secondary antibodies (which are conjugated to horseradish peroxidase (HRP) and allow detection of protein during Western blotting) should not interact with the rabbit primary antibodies that had been used during the co-IP. If this worked then it would not matter that TRAF2 and the rabbit IgG heavy chains were the same size, as only proteins bound by the mouse secondary antibodies would be visible during Western blotting. However, cross-reactivity between antibodies from different species can occur, so it was essential to prove the specificity of the mouse secondary antibody before any progress could be made with the rest of the study.

The data obtained in Figure 5.4 was encouraging in suggesting that there would be no significant cross-reactivity because no bands were detected in the co-IP samples, even

though the primary rabbit IgG chains would have been present. However, the quantities of TRAF2 retained in during interaction with IRE1α had the potential to be extremely low (section 5.2.1.3) and therefore additional evidence was required to be confident that bands appearing at 57 kDa were TRAF2 and not an artefact of the rabbit IgG chains.

In order to achieve this, Flp-In T-REx HEK293 Fv2E-IRE1α cells were treated with tetracycline and/or AP20187 during a 48 h timecourse. The cell lysates were then harvested and the co-IP protocol was carried out as normal (methods section 3.5.7.1). The co-IP samples were then analysed via Western blotting using antibodies against the HA-tag of IRE1α and TRAF2 itself. Having visualised TRAF2, the bottom half of the membrane (containing proteins weighing 70 kDa or less) was stripped and re-probed with rabbit secondary antibodies, which would detect the rabbit IgG chains from the co-IP.

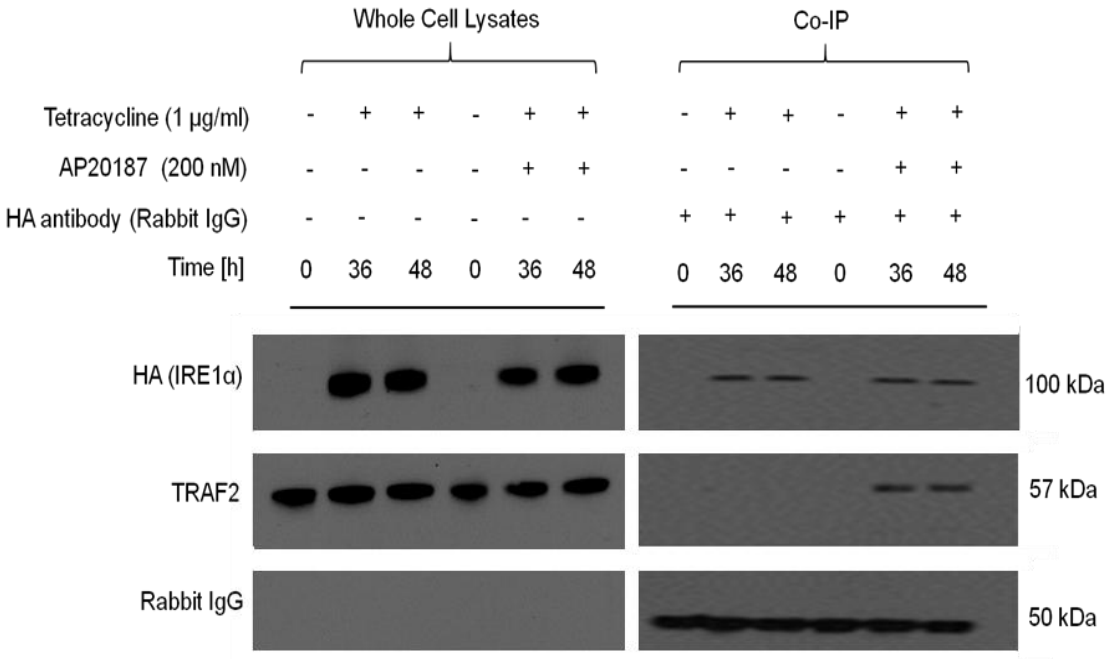

Figure 5.5 – Co-immunoprecipitation of TRAF2 and Fv2E-IRE1α without any detectable cross-reactivity of the mouse secondary antibody and rabbit IgG chains.
Flp-In T-REx HEK293 Fv2E-IRE1α cells were treated with tetracycline and AP20187 as indicated during a 48 h timecourse. The lysates were then collected and a co-immunoprecipitation assay was carried out, during which Fv2E-IRE1α was targeted with an HA-tag antibody. Analysis of the protein retained from the co-immunoprecipitation assay was carried out via Western blotting with the antibodies shown in the figure.

As can be seen from Figure 5.9, when the proteins obtained from the co-IP were probed with rabbit secondary antibodies, bands representing rabbit IgG chains appeared in all six lanes. This result that would be expected because the HA primary antibody (which is a rabbit antibody) was present in all six samples owing to its use during the co-IP. In contrast to this, there are no bands visible in the samples that have not been treated with AP20187 when using mouse secondary antibodies to visualise the TRAF2. Therefore, knowing that the rabbit IgG chains are present, it is clear that the mouse secondary antibody is not

exhibiting detectable cross-reactivity with the HA antibody used during the co-IP and therefore confidence can be held in the fact that bands produced when using the TRAF2 antibody are indeed TRAF2.

5.2.1.3 Fv2E-IRE1α binds to TRAF2 in an AP20187 dependent manner

Fv2E-IRE1α can be successfully induced and isolated during co-IP assays (5.2.1.1) and therefore it is possible to determine if an interaction with TRAF2 can be observed. It is currently believed that IRE1α only interacts with TRAF2 when activated by during ER stress (Urano et al., 2000b, Nishitoh et al., 2002). In wild type cells IRE1α activation is caused by its luminal domain detecting the accumulation of misfolded proteins, a stimulus that causes dimerisation and autophosphorylation of IRE1α (Shamu and Walter, 1996). However, in this system IRE1α does not possess a luminal domain but, instead, the cytoplasmic effector domain of IRE1α is attached to an Fv2E domain. Fv2E domains have been shown to dimerise in the presence of AP20187 (Spencer et al., 1993) and the PERK branch of the UPR has been shown to be induced when cells expressing Fv2E-PERK have been treated with this drug (Deng et al., 2004). Therefore, AP20187 treatment should also cause dimerisation of Fv2E-IRE1α, mimicking the activation caused by misfolded proteins and inducing an interaction with TRAF2 (Figure 5.6).

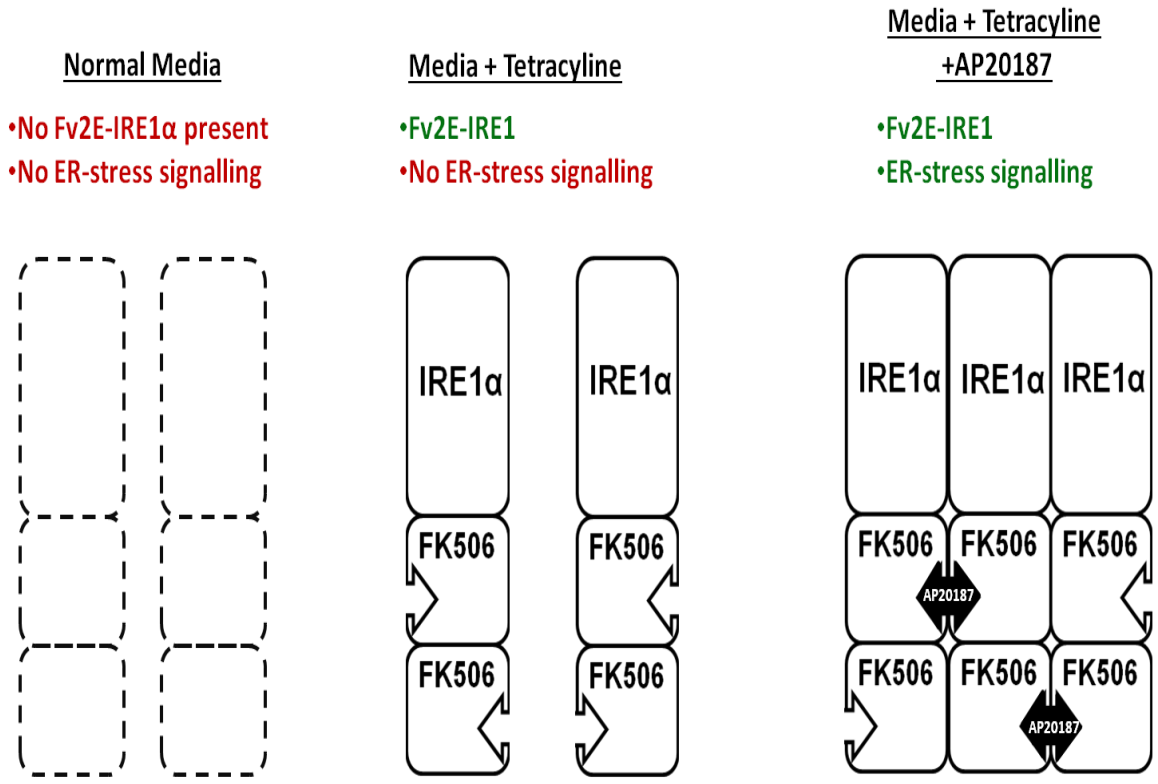

Figure 5.6 – The proposed mechanism by which AP20187 induced FV2E-IRE1α signalling.

To investigate whether AP20187 induces interaction between Fv2E-IRE1α and TRAF2, Flp-In T-REx HEK293 Fv2E-IRE1α cells were treated with tetracycline (1 μg/ml) or AP20187 (200 nM) as indicated for either 36 or 48 h. After the time course a co-immunoprecipitation assay was carried out (section 3.5.7.1) using an HA-tag antibody (at a 1:200 dilution) to retain the Fv2E-IRE1α protein. The resulting lysates were then analysed via Western blotting using antibodies against both IRE1α and TRAF2 proteins (methods section 3.5.12). The experiment was carried out in biological triplicate and the results are shown in figures 5.7 - 5.9.

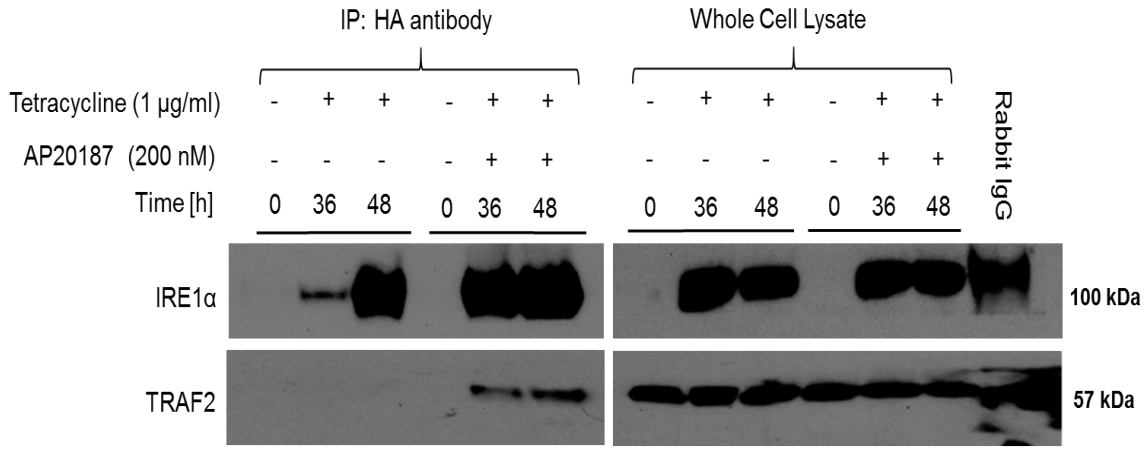

Figure 5.7 –Co-immunoprecipitation of Fv2E-IRE1α and TRAF2.
Flp-In T-REx HEK293 Fv2E-IRE1α cells were treated with tetracycline and AP20187 as indicated during a 48 h timecourse. The lysates were then immunoprecipitated with an HA-tag antibody. Analysis of the protein retained from the co- immunoprecipitation assay was carried out by Western blotting with the antibodies shown in the figure.

Fv2E-IRE1α is only detected when the cells have been treated with tetracycline (Figure 5.7), thus showing that the induction of the Fv2E-IRE1α construct is working as it should. In addition to this, TRAF2 is only retained when the cells have been treated with both tetracycline and AP20187. This confirms that Fv2E-IRE1α only interacts with TRAF2 in the presence of AP20187, which is most likely to be a result of the formation of Fv2E-IRE1α dimers/oligomers. Therefore, these data support the hypothesis thatFv2E-IRE1α protein successfully replicates the initial signalling observed when studying wild type IRE1α during conditions of ER stress (Urano et al., 2000b).

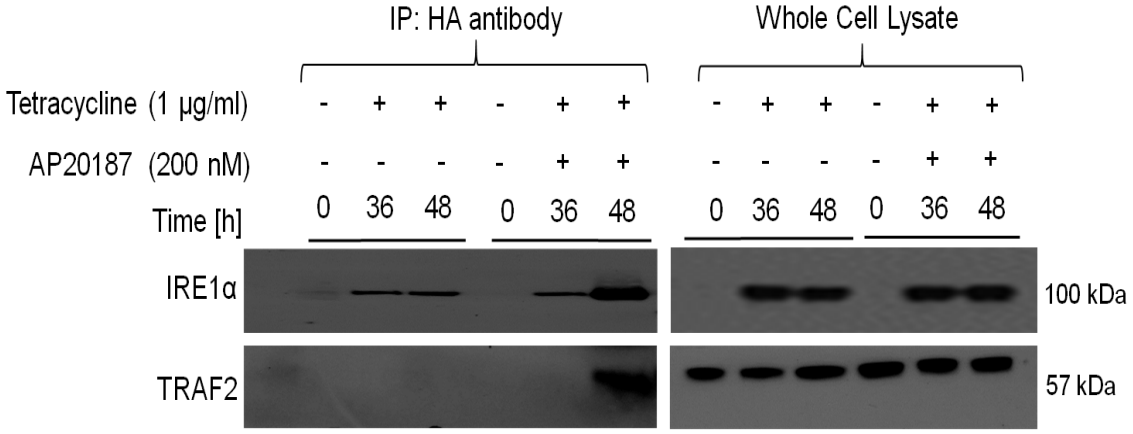

Figure 5.8 - Co-immunoprecipitation of Fv2E-IRE1α and TRAF2.
Flp-In T-REx HEK293 Fv2E-IRE1α cells were treated with tetracycline and AP20187 as indicated during a 48 h timecourse. The lysates were then collected and a co-immunoprecipitation assay was carried out, during which Fv2E-IRE1α was targeted with an HA-tag antibody. Analysis of the protein retained from the co-immunoprecipitation assay was carried out by Western blotting with the antibodies shown in the figure.

Figure 5.8 is a biological repeat of the experiment carried out in Figure 5.7 and re-affirms that Fv2E-IRE1α is only capable of interacting with TRAF2 when it is in the presence of AP20187. Whilst there is no TRAF2 obtained at the 36 h time point, this may have been due to the fact that only a small quantity of IRE1α was retained during the co-IP. However, this is a problem that is very difficult to remedy as the length of the co-IP assay combined with the number of washes makes retaining equal quantities of protein extremely challenging. This is why carrying out repeats is important and, whilst not perfect; this result still supports the hypothesis that dimerised/oligomerised IRE1α binds TRAF2.

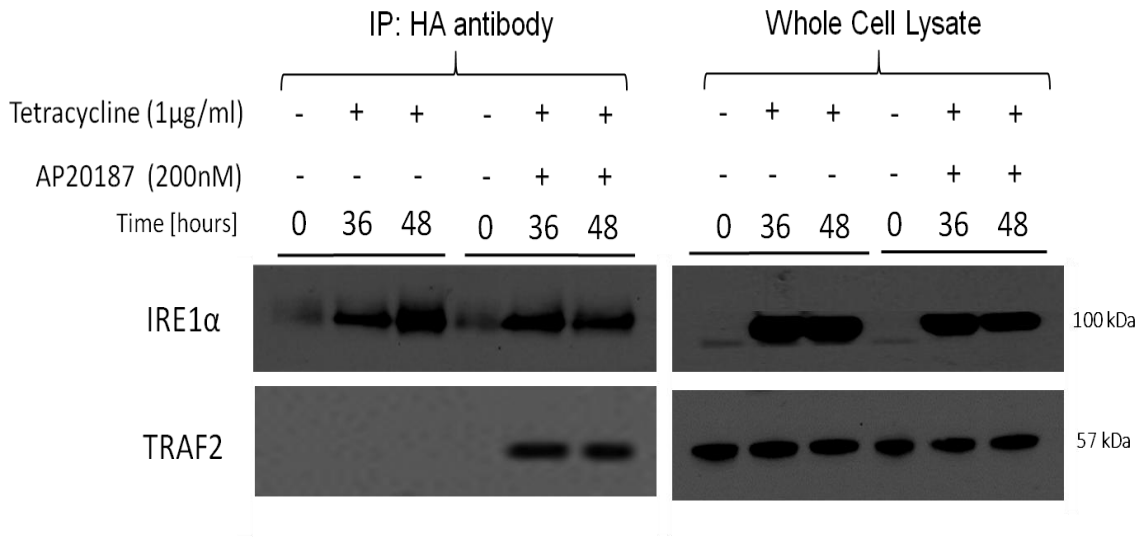

Figure 5.9 - Co-immunoprecipitation of Fv2E-IRE1α and TRAF2.
Flp-In T-REx HEK293 Fv2E-IRE1α cells were treated with tetracycline and AP20187 as indicated during a 48 h timecourse. The lysates were then collected and a co-immunoprecipitation assay was carried out, during which Fv2E-IRE1α was targeted with an HA-tag antibody. Analysis of the protein retained from the co-immunoprecipitation assay was carried out via Western blotting with the antibodies shown in the figure.

Figure 5.9 is the third biological repeat of this series of experiments and provides triplicate data supporting the hypothesis that Fv2E-IRE1α is capable of interacting with TRAF2, but only in the presence of AP20187. This Western blot clearly shows that IRE1α does not interact with TRAF2 in the absence of AP20187, but upon treatment with AP20187 TRAF2 is retained at both 36 h and 48 h. Therefore, from the evidence presented in this section it would appear that Fv2E-IRE1α successfully models the interaction between wild type IRE1α and TRAF2 (Urano et al., 2000b, Nishitoh et al., 2002). In its monomeric form, Fv2E-IRE1α does not interact with TRAF2 and thus replicates the actions of endogenous IRE1α during periods where there is little or no ER stress. However, upon treatment with AP20187 (which assumedly results in dimerisation/oligomerisation), Fv2E-IRE1α binds TRAF2, thus replicating wild type IRE1α during ER-stress.

5.2.2 Dimerisation of Fv2E-IRE1α with AP20187 suffices to cause apoptotic cell death

5.2.2.1 AP20187 specifically activates Fv2E-IRE1α

In order to present this model as an alternative to ER stress mimetic drugs it was important to show that any downstream signalling was the result of AP20187 acting upon IRE1α in isolation and not the result of AP20187 causing a generic ER stress response in a similar way to drugs such as thapsigargin (Thastrup et al., 1990) or tunicamycin (Kaufman, 1999). This would significantly increase the impact of this model because there is currently no method of isolating IRE1α signalling *in vivo*. Therefore, in order to show that AP20187 is specific to Fv2E-IRE1α and does not activate other ER stress sensors, it was decided that it should be determined whether AP20187 treatment causes any detectable activation of PERK signalling.

As discussed during the introduction, PERK mediates its UPR signalling via the phosphorylation of eukaryotic translation initiation factor 2α (eIF2α) (Harding et al., 1999). Therefore, knowing that the phosphorylation of eIF2α is essential for PERK-mediated UPR signalling, it was decided to measure the level of phospho-eIF2α during AP20187 treatment. Thus, Flp-In T-REx HEK293 Fv2E-IRE1α cells were treated with AP20187 at a concentration of 200 nM and/or 1 μg/ml tetracycline at the appropriate time points, whilst negative control samples were treated with the same volume of 100% EtOH. A cell lysate from cells treated with 2 μM thapsigargin for 48 h was also included as a positive control for p-eIF2α (Thastrup et al., 1990). Lysates were obtained as described in sections 3.5.7.1 and antibodies against phospho-eIF2α and total eIF2α were used to visualise the amounts of each protein as detailed in the materials and methods (section 3.5.12).

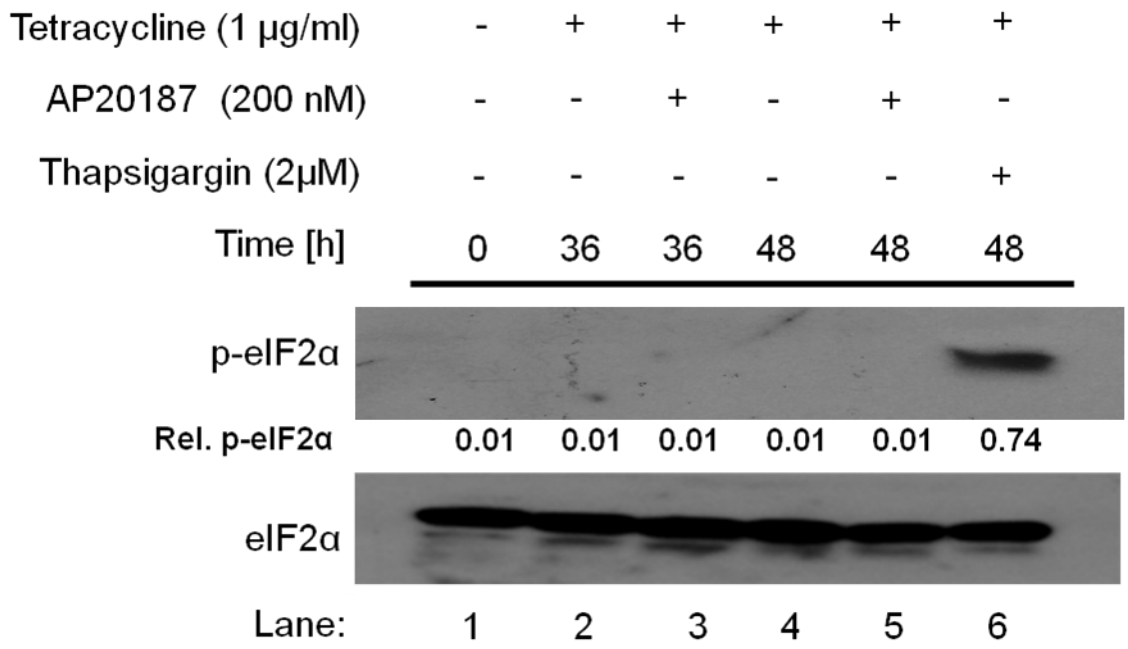

Figure 5.10 – AP20187 does not induce phosphorylation of eIF2α
Cell lysates were collected from Flp-In T-REx HEK293 Fv2E-IRE1α cells that had been treated with thapsigargin, AP20187 and tetracycline as indicated. Western blotting was used to visualise the target proteins and Image J was used to quantify any bands that were detected.

As can be seen from figure 5.10, all lanes contained eIF2α, but phosphorylated eIF2α was only detected in the cell lysate obtained from thapsigargin-treated cells, suggesting that AP20187 treatment does not induce PERK signalling. This combined with other reports stating that AP20187 does not induce ER stress (Lu et al., 2004a, Deng et al., 2004) is sufficient to conclude that AP20187 is unlikely to cause ER stress in Flp-In T-REx HEK293 Fv2E-IRE1α cells. Consequently, this means that the Flp-In T-REx Fv2E-IRE1α system has a significant advantage over traditional ER stress models when it comes to elucidating the precise mechanism of IRE1α signalling because it allows the specific activation of IRE1α, as opposed to the activation of the entire UPR.

5.2.2.2 AP20187 causes cell death in a Fv2E-IRE1α dependent manner

AP20187 treatment causes IRE1α to interact with TRAF2 (see section 5.2.1.3). However, this does not provide evidence that Fv2E-IRE1α is capable of replicating the signalling observed when wild-type IRE1α interacts with TRAF2 *in vivo*. Therefore, this section aims to provide evidence that Fv2E-IRE1α is capable of instigating apoptosis upon treatment with AP20187. In order to achieve this, Flp-In T-REx HEK293 Fv2E-IRE1α cells were subjected to a 48 h time course during which select samples were treated with 1 µg/ml tetracycline and/or 200 nM AP20187 for either 36 or 48 h before being analysed via MTT

colourimetric assay (Gerlier and Thomasset, 1986) in order to quantify any cell death induced during treatment with AP20187 (methods section 3.3.10).

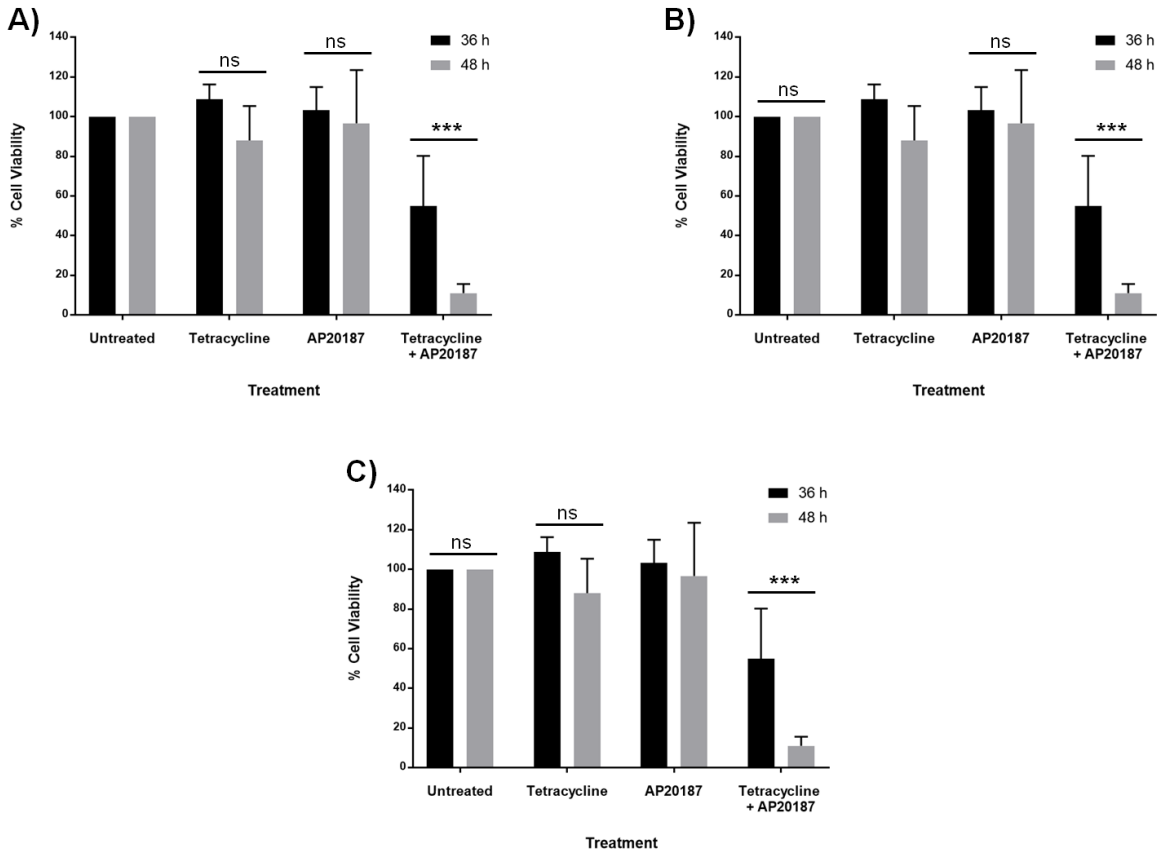

Figure 5.11 – Treatment of Flp-In T-REx HEK293 Fv2E-IRE1α cells with tetracycline and AP20187 causes a significant reduction in cell viability.

Flp-In T-REx HEK293 Fv2E-IRE1α cells were treated with tetracycline (1 µg/ml) and AP20187 (200 nM) as indicated for either 36 h or 48 h before viability was assessed using an MTT assay. The values obtained for the untreated cells were used to set a baseline number for 100% viability and the other samples' viability were calculated based of this. Three biological repeats were carried out to ensure reliability and statistical analysis was performed using Graphpad Prism software, which was used to carry out a two way ANOVA test for significance combined with Tukey's adjustment for multiple comparisons. The bars represent standard error and significance is denoted as not significant (ns), p= ≤0.05 (*), p= ≤0.01 (**), p= ≤0.001 (***).

A) Comparison of the viability detected in untreated cells against all other treatments.
B) Comparison of the viability detected in cells that had only been treated with tetracycline against all other treatments.
C) Comparison of the viability detected in cells that had only been treated with AP20187 against all other treatments.

As can be seen from the data presented in Figure 5.11, there was no significant difference in viability when comparing data obtained from either untreated Flp-In T-REx HEK293 Fv2E-IRE1α cells, cells that had been treated solely with tetracycline or those that had been treated solely with AP20187. However, there was a significant decrease in cell viability when cells from any of these treatments were compared with cells that had been treated with tetracycline in conjunction with AP20187. Therefore, these data indicate that AP20187 instigates cell death in a Fv2E-IRE1α dependent manner, a conclusion that can

be drawn in confidence because neither tetracycline nor AP20187 caused significant changes in cell viability when used in isolation.

5.2.2.3 36 h and 48 h time points represent the best time points to study IRE1α-TRAF2 induced JNK signalling

It has been reported that prolonged IRE1α signalling (>12 h) results in the downstream activation of apoptotic JNK signalling (Urano et al., 2000b, Nishitoh et al., 2002) and therefore, based on the data showing that AP20187 induces cell death in an IRE1α dependent manner (section 5.2.2.2), it was decided that it would be worth investigating whether phospho-JNK levels were elevated during AP20187 treatment. In addition to this it was also decided that Poly (ADP-Ribose) Polymerase 1 (PARP-1) cleavage should be measured. The cleavage of PARP-1 is an event that is well regarded as being a marker for cell death (Kaufmann et al., 1993) and, unlike the MTT assay, which just shows that cells are dying, PARP-1 cleavage would indicate that the mechanism of cell death is apoptosis. Furthermore, PARP-1 cleavage has previously been shown to be mediated by upstream JNK signalling via the mitochondrial cell death pathway (Lei and Davis, 2003, Yang et al., 2006a).

To obtain data on the downstream signalling of Fv2E-IRE1α, Flp-In T-REx HEK293 Fv2E-IRE1α cells were treated with either tetracycline (1 μg/ml) or AP20187 (200 nM) for 12, 24, 36, 48 and 72 h prior to harvesting. Proteins from the cell lysates were then separated via gel electrophoresis and analysed via Western blotting using antibodies against the HA-tag of Fv2E-IRE1α, PARP-1, phospho-JNK, total JNK and GAPDH as described in sections 3.5.9 and 3.5.12 respectively.

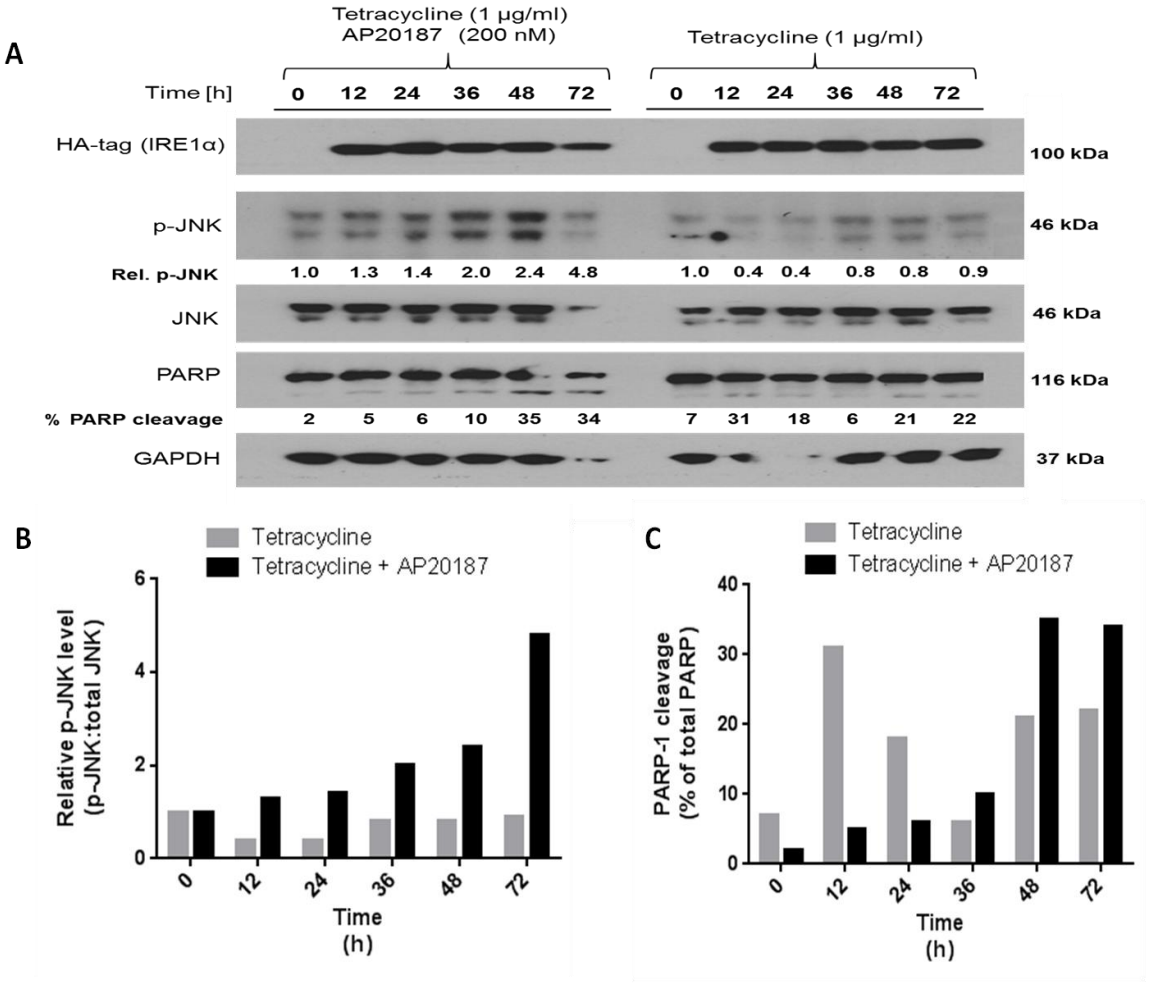

Figure 5.12 –AP20187 treatment induces elevations in p-JNK and PARP-1 cleavage.

A) Western blot showing the amount of p-IRE1α, IRE1α, p-JNK, JNK and PARP-1 proteins obtained from Flp-In T-REx HEK293 Fv2E-IRE1α cells that have been treated with tetracycline and AP20187 as shown. '0 h' samples were treated with 100% EtOH (vehicle) and the antibodies used during Western blotting are shown to the left of the image.

B) Quantification of relative phospho-JNK levels. Untreated cells were normalised to a value of 1.0.

C) Quantification of cleaved PARP-1 levels as a percentage of total PARP-1.

Quantification of protein levels was carried out using Image J software.

The image produced at the end of the 72 h time course revealed that Fv2E-IRE1α is only detectable in the presence of tetracycline, supporting the results presented in section 5.2.1.1. To give an accurate impression as to the levels of JNK signalling, the phospho-JNK bands were quantified using Image J software and then presented as a proportion of the total amount of JNK. The results of this quantification are shown in Figure 5.12 (A) and as a graph in Figure 5.12 (B). As can be seen from these data, the level of phospho-JNK remained fairly consistent over the whole 72 h time course in the cells that were treated solely with tetracycline. This was also the case in the first 24 h of the cells treated with tetracycline and AP20187. However, a steady increase in the relative amount of phospho-JNK was observed during the 36, 48 and 72 h time points in the AP20187-treated

cells. These data therefore gave an early indication that AP20187 was eliciting an inflammatory stress response in an Fv2E-IRE1α dependent manner.

The other marker that was used to measure stress in this preliminary investigation was PARP-1 cleavage, which was measured using Image J and presented as a percentage of total PARP-1 protein (Figure 5.12 (A) and 5.12 (C)). PARP-1 cleavage remained at a low basal level in the cells that had only been treated with tetracycline barring the 12 h time point, which may be an anomaly, but without repeating the experiment it is impossible to tell. The cells that had been treated with AP20187, as well as tetracycline, showed a ~3.5-fold increase in the amount of PARP-1 cleavage between 36 h and 48 h. This would therefore fit a model that proposes IRE1α signalling results in an increase in phospho-JNK (observed at 36 h) and that increasing phospho-JNK signalling results apoptotic signalling and the activation of PARP-1 cleavage (at 48 h).

5.2.2.4 AP20187 causes IRE1α autophosphorylation and downstream activation of JNK and PARP-1

In addition to quantifying elevations in phospho-JNK and PARP-1 cleavage, it was also decided that phospho-IRE1α should be measured as well. This was decided because in wild type cells IRE1α undergoes autophosphorylation after dimerisation during ER stress and therefore it should also be determined if treatment with AP20187 causes phosphorylation of Fv2E-IRE1α. If it were found that treatment with AP20187 did cause significant increases in phospho-IRE1α it would provide strong foundations for determining if this phosphorylation was essential for interaction with TRAF2 and subsequent apoptotic signalling when using point mutants of IRE1α (section 5.2.4).

Based on the data shown in Figure 5.12, it was decided that the 36 h and 48 h time points would be most useful for studying signalling downstream of Fv2E-IRE1α because these time points exhibited the sharpest increases in phospho-JNK and PARP-1 cleavage. The decision to disregard the 72 h time point was made because there was so much cell death by this time that it was difficult to obtain enough protein for western blotting. Another reason for not wanting to use the 72 h time point is that, when large amounts of cell death are occurring, there will be strong signalling across a variety of different stress signalling pathways and many of these will contribute to the elevation of markers such as phospho-JNK and PARP-1 cleavage (Weston and Davis, 2002). This is a scenario which is not conducive to trying to study the IRE1α signalling pathway in isolation and, whilst it is impossible to completely avoid cross-talk between signalling pathways *in vivo*, it is

preferable to avoid it as much as possible when trying to elucidate the actions of a single effector.

To obtain data regarding the effect of AP20187 treatment upon the level of phospho-IRE1α, phospho-JNK and PARP-1 cleavage, Flp-In T-REx HEK293 Fv2E-IRE1α cells were treated with AP20187 at a concentration of 200 nM and/or 1 μg/ml tetracycline, whilst control samples were treated with the same volume of 100% EtOH. Proteins were then harvested as described in section 3.5.7.1, before being separated via gel electrophoresis (section 3.5.9.1) and quantified via Western blotting (section 3.5.12). During Western blotting, antibodies against phospho-IRE1α, phospho-JNK, the HA-tag of Fv2E-IRE1α, total JNK and PARP-1 were used and all of the results were obtained in biological triplicate in order to ensure validity.

Figure 5.13 (A) shows that the addition of AP20187 causes an observable increase in IRE1α and JNK phosphorylation and PARP-1 cleavage at both the 36 h and 48 h time points when compared to their untreated counterparts. Statistical analysis revealed that treatment with tetracycline alone had no significant effect on the level of either phospho-JNK or PARP-1 cleavage after 36 h or 48 h (Figure 5.13 C and D). However, tetracycline used in combination with AP20187 resulted in a significant increase in both JNK phosphorylation and PARP-1 cleavage at both time points (Figure 5.13 C and D). When investigating the phosphorylation of IRE1α it wasn't possible to use untreated cells as a control because the Fv2E-IRE1α protein is only transcribed in the presence of AP2187. Therefore, a one way ANOVA was used to compare all samples against one another. The results of this analysis showed no significant difference between cells that had received the same treatment. However, there was a significant increase in IRE1α phosphorylation in cells that were treated with both AP20187 and tetracycline when compared those that had been treated with tetracycline alone (Figure 5.13 B). Therefore, the data presented in Figure 5.13 clearly indicates that AP20187 causes IRE1α phosphorylation, JNK phosphorylation and PARP-1 cleavage in cells where FV2E-IRE1α is expressed. However, induction of Fv2E-IRE1α synthesis in the absence of AP20187 does not result in the aforementioned effects.

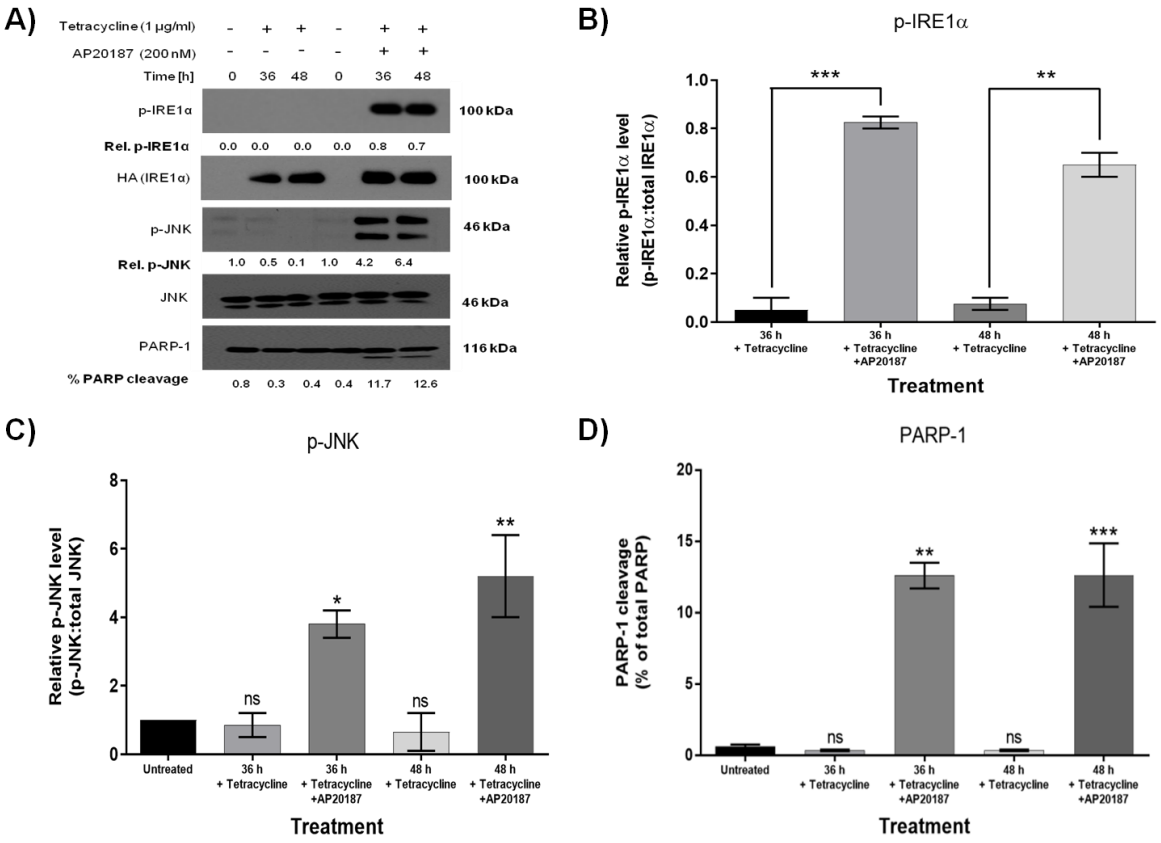

Figure 5.13 –AP20187 treatment of Flp-In T-REx HEK293 Fv2E-IRE1α cells induces elevations in p-IRE1α, p-JNK and PARP-1 cleavage.

A) Western blot showing the amount of p-IRE1α, IRE1α, p-JNK, JNK and PARP-1 proteins obtained from Flp-In T-REx HEK293 Fv2E-IRE1α cells that had been treated with tetracycline and AP20187 as shown. '0 h' samples were treated with 100% EtOH (vehicle) and the antibodies used during Western blotting are shown to the left of the image.

B) Quantification and statistical analysis of relative phospho-IRE1α levels. Different treatments were compared with one another by way of a one way ANOVA test for significance combined with Tukey's adjustment for multiple comparisons. Whilst all of the samples were compared to another, the graph shows the significance of differences between cells that had been treated for the same amount of time.

C) Quantification and statistical analysis of relative phospho-JNK levels. Untreated cells were normalised to a value of 1.0 and then compared to the other samples by way of a one way ANOVA test for significance combined with Dunnett's method for multiple comparisons.

D) Quantification and statistical analysis of cleaved PARP-1 levels as a percentage of total PARP-1. Untreated cells were compared to the other samples by way of a one way ANOVA test for significance combined with Dunnett's method for multiple comparisons.

5.2.3 TRAF2 is required for the apoptotic cell death induced by active Fv2E-IRE1α

5.2.3.1 siRNAs targeting TRAF2 successfully reduce TRAF2 protein levels

Thus far, the data collected have indicated that AP20187 causes Fv2E-IRE1α to interact with TRAF2 (section 5.2.1.3) and induces cell death (section 5.2.2.2) via a pathway that involves signalling via JNK and PARP-1 (section 5.2.2.4). However, in order to confirm that apoptosis caused by Fv2E-IRE1α is dependent upon TRAF2, it was important to investigate what effect inhibiting/removing these proteins had upon Fv2E-IRE1α signalling. Therefore, in order to assess the role of TRAF2 in the IRE1α signalling cascade, siRNAs (materials section 2.7) were used to reduce TRAF2 protein translation (Figure 5.16).

To assess if the TRAF2 siRNA could be used to reduce TRAF2 protein levels, Flp-In T-REx HEK293 Fv2E-IRE1α cells were transfected with TRAF2 siRNA at a concentration of either 10 nM or 20 nM for 96 h in order to determine if the knockdown would work and, if so, which time points would see the greatest reduction in the amount of TRAF2 protein (for the method, see section 3.3.8). Protein samples were then harvested from the cells and analysis was carried out via Western blotting, as described in the materials and methods (section 3.5). During Western blotting antibodies raised against TRAF2 were used to measure the amount of TRAF2 and GAPDH was measured as a loading control.

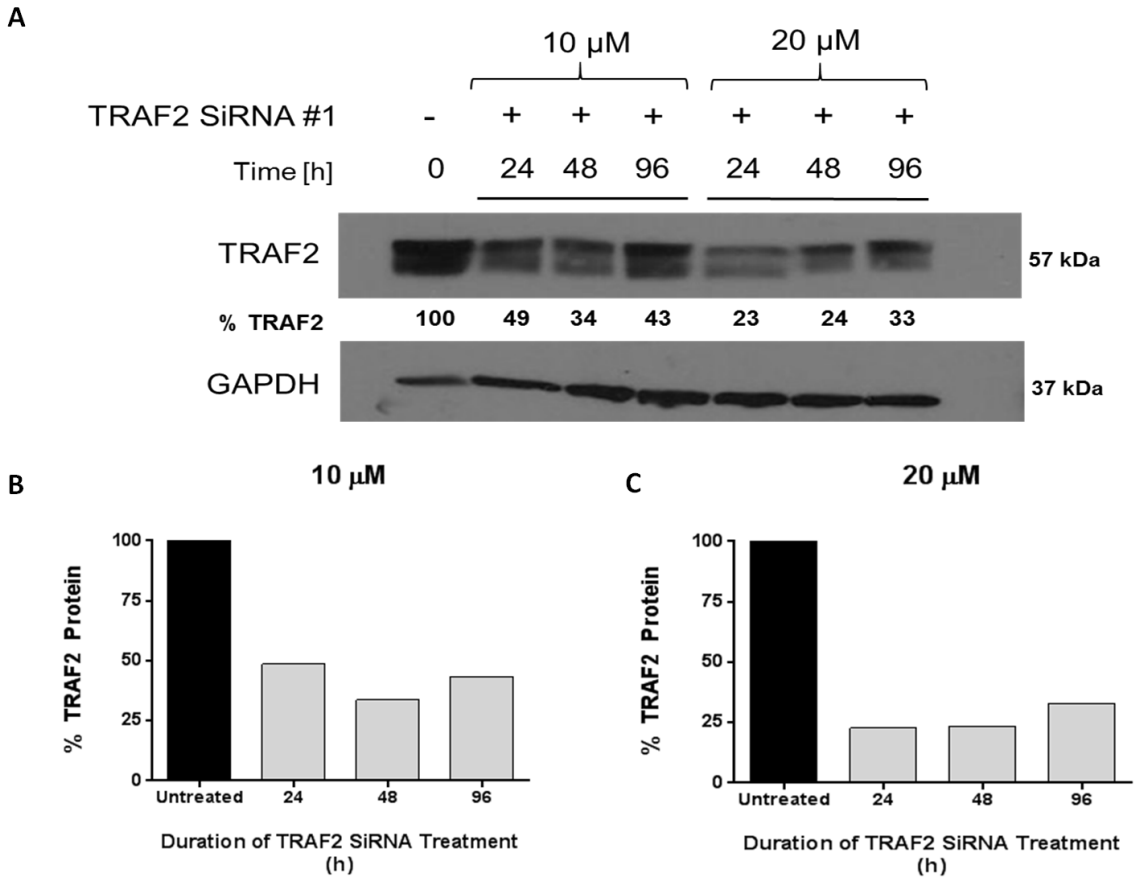

Figure 5.14- Transfection of Flp-In T-REx HEK293 Fv2E-IRE1α cells with TRAF2 siRNA reduces TRAF2 protein levels.

A) Western blot showing the amount of TRAF2 and GAPDH (loading control) proteins obtained from Flp-In T-REx HEK293 Fv2E-IRE1α cells that had been transfected with either 10 µM or 20 µM TRAF2 siRNA.

B) Quantification of the amount of TRAF2 protein when cells were transfected with 10 µM TRAF2 siRNA. Data were collected by quantifying the Western blot (A) using ImageJ software.

C) Quantification of the amount of TRAF2 protein when cells were transfected with 20 µM TRAF2 siRNA. Data were collected by quantifying the Western blot (A) using ImageJ software.

Figure 5.14 confirms that the TRAF 2 siRNA was successful in reducing the amount of TRAF2 protein as 20 µM of TRAF2 siRNA reduced the amount of TRAF2 protein by up to 77%. Therefore, having successfully knocked-down TRAF2, it was decided that it was possible to proceed to investigate the effects of this knock-down upon Fv2E-IRE1α signalling.

5.2.3.2 TRAF2 is required for Fv2E-IRE1α mediated JNK signalling and PARP-1 cleavage

In order to investigate the effects of TRAF2 knock-down upon JNK and PARP-1 signalling, Flp-In T-REx HEK293 Fv2E-IRE1α cells were treated with 20 μM of TRAF2 siRNA 24 h prior to the start of the time course. During the time course the cells were treated with tetracycline and AP20187 for either 36 or 48 h as in previous experiments (section 5.2.2.4). Protein samples were then harvested from the cells and analysed via Western blotting using antibodies against p-IRE1α, the HA tag of Fv2E-IRE1α, p-JNK, JNK and PARP-1 (materials and methods section 3.5). All of the experiments were carried out in triplicate and a representative Western blots is shown on the next page (Figure 5.15). The repeats of this experiment are shown in the appendices (appendices 2a and 2b).

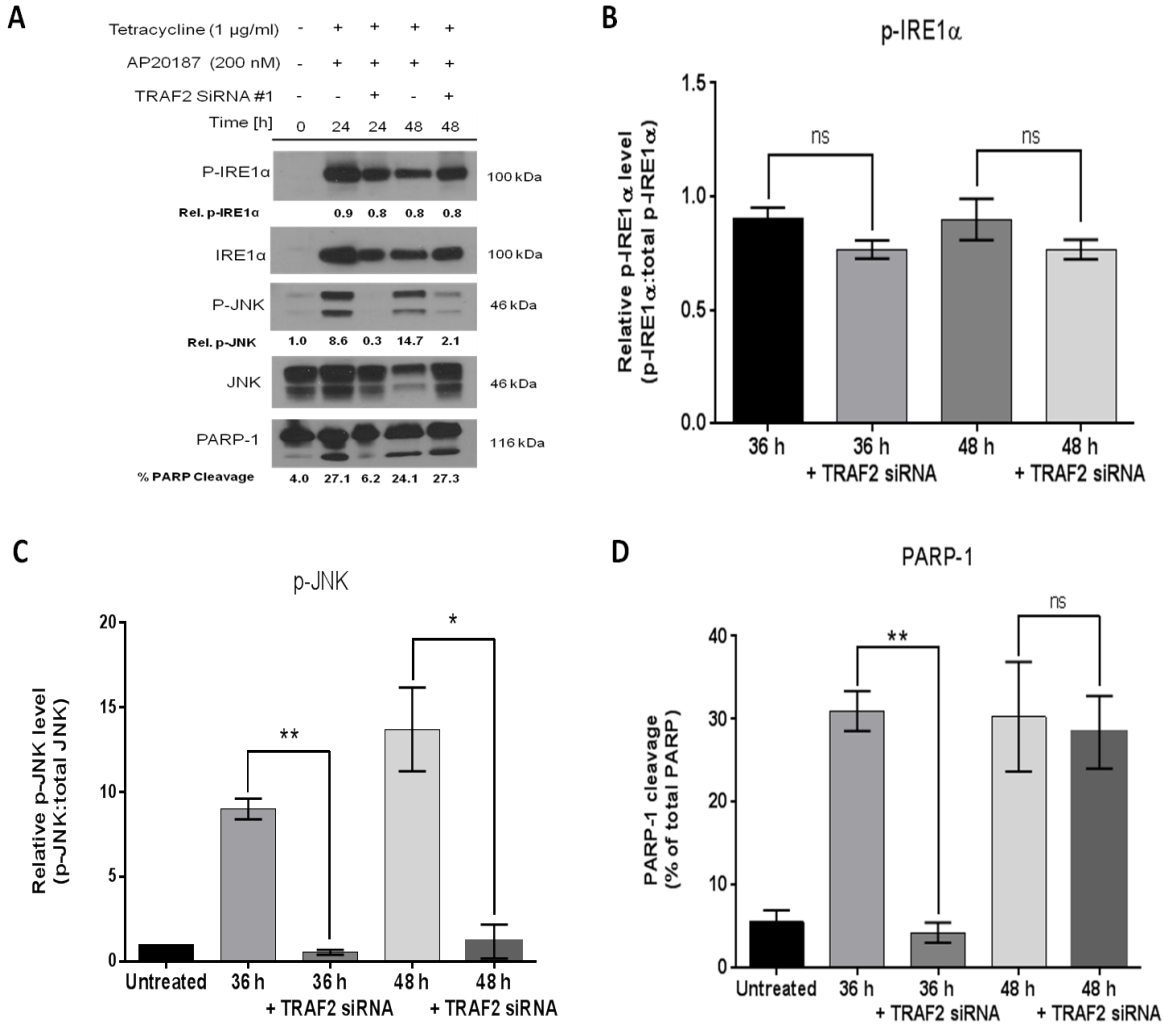

Figure 5.15 - TRAF2 knockdown reduces the amount of p-JNK and PARP-1 cleavage during Fv2E-IRE1α signalling.

A) Western blot showing the amounts of p-IRE1α, p-JNK and PARP-1 proteins obtained from Flp-In T-REx HEK293 Fv2E-IRE1α cells that had been treated with tetracycline (1 µg/ml), AP20187 (200 nM) and TRAF2 siRNA (20 µM) as indicated. Untreated p-JNK samples were normalised to '1.0' as a control and the same was done for the 24 h treatment without TRAF2 siRNA for p-IRE1α. The reason for this was because IRE1α was below detectable limits in the untreated samples.

B) Quantification and statistical analysis of the effect that TRAF2 knockdown has upon the level of p-IRE1α in cells that have been treated with tetracycline (1 µg/ml) and AP20187 (200 nM).

C) Quantification and statistical analysis of the effect that TRAF2 knockdown has upon the level of p-JNK in cells that have been treated with tetracycline (1 µg/ml) and AP20187 (200 nM).

D) Quantification and statistical analysis of the effect of TRAF2 knockdown upon the level of PARP-1 cleavage in cells that have been treated with tetracycline (1 µg/ml) and AP20187 (200 nM).

Quantification of protein levels was carried out using Image J software. 3 biological repeats were carried out to ensure reliability (appendices 3a and 3b) and statistical analysis was performed using Graphpad Prism software, which was used to carry out unpaired t-test with Welch's correction unequal variances in order to determine the significance of the results. The bars represent standard error and significance is denoted as not significant (ns), p= ≤0.05 (*), p= ≤0.01 (**) or p= ≤0.001 (***).

Figure 5.15 shows that reducing TRAF2 protein levels had no significant effect on Fv2E-IRE1α phosphorylation during AP20187 treatment, confirming that Fv2E-IRE1α autophosphorylation occurs upstream of the interaction with TRAF2 in the same way as in wild type cells (Tirasophon et al., 1998). In contrast to this, there were significant reductions in both the amount of phospho-JNK (p = ≤ 0.01) and PARP-1cleavage (p = ≤

0.01) when cells that had been treated with AP20187 were also treated with TRAF2 siRNA. Furthermore, there was also a significant reduction in p-JNK after 48 h ($p = \leq 0.05$). In contrast to this, siRNA treatment has no significant impact on the amount of PARP-1 cleavage that occurred after 48 h. The reason for this is unknown, but it may have been because TRAF2 levels were starting to recover or because other events were causing apoptosis by this point. However, the data collected from the 36 h time point suffices to confirm that the elevations in both p-JNK and PARP-1 that occur during Fv2E-IRE1α signalling (section 5.2.2.4) do so in a TRAF2 dependent manner.

5.2.3.3 The JNK inhibitor SP600125 fails to inhibit c-Jun phosphorylation

To assess the contribution of JNK to Fv2E-IRE1α signalling, Flp-In T-REx HEK293 Fv2E-IRE1α cells were treated with one or a combination of either tetracycline (1 μg/ml), AP20187 (200 nM) and a JNK inhibitor known as SP600125 (20 μM) (Bennett et al., 2001) during a 48 h timecourse. SP600125 was utilised in order to see downstream activation of PARP-1 could be abolished when JNK is prevented from activating its canonical downstream target c-jun (Morton et al., 2003). Once the time course had been completed the cells were harvested to produce lysates (section 3.5.7.1) that could be analysed via Western blotting (section 3.5.12), which was carried out using antibodies against the HA tag of Fv2E-IRE1α, c-jun, and PARP (Figure 5.16).

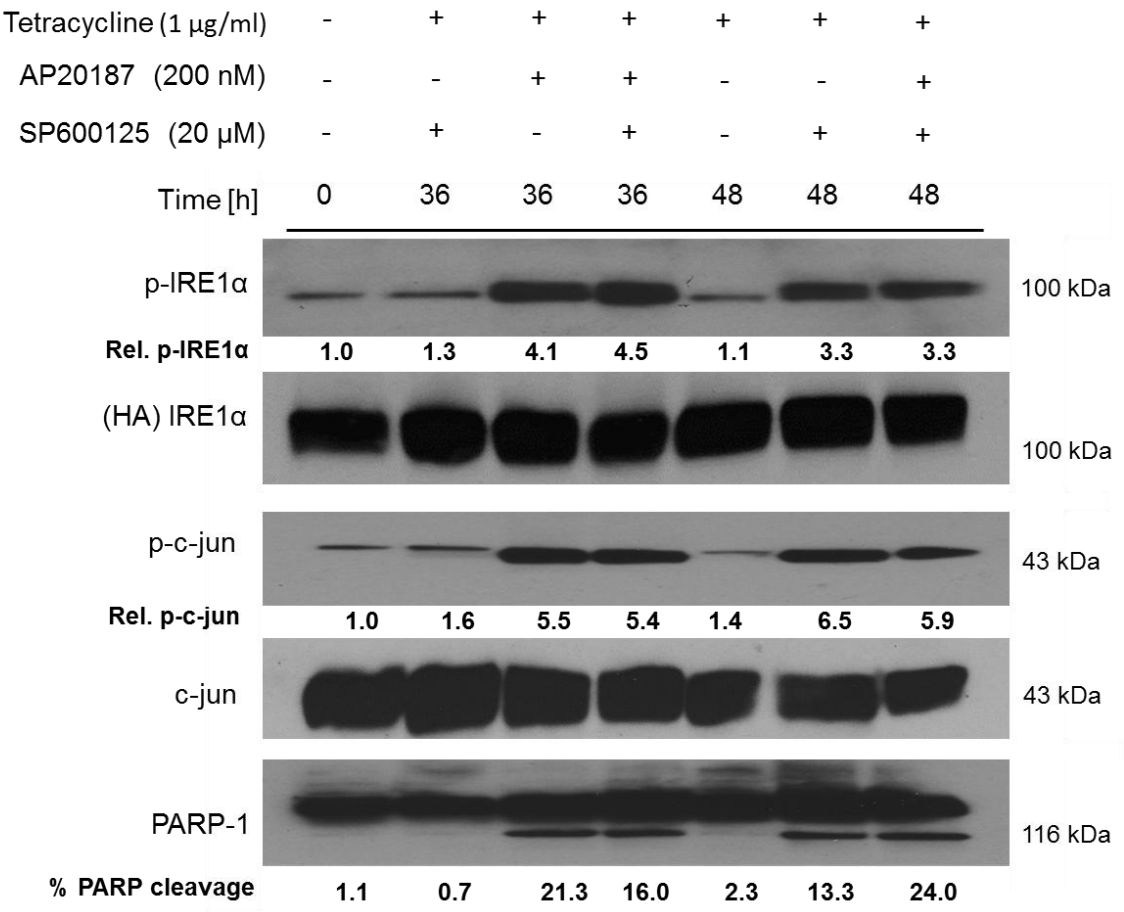

Figure 5.16 –SP600125 has no effect on JNK and PARP-1 signalling in Flp-In T-REx HEK293 Fv2E-IRE1α cells.
Flp-In T-REx HEK293 Fv2E-IRE1α cells were treated with tetracycline, AP20187 and SP600125 as indicated during a 48 h timecourse. Cell lysates were analysed by Western blotting. p-JNK and p-IRE1α were normalised to '1.0' in control samples so that comparisons could be made. PARP-1 cleavage is shown as a % of total PARP.

Despite several attempts, SP600125 treatment did not produce any detectable inhibition of c-jun phosphorylation during either the 36 or 48 h treatments with tetracycline and AP20187. Therefore, it is unsurprising to observe that PARP-1 cleavage still occurred, despite the addition of SP600125. However, the data obtained in Figure 5.16 did provide evidence that Fv2E-IRE1α may mediate cell death via activation of c-jun rather than relying on the assumption that increased phospho-JNK signalling results in the activation of c-jun (Morton et al., 2003). However, in order to confirm this, data linking elevations in phospho-c-jun to cell death would need to be obtained, which is something that will be discussed further at the end of this chapter.

5.2.4 Fv2E-IRE1α^{K599A} does not interact with TRAF2 and does not cause cell death when upon treatment with AP20187.

5.2.4.1 IRE1α^{K599A} is incapable of interacting with TRAF2

The results in this chapter have confirmed that AP20187 causes Fv2E-IRE1α to interact with TRAF2 (5.2.1.3), resulting in elevations in phospho-JNK, PARP-1 cleavage (section 5.2.2.4 and 5.2.3.2) and ultimately cell death (5.2.2.2). Therefore, to advance our understanding of the mechanism by which IRE1α and TRAF2 interact, and the signalling pathway this induces, it was decided that point mutants of the IRE1α cytoplasmic domain would be used. These mutants were stably integrated into Flp-In T-REx HEK293 cells in the same manner as the wild type Fv2E-IRE1α protein (described in section 6.1), with the only difference being the point mutations in IRE1α, which will be highlighted as they are encountered during this section.

The first mutant of IRE1α to be used was IRE1α^{K599A} which, as discussed in the introduction, is a kinase and RNase deficient mutant owing to the loss of the positive charge of lysine 599, which is required for the correct positioning of the triphosphate group of the ATP molecule. This in turn results in the loss of kinase function and an inability to splice *XBP-1* (Papa et al., 2003, Iwawaki et al., 2001). Therefore, if either kinase or RNase activity is required for the interaction between Fv2E-IRE1α and TRAF2, as it is for wild type IRE1α (Urano et al., 2000b), then the use of Fv2E-IRE1α^{K599A} should disrupt the interaction between IRE1α and TRAF2 that was observed upon the addition of AP20187 when using Fv2E-IRE1α (section 5.2.1.3).

In order to investigate whether Fv2E-IRE1α^{K599A} can interact with TRAF2, Flp-In T-REx HEK293 Fv2E-IRE1α^{K599A} cells were treated with tetracycline (1 μg/ml) and AP20187 (200 nM) as indicated for 36 or 48 h. Cell lysates were obtained and subject to a co-IP assay in the same way as was done when investigating Fv2E-IRE1α (section 5.2.1.3), whilst an additional cell lysate, obtained from Flp-In T-REx HEK293 Fv2E-IRE1α cells that had been treated in the same manner, was used as a positive control (Figure 5.17).

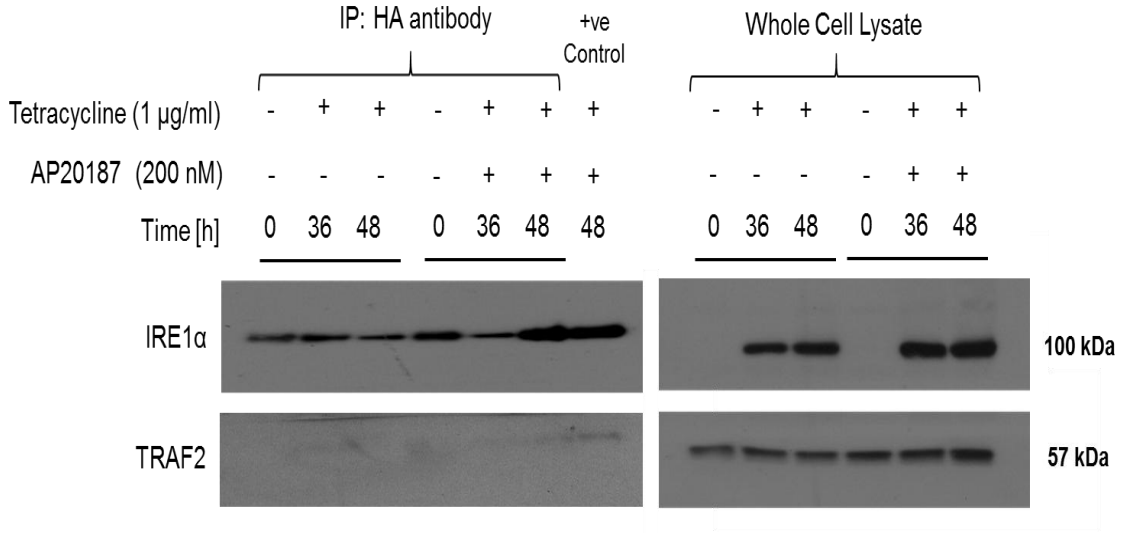

Figure 5.17 - Fv2E-IRE1α^{K599A} fails to interact with TRAF2.
Flp-In T-REx HEK293 Fv2E-IRE1α^{K599A} cells were treated with tetracycline and AP20187 as indicated during a 48 h timecourse. Cell lysates were immunoprecipitated with an HA-tag antibody and the proteins that were retained were analysed by Western blotting. An additional cell lysate obtained from Flp-In T-REx HEK293 Fv2E-IRE1α cells, which had been treated as indicated, was used as a positive control.

The absence of TRAF2 in Figure 5.17 suggests that Fv2E-IRE1α^{K599A} does not interact with TRAF2 even in the presence of AP20187 and this would indicate that lysine 599 is essential for interaction of IRE1α with TRAF2. The reason for this could be the loss of kinase and RNase activity or alternately the mutation of lysine 599 to alanine could cause other structural changes that inhibit interaction with TRAF2.

The positive control in Figure 5.17 produced a very weak band and this could be criticised for not being strong enough to confirm TRAF2 detectability. However, the fact that previous results have proven that TRAF2 can be detected (section 5.2.1.3), combined the data showing that Fv2E-IRE1α^{K599A} is incapable of transducing UPR signalling (Zhou et al., 2006, Urano et al., 2000b), allow a certain confidence when arguing that the K599A mutation prevents interaction with TRAF2.

5.2.4.2 IRE1α^{K599A} does not induce cell death during treatment with AP20187

AP20187 treatment causes Fv2E-IRE1α to interact with TRAF2 (section 5.2.1.3) and initiate apoptotic cell death (section 5.2.2.2). Therefore, having found a mutant that did not interact with TRAF2 (section 5.2.4.1), it was decided to investigate whether cells expressing Fv2E-IRE1α^{K599A} would fail to initiate cell death during AP20187 treatment as well.

In order to achieve this, Flp-In T-REx HEK293 Fv2E-IRE1α^{K599A} cells were treated with tetracycline (1 µg/ml) and AP20187 (200 nM) as indicated for 36 or 48 h before being

subjected to an MTT colorimetric assay to determine cell viability (section 3.3.10). Therefore, the data presented in Figure 5.18 were collected under the same conditions that had been used whilst assessing cells expressing Fv2E-IRE1α (section 5.2.2.2). Once the timecourse was complete the MTT colorimetric assay was carried out as described in methods section 3.3.10.

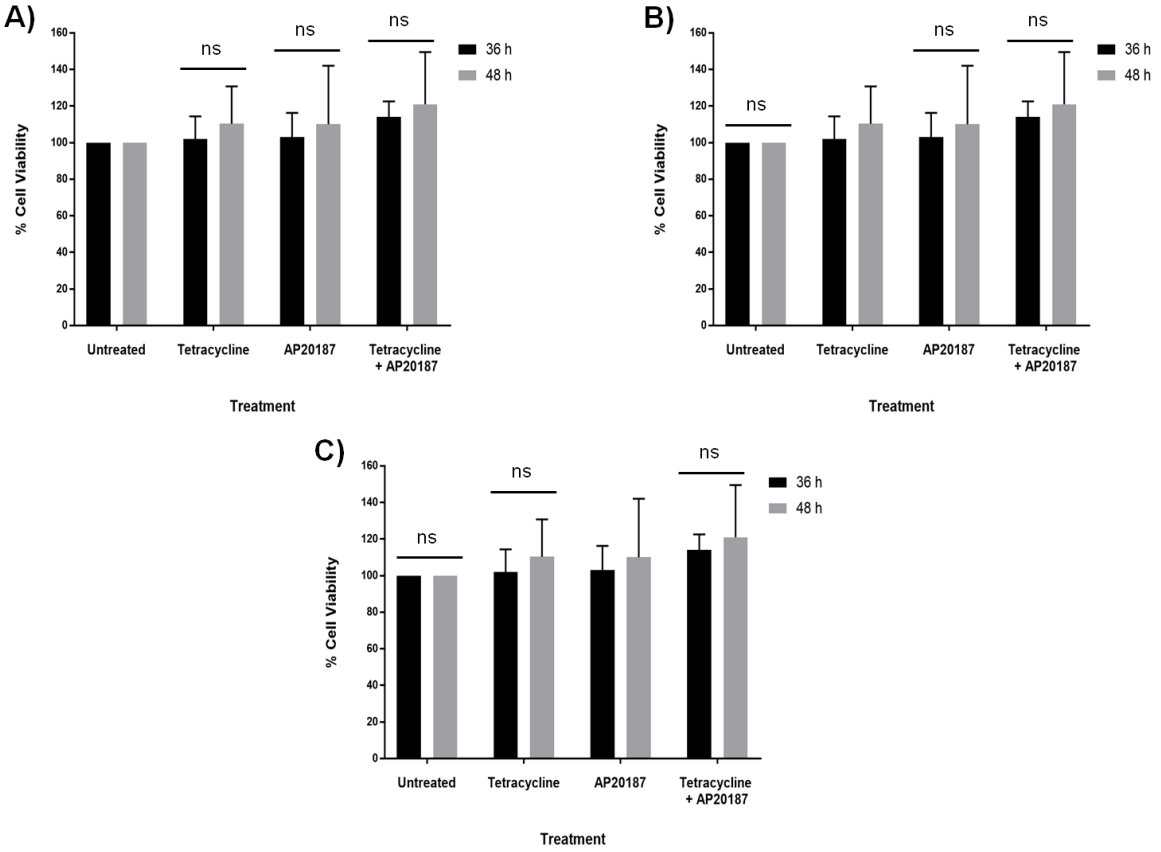

Figure 5.18 – AP20187 treatment has no significant affect on the viability of Flp-In T-REx HEK293 Fv2E-IRE1α^{K599A} cells.
Flp-In T-REx HEK293 Fv2E-IRE1α^{K599A} cells were treated with tetracycline (1 µg/ml) and AP20187 (200 nM) as indicated for either 36 h or 48 h before viability was assessed using an MTT assay. The values obtained for the untreated cells were used to set a baseline number for 100% viability and the other samples' viability were calculated based of this. Three biological repeats were carried out to ensure reliability and statistical analysis was performed using Graphpad Prism software, which was used to carry out a two way ANOVA test for significance combined with Tukey's adjustment for multiple comparisons. The bars represent standard error and significance is denoted as not significant (ns), p= ≤0.05 (*), p= ≤0.01 (**), p= ≤0.001 (***).

A) Comparison of the viability detected in untreated cells against all other treatments.
B) Comparison of the viability detected in cells that had been treated only with tetracycline against all other treatments.
C) Comparison of the viability detected in cells that had been treated only with AP20187 against all other treatments.

During the co-IP testing Fv2E-IRE1α^{K599A} mutant did not bind to TRAF2 (section 5.2.4.1) and therefore, based on current literature, it would be assumed that this mutant would not be able to instigate cell death via the IRE1α apoptotic signalling pathway (Urano et al., 2000b, Nishitoh et al., 2002). Indeed, upon collecting the data from the MTT assay it

became apparent that this was the case, with viability remaining unaffected by the addition of tetracycline and AP20187 (Figure 5.18) despite the fact that, under the same conditions, cells expressing Fv2E-IRE1α exhibited an 89% reduction in viability (section 5.2.2.2). Therefore, it can be concluded that the mutation of lysine 599 to alanine prevents Fv2E-IRE1α transducing apoptotic UPR signalling during treatment with AP20187.

5.2.5 Fv2E- IRE1α^{D711A} interacts with TRAF2 but does not cause cell death.

5.2.5.1 IRE1α^{D711A} interacts with TRAF2

The second IRE1α mutant to be investigated was IRE1α^{D711A}, which has been characterised as a kinase deficient, endoribonuclease active IRE1 protein using the analogous D828A mutant in yeast (Chawla et al., 2011). As explained in the introduction, this is believed to be the result of the disruption of an essential Asp-Phe-Gly motif in the magnesium binding loop of the IRE1α kinase domain, resulting in the inability to position ATP correctly for phosphate cleavage. However, whilst inhibiting phosphotransfer, it does not appear to disrupt the conformational change that activates endoribonuclease activity upon nucleotide binding (Papa et al., 2003). This is shown by reports that *HAC1* splicing continues in yeast Ire1^{D828A} (Chawla et al., 2011) cells and IRE1α^{D711A} restores *XBP1* splicing in *ire1α*$^{-/-}$ MEFs (Sutcliffe, 2012).

In order to investigate the effect of the D711A mutation on the ability of Fv2E-IRE1α to interact with TRAF2, Flp-In T-REx HEK293 Fv2E- IRE1α^{D711A} cells were treated with tetracycline (1 μg/ml) and AP20187 (200 nM) as indicated for 36 or 48 h. After the time course the cell lysates were subjected to a co-immunoprecipitation reaction (see methods 3.6.7) and the proteins retained during this assay were separated by gel electrophoresis (section 3.5.9.1) before being visualised via Western blotting (section 3.5.12). A cell lysate obtained from Flp-In T-REx HEK293 Fv2E-IRE1α cells that had been treated in the same way was used as a positive control (Figure 5.19).

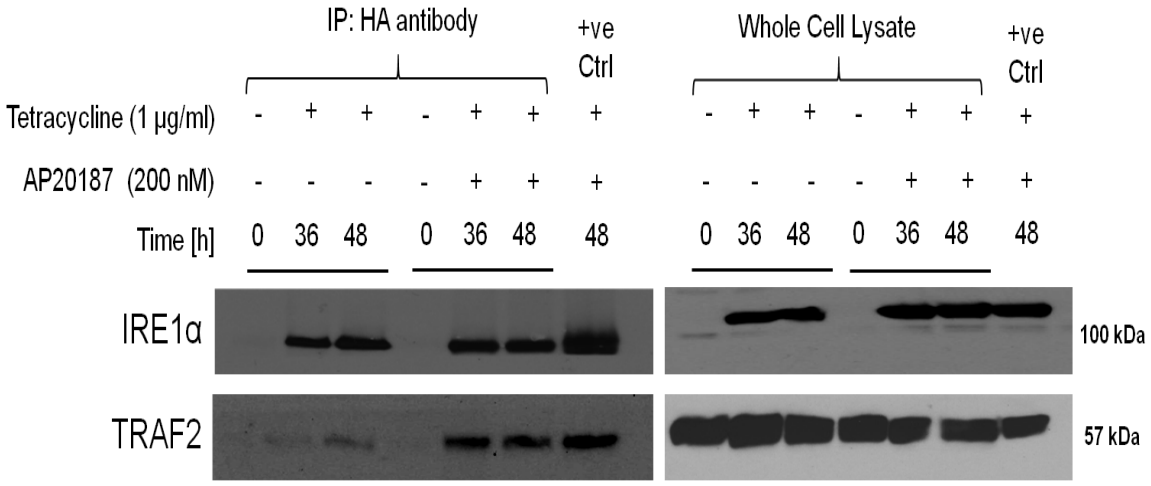

Figure 5.19 - Fv2E-IRE1α^{D711A} binds to TRAF2 upon treatment with AP20187.
Flp-In T-REx HEK293 Fv2E-IRE1α^{D711A} cells were treated with tetracycline and AP20187 as indicated during a 48 h time course. The lysates were then collected a co-immunoprecipitation assay was carried out, during which Fv2E-IRE1α was targeted with an HA-tag antibody. Analysis of the protein retained from the co- immunoprecipitation assay was carried out via Western blotting with the antibodies shown in the figure.

Figure 5.19 shows that TRAF2 binds to Fv2E-IRE1α^{D711A} in AP20187 treated cells, a result which was replicated in Figure 5.20.

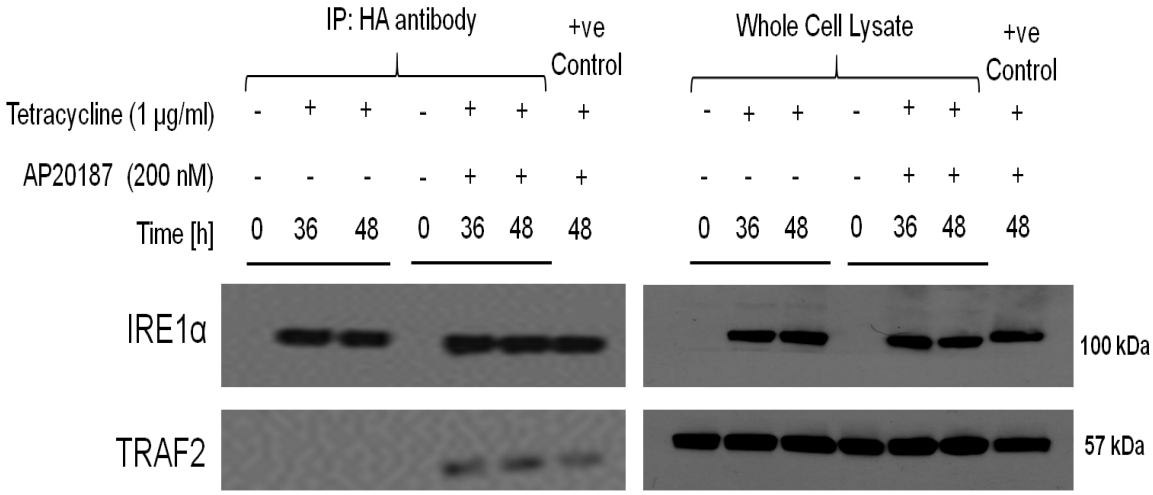

Figure 5.20 – A biological repeat showing that IRE1α^{D711A} binds to TRAF2 upon treatment with AP20187
Flp-In T-REx HEK293 Fv2E-IRE1α^{D711A}cells were treated with tetracycline and AP20187 as indicated during a 48 h timecourse. The lysates were then collected a co-immunoprecipitation assay was carried out, during which Fv2E-IRE1α was targeted with an HA-tag antibody. An additional cell lysate obtained from Flp-In T-REx HEK293 Fv2E-IRE1α cells, which had been treated as indicated, was used as a positive control. Analysis of the protein retained from the co- immunoprecipitation assay was carried out via Western blotting with the antibodies shown in the figure.

The data shown in Figures 5.19 and 5.20 indicate that mutation of aspartate 711 to alanine does not prevent IRE1α from interacting with TRAF2. This is interesting because substitution of aspartate D771 with alanine has been reported to disrupt kinase activity, which up until this point, has been believed to be essential for interaction with TRAF2

(Urano et al., 2000b). However, it was important to confirm that the Fv2E-IRE1α mutant was unable to phosphorylate itself (section 5.2.6.1) before drawing further conclusions regarding the mechanism by which IRE1α initiates apoptotic cell signalling.

5.2.5.2 IRE1α^{D711A} fails to induce cell death upon treatment with AP20187

Section 5.2.5.1 provided evidence that Fv2E-IRE1α^{D711A} can interact with TRAF2 upon treatment with AP20187 and therefore it would be logical to assume that cells expressing Fv2E-IRE1α^{D711A} would induce cell death in a manner similar to those expressing Fv2E-IRE1α. In order to determine if this was the case, Flp-In T-REx HEK293 Fv2E-IRE1α^{D711A} cells were treated with tetracycline (1 μg/ml) and AP20187 (200 nM) for 36 or 48 h before cell viability was assed using an MTT colorimetric assay (section 3.3.10) (Figure 5.21).

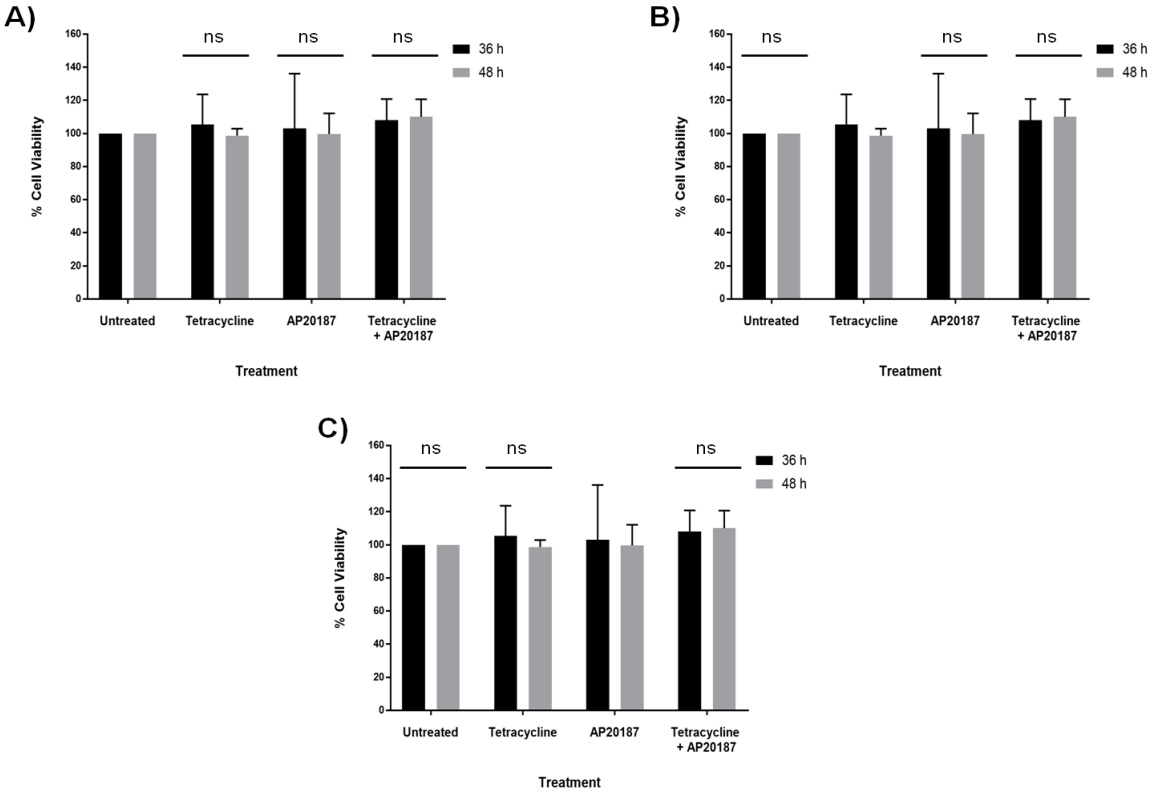

Figure 5.21 – AP20187 treatment has no significant affect on the viability of Flp-In T-REx HEK293 Fv2E-IRE1α^{D711A} cells.

Flp-In T-REx HEK293 Fv2E-IRE1α^{D711A} cells were treated with tetracycline (1 μg/ml) and AP20187 (200 nM) as indicated for either 36 h or 48 h before viability was assessed using an MTT assay. The values obtained for the untreated cells were used to set a baseline number for 100% viability and the other samples' viability were calculated based of this. Three biological repeats were carried out to ensure reliability and statistical analysis was performed using Graphpad Prism software, which was used to carry out a two way ANOVA test for significance combined with Tukey's adjustment for multiple comparisons. The bars represent standard error and significance is denoted as not significant (ns), p= ≤0.05 (*), p= ≤0.01 (**), p= ≤0.001 (***).

A) Comparison of the viability detected in untreated cells against all other treatments.
B) Comparison of the viability detected in cells that had been treated only with tetracycline against all other treatments.
C) Comparison of the viability detected in cells that had been treated only with AP20187 against all other treatments.

The data presented in Figure 5.21 shows that treatment with AP20187 does not cause any significant change to cell viability in cells expressing Fv2E-IRE1α^{D711A}, despite the fact that Fv2E-IRE1α^{D711A} is able to bind to TRAF2 (section 5.2.5.1). Therefore, these data suggest that interaction with TRAF2 does not suffice for IRE1α induced cell death and that another event, which requires the D711 residue, is required for cell death to be initiated.

5.2.6 Characterisation of downstream signalling in Fv2E-IRE1α^{K599A} and Fv2E-IRE1α^{D711A} cells

5.2.6.1 IRE1α^{D711A} and IRE1α^{K599A} fail to autophosphorylate or upregulate JNK phosphorylation and PARP-1 cleavage

Mutating either aspartate 711 (section 5.2.5.2) or lysine 599 (section 5.2.4.2) to alanine prevents Fv2E-IRE1α from initiating apoptotic signalling. However, whilst this disruption could be attributed to a failure to interact with TRAF2 when using the IRE1α^{K599A} (section 5.2.4.1), the same cannot be said for the D711A mutant, which co-immunoprecipitated with TRAF2 during AP20187 treatment (section 5.2.5.1). The ability of IRE1α^{D711A} to interact with TRAF2, combined with its failure to instigate apoptosis, is of particular interest, because, up until this point, it had been believed that interaction between IRE1α and TRAF2 was sufficient for the activation of apoptotic signalling via JNK (Urano et al., 2000b, Nishitoh et al., 2002). However, having observed no significant change in cell viability, despite interaction with TRAF2, these findings challenge what is currently known about the mechanism by which IRE1α signals for apoptosis, suggesting that interaction with TRAF2 is not sufficient for IRE1α to instigate apoptotic signalling. Therefore, in order to investigate this hypothesis futher, experiments were carried out to determine whether mutation of aspartate 711 to alanine prevents downstream activation of JNK, which is currently regarded to be the pathway by which IRE1α instigates apoptosis during prolonged periods of ER stress (Nishitoh et al., 2002, Urano et al., 2000b).

Flp-In T-REx HEK293 Fv2E-IRE1α, IRE1α^{K599A} and IRE1α^{D711A} cells were subjected to a 48 h time course during which they were treated with tetracycline (1 μg/ml) and AP20187 (200 nM) for either 36 or 48 h. Once the time course had been completed, cell lysates were obtained (section 3.5.7.1) and analysed via Western blotting (section 3.5.12), which was carried out using antibodies against p-IRE1α, the HA tag of Fv2E-IRE1α, p-JNK, JNK and PARP-1 (Figure 5.22).

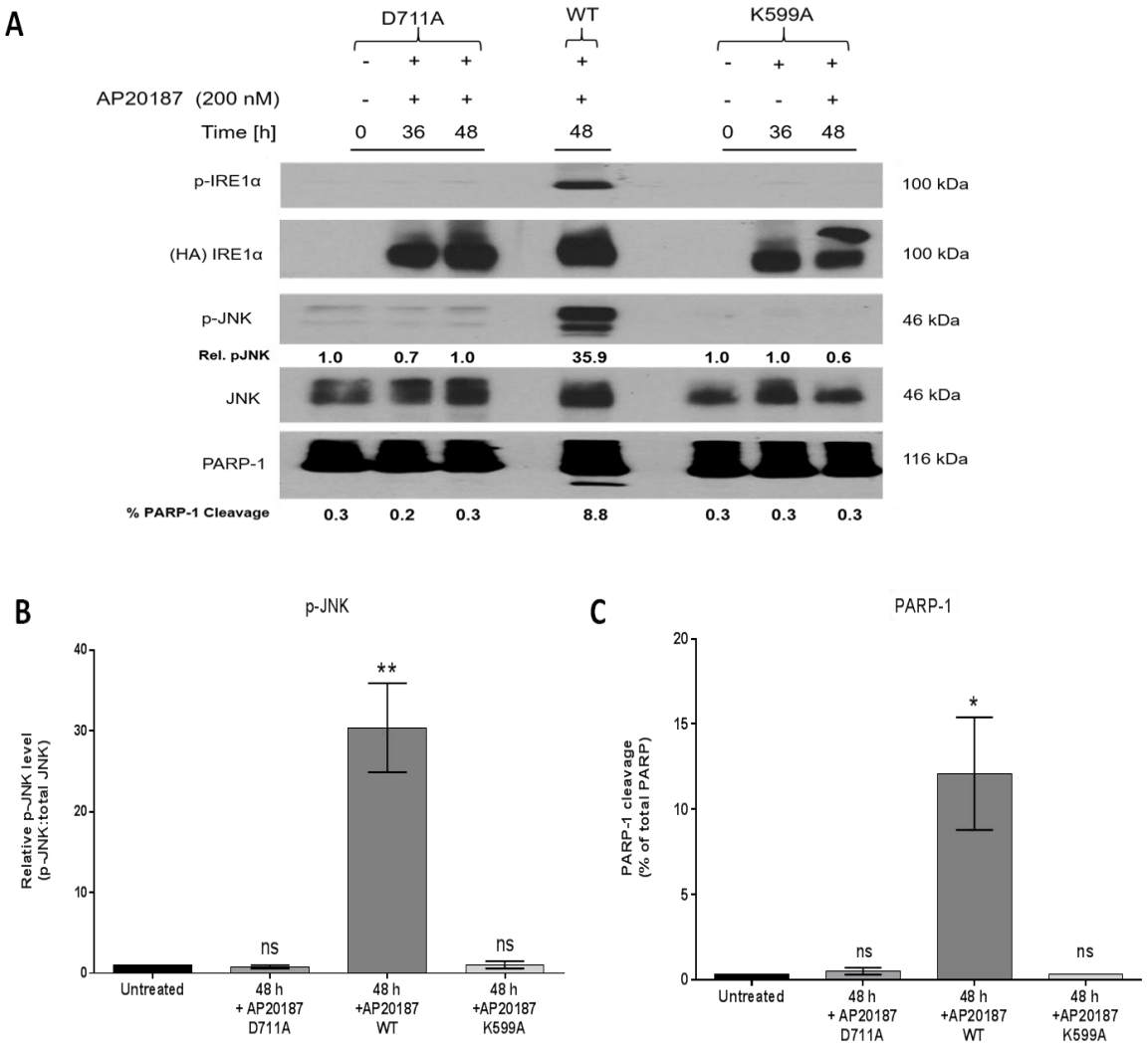

Figure 5.22 –IRE1α^{K599A} and IRE1α^{D711A} mutants fail to autophosphorylate JNK or initiate PARP-1 cleavage.

A) Western blot analysis of p-IRE1α, IRE1α, p-JNK, JNK and PARP-1 in Flp-In T-REx HEK293 cells that have been stably transfected with the Fv2E-IRE1α constructs indicated and then treated with tetracycline (1 μg/ml) and AP20187(200 nM) for either 36 or 48 h. Phospho-JNK levels have been normalised to '1.0' in untreated cells to allow for comparison between treatments.

B) Quantification of p-JNK signalling.

C) Quantification of PARP-1 cleavage.

Three biological repeats (see appendices 3a and 3b) were carried out to ensure reliability and statistical analysis was performed using Prsim Graphpad software, which was used to carry out a one way ANOVA test for significance combined with Šidák correction for multiple comparisons. The bars represent standard error and significance is denoted as not significant (ns), p= ≤0.05 (*), p= ≤0.01 (**) or p= ≤0.001 (***).

Figure 5.22 panel A shows that 48 h treatment with AP20187 results in Fv2E-IRE1α phosphorylation and significant increases in both JNK phosphorylation (p = >0.01) and PARP-1 cleavage (p = ≤0.05), further reinforcing the data obtained in section 5.2.2.4, which suggest that AP20187 treatment promotes IRE1α activation and subsequent apoptotic signalling via JNK. However, under the same conditions, there was no detectable phosphorylation of either IRE1α^{K599A} or IRE1α^{D711A}, which suggests mutation of K599 or D711 to alanine prevents IRE1α from acting as a kinase. Furthermore, 48 h treatment with

AP20187 resulted in no significant change in the levels of phospho-JNK or PARP-1 cleavage in either Flp-In T-REx HEK293 Fv2E-IRE1α^{K599A} or Flp-In T-REx HEK293 Fv2E-IRE1α^{D711A} cells. Therefore, the data shown in Figure 5.22 supports the conclusions drawn from section 5.2.5.2 that interaction with TRAF2 is not sufficient for apoptotic signalling via JNK. Furthermore, these data suggest that whilst kinase activity is not essential for an interaction between IRE1α and TRAF2, it is essential for both the downstream activation of JNK and the cleavage of PARP-1.

5.2.6.2 Endoribonuclease activity is retained by Fv2E-IRE1α, but lost in both Fv2E-IRE1α^{D711A} and Fv2E-IRE1α^{K599A} cells

Our current understanding of IRE1α states that it has two main functions during endoplasmic reticulum stress. During short periods of low level stress IRE1α has a protective role that is mediated by its capacity as an endoribonuclease (Shen et al., 2001, Lee et al., 2003, Yoshida et al., 2003, Oda et al., 2006), whilst during periods of prolonged stress IRE1α instigates a cell death signalling cascade via its kinase domain (Huang et al., 2014, Jung et al., 2012, Jung et al., 2014, Smith and Deshmukh, 2007, Wang et al., 2008, Zhang et al., 2001). The data obtained thus far shows that the Fv2E- IRE1α^{D711A} mutant is able to interact with TRAF2 upon activation (section 5.2.5.1), but does not undergo autophosphorylation and fails to induce apoptosis via the phosphorylation of JNK (sections 5.2.5.2 and 5.2.6.1). These results could be explained owing to the fact that IRE1α^{D711A} lacks kinase activity or because it lacks endoribonuclease activity (Han et al., 2009). The former of these suggestions would currently appear to be more likely as the D711A mutant has been reported to splice *XBP1* in MEFs and also in yeast when using the analogous D828A mutant (Chawla et al., 2011). However, the endoribonuclease activity of Fv2E-IRE1α has not yet been assessed and therefore it was imperative to carry out an assay to determine the ability of Fv2E-IRE1α, Fv2E-IRE1α^{D711A} and Fv2E-IRE1α^{K599A} to splice *XBP1* before drawing any further conclusions regarding the lack of apoptosis observed in AP20187 treated Flp-In T-REx HEK293 Fv2E-IRE1α^{D711A} cells.

In order to investigate the capacity of Fv2E-IRE1α to splice *XBP1 in vivo* Flp-In T-REx HEK293 cells that had been stably transfected with Fv2E-IRE1α, Fv2E-IRE1α^{D711A} or Fv2E-IRE1α^{K599A} were subjected to a 48 h timecourse in which they were treated with tetracycline (1 µg/ml) and AP20187 (200 nM) (as showin in Figure 5.23) for either 36 or 48 h. RNA was then harvested as detailed in methods section 3.4. Having been quantified, RNA samples were reverse transcribed to produce *XBP1* cDNA, which was amplified via

PCR using the protocol outlined in methods section 3.4.5. The cDNA was then run on a 2% agarose gel before being visualised using a UV transilluminator. The results obtained from this process are shown in Figure 5.23.

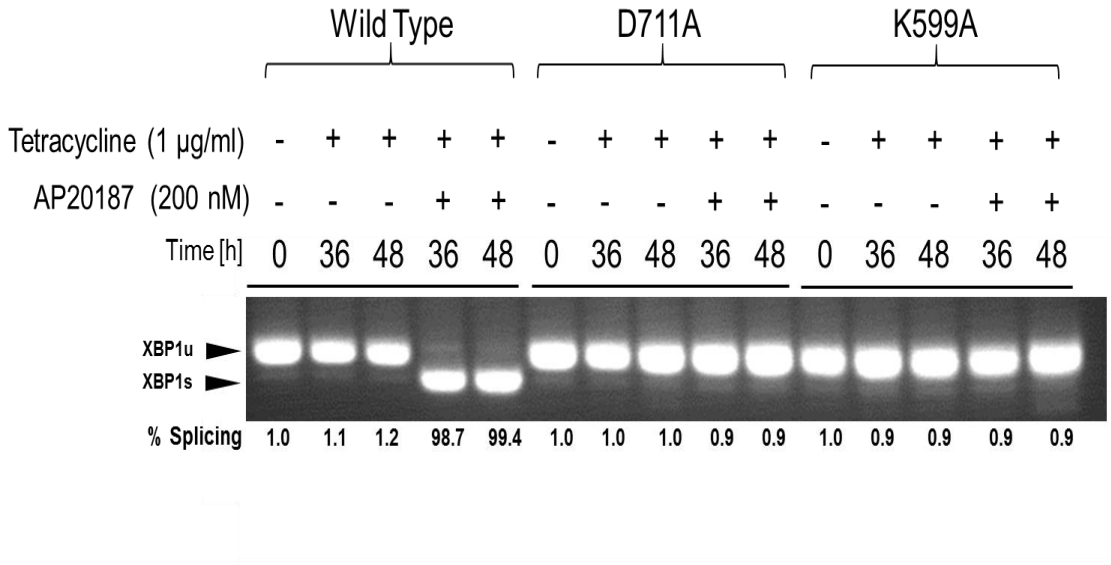

Figure 5.23 –Mutation of D711 and K599 abolish the ability of Fv2E-IRE1α to splice *XBP1* mRNA.

A) RT-PCR analysis of *XBP1* splicing in Flp-In T-REx HEK293 cells that have been stably transfected with Fv2E-IRE1α, Fv2E-IRE1α^{D711A} or Fv2E-IRE1α^{K599A}. The cells were treated with tetracycline and AP20187 as indicated. *XBP1u* = unspliced *XBP1* mRNA and *XBP1s* = spliced *XBP1* mRNA. The percentage of total *XBP1* that had been spliced was calculated using Image J to quantify both sets of bands.

Figure 5.23 shows that Fv2E-IRE1α spliced >98% of the total *XBP1* when activated with AP20187 compared with just 1.2% in the absence of AP20187, which is most likely attributable to either basal *XBP1* splicing being carried out by endogenous IRE1α or basal levels of dimerisation between Fv2E-IRE1α chimeras. These data therefore support the hypothesis that Fv2E-IRE1α retains both its endoribonuclease (Figure 5.23) and kinase (Figure 5.13) functions. In contrast to Fv2E-IRE1α, neither mutant displayed endoribonuclease function, with less than 2% of the total *XBP1* mRNA being spliced. Once again, this was to be expected when using Fv2E-IRE1^{K599A} as this mutation has been documented as lacking endoribonuclease activity (Tirasophon et al., 1998, Tirasophon et al., 2000). However, the failure of Fv2E-IRE1^{D711A} to splice *XBP1* mRNA was surprising as the full length version of this mutant has been reported to restore *XBP1* splicing in *ire1α*$^{-/-}$ MEFs (Sutcliffe, 2012) and in yeast when using the analogous D828A mutant (Chawla et al., 2011).

5.2.7 Fv2E-IRE1α^{K599R} and Fv2E-IRE1α$^{I642G-D711A}$ also fail to splice *XBP1* mRNA

5.2.7.1 Endoribonuclease activity is also absent in Fv2E-IRE1α^{K599R} and Fv2E-IRE1α$^{I642G/D711A}$ cells

With data indicating that Fv2E-IRE1α^{D711A} is unable to splice *XBP1* it was decided that it would be worth investigating other IRE1α mutants to determine if it would be possible to obtain an IRE1α mutant that lacked kinase activity but retained the functionality of its endoribonuclease domain. All the results were obtained using the same methodology as those using the Flp-In T-REx HEK293 Fv2E-IRE1α cells (section 5.2.6.2) and the results obtained are shown below.

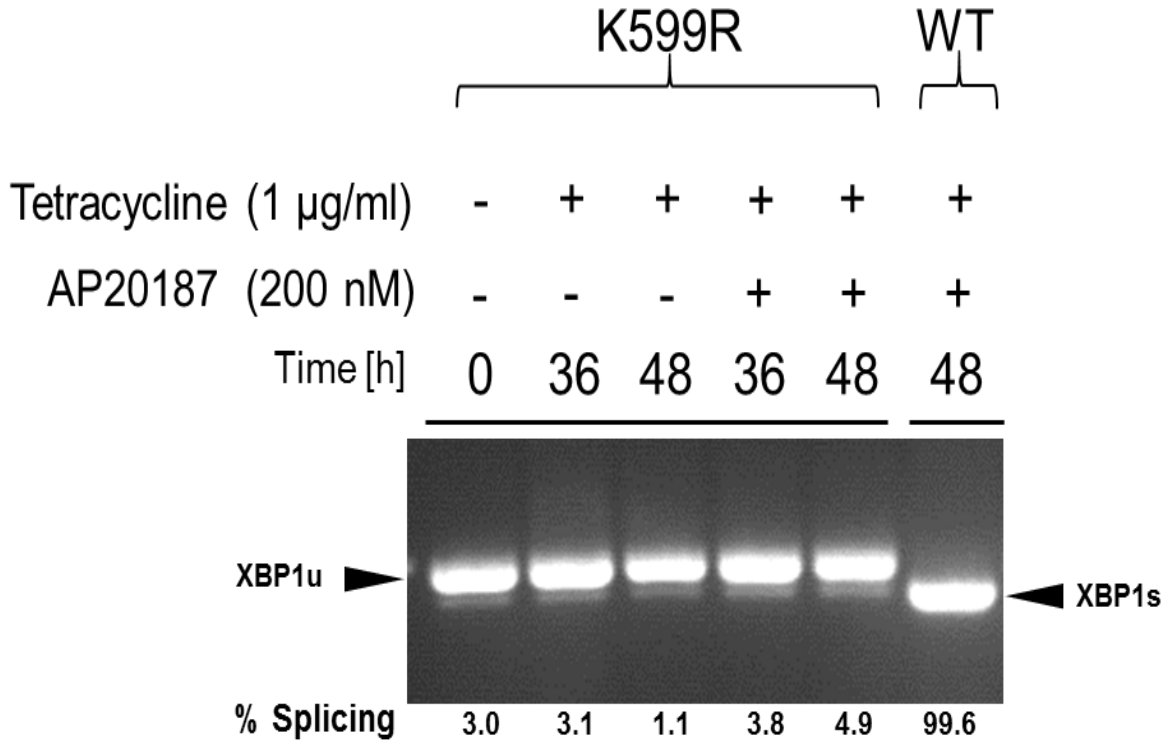

Figure 5.24 –Fv2E-IRE1α^{K599R} is unable to splice *XBP1* mRNA.
RT-PCR analysis of *XBP1* splicing in Flp-In T-REx HEK293 Fv2E-IRE1α^{K599R} cells that had been treated with tetracycline and AP20187 as indicted. *XBP1u* = unspliced *XBP1* mRNA and *XBP1s* = spliced *XBP1* mRNA. The percentage of total *XBP1* that had been spliced was calculated using imageJ to quantify both sets of bands.

The first mutant that was used whilst searching for an IRE1α protein with endoribonuclease activity was IRE1α^{K599R}. This mutant is similar to K599A, but instead of mutating lysine 599 to the neutral amino acid alanine, this mutant retains the positive charge imbued by lysine through use of arginine. This is believed to create a slightly less disruptive change than the one caused by the K599A mutation and has been reported to

reduce kinase and endoribonuclease activity, without leading to full abolition of signalling, in yeast whilst using the analogous K702R mutant (Shamu and Walter, 1996, Mori et al., 1993). However, the results obtained in Figure 5.24 revealed that Fv2E-IRE1α^{K599R} also fails to splice *XBP1* mRNA.

Another IRE1α mutant that has been reported to possess endoribonuclease activity in the absence of a functional kinase domain is IRE1α $^{I642G/D711A}$. The D711A mutation prevents kinase activity (as described in sections 1.4.3.1 and 5.2.5.1), whilst the mutation of isoleucine 642 to glycine enlarges the ATP-binding pocket of the IRE1α kinase domain, preventing kinase or endoribonuclease activity (described further in section 1.4.3.2). However, it has been reported that the use of an ATP analogue, 1NM-PP1, can restore endoribonuclease activity in IRE1α^{I642G} mutants by binding to the enlarged ATP-binding pocket (Papa et al., 2003). Therefore, Fv2E- IRE1α $^{I642G/D711A}$ had the potential to act as the kinase deficient, endoribonuclease functional mutant, which would allow further characterisation of the IRE1α signalling pathway. Thus, *XBP1* mRNA was obtained from Flp-In T-REx HEK293 Fv2E-IRE1α$^{I642G/D711A}$ cells, and subsequently analysed, using same methodology as described in section 5.2.6.2 and the results are shown in Figure 5.25.

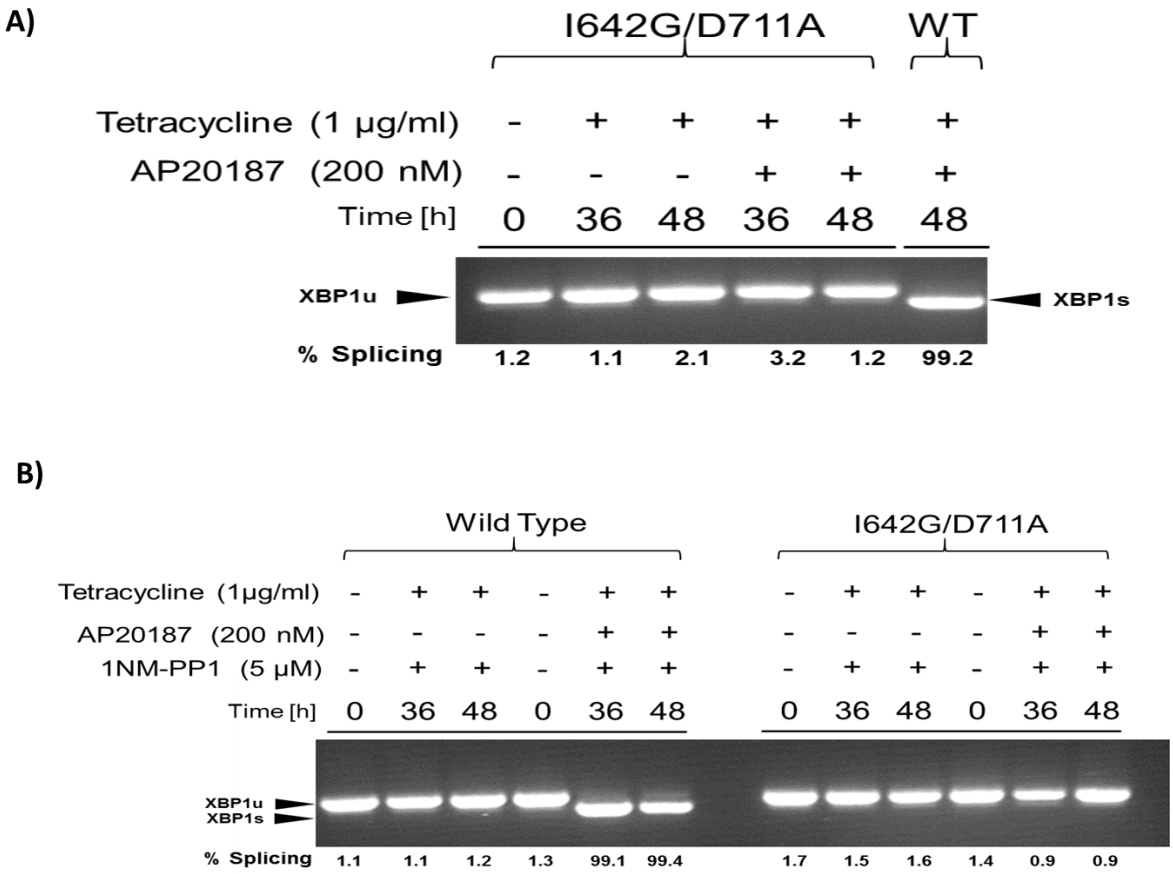

Figure 5.25 - Fv2E-IRE1α$^{I642G/D711A}$ fails to splice *XBP1* mRNA.
RT-PCR analysis of *XBP1* splicing in Flp-In T-REx HEK293 Fv2E-IRE1α$^{I642G/D711A}$ cells that had been treated with tetracycline and AP20187 as indicted. *XBP1u* = unspliced *XBP1* mRNA and *XBP1s* = spliced *XBP1* mRNA. The percentage of total *XBP1* that had been spliced was calculated using Image J to quantify both sets of bands.

As can be seen from Figure 5.25 panel A, without 1NM-PP1 treatment IRE1α$^{I642G/D711A}$ fails to splice *XBP1*, which was expected based on previous findings (Papa et al., 2003). However, panel B also shows a lack of *XBP1* splicing, despite treatment with 1NM-PP1. Therefore, it would seem that Fv2E-IRE1α $^{I642G/D711A}$ responds differently to the full-length, membrane-bound proteins (L745G and L745G/D828A) studied by *Papa et al.* (Papa et al., 2003) and does not have endoribonuclease activity rescued by treatment with1NM-PP1. Thus the data obtained suggests that neither IRE1α^{K599R} nor IRE1α $^{I642G/D711A}$ have the capacity to act as kinase deficient, endoribonuclease competent mutants of IRE1α whilst using the Fv2E system.

5.3 Discussion of the Fv2E-IRE1α System

The co-immunoprecipitation (co-IP) assay that was used in Chapter 5 formed the foundations on which the rest of the data would be collected as it allowed the identification of proteins that interact with IRE1α and, therefore, held the key to characterising the IRE1α signalling cascade. As a result of this, a large amount of time was spent optimising the co-IP protocol in order to ensure clean and reliable detection of Fv2E-IRE1α and proteins that bind to it. Despite initial concerns, Figure 5.9 demonstrated that TRAF2 can be detected without the appearance of artificial bands caused by detection of the heavy IgG chains of the antibodies that were used during the co-IP procedure (section 3.5.7.1) and the assay proved reliable enough to obtain biological repeats for the work with both Fv2E-IRE1α (Figures 5.5-5.7) and Fv2E-IRE1α^{D711A} (Figures 5.22-5.23). Therefore, the biggest flaw in the co-immunoprecipitation assay is the fact that it is susceptible to variations in the amount of protein that is retained. However, there is very little that can be done to avoid this given that there are so many stages in which protein can be lost (methods section 3.6.7). Therefore, all that can be done is to ensure that all the assays contain clean controls and that biological repeats are obtained. This is why so much time was expended ensuring that the smearing and appearance of unknown bands observed during early attempts to detect TRAF2 (data not shown) were abolished before collecting the data that would be used to draw conclusions as to the activity of IRE1α. However, all of the results that have been used to argue for a positive interaction with TRAF2 have clear controls and biological repeats associated with them. Therefore, whilst variations in the level of IRE1α protein can be criticised, they cannot be avoided, and stringent regulations have been put in place to ensure that the data are as reliable as possible. As such, the data obtained for both Fv2E-IRE1α and Fv2E-IRE1α^{D711A} is sufficient to allow the conclusion that both proteins interact with TRAF2.

Providing evidence that the Fv2E-IRE1α system allows isolated activation of IRE1α was a requirement for it to be presented as being an alternative assay to normal ER stress mimetic drugs. Previous research involving PERK (Deng et al., 2004) has suggested that the fusion of the cytosolic effector domain of IRE1α to FK506 (Fv) binding domains may allow isolated dimerisation, and subsequent activation, of IRE1α through use of the chemical AP20187. However, up until this point, there has only been one reported use of an IRE1α-Fv protein (Back et al., 2006). *Back et al.* fused the cytosolic domain of IRE1α to a single FK506 domain in order to investigate if dimerisation of IRE1α was sufficient for *XBP1* splicing to occur in the absence of ER stress. However, whilst their fusion protein (F_v-IRE1αΔN-HA) did undergo phosphorylation, the amount of phosphorylated F_v-

IRE1αΔN-HA varied very little between cells that had been treated with AP20187 and those that had not. Therefore, the phosphorylation observed could have been the result of overexpressing F_v-IRE1αΔN-HA, rather than treatment with AP20187. Furthermore, similar results were obtained whilst investigating *XBP1* splicing and there was no significant increase in spliced *XBP1* observed when cells were treated with AP20187. As such, the ~2-fold increase in *XBP1* splicing observed when cells were transfected with F_v-IRE1αΔN-HA, may well have been the result of overexpression generating ER stress and causing *XBP1* to be spliced by endogenous IRE1α. Therefore, in order to present the Fv2E-IRE1α system as one that can be used as a model for studying IRE1α signalling in isolation, it was vital to provide evidence that Fv2E-IRE1α signalling was initiated by treatment with AP20197 and not as a result of overexpression. This evidence is provided in section 5.2.6, whereby the Fv2E-IRE1α mutants act as controls in order to establish that the phosphorylation of IRE1α, elevations in JNK signalling and splicing of *XBP1* are the result of AP20187 treatment. If any of these events were the result of overexpression, then they should have occurred in untreated cells and/or cells that had been transfected with Fv2E-IRE1α^{D711A} and/or Fv2E-IRE1α^{K599A}. Therefore, with similar levels of expression between constructs and clear activation of both *XBP1* splicing and JNK signalling when using Fv2E-IRE1α, the data presented in section 5.2.6 suggest that the Fv2E-IRE1α allows activation of IRE1α signalling via AP20187 treatment and that this is not an artefact created by the overexpression of the fusion protein.

In addition to providing evidence that induction of Fv2E-IRE1α is caused by AP20817, as opposed to ER stress generated by the overexpression of the fusion protein, it was important to provide evidence that AP20187 treatment itself does not cause ER stress, otherwise it would be no different to ER stress mimetic drugs. This is something that was achieved by showing that AP20187 does not cause phosphorylation of eIF2α (Figure 5.14) and this, combined with other papers reporting that AP20187 does not cause ER stress (Deng et al., 2004) and the fact that AP20187 failed to induce cell death (section 5.2.2.2) or activation of JNK and PARP-1 cleavage in the absence of Fv2E-IRE1α (section 5.2.2.4), is sufficient to support the conclusion that this system allows the specific activation of IRE1α and therefore the isolated study of its downstream targets. However, in order to support this conclusion further, it would be valuable to obtain data to show that AP20187 treatment does not initiate ATF6 signalling. Thus far our lab has not found an antibody that reliably detects ATF6, however, it may be possible to avoid having to use ATF6 antibodies by transfecting cells with a HA-tagged ATF6 protein and then use antibodies against the

tag to determine if ATF6 is cleaved, and therefore activated (Ye et al., 2000), during AP20187 treatment.

The work carried out in order to characterise the impact of Fv2E-IRE1α signalling was again convincing, with Western blotting confirming the repeatable and significant activation of p-JNK and cleavage of PARP-1 (section 5.2.2.4), whilst MTT assays provided similar data for increased apoptosis (5.2.2.2). This was complemented by data showing that untreated cells, or cells expressing kinase deficient IRE1α mutants, did not induce any significant changes in UPR signalling or cell death (sections 5.2.4-5.2.6). As with any work done *in vivo*, these results exhibited some fairly large variations between biological repeats, but statistical analysis was able to show that, even taking these variations into account, the effects of Fv2E-IRE1α signalling on the UPR and cell viability are significant (section 5.2.2). Therefore, the methods used were sufficient to present a model whereby IRE1α induces cell death via the activation of JNK signalling and PARP-1 cleavage.

The other downstream target of IRE1α that was measured during this study was *XBP1* mRNA and the results obtained provided repeatable data exhibiting over 98% of *XBP1* mRNA being spliced in cells expressing Fv2E-IRE1α, whilst <5% splicing occurring in untreated cells or cells expressing IRE1α mutants (section 5.2.6). These results were to be expected when using the lysine 599 mutant, as substitution of this residue has already been reported to produce mutants that have significantly reduced endoribonuclease activity (Mori et al., 1993, Shamu and Walter, 1996) or fail to splice *XBP1* (Iwawaki et al., 2001, Zhou et al., 2006). In contrast, the failure of Fv2E-IRE1^{D711A} to splice *XBP1* mRNA was surprising because the full length version of this mutant has been reported to restore *XBP1* splicing in *ire1α*$^{-/-}$ MEFs (Sutcliffe, 2012) and in yeast, when using the analogous D828A mutant (Chawla et al., 2011). However, the data presented in section 5.2.6 provides strong evidence that Fv2E-IRE1α^{D711A} lacks endoribonuclease activity and, thus, differs from its membrane-bound counterparts. Therefore, with evidence to support the conclusion that Fv2E-IRE1α retains endoribonuclease activity, whilst IRE1α^{D711A} lacks the ability to splice *XBP1* (section 5.2.6.2), it is possible that future work can be carried out, through use of the IRE1α-Fv2E system, in order to characterise not only signalling via interaction with TRAF2, but also via the endoribonuclease domain.

One issue that may be raised with the Fv2E-IRE1α system is that it takes 12 h for the effects of AP20187 treatment to be observed, whilst in wild type cells activation of the

UPR takes approximately 1-2 hours (Nishitoh et al., 2002, Kang et al., 2012). Whilst the reason for this delay is unknown, it could be a result of the fact that Fv2E-IRE1α is a cytoplasmic protein as opposed to being membrane bound. Work carried out in yeast has suggested that there are several foci located in the ER membrane and nuclear envelope where IRE1 monomers form oligomers in response to ER stress (Aragón et al., 2009). In this study, overexpression of Ire1p did not increase the number of foci, merely the number of Ire1p monomers gathered at them. This prompted the authors to postulate that these foci may occur at predetermined locations, proving nucleation sites for oligomerisation, and that they may even allow *HAC1* mRNA to be targeted to them via the cytoskeleton in order to increase the speed of Ire1p signalling. In addition to this, the authors also found that disruption of two luminal dimerisation interfaces, believed to be responsible for dimerisation/oligomerisation of Ire1p (Credle et al., 2005), either slowed down the ER response, when one domain was disrupted, or abolished it, if both domains were disrupted. Furthermore, it was shown that artificial dimerisation of Ire1p restored *HAC1* splicing and cell survival, but only to the same level of Ire1p mutants with one functional dimerisation interface. This lead to the suggestion that, whilst dimerisation is sufficient for Ire1p signalling, oligomerisation is required for an optimal response to ER stress. Therefore, the idea of Ire1p foci (Li et al., 2010, Aragón et al., 2009) could help explain why the Fv2E system exhibits a slower response than observed in wild type cells. Fv2E-IRE1α lacks both a transmembrane domain and a luminal domain and therefore will not be able to cluster at the foci proposed by *Aragón et al*. However, it does have two FK506 domains which, in theory, will allow oligomerisation via treatment with AP20187 (Deng et al., 2004). Therefore, whilst lacking a transmembrane domain to anchor IRE1α monomers to a nucleation sites may result in slower oligomerisation, Fv2E-IRE1α should still form oligomers over time. This would certainly be supported by the evidence provided in Chapter 5, which suggests that treatment with AP20187 suffices to induce oligomerisation by virtue of the fact that downstream signalling still occurs. Interestingly, the only other group to try and utilise an IRE1α-FK506 fusion protein did so using just one FK506 domain (Back et al., 2006) and, in doing so, limited this protein to forming dimers instead of oligomers. Based on the findings of *Aragón et al*. (Aragón et al., 2009), this would result in a diminished signalling response and may explain why *Back et al.* reported minimal autophosphorylation and *XBP1* splicing. Fv2E-IRE1α, on the other hand, possesses two FK506 domains and exhibits strong, albeit delayed, kinase and endoribonuclease activity (Chapter 5.2).

Additionally, the slower response rate in Flp-In T-REx HEK293 Fv2E-IRE1α cells, compared to thapsigargin treated wild-type counterparts, could be a result of the fact that the stress caused by disrupting calcium homeostasis will activate a multitude of stress signalling pathways and, therefore, elicit a much stronger response than the activation of a single sensor. However, despite not knowing the reason behind the delay, the fact that Fv2E-IRE1α is capable of mediating cell death via the same pathway that has been reported in wild-type cells (Urano et al., 2000b, Davis, 2000) means that the time it takes for this pathway to be initiated is a minor concern.

Finally, two different methods were used in order to show that apoptotic signalling is mediated by an Fv2E-IRE1α-TRAF2-JNK pathway. The first of these was an attempt to prove the necessity of JNK in causing apoptosis through use of the JNK inhibitor SP600125 and, whilst this method did not inhibit c-jun phosphorylation, it did show that c-jun is phosphorylated during IRE1α signalling (Figure 5.15). The reason that SP600125 did not inhibit JNK signalling could be a result of the fact that it is very insoluble in water (Bennett et al., 2001) and, for this reason, may have precipitated early on in the experiment. Therefore, future work could attempt to resolve this issue by increasing the DMSO concentration of the culture media to 0.2%, as recommended by *Bennett et al.* or decreasing the concentration of the SP600125 stock solution to avoid high concentrations when it is added to the media. Alternatively, work could be carried out in *jnk1*$^{-/-}$, *jnk2*$^{-/-}$ and/or c-*jun*$^{-/-}$ knock-out cells (or through use of siRNA knockdown of these proteins) in order to determine if the current hypothesis, that JNK-c-jun signalling is essential for the cell death observed during prolonged IRE1α signalling (section 5.2.3.3), is correct.

The second method of showing that apoptotic signalling is mediated via an IRE1α-TRAF2-JNK pathway was the siRNA knockdown of TRAF2 and the data obtained in section 5.2.3.2 show that siRNAs targeting of TRAF2 reduce TRAF2 protein levels (Figure 5.16). Further analysis was then able to show that this in turn reduces the amount of p-JNK and PARP-1 cleavage (Figure 5.17). In order to strengthen the data obtained in section 5.2.3.2, future work could be carried out to show that TRAF2 knockdown results in a reduction in apoptosis during treatment with AP20187. This could be achieved by transfecting Flp-In T-REx HEK293 Fv2E-IRE1α cells with TRAF2 siRNA (methods section 3.3.8) and then treating them with AP20187 before assessing cell viability using an MTT assay (section 3.3.10). It is likely that this would support the data obtained in this chapter, which shows that TRAF2 knockdown disrupts JNK and PARP-1 signalling (Figure 5.17) and, when JNK phosphorylation and PARP-1 cleavage were attenuated during the use of IRE1α^{D711A}

and IRE1α^{K599A}, cell death was reduced to untreated levels (sections 5.2.5 and 5.2.6). Furthermore, it would also be useful to obtain data showing TRAF2 mRNA levels decrease during treatment with TRAF2 siRNA in order to complement the data in Figure 5.16, which shows that the amount of TRAF2 protein is reduced by treatment with TRAF2 siRNA.

Having made progress in characterising the splicing of *XBP1* by Fv2E-IRE1α and apoptotic signalling via the Fv2E-IRE1α-TRAF2-JNK pathway, the one aspect of Fv2E-IRE1α signalling that has yet to be studied is signalling via NF-κB. A minor investigation into the role of NF-κB during IRE1α signalling was carried out as part of this thesis (summarised in Appendix 4), but difficulties optimising the assays, combined with the fact that this avenue diverged significantly from the main line of investigation, meant that this was not pursued. Therefore, further work could be centred on characterising the activation of NF-κB, as there is a large body of evidence that links ER stress to elevations in NF-κB signalling (Hu et al., 2006, Tam et al., 2012, Deng et al., 2004), but there is some dispute over how much IRE1α contributes to this. Furthermore, there is also debate as to whether NF-κB signalling is protective or apoptotic. Therefore future work determining if AP20187 treatment results in elevations of NF-κB in nuclear lysates obtained from Flp-In T-REx HEK293 Fv2E-IRE1α cells would be valuable, as this would show that IRE1α activation is sufficient for NF-*κ*B activation. This could then be followed by treatment with TRAF2 siRNA to determine if this activation is dependent on IRE1α-TRAF2 signalling. Finally, carrying out an MMT assay on AP20187 treated Flp-In T-REx HEK293 Fv2E-IRE1α cells in the presence of either an NF-κB inhibitor, such as BAY 11-7085 (Pierce et al., 1997) or MG-132(Arlt et al., 2001), or siRNA targeting NF-κB (Lee et al., 2008b) could help to determine if IRE1α mediated activation of NF-κB is protective or apoptotic.

As stated at the beginning of this thesis, the primary aim of this work was to isolate and characterise the mechanisms by which IRE1α signalling occurs *in vivo*. This is because greater understanding of the downstream signalling events may provide insight as to how apoptotic signalling can be disrupted, whilst leaving protective signalling intact. The most efficient way to do this would be to find a mechanism by which the IRE1α-TRAF2 interaction could be disrupted, as shown by the effectiveness of knocking down TRAF2 (section 5.2.3.2). Therefore, future work could be carried out whereby the Fv2E-IRE1α construct is expressed in *traf2*$^{-/-}$ cells. Assumedly in this scenario Fv2E-IRE1α signalling would be abolished, but could also be reconstituted via the exogenous expression of wild type TRAF2. If this were the case, then TRAF2 mutants with alterations to their TRAF-C

domains could then be used to try and isolate the motifs required for interaction with IRE1α (Chung et al., 2007), although it should be noted that TRAF2 has been reported to autoactivate when overexpressed (Tsitsikov et al., 1997). Targeting TRAF2 in this way would avoid the problem of trying to interfere with the IRE1α kinase domain, but would have the drawback of targeting an adaptor protein that is involved in various other signalling cascades, such as that of TNF-α (Baud and Karin, 2001).

Another route of investigation that could prove useful would be to integrate the Fv2E-IRE1α system into other cell lines, perhaps even ones that had endogenous IRE1α knocked out (although, once the co-IP had been optimised, the presence of endogenous IRE1α did not appear to be detrimental). This would be useful because, as mentioned in the introduction, IRE1α-TRAF2 signalling would appear to instigate the formation of a signalling complex or 'UPRosome' and a vast number of proteins have been mooted as being involved (Woehlbier and Hetz, 2011). However, that fact that many of these proteins have only been shown to interact with IRE1α in specific cell lines suggests that the IRE1α signalling scaffold is likely to be cell specific. Integration of the Fv2E-IRE1α system into multiple cell lines would therefore be useful as it would allow co-immunoprecipitation, using Fv2E-IRE1α as bait, to elucidate key components of the IRE1α signalling cascade in a cell specific manner, without cross-talk from other signalling pathways. In addition to this, the use of different cell lines would allow specific studies regarding the role of IRE1α in different diseases. For example, when looking for therapeutic treatments for JNK-mediated insulin resistance, the use of hepatocytes or skeletal muscle cells would be more useful than the embryonic kidney cells used during this project. Alternatively, rather than making multiple cell lines, it may also be possible to create a transgenic mouse, with the Fv2E-IRE1α protein under tissue specific promoters, and then either feed it, or inject it, with AP20187. This would allow an assessment of IRE1α signalling in different tissues on the whole organism scale.

5.3.1 Summary

The data presented in Chapter 5 show that AP20187 causes the activation and autophosphorylation of Fv2E-IRE1α (5.2.2.4), replicating the signalling that is observed when ER stress mimetic drugs are used to activate wild type IRE1α. However, unlike ER stress mimetic drugs, AP20187 appears to activate IRE1α in isolation (5.2.2.1). Upon activation, Fv2E-IRE1α was shown to undergo autophosphorylation (5.2.2.4) and to bind to TRAF2 (5.2.1.3), inducing elevated levels of phospho-JNK, phospho-c-jun, PARP-1 cleavage (5.2.2.4) and cell death (5.2.2.2). Furthermore, it was established that this apoptotic signalling occurs in a TRAF2-dependent manner, with siRNA-induced reductions of TRAF2 protein levels resulting in reduced levels of phospho-JNK and PARP-1 cleavage (5.2.3.2). It was also shown that Fv2E-IRE1α retains both kinase (5.2.2.4) and endoribonuclease activity (5.2.6.2).

Further study revealed that mutations that disrupt the kinase activity of IRE1α abolish downstream stress signalling and apoptosis, as evidenced by the K599A (section 5.2.4) and D711A (section 5.2.5) mutants. However, whilst the D711A mutation prevented apoptotic signalling, it did not prevent interaction with TRAF2 (5.2.5.1). This is a novel finding and contrasts with current literature, which proposes that an active IRE1α kinase domain is required for interaction with TRAF2 and that this interaction with TRAF2 is sufficient for downstream activation of JNK (Urano et al., 2000b). The work with the mutant variants of IRE1α also showed that disruption of the kinase domain abolishes endoribonuclease activity with the K599A, K599R, D711A and D711A/I642G mutants all failing to splice *XBP1* (sections 5.2.6 and 5.2.7).

Therefore, the work carried out in this section has provided a system that allows the specific activation of IRE1α *in vivo* and a method that can be used to isolate the proteins involved in the IRE1α-TRAF2 signalling scaffold. Furthermore, the work with the D711A mutant has provided a potentially novel insight into the mechanism by which IRE1α and TRAF2 instigate apoptotic signalling and this, plus the potential impact of the Fv2E-IRE1α system in a broader context, will be discussed in Chapter 6.

6 Discussion

Having evaluated the experimental design implemented whilst obtaining the data presented in this thesis and the consequences it may have on our understanding of the contribution of the kinase and RNase activities of IRE1α to the activation of apoptotic JNK signalling, the focus of this final chapter will be to switch from a myopic dissection of the IRE1α-TRAF2 interaction and provide a broader perspective as to how the Fv2E-IRE1α system fits into the context of the unfolded protein response, inflammatory signalling and the pathologies associated with them.

6.1 Fv2E-IRE1α in the context of the unfolded protein response

The work carried out in this project provides a model in which IRE1α signalling can be studied in isolation through the use of AP20187, a chemical which causes activation of both the IRE1α kinase domain and endoribonuclease activity without initiating the generic ER stress that is observed when using ER stress mimetic drugs such as thapsigargin or tunicamycin. The specificity of the Fv2E-IRE1α system therefore makes it more powerful than traditional models when trying to elucidate the mechanisms by which IRE1α signals for cytoprotection and apoptosis because it avoids the initiation of global stress signalling and the complex web of interrelated downstream interactions that ultimately follow. The significance of this model has already been highlighted by the fact that data collected during this thesis provides novel insight into how IRE1α signalling occurs.

It is believed IRE1α signalling is initiated when IRE1α monomers form dimers/oligomers (Shamu and Walter, 1996) in response to the dissociation of BiP and direct binding to misfolded proteins within the ER lumen (Kimata et al., 2007, Pincus et al., 2010). The process of dimerisation/oligomerisation allows IRE1α to undergo autophosphorylation (Shamu and Walter, 1996) and a conformational change (Korennykh et al., 2009, Lee et al., 2008a), which allow signalling via the kinase domain and RNase domains respectively. Up until this point, it was believed that nucleotide binding during autophosphorylation, but not autophosphorylation itself, was responsible for the conformational change that allows *XBP1* splicing to occur (Papa et al., 2003). This was based on work using a yeast analogue of the mammalian D711A mutant (D828A), which lacks kinase activity, but retains both the ability to bind ATP and splice *XBP1* (Papa et al., 2003). However, the data presented in this thesis contrasts with this theory as the Fv2E-IRE1α^{D711A} mutant fails to splice *XBP1* (section 5.2.6.2). The reason for this is unknown, but the lack of *XBP1* splicing observed whilst using Fv2E- IRE1α$^{D711A/I624G}$ and 1NM-PP1 (section 5.2.7) would suggest that it is

not a lack of nucleotide binding and the ability of Fv2E-IRE1α^{D711A} to interact with TRAF2 (section 5.2.5.1) would suggest it is not an issue with folding either. Therefore, it could be possible that human IRE1α differs slightly from its yeast homologue and requires autophosphorylation to occur in order to initiate endoribonuclease activity. Clearly this is a conclusion that cannot be drawn from the current data, but what is evident is that the Fv2E-IRE1α system challenges our current knowledge regarding the mechanism by which IRE1α-XBP1 signalling occurs during the UPR and provides a new perspective from which to study this pathway in the future.

The other aspect of IRE1α signalling occurs via the IRE1α-TRAF2-JNK pathway, which is complicated by the fact that JNK signalling during ER stress appears to be biphasic. During shorter, transient periods of ER stress ≤8 h it is believed that JNK signalling is cytoprotective (Brown et al., 2016), whilst during prolonged stress ≥12 hours, JNK signalling becomes apoptotic (Nishitoh et al., 2002, Urano et al., 2000b). However, the mechanism and conditions required for this switch to occur remain elusive. Therefore, whilst the data collected in this thesis only deal with prolonged, apoptotic signalling, the ability to study IRE1α signalling isolation will prove useful during future attempts to elucidate how IRE1α-TRAF2- JNK signalling can be both protective and apoptotic.

Apoptotic signalling via the IRE1α kinase domain is thought to occur as a result of interaction with TRAF2 which, up until now, was believed to require a functional IRE1α kinase domain (Urano et al., 2000b). However, the data collected using Fv2E-IRE1α^{D711A} suggests that the kinase activity of IRE1α is not required for an interaction with TRAF2 to occur, but is required for downstream signal transduction (sections 5.2.5 and 5.2.6.1). This therefore opens the possibility that there are other targets of the IRE1α kinase domain, which contrasts to our current understanding that IRE1α is only capable of autophosphorylation (Shamu and Walter, 1996). The potential targets of the IRE1α kinase domain are numerous because TRAF2 binding is believed to stimulate the formation of a tissue-specific, multi-protein scaffold or 'UPRosome' (Woehlbier and Hetz, 2011). However, based on current understanding, ASK1 (Nishitoh et al., 2002), IKK (Hu et al., 2006) and TRAF2 (Urano et al., 2000b) would be the primary candidates. In support of the idea that IRE1α may phosphorylate members of the UPRosome, *Yoneda et al.* have previously presented data that show elevations in TRAF2 phosphorylation result in increased downstream activation of JNK (Yoneda et al., 2001). An alternative view of this data, and its implications on the mechanism by which apoptotic JNK signalling occurs, could be that an active endoribonuclease domain (lacked by Fv2E-IRE1α^{D711A} and Fv2E-

IRE1α^{K599A}, but possessed by Fv2E-IRE1α) is required for downstream JNK activation. However, whilst this is a logical question to ask based on the data, it is currently difficult to see how this model would fit with current literature on the activation and transduction of IRE1α signalling. Therefore, whilst more work will need to be done to elucidate the nuances of IRE1α-TRAF2-JNK signalling, the Fv2E-IRE1α system has provided novel insight into this pathway and may hold the key to determining how apoptotic signalling via JNK differs from protective signalling.

Downstream of the IRE1α-TRAF2 interaction, data obtained in this thesis shows that prolonged signalling results in elevated levels of phospho-JNK, c-jun and PARP-1 cleavage (≥12 h), which ultimately lead to an increase in cell death (≥24 h). Therefore, the data collected using the Fv2E-IRE1α system would present a model for apoptotic IRE1α signalling as follows: IRE1α forms dimers/oligomers, allowing the recruitment of TRAF2 (section 5.2.1.3). This interaction between IRE1α and TRAF2 allows the formation of a signalling scaffold in which IRE1α phosphorylates itself and other, as yet unknown, targets (section 5.2.2). It is likely that these targets are proteins such as ASK1, which are capable of phosphorylating and activating JNK (section 5.2.2.4). JNK then phosphorylates c-jun (section 5.2.3.3), which can activate the transcription of genes involved in apoptotic signalling (Bossy-Wetzel et al., 1997). In addition JNK may also stimulate apoptotic signalling via the mitochondrial cell death pathway, through activation of Bcl-2 family members (Ghatan et al., 2000), which have been shown to induce PARP-1 cleavage and cell death (Yang et al., 2006a).

6.2 Fv2E-IRE1α in the context of inflammatory signalling

Many receptors exert their effects via JNK signalling and, with IRE1α being a protein that acts in this manner, the work in this thesis has the potential to contribute to a broader understanding of the role that JNK plays in inflammatory signalling. As described during the introduction, signalling via JNK is extremely complex, with a large number signalling pathways converging to activate JNK and an equally large number of pathways diverging to produce disparate effects once JNK has been activated (Nishina et al., 2004). Therefore, despite extensive study, it is still unclear if the function of JNK is apoptotic or pro-survival (Molton et al., 2005, Huang et al., 2014). In addition to this, defining the role of JNK can be complicated further when, similar to its apparent role in the unfolded protein response, JNK appears to carry out both these roles depending on the intensity and duration of the stress (Brown et al., 2016, Urano et al., 2000b).

The ability of JNK to be such a versatile signalling molecule appears to arise from its association with scaffolding proteins, which allow the integration of various signals via the binding of proteins that act both upstream and downstream of JNK. This occurs because these scaffolding proteins tend to have numerous protein-protein interaction motifs and, therefore, create the possibility of a wide range of potential scaffold configurations which, assumedly, cater for the vast number of effects that can be observed when JNK is activated.

Generally, the foundation of these signalling scaffolds will be a member of the JNK interacting protein (JIP) family, of which there are currently four known members (Whitmarsh, 2006). The most abundant and best characterised member of the family is JNK interacting protein 1 (JIP1) (Dickens et al., 1997), which is of particular interest in the context of UPR signalling because it exhibits elevated expression in pancreatic β cells (Martin et al., 2003). Furthermore there is evidence to suggest that JIP1 is directly involved in the development of obesity related type 2 diabetes (Jaeschke et al., 2004). However, JIP3 also has the potential to be involved in ER stress signalling as it has been shown to interact with ASK1 (also known as mitogen-activated kinase kinase kinase 5), which is recruited during UPR-mediated apoptosis in neuronal cells (Nishitoh et al., 1998). The N-termini of all JIPs possess a JNK docking domain, whilst the C-termini possesses various protein-protein interaction domains such as src-homology 3 domains and phosphor-tyrosine binding domains, both of which are found in the C-termini of JIP1 and JIP2 (Sharrocks et al., 2000). This structure allows JIPs to act as scaffolds by bringing JNK into close proximity to both upstream activators, such as MKK7 (Ikeda et al., 2001), and downstream targets such as amyliod precursor protein (Muresan et al., 2014). The ability of JIPs to form a variety of protein signalling scaffolds is further exhibited by the fact that JIPs can recruit mixed lineage kinases as well (Whitmarsh et al., 1998). Furthermore, the scaffolds formed can diversify further by not only interacting with a variety of proteins that activate JNK, but also proteins that inhibit JNK. This is shown by evidence to suggest that JIP1 is capable of recruiting negative regulators of JNK such as MAPK phosphatase 7 and the JNK phosphatase M3/6 (Willoughby et al., 2003).

The diversity allowed by JIP scaffolds may well hold the key to understanding how JNK can be finely tuned to instigate both pro-survival and apoptotic signalling in response to a single stress, as exhibited during the UPR. In these scenarios it could be possible that the combination of proteins recruited to the signalling scaffold will be altered depending on the duration and intensity of the stress. In this model, short periods of stress may recruit

different MEKs/MLKs when compared to periods of prolonged stress. This difference could result in different downstream targets of JNK binding to the scaffold, such as Bcl-2 (Deng et al., 2001) during short periods of stress and c-jun during prolonged periods of stress (Sabapathy and Wagner, 2004). This could be applied to IRE1α, especially if the data presented in this thesis is correct in suggesting that the kinase domain of IRE1α may have multiple targets. Thus, it may be that IRE1α phosphorylates and activates an upstream activator of JNK that causes apoptotic signalling, but this protein has to compete with other, pro-survival kinases for binding sites or residues on the JIP. During low levels of stress, the amount of active IRE1α will also be low and, therefore, the number of apoptotic upstream kinases may be outcompeted, giving the JNK activation scaffold a pro-survival configuration and resulting in the recruitment of pro-survival targets of JNK. However, as more IRE1α is activated, more apoptotic kinases would be recruited and this would change the configuration of the scaffold, causing apoptotic targets of JNK to be recruited. Thus, even though JNK is always recruited and activated, the downstream targets that are recruited for phosphorylation by JNK will differ depending on the duration and intensity of the stress.

Alternatively, it could be that JIPs are recruited to the IRE1α-TRAF2 scaffold and are then modified directly by IRE1α in order to create a multi-scaffold, apoptotic signalling complex. This idea would be supported by evidence suggesting that, not only can JIPs form dimmers with one another, but they can also bind to other scaffolding proteins in order to form multi-scaffold complexes (Kukekov et al., 2006). Furthermore, there is evidence to suggest that JIP undergoes extensive post-translational modification, displaying over 30 phosphorylation sites during stress (D'Ambrosio et al., 2006). Therefore, if the data in this thesis is correct in suggesting that the IRE1α kinase domain may have multiple targets, it may be possible that IRE1α could phosphorylate JIP1. In this scenario, the level of JIP1 phosphorylation could determine the JNK targets that it recruits. Low levels of phosphorylation, which would occur during transient periods of stress, could result in the recruitment of prosurvival JNK targets, whilst high levels of phosphorylation, occurring during prolonged stress, could result in the recruitment of apoptotic JNK targets.

6.3 Fv2E-IRE1α in the context of disease

Proteins are essential in governing virtually every aspect of cellular activity and therefore it is unsurprising that defects in the regulation of protein synthesis cause a plethora of diseases (Ellisdon and Bottomley, 2004). With the ER being responsible for the folding and maturation of the majority of the cell's proteins, it is logical that diseases caused by aberrant proteins will initiate the unfolded protein response and, therefore, the UPR becomes incorporated into the pathology of the disease. This is true of a wide variety of cancers, inflammatory disorders, neurodegenerative diseases and cardiovascular diseases (Park and Ozcan, 2013), which have been all been linked to the UPR, as well as more specific diseases such as Wolcott-Rallison syndrome (Julier and Nicolino, 2010), α1-AT deficiency (Stoller and Aboussouan, 2012) and even certain viral infections (Jheng et al., 2010).

Persistent accumulation of misfolded proteins is well documented in causing UPR mediated cell death and this is a situation that is observed in many neurodegenerative diseases, with a substantial number of them being caused by mutations in genes that result in the accumulation of misfolded proteins. For example, Parkinson's disease is caused by a mutation on the Parkin gene, causing the production of a mutant E3 ligase and subsequent defects in the degradation of proteins (Kitada et al., 1998). Huntington's disease causes the production of mutant Huntington protein, which contains a series of CAG repeats that prevent its correct folding, whilst Alzheimer's disease is caused by a mutation in the protein presenilin (Hardy and Allsop, 1991). Hence, all of these examples result in an accumulation of misfolded proteins and prolonged ER stress signalling resulting in JNK and CHOP mediated neuronal cell death. Consequently, whilst these neurodegenerative diseases cause activation of the UPR, it is the resultant UPR signalling that stimulates the neuronal cell death that characterises the diseases (Bucciantini et al., 2002).

Conversely, whilst the apoptotic signalling of the UPR is responsible for cell death in degenerative diseases, it is believed that the protective branch of the UPR can be attributed to the development of certain cancers (Vandewynckel et al., 2013). Cancers can cause the accumulation of misfolded proteins, and subsequent activation of the UPR, via the transcription of mutated genes, excessive demand for new protein synthesis and hypoxia resulting from insufficient vascularisation during tumour growth (Queitsch et al., 2002). However, in this instance, the UPR can aid disease propagation by promoting adaptation to ER stress, with research showing that *XBP1* splicing (Romero-Ramirez et al., 2009) and increased levels of BiP (Cai et al., 1993) actually aid the survival of cancer cells and

enhance tumour growth. Furthermore, deletion of IRE1, PERK or ATF6 has been shown to slow tumour growth rates and decrease angiogenesis (Auf et al., 2010) (Wang et al., 2012). Therefore, it is clear that a wide variety of diseases can stimulate the UPR and that the UPR contributes significantly to the symptoms associated with these diseases. It is also extremely interesting to note that the UPR can contribute to diseases via either protective or apoptotic signalling. However, when looking at UPR related pathologies, there is one disease which stands out in terms of the volume of literature that has been produced and this is type 2 diabetes.

Thus far research has shown that the contribution of ER stress to the development of type 2 diabetes is twofold. Firstly, JNK signalling causes the phosphorylation and inhibition of IRS1, which prevents insulin signal transmission (Ozcan et al., 2004). This is then combined with the death of insulin producing β-cells as a result of ER stress induced apoptosis in response to excessive demand for *de novo* insulin synthesis during over-nutrition. Therefore, the cumulative effect of these two factors is a decrease in insulin production and sensitivity, which are the hallmarks of the pathology exhibited in type 2 diabetes.

The idea that JNK has a major role in the development of obesity related insulin resistance was first proposed by *Hirosumi et al.* (Hirosumi et al., 2002) as a result of Western blot analysis revealing that the amount of phosphorylated JNK is significantly higher in obese mice when compared to lean counterparts. In addition to this, $jnk^{-/-}$ mice exhibited a significant reduction in adiposity and enhanced insulin sensitivity. The molecular link between elevated JNK signalling and inhibition of insulin signalling was provided by *Ozcan et al.* who showed that, during ER stress, JNK phosphorylates serine residues on insulin receptor substrate 1 (IRS1) (Ozcan et al., 2004). This event prevents IRS1 from being phosphorylated by the insulin receptor, which has a substrate preference for tyrosine rather than serine or threonine (Hubbard et al., 1994).

However, targeting the UPR whilst searching for therapeutic treatments for type 2 diabetes is complicated by the fact that some aspects of UPR signalling also protect β-cells from cell death during excessive demand for *de novo* insulin synthesis. The protective function of the UPR during excessive insulin demand is mediated by PERK stimulated translational arrest and the activation of genes that increase the ER's folding capacity by IRE1/XBP1 and ATF6. This is evidenced by the fact that perturbation of these processes has been shown to exacerbate cell death and speed up the onset of diabetes. For example, $perk^{-/-}$ mice (Liu et al., 2005) or cells expressing $eIF2\alpha^{S51A}$ (which cannot be phosphorylated)

(Scheuner et al., 2001) have been shown to develop severely decreased β cell mass and overt diabetes mellitus due to an accumulation of misfolded proinsulin (Back et al., 2009), whilst deletion of the XBP1 gene in mice causes them to develop insulin resistance (Ozcan et al., 2004). However, the UPR is also capable of exacerbating insulin resistance by instigating an increase in apoptosis via PERK/ATF6 activation of CHOP and IRE1α activation of JNK/NFκ-B (Han et al., 2013, Hasnain et al., 2014).

Thus, with the UPR being linked to a plethora of diseases, and possessing the ability to amplify the effects of their pathogenesis by either promoting cell survival or instigating cell death (Yoshida, 2007), it is unsurprising that many research groups are choosing to investigate the UPR as a potential target for therapeutic drug treatments (Hetz et al., 2013). However, this is complicated by the fact that the UPR can either provide protection, which is useful in degenerative diseases, or signal for apoptosis, which is useful for diseases exhibiting excessive proliferation, such as cancer. Therefore, when searching for therapeutic treatments it is not possible to inhibit or amplify the UPR as a whole. Instead, there needs to be a way of promoting certain branches of the UPR, whilst inhibiting others. With PERK and ATF6 this is difficult, because they mediate both their apoptotic and their protective functions via the same method. PERK phosphorylates eIF2α to initiate attenuation of translation (protective) (Harding et al., 2000b) and CHOP upregulation (apoptotic) (Averous et al., 2004), whist ATF6 upregulates genes involved in increasing the ER's folding capacity (protective) (Yoshida et al., 1998) and once again CHOP (Fawcett et al., 1999), which is apoptotic. In this respect IRE1α becomes a prime candidate for the design of therapeutic drugs as it is a bifunctional enzyme that mediates protection via its endoribonuclease domain and apoptosis via its kinase domain. Therefore, if drugs could be developed to switch off one pathway, whilst leaving the other intact, there is a strong possibility of being able to choose which function of the UPR is predominant depending on the disease (Jiang et al., 2015). For example, inhibiting endoribonuclease function, and subsequent *XBP1* splicing, could be useful in halting the progression of certain cancers (Romero-Ramirez et al., 2009), whilst inhibiting the kinase signalling pathway could help reduce the inflammatory signalling and cell death exhibited in type 2 diabetes. As a result of this potential, many research groups have started working on drugs that can effect IRE1α signalling and these are outlined in the table below:

Table 6.1 – Drugs that have been reported to affect IRE1α signalling

Name	Mode of action	Reference
STF-083010	Inhibits endoribonuclease activity	(Papandreou et al., 2011)
Salicylaldehyde analogs	Non-competitive-inhibition of XBP-1 mRNA binding	(Volkmann et al., 2011)
4μ8C	Competitive-inhibition of XBP1 and RIDD substrates	(Cross et al., 2012)
MKC-3946	Endoribonuclease domain inhibitor	(Mimura et al., 2012)
Toyocamycin	Prevents XBP1 splicing	(Ri et al., 2012).
8-formyltetrahydrochromeno [3,4-c]pyridines	Inhibit endoribonuclease activity	(Ranatunga et al., 2014)
Hydroxy aryl aldehydes	Inhibit IRE1α endoribonuclease activity	(Ranatunga et al., 2014)

Unfortunately, as can be seen from Table 6.1, there are currently only inhibitors of endoribonuclease activity being reported. The reason for this bias is likely to be because, whilst the kinase activity of IRE1α acts independently of the RNase domain, the endoribonuclease function of wild type IRE1α is dependent on the IRE1α's ability to autophosphorylate itself. Therefore, inhibiting apoptotic signalling is not a simple case of targeting the kinase domain, but instead requires intervention downstream of autophosphorylation. This process would require an intimate knowledge of the IRE1α-TRAF2 signalling cascade; knowledge that could be attained through use of co-immunoprecipitation assays. Thus, data obtained using the Fv2e-IRE1α system would be especially valuable if, as suggested by the work with D711A, IRE1α modifies some of the proteins in the signalling scaffold via phosphorylation. Under these circumstances, identifying and disrupting the interaction between IRE1α and these proteins could allow the apoptotic signalling via JNK to be switched off whilst maintaining protective *XBP1* splicing. Furthermore, if there were a situation whereby different proteins were recruited to the scaffold during short-term, protective JNK signalling, when compared to prolonged, apoptotic signalling, it may even be possible to differentiate between the two and maintain protective JNK signalling.

In summary, the data obtained in this thesis provides new insight into the mechanism by which IRE1α-controls cell fate decisions via the characterisation of signalling by both the endoribonuclease and kinase domains. Furthermore, as a result of the specificity afforded by the Fv2E-IRE1α model, future research has the potential to elucidate motifs and protein interactions that can be targeted in order to disrupt apoptotic JNK signalling, whilst retaining cytoprotective signalling via JNK and XBP1. Therefore, this system could be used to develop strategies that will allow manipulation of the cell fate decisions made by IRE1α, which would have a significant impact when investigating diseases that incorporate apoptotic UPR signalling as part of their pathology, such as neurodegenerative disorders and type 2 diabetes.

APPENDIX 1a – A second biological repeat of data showing that AP20187 treatment of Flp-In T-REx HEK293 Fv2E-IRE1α cells induces elevations in p-IRE1α, p-JNK and PARP-1 cleavage.

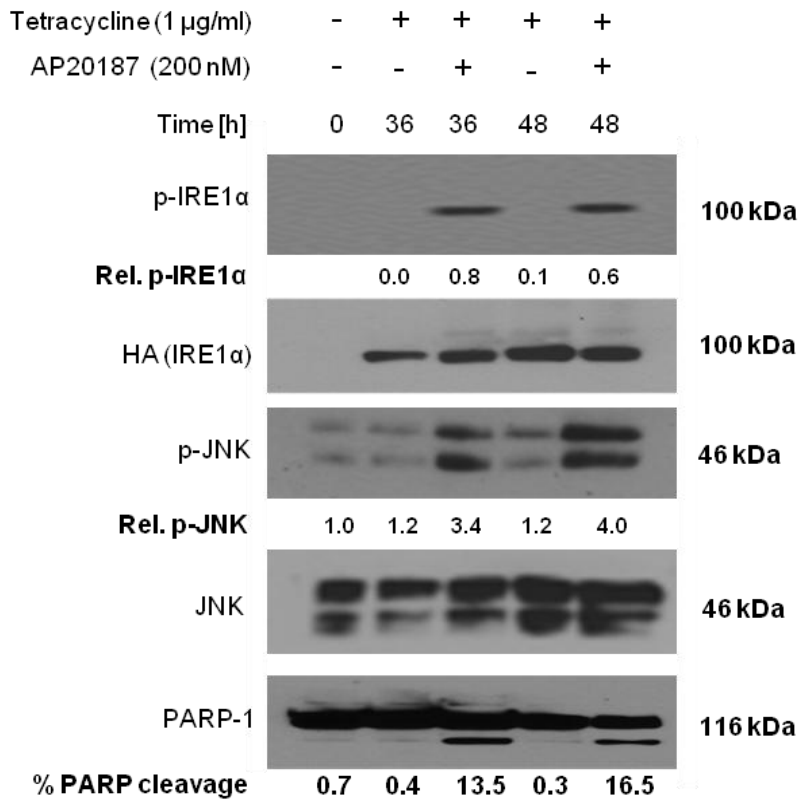

Figure 6.1 –AP20187 treatment of Flp-In T-REx HEK293 Fv2E-IRE1α cells induces elevations in p-IRE1α, p-JNK and PARP-1 cleavage.
Western blot showing the amount of p-IRE1α, IRE1α, p-JNK, JNK and PARP-1 proteins obtained from Flp-In T-REx HEK293 Fv2E-IRE1α cells that had been treated with tetracycline and AP20187 as shown. '0 h' samples were treated with 100% EtOH (vehicle) and the antibodies used during Western blotting are shown on the left hand side.

APPENDIX 1b – A third biological repeat of data showing that AP20187 treatment of Flp-In T-REx HEK293 Fv2E-IRE1α cells induces elevations in p-IRE1α, p-JNK and PARP-1 cleavage.

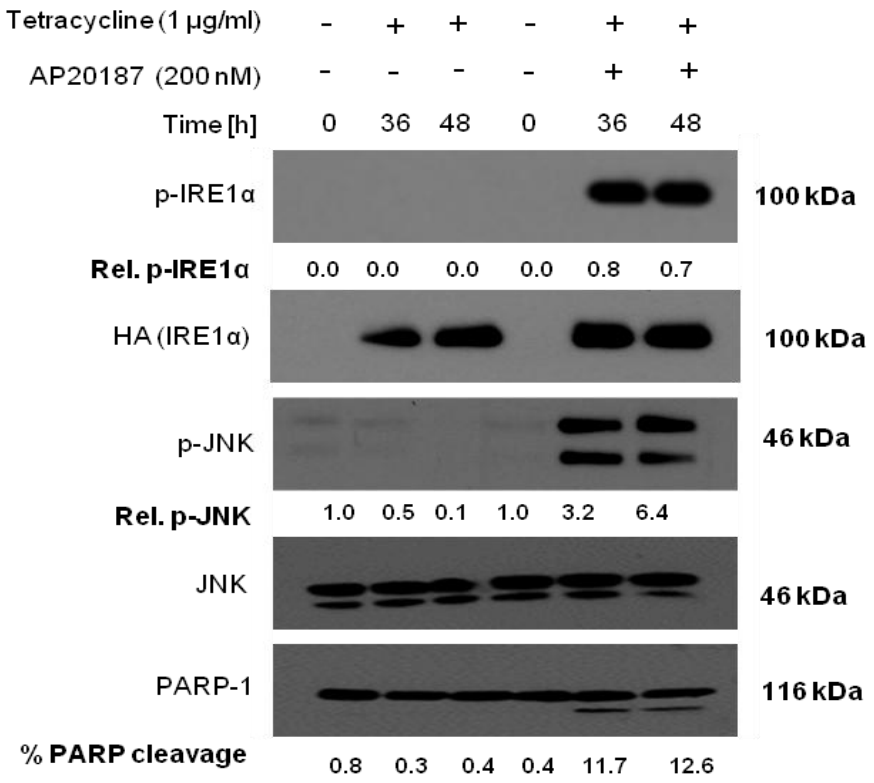

Figure 6.2 –AP20187 treatment of Flp-In T-REx HEK293 Fv2E-IRE1α cells induces elevations in p-IRE1α, p-JNK and PARP-1 cleavage.
Western blot showing the amount of p-IRE1α, IRE1α, p-JNK, JNK and PARP-1 proteins obtained from Flp-In T-REx HEK293 Fv2E-IRE1α cells that had been treated with tetracycline and AP20187 as shown. '0 h' samples were treated with 100% EtOH (vehicle) and the antibodies used during Western blotting are shown to the left of the image.

APPENDIX 2a – A second biological repeat of data showing that TRAF2 is required for Fv2E-IRE1α mediated JNK signalling and PARP-1 cleavage.

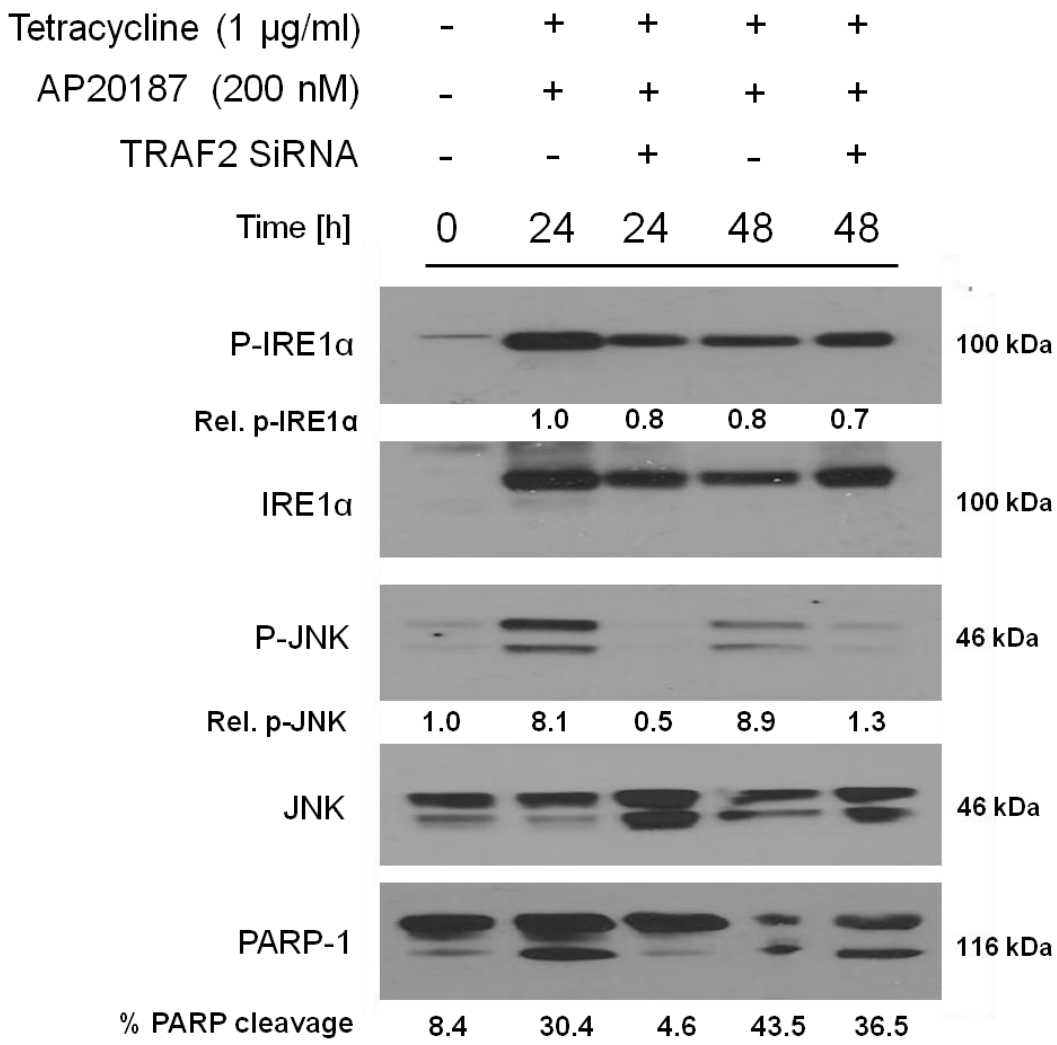

Figure 6.3 –TRAF2 knockdown reduces the amount of p-JNK and PARP-1 cleavage during Fv2E-IRE1α signalling.
Western blot showing the amounts of p-IREα, p-JNK and PARP-1 proteins obtained from Flp-In T-REx HEK293 Fv2E-IRE1α cells that had been treated with tetracycline (1 µg/ml), AP20187 (200 nM) and TRAF2 siRNA (20 µM) as indicated. Untreated p-JNK samples were normalised to '1.0' as a control and the same was done for the 24 h treatment without TRAF2 siRNA for p-IRE1α. The reason for this was because IRE1α was below detectable limits in the untreated samples.

APPENDIX 2b – A third biological repeat of data showing that TRAF2 is required for Fv2E-IRE1α mediated JNK signalling and PARP-1 cleavage.

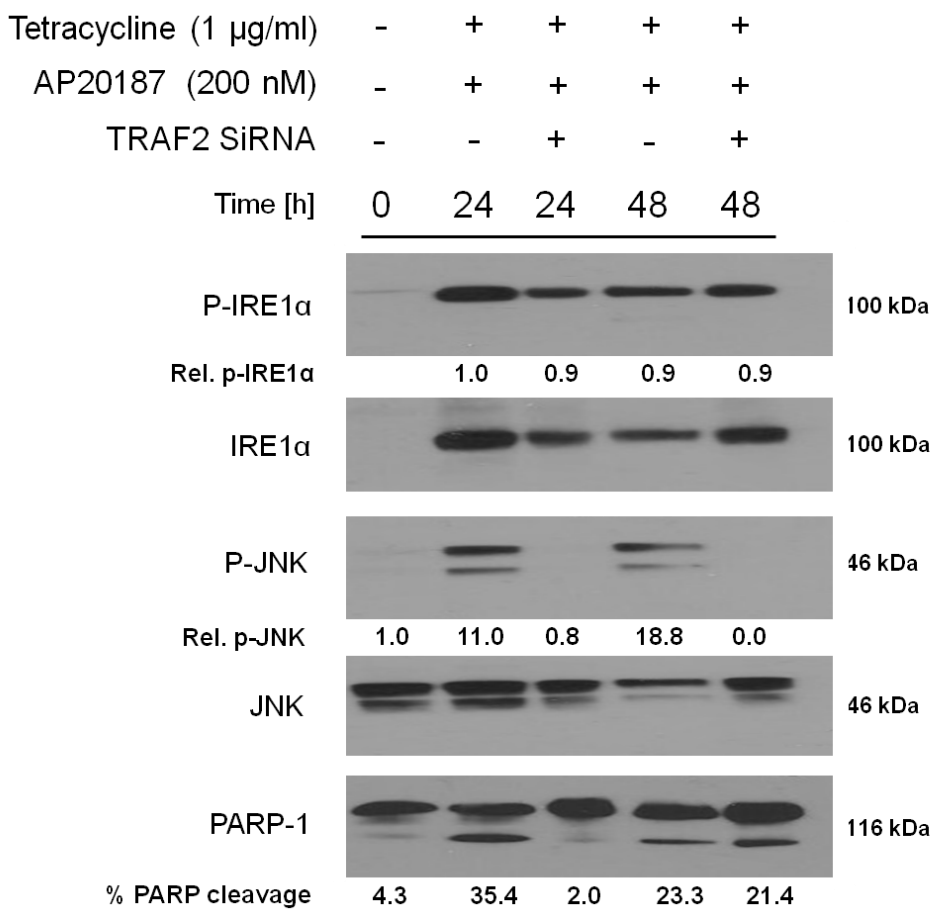

Figure 6.4 – Third biological repeat showing that TRAF2 knockdown reduces the amount of p-JNK and PARP-1 cleavage during Fv2E-IRE1α signalling.
Western blot showing the amounts of p-IREα, p-JNK and PARP-1 proteins obtained from Flp-In T-REx HEK293 Fv2E-IRE1α cells that had been treated with tetracycline (1 µg/ml), AP20187 (200 nM) and TRAF2 siRNA (20 µM) as indicated. Untreated p-JNK samples were normalised to '1.0' as a control and the same was done for the 24 h treatment without TRAF2 siRNA for p-IRE1α. The reason for this was because IRE1α was below detectable limits in the untreated samples.

APPENDIX 3a – A second biological repeat of data showing that IRE1α^{D711A} and IRE1α^{K599A} fail to initiate JNK phosphorylation and PARP-1 cleavage.

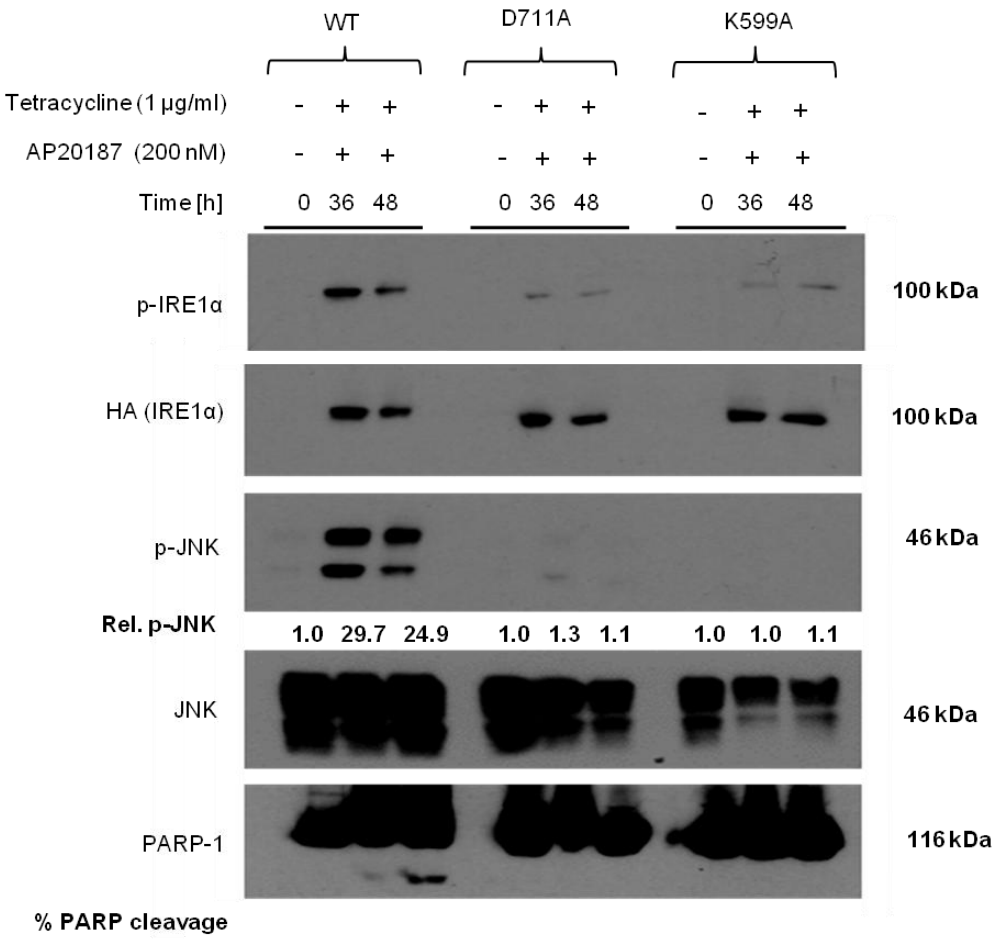

Figure 6.5 –IRE1α^{D711A} and IRE1α^{K599A} fail to initiate JNK phosphorylation and PARP-1 cleavage.
Western blot analysis of p-IRE1α, IRE1α, p-JNK, JNK and PARP-1 in Flp-In T-REx HEK293 cells that have been stably transfected with the Fv2E-IRE1α constructs indicated and then treated with tetracycline (1 µg/ml) and AP20187(200 nM) for either 36 or 48 h. Phospho-JNK levels have been normalised to '1.0' in untreated cells to allow for comparison between treatments.

APPENDIX 3b – A third biological repeat of data showing that IRE1α^{D711A} and IRE1α^{K599A} fail to initiate JNK phosphorylation and PARP-1 cleavage.

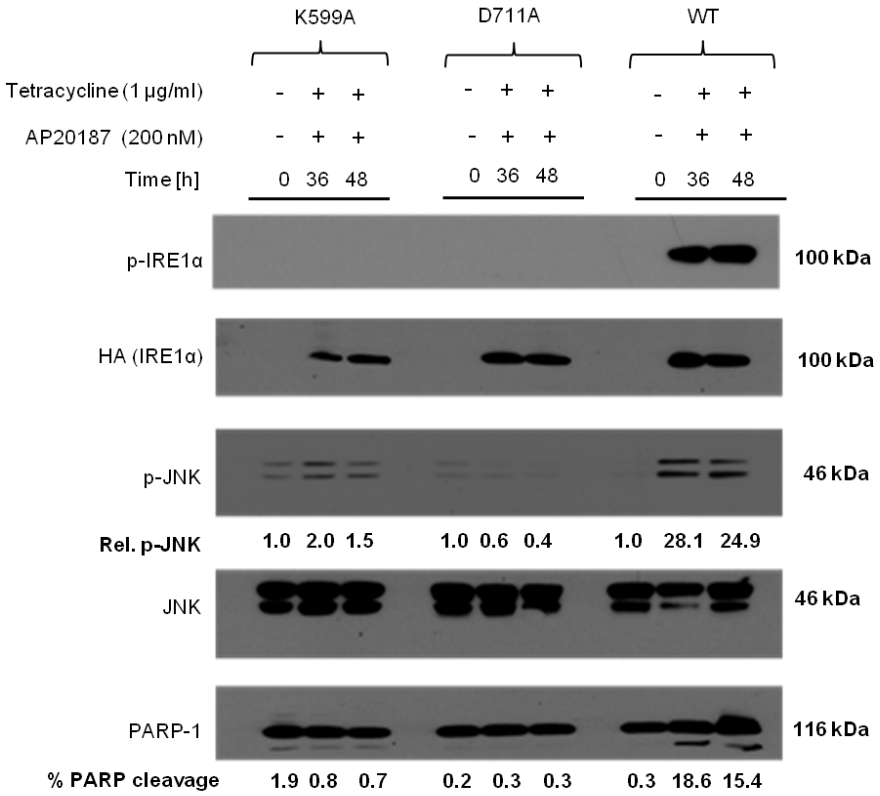

Figure 6.6 –IRE1α^{D711A} and IRE1α^{K599A} fail to initiate JNK phosphorylation and PARP-1 cleavage.
Western blot analysis of p-IRE1α, IRE1α, p-JNK, JNK and PARP-1 in Flp-In T-REx HEK293 cells that have been stably transfected with the Fv2E-IRE1α constructs indicated and then treated with tetracycline (1 µg/ml) and AP20187(200 nM) for either 36 or 48 h. Phospho-JNK levels have been normalised to '1.0' in untreated cells to allow for comparison between treatments.

APPENDIX 4 – Investigating NF-κB signalling in response to ER stress.

Rationale

There is growing support for the theory that NF-κB signalling contributes to the apoptosis observed during ER stress and that the IRE1α kinase domain has a major role in transducing this signal by activating IκB kinase (IKK), which is an upstream activator of NF-κB (Hu et al., 2006, Tam et al., 2012). However, before being able to study the IRE1α-TRAF2-NF-κB pathway, there were technical issues regarding the assay used to measure NF-κB that had to be resolved as a result of the mechanism by which canonical NF-κB signalling is regulated *in vivo*.

In unstimulated cells, NF-κB is sequestered by IκBα, which masks the nuclear localisation signal (NLS) of NF-κB and prevents it from translocating to the nucleus. However, upon the detection of stress, IκBα is phosphorylated by IκB kinase (IKK), which targets IκBα for ubiquitination and subsequent degradation by the proteasome (DiDonato et al., 1996). With IκBα degraded the NLS of NF-κB is exposed and it is free to translocate to the nucleus where it can fulfil its role as a transcriptional activator by binding to κB promoter sites (Gilmore, 2006). However, the NF-κB probe, which was supplied as part of Promega's '*Gel shift assay system'* and used to monitor NF-κB activity (see methods section 3.5.8), is unable to distinguish between active NF-κB and the inactive IκBα sequestered version. Therefore, in order to measure elevations in NF-κB activity, as opposed to elevations in NF-κB protein, it was essential to find a method of isolating active NF-κB from the inactive form. Owing to the fact that the inactive, sequestered form of NF-κB is located in the cytoplasm and the active transcription factor is located in the nucleus, it was decided that the best way to isolate active NF-κB would be to separate the nuclear and cytoplasmic cellular fractions during protein harvesting. This would allow inactive NF-κB to be discarded and ensure that any elevations in the amount of NF-κB were representative of increased NF-κB signalling. The next section therefore details the development of a protocol to isolate nuclear NF-κB and the data that was obtained regarding NF-κB activation in response to ER stress.

Separation of nuclear and cytosolic fractions

Initially it was unknown if it would be possible to obtain clean nuclear protein extracts and it took several attempts and modifications of the original protocol to produce the Western blot in Figure 6.7. However, after a period of optimisation, nuclear and cytosolic protein fractions were harvested from 3T3-F442A cells using the methods outlined in methods section 3.5.5. This involved using a sucrose buffer to lyse the cell membrane and extract the cytosolic proteins before using salt buffers of varying concentration to lyse the nuclei and collect the nuclear proteins. Having collected the cytosolic and nuclear protein fractions, the samples were subjected to Western blotting with antibodies against lamin A (which was used as a positive control for proteins located in the nuclear fraction (Goldman et al., 2002)) and α-tubulin (used as a cytoplasmic protein control (Katsuno et al., 2003)). Samples were also compared between cells that had been treated with 2 μM thapsigargin and those that had not, so as to confirm that thapsigargin treatment did not affect the assay.

As can be seen across the top row of Figure 6.7, when the cytosolic samples were probed with the Jol4 lamin A antibody no bands were detected in either the untreated or treated cells. However, when the nuclear lysates were probed with the same antibody bands can be seen in both the control and thapsigargin treated samples. Conversely, when the lysates were tested with an anti-α-tubulin antibody the opposite was true, with two clear bands appearing in the cytosolic fraction, but no bands being detected in the nuclear fraction. Combined these data suggest that the protocol for isolating separate nuclear and cytosolic fractions had been successful because the nuclear protein (lamin A) is only detected in the nuclear fraction and the cytosolic protein (α-tubulin) is only visible in the cytosolic fraction. Therefore, it was decided that this protocol was suitable for obtaining clean nuclear protein fractions for use in the NF-κB gel shift assay.

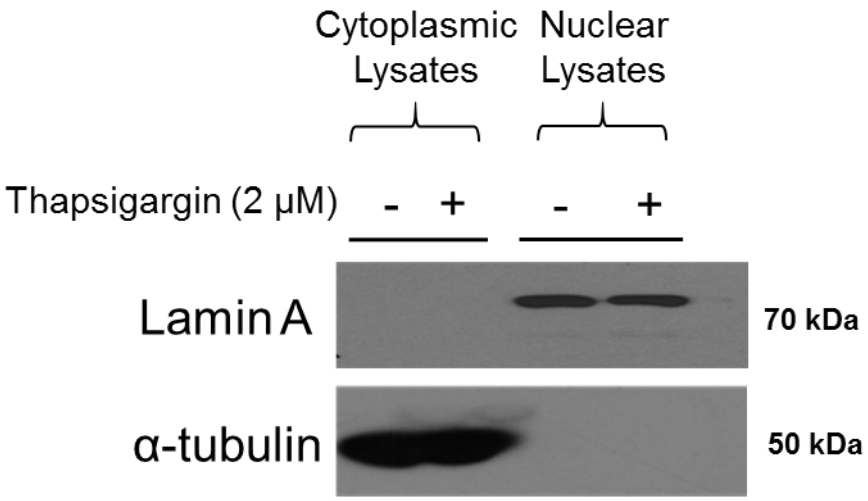

Figure 6.7 – Separation of cytoplasmic and nuclear lysates.
Separate nuclear and cytosolic protein fractions were obtained from 3T3-F442A cells. Antibodies were then used against a nuclear protein (lamin A) and a cytoplasmic protein (α-tubulin) during Western Blot analysis in order to show that the nuclear protein fraction and the cytosolic protein fraction had been successfully separated.

Thapsigargin treatment produces a bell shaped NF-κB response

To investigate the effect of ER stress on NF-κB signalling, 3T3-F442A cells were seeded at approximately 50% confluency 24 h before harvesting and individual samples were treated with either 2 μM, 1 μM or 0.5 μM thapsigargin for up to 6 h, whilst the control group were treated with an equal amount of DMSO to act as a negative control. Nuclear proteins were harvested as detailed in section 3.5.5 and 5 μg of nuclear proteins were then incubated with a radiolabelled NF-κB probe before being separated on a 6% DNA retardation gel and imaged using a phosphorimager as detailed in section 3.5.10.

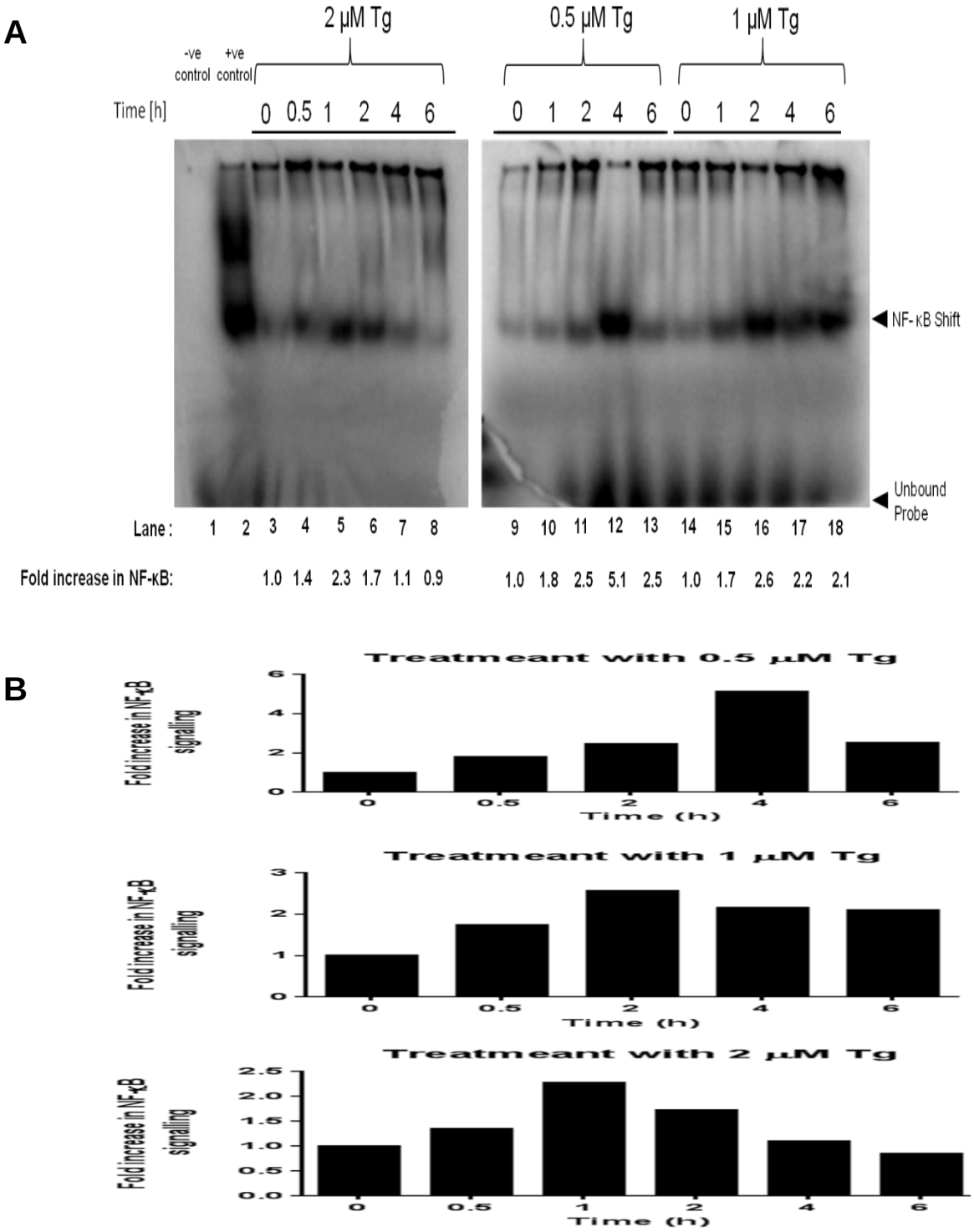

Figure 6.8 – Treatment with thapsigargin results in elevations in NF-κB signalling.

A) Phosphor images showing protein lysates obtained from 3T3-F442A cells that had been treated with a variety of thapsigargin concentrations over a range of time points. The lysates were combined with an NF-κB probe before being run on a 6% DNA retardation gel. The negative control contained a 3T3-F442A cell lysate that treated with 2.0 µM thapsigargin for 0.5 h and then with a non-specific probe, whilst the positive control contained a HeLa cell lysate (provided with the kit) that had been treated with the NF-κB probe.

B) Graphs showing quantification of the amount of NF-κB. Data was obtained using Image J software to quantify the bands from the phosphor images in (A).

Before discussing the individual samples in Figure 6.8 it is important to mention that the bottom of the gel, which contained the unbound probe, had to be removed. This was because the intensity of the band produced by the unbound probe was so strong the phosphor imager was automatically reducing the exposure on the image. This reduction in exposure meant that the fainter bands further up the gel fell below detectable limits and did not appear. However, upon removing the unbound probe, the shifted bands became detectable. Despite having to take this action, it is still possible to see the tops of the unbound probe at the bottom of the image, and therefore they still serve their purpose as a control.

The specificity of the NF-κB probe used in Figure 6.8 was confirmed by the fact that the non-specific probe failed to produce a gel shift (Lane 1), whilst the NF-κB probe successfully induced a gel shift in the HeLa cell lysates provided by Promega (Lane 2). However, whilst the occurrence of a gel shift in this sample was expected, the appearance of two bands was a surprise. The smaller of the two protein-DNA complexes (the one which travelled furthest down the gel) appears to be the same size at the bands representing NF-κB in other samples and it would therefore be logical to assume that this band represents nuclear NF-κB. The larger of the two protein-DNA complexes (the one which travelled less distance and is therefore closer to the top of the gel) could therefore be argued to be the inactive sequestered form of NF-κB. Whilst the lack of molecular weight markers means that this cannot be confirmed, it would make sense if this were the case owing to the fact that the HeLa cell extract is a whole cell lysate and not a nuclear fraction. As discussed above, the probe cannot distinguish between the inactive and active forms of NF-κB and will bind to both forms, which is why it was essential to design a protocol to separate nuclear and cytosolic protein fractions. However, in a sample containing both inactive and active NF-κB you would expect that the inactive form would run more slowly through a gel owing to the fact that is bound to IκBα and has a larger molecular weight (DiDonato et al., 1996). Therefore, it is plausible that the larger protein-DNA complex that appeared in the second lane is actually the result of the radio-labelled probe binding to cytoplasmic NF-κB·IκBα complexes. If this were to be the case then this would provide a second layer of control for the assay as it shows that the nuclear extracts were clean and do not contain detectable levels of cytosolic NF-κB. However, it would also mean that there was no need to separate the nuclear and cytosolic protein fractions as IκBα bound NF-κB is distinguishable from unbound NF-κB. Either way, the fact that a band representing active NF-κB appeared meant that the second lane served its purpose as a positive control and, without being able to confirm the identity of the second band, it was prudent to continue

isolating the nuclear proteins from their cytosolic counterparts.

Figure 6.8 shows that there was an observable increase in the amount of NF-κB in cells that has been treated with thapsigargin (lanes 4-8, 10-13 and 15) when compared with untreated samples (lanes 3, 9 and 14). This observation complements previous studies which show that thapsigargin induces ER stress (Thastrup et al., 1990) and that induction of the UPR causes downstream activation of NF-κB (Tam et al., 2012, Pahl and Baeuerle, 1995). To further understand the effects of thapsigargin treatment, the intensity of the shifted bands was measured using Image J software and the data obtained were used to produce graphs. As can be seen from panel B of Figure 6.8, all three thapsigargin concentrations produced bell-shaped curves, with band intensities increasing to a certain point and then tailing off afterwards. This may suggest that there is a negative feedback loop regulating NF-κB signalling over time or that the cells are able to adapt to the stress caused by the treatment. It was also observed that the speed in which cells initiate NF-κB signalling is dependent on the concentration of thapsigargin used. The highest concentration of thapsigargin (2 μM) produced the fastest response, with cells reaching the peak of their NF-κB signalling after just 1 h compared to the cells that had been treated with 0.5 μM thapsigargin, which reached the peak of their NF-κB signalling after 4 h.

One unexpected result observed in Figure 6.8 is that the maximal intensity of NF-κB signalling seems to be inversely proportional to thapsigargin concentration with 0.5 μM producing the strongest increase in NF-κB signalling (a 5.1-fold increase) and 2 μM thapsigargin producing the lowest (a 2.2-fold increase). There are a number of reasons that could explain this pattern, with one of them being that NF-κB is part of a signalling pathway induced at low levels of ER stress, but this pathway is then switched off once the stress pushes through a certain threshold. This would not fit in with reported role of NF-κB in stimulating apoptosis during ER stress (Hu et al., 2006), although this does not necessarily mean that the results are not representative of the signalling that is occurring because NF-κB has been shown to be prosurvival in many other stress responses (Luo et al., 2005). However, further data will need to be collected to determine whether the transient activation of NF-κB observed in Figure 6.8 is representative of protective signalling, which gets switched off more quickly during stronger stress in favour of apoptotic signalling, or merely an artefact created by this particular assay.

Summary

The data obtained in these experiments show that it is possible to monitor increases in NF-κB signalling by separating the nuclear fraction from whole-cell lysates (Figure 6.7) and then using a gel shift assay to determine the amount of NF-κB present (Figure 6.8). The data collected indicate that NF-κB is transiently activated in response to ER stress and that this response is stronger at lower concentrations of thapsigargin (Figure 6.8). This could potentially indicate that NF-κB actually has a protective role at low levels of stress and gets switched off in favour of apoptotic signalling during intense or prolonged periods of stress. However, far more data, and improvements to the reliability of the protocol, are required before conclusion of this nature can be drawn.

Figure 6.7 presents data indicating the successful separation of nuclear and cytoplasmic protein fractions and, therefore, provides a method that allows the separation of inactive and active NF-κB. The conclusion that this protocol can separate active NF-κB in the nucleus from inactive cytoplasmic NF-κB is further strengthened by Figure 6.8, whereby the NF-κB probe produces two bands when using whole cell lysates (lane 2) and just one band in nuclear lysates (lanes 3-18). The band that appears at a smaller molecular weight across all samples in this figure is most likely representative of non-sequestered, active NF-κB, whilst it is reasonable to assume that the band at the higher molecular weight represents 'super-shifted' inactive NF-κB in association with IκBα. Future work could be done in order to strengthen the conclusion by incubating cell lysates with antibodies against NF-κB, IκBα and control antibodies to confirm specificity. This should result in super-shifts in whole cell lysates and single bands in samples that only contain nuclear lysates. However, owing to previous reports observing super-shifted NF-κB in association with IκBα (Wulczyn et al., 1998), there can be confidence in the conclusion that the protocol detailed in methods sections 3.5.5 and 3.5.8 is capable of detecting changes in NF-κB signalling, as opposed to just the total amount of NF-κB.

The data obtained in Figure 6.8 initially seemed very positive; with all three thapsigargin concentrations producing similar curves, however, one concern with the data was that the 4 h treatment with 0.5 μM thapsigargin produced an unusually intense band. At first this was written off as an anomaly, but similar sporadic results continued to be obtained and it was noticed that varying amounts of the samples were being retained in the wells of the gel. Therefore, the increased intensity of the anomalous results may be a consequence of more protein being released from the well rather than the samples containing more NF-κB. Comparing NF-κB levels in samples that had different amounts of protein running through

the gel obviously does not give a representative picture of the stress that was being induced. Thus, future work would aim to resolve the issue of sample retention, something that could be achieved by making a few alterations the protocol described in section 3.5. Firstly, it would be worth reducing the gel percentage to make it easier for sample migration to occur and, secondly, it would be worthwhile reducing the salinity of the nuclear samples that were being used. As detailed in the methodology (section 3.5.5), nuclear protein samples were isolated using a 'high salt buffer' and it has been well documented that high salt concentrations can cause aberrant sample migration during electrophoresis (Garfin, 2003). Therefore, using techniques such as dialysis or gel filtration chromatography would be worthwhile when trying to resolve the aforementioned issues. Alternatively, the signal from the wells could have been caused by the probe annealing to remaining DNA or RNA or the probe binding to large protein complexes that may contain NF-κB. The former could be resolved by performing a nuclease digestion on the lysates, whilst the latter may require the use of a different buffer during the binding assay to suppress the formation of large protein complexes, should they from post-lysis, or dissociate the complexes, if they are present within the cell before lysis occurs.

Ultimately, the work carried out in this chapter deviated too far from the original question posed by this thesis and this, combined with the time required to optimise the gel shift assay and collect sufficient data, resulted in it being constrained to the appendices.

7 Bibliography

Bibliography

ACOSTA-ALVEAR, D., ZHOU, Y., BLAIS, A., TSIKITIS, M., LENTS, N. H., ARIAS, C., LENNON, C. J., KLUGER, Y. & DYNLACHT, B. D. 2007. XBP1 controls diverse cell type- and condition-specific transcriptional regulatory networks. *Mol Cell,* 27**,** 53-66.

ADACHI, Y., YAMAMOTO, K., OKADA, T., YOSHIDA, H., HARADA, A. & MORI, K. 2008. ATF6 is a transcription factor specializing in the regulation of quality control proteins in the endoplasmic reticulum. *Cell Struct Funct,* 33**,** 75-89.

AGUIRRE, V., WERNER, E. D., GIRAUD, J., LEE, Y. H., SHOELSON, S. E. & WHITE, M. F. 2002. Phosphorylation of Ser307 in insulin receptor substrate-1 blocks interactions with the insulin receptor and inhibits insulin action. *J Biol Chem,* 277**,** 1531-7.

ALI, M. M., BAGRATUNI, T., DAVENPORT, E. L., NOWAK, P. R., SILVA-SANTISTEBAN, M. C., HARDCASTLE, A., MCANDREWS, C., ROWLANDS, M. G., MORGAN, G. J., AHERNE, W., COLLINS, I., DAVIES, F. E. & PEARL, L. H. 2011. Structure of the Ire1 autophosphorylation complex and implications for the unfolded protein response. *EMBO J,* 30**,** 894-905.

ALVAREZ, S. E., HARIKUMAR, K. B., HAIT, N. C., ALLEGOOD, J., STRUB, G. M., KIM, E. Y., MACEYKA, M., JIANG, H., LUO, C., KORDULA, T., MILSTIEN, S. & SPIEGEL, S. 2010. Sphingosine-1-phosphate is a missing cofactor for the E3 ubiquitin ligase TRAF2. *Nature,* 465**,** 1084-1088.

ANTIGNANI, A. & YOULE, R. J. 2006. How do Bax and Bak lead to permeabilization of the outer mitochondrial membrane? *Current Opinion in Cell Biology,* 18**,** 685-689.

ARAGON, T., VAN ANKEN, E., PINCUS, D., SERAFIMOVA, I. M., KORENNYKH, A. V., RUBIO, C. A. & WALTER, P. 2009. Messenger RNA targeting to endoplasmic reticulum stress signalling sites. *Nature,* 457**,** 736-40.

ARAGÓN, T., VAN ANKEN, E., PINCUS, D., SERAFIMOVA, I. M., KORENNYKH, A. V., RUBIO, C. A. & WALTER, P. 2009. mRNA Targeting to ER Stress Signaling Sites. *Nature,* 457**,** 736-740.

ARAKI, K. & NAGATA, K. 2011. Protein folding and quality control in the ER. *Cold Spring Harb Perspect Biol,* 3**,** a007526.

ARLT, A., VORNDAMM, J., BREITENBROICH, M., FOLSCH, U. R., KALTHOFF, H., SCHMIDT, W. E. & SCHAFER, H. 2001. Inhibition of NF-kappaB sensitizes human pancreatic carcinoma cells to apoptosis induced by etoposide (VP16) or doxorubicin. *Oncogene,* 20**,** 859-68.

AUF, G., JABOUILLE, A., GUERIT, S., PINEAU, R., DELUGIN, M., BOUCHECAREILH, M., MAGNIN, N., FAVEREAUX, A., MAITRE, M., GAISER, T., VON DEIMLING, A., CZABANKA, M., VAJKOCZY, P., CHEVET, E., BIKFALVI, A. & MOENNER, M. 2010. Inositol-requiring enzyme 1alpha is a key regulator of angiogenesis and invasion in malignant glioma. *Proc Natl Acad Sci U S A,* 107**,** 15553-8.

AVEROUS, J., BRUHAT, A., JOUSSE, C., CARRARO, V., THIEL, G. & FAFOURNOUX, P. 2004. Induction of CHOP expression by amino acid limitation requires both ATF4 expression and ATF2 phosphorylation. *J Biol Chem,* 279**,** 5288-97.

AVIVAR-VALDERAS, A., SALAS, E., BOBROVNIKOVA-MARJON, E., DIEHL, J. A., NAGI, C., DEBNATH, J. & AGUIRRE-GHISO, J. A. 2011. PERK integrates autophagy and oxidative stress responses to promote survival during extracellular matrix detachment. *Mol Cell Biol,* 31**,** 3616-29.

BACK, S. H., LEE, K., VINK, E. & KAUFMAN, R. J. 2006. Cytoplasmic IRE1alpha-mediated XBP1 mRNA splicing in the absence of nuclear processing and endoplasmic reticulum stress. *J Biol Chem,* 281**,** 18691-706.

BACK, S. H., SCHEUNER, D., HAN, J., SONG, B., RIBICK, M., WANG, J., GILDERSLEEVE, R. D., PENNATHUR, S. & KAUFMAN, R. J. 2009. Translation attenuation through eIF2alpha phosphorylation prevents oxidative stress and maintains the differentiated state in beta cells. *Cell Metab,* 10**,** 13-26.

BATES, G. P. 2005. History of genetic disease: the molecular genetics of Huntington disease - a history. *Nat Rev Genet,* 6**,** 766-73.

BAUD, V. & KARIN, M. 2001. Signal transduction by tumor necrosis factor and its relatives. *Trends Cell Biol,* 11**,** 372-7.

BAUD, V., LIU, Z.-G., BENNETT, B., SUZUKI, N., XIA, Y. & KARIN, M. 1999. Signaling by proinflammatory cytokines: oligomerization of TRAF2 and TRAF6 is sufficient for JNK and IKK activation and target gene induction via an amino-terminal effector domain. *Genes & Development,* 13**,** 1297-1308.

BELMONT, P. J., CHEN, W. J., THUERAUF, D. J. & GLEMBOTSKI, C. C. 2012. Regulation of microRNA expression in the heart by the ATF6 branch of the ER stress response. *J Mol Cell Cardiol,* 52**,** 1176-82.

BENNETT, B. L., SASAKI, D. T., MURRAY, B. W., O'LEARY, E. C., SAKATA, S. T., XU, W., LEISTEN, J. C., MOTIWALA, A., PIERCE, S., SATOH, Y., BHAGWAT, S. S., MANNING, A. M. & ANDERSON, D. W. 2001. SP600125, an anthrapyrazolone inhibitor of Jun N-terminal kinase. *Proceedings of the National Academy of Sciences,* 98**,** 13681-13686.

BENOSMAN, S., RAVANAN, P., CORREA, R. G., HOU, Y. C., YU, M., GULEN, M. F., LI, X., THOMAS, J., CUDDY, M., MATSUZAWA, Y., SANO, R., DIAZ, P., MATSUZAWA, S. & REED, J. C. 2013. Interleukin-1 receptor-associated kinase-2 (IRAK2) is a critical mediator of endoplasmic reticulum (ER) stress signaling. *PLoS One,* 8**,** e64256.

BERNALES, S., MCDONALD, K. L. & WALTER, P. 2006. Autophagy counterbalances endoplasmic reticulum expansion during the unfolded protein response. *PLoS Biol,* 4**,** e423.

BERTOLOTTI, A. & RON, D. 2001. Alterations in an IRE1-RNA complex in the mammalian unfolded protein response. *J Cell Sci,* 114**,** 3207-12.

BERTOLOTTI, A., WANG, X., NOVOA, I., JUNGREIS, R., SCHLESSINGER, K., CHO, J. H., WEST, A. B. & RON, D. 2001. Increased sensitivity to dextran sodium sulfate colitis in IRE1beta-deficient mice. *J Clin Invest,* 107**,** 585-93.

BERTOLOTTI, A., ZHANG, Y., HENDERSHOT, L. M., HARDING, H. P. & RON, D. 2000a. Dynamic interaction of BiP and ER stress transducers in the unfolded-protein response. *Nat Cell Biol,* 2**,** 326-332.

BERTOLOTTI, A., ZHANG, Y., HENDERSHOT, L. M., HARDING, H. P. & RON, D. 2000b. Dynamic interaction of BiP and ER stress transducers in the unfolded-protein response. *Nat Cell Biol,* 2**,** 326-32.

BIRNBOIM, H. C. & DOLY, J. 1979. A rapid alkaline extraction procedure for screening recombinant plasmid DNA. *Nucleic Acids Res,* 7**,** 1513-23.

BISHOP, A. C., UBERSAX, J. A., PETSCH, D. T., MATHEOS, D. P., GRAY, N. S., BLETHROW, J., SHIMIZU, E., TSIEN, J. Z., SCHULTZ, P. G., ROSE, M. D., WOOD, J. L., MORGAN, D. O. & SHOKAT, K. M. 2000. A chemical switch for inhibitor-sensitive alleles of any protein kinase. *Nature,* 407**,** 395-401.

BOGOYEVITCH, M. A. & KOBE, B. 2006. Uses for JNK: the many and varied substrates of the c-Jun N-terminal kinases. *Microbiol Mol Biol Rev,* 70**,** 1061-95.

BOMMIASAMY, H., BACK, S. H., FAGONE, P., LEE, K., MESHINCHI, S., VINK, E., SRIBURI, R., FRANK, M., JACKOWSKI, S., KAUFMAN, R. J. & BREWER, J. W. 2009. ATF6alpha induces XBP1-independent expansion of the endoplasmic reticulum. *J Cell Sci,* 122**,** 1626-36.

BOSSY-WETZEL, E., BAKIRI, L. & YANIV, M. 1997. Induction of apoptosis by the transcription factor c-Jun. *The EMBO Journal,* 16**,** 1695-1709.

BREWER, J. W. & DIEHL, J. A. 2000. PERK mediates cell-cycle exit during the mammalian unfolded protein response. *Proc Natl Acad Sci U S A,* 97**,** 12625-30.

BROWN, M., STRUDWICK, N., SUWARA, M., SUTCLIFFE, L. K., MIHAI, A. D., ALI, A. A., WATSON, J. N. & SCHRÖDER, M. 2016. An initial phase of JNK activation inhibits cell death early in the endoplasmic reticulum stress response. *Journal of Cell Science*.

BUCCIANTINI, M., GIANNONI, E., CHITI, F., BARONI, F., FORMIGLI, L., ZURDO, J., TADDEI, N., RAMPONI, G., DOBSON, C. M. & STEFANI, M. 2002. Inherent toxicity of aggregates implies a common mechanism for protein misfolding diseases. *Nature,* 416**,** 507-11.

CAI, J.-W., HENDERSON, B. W., SHEN, J.-W. & SUBJECK, J. R. 1993. Induction of glucose regulated proteins during growth of a murine tumor. *Journal of Cellular Physiology,* 154**,** 229-237.

CALFON, M., ZENG, H., URANO, F., TILL, J. H., HUBBARD, S. R., HARDING, H. P., CLARK, S. G. & RON, D. 2002. IRE1 couples endoplasmic reticulum load to secretory capacity by processing the XBP-1 mRNA. *Nature,* 415**,** 92-6.

CHANG, L., JONES, Y., ELLISMAN, M. H., GOLDSTEIN, L. S. B. & KARIN, M. 2003. JNK1 Is Required for Maintenance of Neuronal Microtubules and Controls Phosphorylation of Microtubule-Associated Proteins. *Developmental Cell,* 4**,** 521-533.

CHAUDHARI, N., TALWAR, P., PARIMISETTY, A., LEFEBVRE D'HELLENCOURT, C. & RAVANAN, P. 2014. A molecular web: endoplasmic reticulum stress, inflammation, and oxidative stress. *Front Cell Neurosci,* 8**,** 213.

CHAWLA, A., CHAKRABARTI, S., GHOSH, G. & NIWA, M. 2011. Attenuation of yeast UPR is essential for survival and is mediated by IRE1 kinase. *J Cell Biol,* 193**,** 41-50.

CHEN, J. J. & LONDON, I. M. 1995. Regulation of protein synthesis by heme-regulated eIF-2 alpha kinase. *Trends Biochem Sci,* 20**,** 105-8.

CHEN, X., SHEN, J. & PRYWES, R. 2002. The luminal domain of ATF6 senses endoplasmic reticulum (ER) stress and causes translocation of ATF6 from the ER to the Golgi. *J Biol Chem,* 277**,** 13045-52.

CHEN, Y. & BRANDIZZI, F. 2013. IRE1: ER stress sensor and cell fate executor. *Trends Cell Biol,* 23**,** 547-55.

CHOW, C.-W., RINCÓN, M., CAVANAGH, J., DICKENS, M. & DAVIS, R. J. 1997. Nuclear Accumulation of NFAT4 Opposed by the JNK Signal Transduction Pathway. *Science,* 278**,** 1638-1641.

CHUNG, C. T., NIEMELA, S. L. & MILLER, R. H. 1989. One-step preparation of competent Escherichia coli: transformation and storage of bacterial cells in the same solution. *Proceedings of the National Academy of Sciences,* 86**,** 2172-2175.

CHUNG, J. Y., LU, M., YIN, Q., LIN, S. C. & WU, H. 2007. Molecular basis for the unique specificity of TRAF6. *Adv Exp Med Biol,* 597**,** 122-30.

CONNOR, J. H., WEISER, D. C., LI, S., HALLENBECK, J. M. & SHENOLIKAR, S. 2001. Growth arrest and DNA damage-inducible protein GADD34 assembles a novel signaling complex containing protein phosphatase 1 and inhibitor 1. *Mol Cell Biol,* 21**,** 6841-50.

COX, J. S., SHAMU, C. E. & WALTER, P. 1993. Transcriptional induction of genes encoding endoplasmic reticulum resident proteins requires a transmembrane protein kinase. *Cell,* 73**,** 1197-206.

COX, J. S. & WALTER, P. 1996. A novel mechanism for regulating activity of a transcription factor that controls the unfolded protein response. *Cell,* 87**,** 391-404.

CREDLE, J. J., FINER-MOORE, J. S., PAPA, F. R., STROUD, R. M. & WALTER, P. 2005. On the mechanism of sensing unfolded protein in the endoplasmic reticulum. *Proc Natl Acad Sci U S A,* 102**,** 18773-84.

CROSS, B. C., BOND, P. J., SADOWSKI, P. G., JHA, B. K., ZAK, J., GOODMAN, J. M., SILVERMAN, R. H., NEUBERT, T. A., BAXENDALE, I. R., RON, D. & HARDING, H. P. 2012. The molecular basis for selective inhibition of unconventional mRNA splicing by an IRE1-binding small molecule. *Proc Natl Acad Sci U S A,* 109**,** E869-78.

CUENDA, A. 2000. Mitogen-activated protein kinase kinase 4 (MKK4). *Int J Biochem Cell Biol,* 32**,** 581-7.

CUI, W., LI, J., RON, D. & SHA, B. 2011. The structure of the PERK kinase domain suggests the mechanism for its activation. *Acta Crystallogr D Biol Crystallogr,* 67**,** 423-8.

CULLINAN, S. B., ZHANG, D., HANNINK, M., ARVISAIS, E., KAUFMAN, R. J. & DIEHL, J. A. 2003. Nrf2 is a direct PERK substrate and effector of PERK-dependent cell survival. *Mol Cell Biol,* 23**,** 7198-209.

D'AMBROSIO, C., ARENA, S., FULCOLI, G., SCHEINFELD, M. H., ZHOU, D., D'ADAMIO, L. & SCALONI, A. 2006. Hyperphosphorylation of JNK-interacting protein 1, a protein associated with Alzheimer disease. *Mol Cell Proteomics,* 5**,** 97-113.

DAVIS 2002. *Basic Cell Culture*.

DAVIS, R. J. 2000. Signal Transduction by the JNK Group of MAP Kinases. *Cell,* 103**,** 239-252.

DENG, J., LU, P. D., ZHANG, Y., SCHEUNER, D., KAUFMAN, R. J., SONENBERG, N., HARDING, H. P. & RON, D. 2004. Translational repression mediates activation of nuclear factor kappa B by phosphorylated translation initiation factor 2. *Mol Cell Biol,* 24**,** 10161-8.

DENG, X., XIAO, L., LANG, W., GAO, F., RUVOLO, P. & MAY, W. S., JR. 2001. Novel role for JNK as a stress-activated Bcl2 kinase. *J Biol Chem,* 276**,** 23681-8.

DICKENS, M., ROGERS, J. S., CAVANAGH, J., RAITANO, A., XIA, Z., HALPERN, J. R., GREENBERG, M. E., SAWYERS, C. L. & DAVIS, R. J. 1997. A cytoplasmic inhibitor of the JNK signal transduction pathway. *Science,* 277**,** 693-6.

DIDONATO, J., MERCURIO, F., ROSETTE, C., WU-LI, J., SUYANG, H., GHOSH, S. & KARIN, M. 1996. Mapping of the inducible IkappaB phosphorylation sites that signal its ubiquitination and degradation. *Molecular and Cellular Biology,* 16**,** 1295-1304.

DONG, B. & SILVERMAN, R. H. 1995. 2-5A-dependent RNase molecules dimerize during activation by 2-5A. *J Biol Chem,* 270**,** 4133-7.

DONG, B., XU, L., ZHOU, A., HASSEL, B. A., LEE, X., TORRENCE, P. F. & SILVERMAN, R. H. 1994. Intrinsic molecular activities of the interferon-induced 2-5A-dependent RNase. *J Biol Chem,* 269**,** 14153-8.

ELLISDON, A. M. & BOTTOMLEY, S. P. 2004. The role of protein misfolding in the pathogenesis of human diseases. *IUBMB Life,* 56**,** 119-23.

FAN, E., MERRITT, E. A., VERLINDE, C. L. M. J. & HOL, W. G. J. 2000. AB5 toxins: structures and inhibitor design. *Current Opinion in Structural Biology,* 10**,** 680-686.

FAWCETT, T. W., MARTINDALE, J. L., GUYTON, K. Z., HAI, T. & HOLBROOK, N. J. 1999. Complexes containing activating transcription factor (ATF)/cAMP-responsive-element-binding protein (CREB) interact with the CCAAT/enhancer-binding protein (C/EBP)-ATF composite site to regulate Gadd153 expression during the stress response. *Biochem J,* 339 (Pt 1)**,** 135-41.

FEDOROFF, N. 2006. Redox Regulatory Mechanisms in Cellular Stress Responses. *Annals of Botany,* 98**,** 289-300.

FERNANDEZ, J., BODE, B., KOROMILAS, A., DIEHL, J. A., KRUKOVETS, I., SNIDER, M. D. & HATZOGLOU, M. 2002. Translation mediated by the internal ribosome entry site of the cat-1 mRNA is regulated by glucose availability in a PERK kinase-dependent manner. *J Biol Chem,* 277**,** 11780-7.

FUCHS, S. Y., ADLER, V., PINCUS, M. R. & RONAI, Z. 1998. MEKK1/JNK signaling stabilizes and activates p53. *Proc Natl Acad Sci U S A,* 95**,** 10541-6.

FUJINO, G., NOGUCHI, T., MATSUZAWA, A., YAMAUCHI, S., SAITOH, M., TAKEDA, K. & ICHIJO, H. 2007. Thioredoxin and TRAF Family Proteins Regulate Reactive Oxygen Species-Dependent Activation of ASK1 through Reciprocal Modulation of the N-Terminal Homophilic Interaction of ASK1. *Molecular and Cellular Biology,* 27**,** 8152-8163.

GALLAGHER, E., GAO, M., LIU, Y. C. & KARIN, M. 2006. Activation of the E3 ubiquitin ligase Itch through a phosphorylation-induced conformational change. *Proc Natl Acad Sci U S A,* 103**,** 1717-22.

GARDNER, B. M. & WALTER, P. 2011. Unfolded proteins are Ire1-activating ligands that directly induce the unfolded protein response. *Science,* 333**,** 1891-4.

GARFIN, D. E. 2003. Two-dimensional gel electrophoresis: an overview. *TrAC Trends in Analytical Chemistry,* 22**,** 263-272.

GERLIER, D. & THOMASSET, N. 1986. Use of MTT colorimetric assay to measure cell activation. *Journal of Immunological Methods,* 94**,** 57-63.

GHATAN, S., LARNER, S., KINOSHITA, Y., HETMAN, M., PATEL, L., XIA, Z., YOULE, R. J. & MORRISON, R. S. 2000. p38 MAP kinase mediates bax translocation in nitric oxide-induced apoptosis in neurons. *J Cell Biol,* 150**,** 335-47.

GILMORE, T. D. 2006. Introduction to NF-kappaB: players, pathways, perspectives. *Oncogene,* 25**,** 6680-4.

GOLDMAN, R. D., GRUENBAUM, Y., MOIR, R. D., SHUMAKER, D. K. & SPANN, T. P. 2002. Nuclear lamins: building blocks of nuclear architecture. *Genes Dev,* 16**,** 533-47.

GORLACH, A., KLAPPA, P. & KIETZMANN, T. 2006. The endoplasmic reticulum: folding, calcium homeostasis, signaling, and redox control. *Antioxid Redox Signal,* 8**,** 1391-418.

GRANT, C. M., MILLER, P. F. & HINNEBUSCH, A. G. 1995. Sequences 5' of the first upstream open reading frame in GCN4 mRNA are required for efficient translational reinitiation. *Nucleic Acids Res,* 23**,** 3980-8.

GUPTA, S., DEEPTI, A., DEEGAN, S., LISBONA, F., HETZ, C. & SAMALI, A. 2010. HSP72 protects cells from ER stress-induced apoptosis via enhancement of IRE1alpha-XBP1 signaling through a physical interaction. *PLoS Biol,* 8**,** e1000410.

HA, H., HAN, D. & CHOI, Y. 2009. TRAF-mediated TNFR-family signaling. *Curr Protoc Immunol,* Chapter 11**,** Unit11 9D.

HAMANAKA, R. B., BENNETT, B. S., CULLINAN, S. B. & DIEHL, J. A. 2005. PERK and GCN2 contribute to eIF2alpha phosphorylation and cell cycle arrest after activation of the unfolded protein response pathway. *Mol Biol Cell,* 16**,** 5493-501.

HAMANAKA, R. B., BOBROVNIKOVA-MARJON, E., JI, X., LIEBHABER, S. A. & DIEHL, J. A. 2009. PERK-dependent regulation of IAP translation during ER stress. *Oncogene,* 28**,** 910-20.

HAN, D., LERNER, A. G., VANDE WALLE, L., UPTON, J. P., XU, W., HAGEN, A., BACKES, B. J., OAKES, S. A. & PAPA, F. R. 2009. IRE1alpha kinase activation modes control alternate endoribonuclease outputs to determine divergent cell fates. *Cell,* 138**,** 562-75.

HAN, J., BACK, S. H., HUR, J., LIN, Y.-H., GILDERSLEEVE, R., SHAN, J., YUAN, C. L., KROKOWSKI, D., WANG, S., HATZOGLOU, M., KILBERG, M. S., SARTOR, M. A. & KAUFMAN, R. J. 2013. ER-stress-induced transcriptional regulation increases protein synthesis leading to cell death. *Nat Cell Biol,* 15**,** 481-490.

HARDING, H. P., NOVOA, I., ZHANG, Y., ZENG, H., WEK, R., SCHAPIRA, M. & RON, D. 2000a. Regulated translation initiation controls stress-induced gene expression in mammalian cells. *Mol Cell,* 6**,** 1099-108.

HARDING, H. P., ZHANG, Y., BERTOLOTTI, A., ZENG, H. & RON, D. 2000b. Perk is essential for translational regulation and cell survival during the unfolded protein response. *Mol Cell,* 5**,** 897-904.

HARDING, H. P., ZHANG, Y. & RON, D. 1999. Protein translation and folding are coupled by an endoplasmic-reticulum-resident kinase. *Nature,* 397**,** 271-4.

HARDING, H. P., ZHANG, Y., ZENG, H., NOVOA, I., LU, P. D., CALFON, M., SADRI, N., YUN, C., POPKO, B., PAULES, R., STOJDL, D. F., BELL, J. C., HETTMANN, T., LEIDEN, J. M. & RON, D. 2003. An Integrated Stress Response Regulates Amino Acid Metabolism and Resistance to Oxidative Stress. *Molecular Cell,* 11**,** 619-633.

HARDY, J. & ALLSOP, D. 1991. Amyloid deposition as the central event in the aetiology of Alzheimer's disease. *Trends Pharmacol Sci,* 12**,** 383-8.

HASNAIN, S. Z., BORG, D. J., HARCOURT, B. E., TONG, H., SHENG, Y. H., NG, C. P., DAS, I., WANG, R., CHEN, A. C. H., LOUDOVARIS, T., KAY, T. W., THOMAS, H. E., WHITEHEAD, J. P., FORBES, J. M., PRINS, J. B. & MCGUCKIN, M. A. 2014. Glycemic control in diabetes is restored by therapeutic manipulation of cytokines that regulate beta cell stress. *Nat Med,* 20**,** 1417-1426.

HAYES, S. E., CONNER, L. J., STRAMM, L. E. & SHI, Y. 1999. Assignment of pancreatic eIF-2alpha kinase (EIF2AK3) to human chromosome band 2p12 by radiation hybrid mapping and in situ hybridization. *Cytogenet Cell Genet,* 86**,** 327-8.

HAZE, K., YOSHIDA, H., YANAGI, H., YURA, T. & MORI, K. 1999. Mammalian transcription factor ATF6 is synthesized as a transmembrane protein and activated by proteolysis in response to endoplasmic reticulum stress. *Mol Biol Cell,* 10**,** 3787-99.

HE, Y., BEATTY, A., HAN, X., JI, Y., MA, X., ADELSTEIN, R. S., YATES, J. R., 3RD, KEMPHUES, K. & QI, L. 2012. Nonmuscle myosin IIB links cytoskeleton to IRE1alpha signaling during ER stress. *Dev Cell,* 23**,** 1141-52.

HETZ, C. 2012. The unfolded protein response: controlling cell fate decisions under ER stress and beyond. *Nat Rev Mol Cell Biol,* 13**,** 89-102.

HETZ, C., BERNASCONI, P., FISHER, J., LEE, A. H., BASSIK, M. C., ANTONSSON, B., BRANDT, G. S., IWAKOSHI, N. N., SCHINZEL, A., GLIMCHER, L. H. & KORSMEYER, S. J. 2006. Proapoptotic BAX and BAK modulate the unfolded protein response by a direct interaction with IRE1alpha. *Science,* 312**,** 572-6.

HETZ, C., CHEVET, E. & HARDING, H. P. 2013. Targeting the unfolded protein response in disease. *Nat Rev Drug Discov,* 12**,** 703-719.

HETZ, C. & GLIMCHER, L. H. 2009. Fine-tuning of the unfolded protein response: Assembling the IRE1alpha interactome. *Mol Cell,* 35**,** 551-61.

HILL, D. S., MARTIN, S., ARMSTRONG, J. L., FLOCKHART, R., TONISON, J. J., SIMPSON, D. G., BIRCH-MACHIN, M. A., REDFERN, C. P. F. & LOVAT, P. E. 2009. Combining the ER-stress inducing agents bortezomib and fenretinide as a novel therapeutic strategy for metastatic melanoma. *Clinical cancer research : an official journal of the American Association for Cancer Research,* 15**,** 1192-1198.

HILLEN, W. & BERENS, C. 1994. Mechanisms underlying expression of Tn10 encoded tetracycline resistance. *Annu Rev Microbiol,* 48**,** 345-69.

HINNEBUSCH, A. G. 1994. The eIF-2 alpha kinases: regulators of protein synthesis in starvation and stress. *Semin Cell Biol,* 5**,** 417-26.

HIROSUMI, J., TUNCMAN, G., CHANG, L., GORGUN, C. Z., UYSAL, K. T., MAEDA, K., KARIN, M. & HOTAMISLIGIL, G. S. 2002. A central role for JNK in obesity and insulin resistance. *Nature,* 420**,** 333-6.

HOLLIEN, J., LIN, J. H., LI, H., STEVENS, N., WALTER, P. & WEISSMAN, J. S. 2009. Regulated Ire1-dependent decay of messenger RNAs in mammalian cells. *J Cell Biol,* 186**,** 323-31.

HOLLIEN, J. & WEISSMAN, J. S. 2006. Decay of endoplasmic reticulum-localized mRNAs during the unfolded protein response. *Science,* 313**,** 104-7.

HU, P., HAN, Z., COUVILLON, A. D., KAUFMAN, R. J. & EXTON, J. H. 2006. Autocrine tumor necrosis factor alpha links endoplasmic reticulum stress to the membrane death receptor pathway through IRE1alpha-mediated NF-kappaB activation and down-regulation of TRAF2 expression. *Mol Cell Biol,* 26**,** 3071-84.

HUANG, C., RAJFUR, Z., BORCHERS, C., SCHALLER, M. D. & JACOBSON, K. 2003. JNK phosphorylates paxillin and regulates cell migration. *Nature,* 424**,** 219-23.

HUANG, Y., LI, X., WANG, Y., WANG, H., HUANG, C. & LI, J. 2014. Endoplasmic reticulum stress-induced hepatic stellate cell apoptosis through calcium-mediated JNK/P38 MAPK and Calpain/Caspase-12 pathways. *Molecular and Cellular Biochemistry,* 394**,** 1-12.

HUBBARD, S. R., MOHAMMADI, M. & SCHLESSINGER, J. 1998. Autoregulatory mechanisms in protein-tyrosine kinases. *J Biol Chem,* 273**,** 11987-90.

HUBBARD, S. R., WEI, L., ELLIS, L. & HENDRICKSON, W. A. 1994. Crystal structure of the tyrosine kinase domain of the human insulin receptor. *Nature,* 372**,** 746-54.

ICHIJO, H., NISHIDA, E., IRIE, K., TEN DIJKE, P., SAITOH, M., MORIGUCHI, T., TAKAGI, M., MATSUMOTO, K., MIYAZONO, K. & GOTOH, Y. 1997. Induction of apoptosis by ASK1, a mammalian MAPKKK that activates SAPK/JNK and p38 signaling pathways. *Science,* 275**,** 90-4.

IKEDA, A., HASEGAWA, K., MASAKI, M., MORIGUCHI, T., NISHIDA, E., KOZUTSUMI, Y., OKA, S. & KAWASAKI, T. 2001. Mixed lineage kinase LZK forms a functional signaling complex with JIP-1, a scaffold protein of the c-Jun NH(2)-terminal kinase pathway. *J Biochem,* 130**,** 773-81.

IMAGAWA, Y., HOSODA, A., SASAKA, S., TSURU, A. & KOHNO, K. 2008. RNase domains determine the functional difference between IRE1alpha and IRE1beta. *FEBS Lett,* 582**,** 656-60.

IP, Y. T. & DAVIS, R. J. 1998. Signal transduction by the c-Jun N-terminal kinase (JNK)--from inflammation to development. *Curr Opin Cell Biol,* 10**,** 205-19.

IQBAL, J., DAI, K., SEIMON, T., JUNGREIS, R., OYADOMARI, M., KURIAKOSE, G., RON, D., TABAS, I. & HUSSAIN, M. M. 2008. IRE1beta inhibits chylomicron production by selectively degrading MTP mRNA. *Cell Metab,* 7**,** 445-55.

IWAWAKI, T., AKAI, R., YAMANAKA, S. & KOHNO, K. 2009. Function of IRE1 alpha in the placenta is essential for placental development and embryonic viability. *Proc Natl Acad Sci U S A,* 106**,** 16657-62.

IWAWAKI, T., HOSODA, A., OKUDA, T., KAMIGORI, Y., NOMURA-FURUWATARI, C., KIMATA, Y., TSURU, A. & KOHNO, K. 2001. Translational control by the ER transmembrane kinase/ribonuclease IRE1 under ER stress. *Nat Cell Biol,* 3**,** 158-64.

JACKSON, R. J., HELLEN, C. U. T. & PESTOVA, T. V. 2010. The mechanism of eukaryotic translation initiation and principles of its regulation. *Nat Rev Mol Cell Biol,* 11**,** 113-127.
JAESCHKE, A., CZECH, M. P. & DAVIS, R. J. 2004. An essential role of the JIP1 scaffold protein for JNK activation in adipose tissue. *Genes Dev,* 18**,** 1976-80.
JHENG, J. R., LAU, K. S., TANG, W. F., WU, M. S. & HORNG, J. T. 2010. Endoplasmic reticulum stress is induced and modulated by enterovirus 71. *Cell Microbiol,* 12**,** 796-813.
JIANG, D., NIWA, M. & KOONG, A. C. 2015. Targeting the IRE1α–XBP1 branch of the unfolded protein response in human diseases. *Seminars in Cancer Biology*.
JIANG, H. Y., WEK, S. A., MCGRATH, B. C., SCHEUNER, D., KAUFMAN, R. J., CAVENER, D. R. & WEK, R. C. 2003. Phosphorylation of the alpha subunit of eukaryotic initiation factor 2 is required for activation of NF-kappaB in response to diverse cellular stresses. *Mol Cell Biol,* 23**,** 5651-63.
JULIER, C. & NICOLINO, M. 2010. Wolcott-Rallison syndrome. *Orphanet J Rare Dis,* 5**,** 29.
JUNG, T. W., HWANG, H.-J., HONG, H. C., CHOI, H. Y., YOO, H. J., BAIK, S. H. & CHOI, K. M. 2014. Resolvin D1 reduces ER stress-induced apoptosis and triglyceride accumulation through JNK pathway in HepG2 cells. *Molecular and Cellular Endocrinology,* 391**,** 30-40.
JUNG, T. W., LEE, M. W., LEE, Y. J. & KIM, S. M. 2012. Metformin prevents endoplasmic reticulum stress-induced apoptosis through AMPK-PI3K-c-Jun NH2 pathway. *Biochemical and Biophysical Research Communications,* 417**,** 147-152.
JURKIN, J., HENKEL, T., NIELSEN, A. F., MINNICH, M., POPOW, J., KAUFMANN, T., HEINDL, K., HOFFMANN, T., BUSSLINGER, M. & MARTINEZ, J. 2014. The mammalian tRNA ligase complex mediates splicing of XBP1 mRNA and controls antibody secretion in plasma cells. *EMBO J,* 33**,** 2922-36.
KAKIZUKA, A. 1998. Protein precipitation: a common etiology in neurodegenerative disorders? *Trends Genet,* 14**,** 396-402.
KANEKO, M., NIINUMA, Y. & NOMURA, Y. 2003. Activation signal of nuclear factor-kappa B in response to endoplasmic reticulum stress is transduced via IRE1 and tumor necrosis factor receptor-associated factor 2. *Biol Pharm Bull,* 26**,** 931-5.
KANG, M.-J., CHUNG, J. & RYOO, H. D. 2012. CDK5 and MEKK1 mediate pro-apoptotic signalling following endoplasmic reticulum stress in an autosomal dominant retinitis pigmentosa model. *Nat Cell Biol,* 14**,** 409-415.
KATSUNO, M., ADACHI, H., DOYU, M., MINAMIYAMA, M., SANG, C., KOBAYASHI, Y., INUKAI, A. & SOBUE, G. 2003. Leuprorelin rescues polyglutamine-dependent phenotypes in a transgenic mouse model of spinal and bulbar muscular atrophy. *Nat Med,* 9**,** 768-773.
KAUFMAN, R. J. 1999. Stress signaling from the lumen of the endoplasmic reticulum: coordination of gene transcriptional and translational controls. *Genes Dev,* 13**,** 1211-33.
KAUFMANN, S. H., DESNOYERS, S., OTTAVIANO, Y., DAVIDSON, N. E. & POIRIER, G. G. 1993. Specific proteolytic cleavage of poly(ADP-ribose) polymerase: an early marker of chemotherapy-induced apoptosis. *Cancer Res,* 53**,** 3976-85.
KELKAR, N., GUPTA, S., DICKENS, M. & DAVIS, R. J. 2000. Interaction of a mitogen-activated protein kinase signaling module with the neuronal protein JIP3. *Mol Cell Biol,* 20**,** 1030-43.
KHOURY, M. K., PARKER, I. & ASWAD, D. W. 2010. Acquisition of chemiluminescent signals from immunoblots with a digital SLR camera. *Analytical biochemistry,* 397**,** 129-131.
KIM, B. J., RYU, S. W. & SONG, B. J. 2006. JNK- and p38 kinase-mediated phosphorylation of Bax leads to its activation and mitochondrial translocation and to apoptosis of human hepatoma HepG2 cells. *J Biol Chem,* 281**,** 21256-65.
KIMATA, Y., ISHIWATA-KIMATA, Y., ITO, T., HIRATA, A., SUZUKI, T., OIKAWA, D., TAKEUCHI, M. & KOHNO, K. 2007. Two regulatory steps of ER-stress sensor Ire1 involving its cluster formation and interaction with unfolded proteins. *J Cell Biol,* 179**,** 75-86.
KIMATA, Y., OIKAWA, D., SHIMIZU, Y., ISHIWATA-KIMATA, Y. & KOHNO, K. 2004. A role for BiP as an adjustor for the endoplasmic reticulum stress-sensing protein Ire1. *J Cell Biol,* 167**,** 445-56.

KIMMIG, P., DIAZ, M., ZHENG, J., WILLIAMS, C. C., LANG, A., ARAGON, T., LI, H. & WALTER, P. 2012. The unfolded protein response in fission yeast modulates stability of select mRNAs to maintain protein homeostasis. *Elife,* 1**,** e00048.

KITADA, T., ASAKAWA, S., HATTORI, N., MATSUMINE, H., YAMAMURA, Y., MINOSHIMA, S., YOKOCHI, M., MIZUNO, Y. & SHIMIZU, N. 1998. Mutations in the parkin gene cause autosomal recessive juvenile parkinsonism. *Nature,* 392**,** 605-8.

KOHNO, K. 2007. How transmembrane proteins sense endoplasmic reticulum stress. *Antioxid Redox Signal,* 9**,** 2295-303.

KOHNO, K., NORMINGTON, K., SAMBROOK, J., GETHING, M. J. & MORI, K. 1993. The promoter region of the yeast KAR2 (BiP) gene contains a regulatory domain that responds to the presence of unfolded proteins in the endoplasmic reticulum. *Mol Cell Biol,* 13**,** 877-90.

KORENNYKH, A. V., EGEA, P. F., KOROSTELEV, A. A., FINER-MOORE, J., ZHANG, C., SHOKAT, K. M., STROUD, R. M. & WALTER, P. 2009. The unfolded protein response signals through high-order assembly of Ire1. *Nature,* 457**,** 687-93.

KORENNYKH, A. V., KOROSTELEV, A. A., EGEA, P. F., FINER-MOORE, J., STROUD, R. M., ZHANG, C., SHOKAT, K. M. & WALTER, P. 2011. Structural and functional basis for RNA cleavage by Ire1. *BMC Biol,* 9**,** 47.

KOUMENIS, C., NACZKI, C., KORITZINSKY, M., RASTANI, S., DIEHL, A., SONENBERG, N., KOROMILAS, A. & WOUTERS, B. G. 2002. Regulation of protein synthesis by hypoxia via activation of the endoplasmic reticulum kinase PERK and phosphorylation of the translation initiation factor eIF2alpha. *Mol Cell Biol,* 22**,** 7405-16.

KOUROKU, Y., FUJITA, E., TANIDA, I., UENO, T., ISOAI, A., KUMAGAI, H., OGAWA, S., KAUFMAN, R. J., KOMINAMI, E. & MOMOI, T. 2007. ER stress (PERK/eIF2alpha phosphorylation) mediates the polyglutamine-induced LC3 conversion, an essential step for autophagy formation. *Cell Death Differ,* 14**,** 230-9.

KOZUTSUMI, Y., SEGAL, M., NORMINGTON, K., GETHING, M.-J. & SAMBROOK, J. 1988. The presence of malfolded proteins in the endoplasmic reticulum signals the induction of glucose-regulated proteins. *Nature,* 332**,** 462-464.

KUKEKOV, N. V., XU, Z. & GREENE, L. A. 2006. Direct interaction of the molecular scaffolds POSH and JIP is required for apoptotic activation of JNKs. *J Biol Chem,* 281**,** 15517-24.

LAMB, J. A., VENTURA, J. J., HESS, P., FLAVELL, R. A. & DAVIS, R. J. 2003. JunD mediates survival signaling by the JNK signal transduction pathway. *Mol Cell,* 11**,** 1479-89.

LEE, A. H., IWAKOSHI, N. N. & GLIMCHER, L. H. 2003. XBP-1 regulates a subset of endoplasmic reticulum resident chaperone genes in the unfolded protein response. *Mol Cell Biol,* 23**,** 7448-59.

LEE, A. S. 2005. The ER chaperone and signaling regulator GRP78/BiP as a monitor of endoplasmic reticulum stress. *Methods,* 35**,** 373-81.

LEE, K., TIRASOPHON, W., SHEN, X., MICHALAK, M., PRYWES, R., OKADA, T., YOSHIDA, H., MORI, K. & KAUFMAN, R. J. 2002. IRE1-mediated unconventional mRNA splicing and S2P-mediated ATF6 cleavage merge to regulate XBP1 in signaling the unfolded protein response. *Genes Dev,* 16**,** 452-66.

LEE, K. P., DEY, M., NECULAI, D., CAO, C., DEVER, T. E. & SICHERI, F. 2008a. Structure of the dual enzyme Ire1 reveals the basis for catalysis and regulation in nonconventional RNA splicing. *Cell,* 132**,** 89-100.

LEE, U. J., CHOUNG, S. R., PRAKASH, K. V., LEE, E. J., LEE, M. Y., KIM, Y. J., HAN, C. W. & CHOI, Y. C. 2008b. Dual knockdown of p65 and p50 subunits of NF-kappaB by siRNA inhibits the induction of inflammatory cytokines and significantly enhance apoptosis in human primary synoviocytes treated with tumor necrosis factor-alpha. *Mol Biol Rep,* 35**,** 291-8.

LEI, K. & DAVIS, R. J. 2003. JNK phosphorylation of Bim-related members of the Bcl2 family induces Bax-dependent apoptosis. *Proc Natl Acad Sci U S A,* 100**,** 2432-7.

LERNER, A. G., UPTON, J. P., PRAVEEN, P. V., GHOSH, R., NAKAGAWA, Y., IGBARIA, A., SHEN, S., NGUYEN, V., BACKES, B. J., HEIMAN, M., HEINTZ, N., GREENGARD, P., HUI, S., TANG, Q., TRUSINA, A., OAKES, S. A. & PAPA, F. R. 2012. IRE1alpha induces thioredoxin-interacting

protein to activate the NLRP3 inflammasome and promote programmed cell death under irremediable ER stress. *Cell Metab,* 16**,** 250-64.

LI, H., KORENNYKH, A. V., BEHRMAN, S. L. & WALTER, P. 2010. Mammalian endoplasmic reticulum stress sensor IRE1 signals by dynamic clustering. *Proceedings of the National Academy of Sciences of the United States of America,* 107**,** 16113-16118.

LIM, C. P. & CAO, X. 1999. Serine phosphorylation and negative regulation of Stat3 by JNK. *J Biol Chem,* 274**,** 31055-61.

LIN, J. H., LI, H., ZHANG, Y., RON, D. & WALTER, P. 2009. Divergent effects of PERK and IRE1 signaling on cell viability. *PLoS One,* 4**,** e4170.

LISBONA, F., ROJAS-RIVERA, D., THIELEN, P., ZAMORANO, S., TODD, D., MARTINON, F., GLAVIC, A., KRESS, C., LIN, J. H., WALTER, P., REED, J. C., GLIMCHER, L. H. & HETZ, C. 2009. BAX inhibitor-1 is a negative regulator of the ER stress sensor IRE1alpha. *Mol Cell,* 33**,** 679-91.

LIU, C. Y., SCHRODER, M. & KAUFMAN, R. J. 2000. Ligand-independent dimerization activates the stress response kinases IRE1 and PERK in the lumen of the endoplasmic reticulum. *J Biol Chem,* 275**,** 24881-5.

LIU, M., LI, Y., CAVENER, D. & ARVAN, P. 2005. Proinsulin disulfide maturation and misfolding in the endoplasmic reticulum. *J Biol Chem,* 280**,** 13209-12.

LODISH, H. 2008. *Molecular Cell Biology*, W. H. Freeman.

LOGUE, S. E., CLEARY, P., SAVELJEVA, S. & SAMALI, A. 2013. New directions in ER stress-induced cell death. *Apoptosis,* 18**,** 537-46.

LU, P. D., JOUSSE, C., MARCINIAK, S. J., ZHANG, Y., NOVOA, I., SCHEUNER, D., KAUFMAN, R. J., RON, D. & HARDING, H. P. 2004a. Cytoprotection by pre-emptive conditional phosphorylation of translation initiation factor 2. *EMBO J,* 23**,** 169-79.

LU, P. D., JOUSSE, C., MARCINIAK, S. J., ZHANG, Y., NOVOA, I., SCHEUNER, D., KAUFMAN, R. J., RON, D. & HARDING, H. P. 2004b. *Cytoprotection by pre-emptive conditional phosphorylation of translation initiation factor 2*.

LUO, D., HE, Y., ZHANG, H., YU, L., CHEN, H., XU, Z., TANG, S., URANO, F. & MIN, W. 2008. AIP1 is critical in transducing IRE1-mediated endoplasmic reticulum stress response. *J Biol Chem,* 283**,** 11905-12.

LUO, J.-L., KAMATA, H. & KARIN, M. 2005. IKK/NF-κB signaling: balancing life and death – a new approach to cancer therapy. *Journal of Clinical Investigation,* 115**,** 2625-2632.

MA, Y., BREWER, J. W., DIEHL, J. A. & HENDERSHOT, L. M. 2002. Two distinct stress signaling pathways converge upon the CHOP promoter during the mammalian unfolded protein response. *J Mol Biol,* 318**,** 1351-65.

MA, Y. & HENDERSHOT, L. M. 2003. Delineation of a negative feedback regulatory loop that controls protein translation during endoplasmic reticulum stress. *J Biol Chem,* 278**,** 34864-73.

MAO, T., SHAO, M., QIU, Y., HUANG, J., ZHANG, Y., SONG, B., WANG, Q., JIANG, L., LIU, Y., HAN, J. D., CAO, P., LI, J., GAO, X., RUI, L., QI, L., LI, W. & LIU, Y. 2011. PKA phosphorylation couples hepatic inositol-requiring enzyme 1alpha to glucagon signaling in glucose metabolism. *Proc Natl Acad Sci U S A,* 108**,** 15852-7.

MARCINIAK, S. J., YUN, C. Y., OYADOMARI, S., NOVOA, I., ZHANG, Y., JUNGREIS, R., NAGATA, K., HARDING, H. P. & RON, D. 2004. CHOP induces death by promoting protein synthesis and oxidation in the stressed endoplasmic reticulum. *Genes Dev,* 18**,** 3066-77.

MARTIN, D., TAWADROS, T., MEYLAN, L., ABDERRAHMANI, A., CONDORELLI, D. F., WAEBER, G. & HAEFLIGER, J. A. 2003. Critical role of the transcriptional repressor neuron-restrictive silencer factor in the specific control of connexin36 in insulin-producing cell lines. *J Biol Chem,* 278**,** 53082-9.

MEYERS, J. A., SANCHEZ, D., ELWELL, L. P. & FALKOW, S. 1976. Simple agarose gel electrophoretic method for the identification and characterization of plasmid deoxyribonucleic acid. *Journal of Bacteriology,* 127**,** 1529-1537.

MIMURA, N., FULCINITI, M., GORGUN, G., TAI, Y. T., CIRSTEA, D., SANTO, L., HU, Y., FABRE, C., MINAMI, J., OHGUCHI, H., KIZILTEPE, T., IKEDA, H., KAWANO, Y., FRENCH, M., BLUMENTHAL, M., TAM, V., KERTESZ, N. L., MALYANKAR, U. M., HOKENSON, M., PHAM,

T., ZENG, Q., PATTERSON, J. B., RICHARDSON, P. G., MUNSHI, N. C. & ANDERSON, K. C. 2012. Blockade of XBP1 splicing by inhibition of IRE1alpha is a promising therapeutic option in multiple myeloma. *Blood,* 119**,** 5772-81.

MOLTON, S. A., WESTON, C., BALMANNO, K., NEWSON, C., TODD, D. E., GARNER, A. P. & COOK, S. J. 2005. The conditional kinase DeltaMEKK1:ER* selectively activates the JNK pathway and protects against serum withdrawal-induced cell death. *Cell Signal,* 17**,** 1412-22.

MORI, K., MA, W., GETHING, M. J. & SAMBROOK, J. 1993. A transmembrane protein with a cdc2+/CDC28-related kinase activity is required for signaling from the ER to the nucleus. *Cell,* 74**,** 743-56.

MORI, K., OGAWA, N., KAWAHARA, T., YANAGI, H. & YURA, T. 2000. mRNA splicing-mediated C-terminal replacement of transcription factor Hac1p is required for efficient activation of the unfolded protein response. *Proc Natl Acad Sci U S A,* 97**,** 4660-5.

MORI, K., SANT, A., KOHNO, K., NORMINGTON, K., GETHING, M. J. & SAMBROOK, J. F. 1992. A 22 bp cis-acting element is necessary and sufficient for the induction of the yeast KAR2 (BiP) gene by unfolded proteins. *EMBO J,* 11**,** 2583-93.

MORTON, S., DAVIS, R. J., MCLAREN, A. & COHEN, P. 2003. *A reinvestigation of the multisite phosphorylation of the transcription factor c-Jun*.

MOSMANN, T. 1983. Rapid colorimetric assay for cellular growth and survival: application to proliferation and cytotoxicity assays. *J Immunol Methods,* 65**,** 55-63.

MURESAN, V., VILLEGAS, C. & MURESAN, Z. L. 2014. Functional Interaction Between Amyloid-β Precursor Protein and Peripherin Neurofilaments: A Shared Pathway Leading to Alzheimer's Disease and Amyotrophic Lateral Sclerosis? *Neuro-degenerative diseases,* 13**,** 122-125.

NAKAMURA, D., TSURU, A., IKEGAMI, K., IMAGAWA, Y., FUJIMOTO, N. & KOHNO, K. 2011. Mammalian ER stress sensor IRE1beta specifically down-regulates the synthesis of secretory pathway proteins. *FEBS Lett,* 585**,** 133-8.

NGUYEN, D. T., KEBACHE, S., FAZEL, A., WONG, H. N., JENNA, S., EMADALI, A., LEE, E. H., BERGERON, J. J., KAUFMAN, R. J., LAROSE, L. & CHEVET, E. 2004. Nck-dependent activation of extracellular signal-regulated kinase-1 and regulation of cell survival during endoplasmic reticulum stress. *Mol Biol Cell,* 15**,** 4248-60.

NIKAWA, J. & YAMASHITA, S. 1992. IRE1 encodes a putative protein kinase containing a membrane-spanning domain and is required for inositol phototrophy in Saccharomyces cerevisiae. *Mol Microbiol,* 6**,** 1441-6.

NISHINA, H., WADA, T. & KATADA, T. 2004. Physiological roles of SAPK/JNK signaling pathway. *J Biochem,* 136**,** 123-6.

NISHITOH, H., MATSUZAWA, A., TOBIUME, K., SAEGUSA, K., TAKEDA, K., INOUE, K., HORI, S., KAKIZUKA, A. & ICHIJO, H. 2002. ASK1 is essential for endoplasmic reticulum stress-induced neuronal cell death triggered by expanded polyglutamine repeats. *Genes Dev,* 16**,** 1345-55.

NISHITOH, H., SAITOH, M., MOCHIDA, Y., TAKEDA, K., NAKANO, H., ROTHE, M., MIYAZONO, K. & ICHIJO, H. 1998. ASK1 is essential for JNK/SAPK activation by TRAF2. *Mol Cell,* 2**,** 389-95.

NOACK, J., BRAMBILLA PISONI, G. & MOLINARI, M. 2014. Proteostasis: bad news and good news from the endoplasmic reticulum. *Swiss Med Wkly,* 144**,** w14001.

NOVOA, I., ZENG, H., HARDING, H. P. & RON, D. 2001. Feedback inhibition of the unfolded protein response by GADD34-mediated dephosphorylation of eIF2alpha. *J Cell Biol,* 153**,** 1011-22.

NOVOA, I., ZHANG, Y., ZENG, H., JUNGREIS, R., HARDING, H. P. & RON, D. 2003. Stress-induced gene expression requires programmed recovery from translational repression. *The EMBO Journal,* 22**,** 1180-1187.

ODA, Y., OKADA, T., YOSHIDA, H., KAUFMAN, R. J., NAGATA, K. & MORI, K. 2006. Derlin-2 and Derlin-3 are regulated by the mammalian unfolded protein response and are required for ER-associated degradation. *The Journal of Cell Biology,* 172**,** 383-393.

OHOKA, N., YOSHII, S., HATTORI, T., ONOZAKI, K. & HAYASHI, H. 2005. TRB3, a novel ER stress-inducible gene, is induced via ATF4-CHOP pathway and is involved in cell death. *EMBO J,* 24**,** 1243-55.

OIKAWA, D., KIMATA, Y., KOHNO, K. & IWAWAKI, T. 2009. Activation of mammalian IRE1alpha upon ER stress depends on dissociation of BiP rather than on direct interaction with unfolded proteins. *Exp Cell Res,* 315**,** 2496-504.

OIKAWA, D., TOKUDA, M., HOSODA, A. & IWAWAKI, T. 2010. Identification of a consensus element recognized and cleaved by IRE1 alpha. *Nucleic Acids Res,* 38**,** 6265-73.

OKADA, T., YOSHIDA, H., AKAZAWA, R., NEGISHI, M. & MORI, K. 2002. Distinct roles of activating transcription factor 6 (ATF6) and double-stranded RNA-activated protein kinase-like endoplasmic reticulum kinase (PERK) in transcription during the mammalian unfolded protein response. *Biochem J,* 366**,** 585-94.

ORTEGA-PEREZ, I., CANO, E., WERE, F., VILLAR, M., VAZQUEZ, J. & REDONDO, J. M. 2005. c-Jun N-terminal kinase (JNK) positively regulates NFATc2 transactivation through phosphorylation within the N-terminal regulatory domain. *J Biol Chem,* 280**,** 20867-78.

OSTUNI, R., ZANONI, I. & GRANUCCI, F. 2010. Deciphering the complexity of Toll-like receptor signaling. *Cell Mol Life Sci,* 67**,** 4109-34.

OZCAN, U., CAO, Q., YILMAZ, E., LEE, A. H., IWAKOSHI, N. N., OZDELEN, E., TUNCMAN, G., GORGUN, C., GLIMCHER, L. H. & HOTAMISLIGIL, G. S. 2004. Endoplasmic reticulum stress links obesity, insulin action, and type 2 diabetes. *Science,* 306**,** 457-61.

PAHL, H. L. & BAEUERLE, P. A. 1995. A novel signal transduction pathway from the endoplasmic reticulum to the nucleus is mediated by transcription factor NF-kappa B. *EMBO J,* 14**,** 2580-8.

PALADE, G. 1975. Intracellular aspects of the process of protein synthesis. *Science,* 189**,** 867.

PALADE, G. E. 1956. THE ENDOPLASMIC RETICULUM. *The Journal of Biophysical and Biochemical Cytology,* 2**,** 85-98.

PAPA, F. R., ZHANG, C., SHOKAT, K. & WALTER, P. 2003. Bypassing a kinase activity with an ATP-competitive drug. *Science,* 302**,** 1533-7.

PAPANDREOU, I., DENKO, N. C., OLSON, M., VAN MELCKEBEKE, H., LUST, S., TAM, A., SOLOW-CORDERO, D. E., BOULEY, D. M., OFFNER, F., NIWA, M. & KOONG, A. C. 2011. Identification of an Ire1alpha endonuclease specific inhibitor with cytotoxic activity against human multiple myeloma. *Blood,* 117**,** 1311-4.

PARK, J. & LIU, A. Y. 2001. JNK phosphorylates the HSF1 transcriptional activation domain: role of JNK in the regulation of the heat shock response. *J Cell Biochem,* 82**,** 326-38.

PARK, S. W. & OZCAN, U. 2013. Potential for therapeutic manipulation of the UPR in disease. *Semin Immunopathol,* 35**,** 351-73.

PARSONS, M. J. & GREEN, D. R. 2010. *Mitochondria in cell death*.

PATIL, C. K., LI, H. & WALTER, P. 2004. Gcn4p and Novel Upstream Activating Sequences Regulate Targets of the Unfolded Protein Response. *PLoS Biol,* 2**,** e246.

PATON, A. W., BEDDOE, T., THORPE, C. M., WHISSTOCK, J. C., WILCE, M. C. J., ROSSJOHN, J., TALBOT, U. M. & PATON, J. C. 2006. AB5 subtilase cytotoxin inactivates the endoplasmic reticulum chaperone BiP. *Nature,* 443**,** 548-552.

PFAFFENBACH, K. T., NIVALA, A. M., REESE, L., ELLIS, F., WANG, D., WEI, Y. & PAGLIASSOTTI, M. J. 2010. Rapamycin inhibits postprandial-mediated X-box-binding protein-1 splicing in rat liver. *J Nutr,* 140**,** 879-84.

PIERCE, J. W., SCHOENLEBER, R., JESMOK, G., BEST, J., MOORE, S. A., COLLINS, T. & GERRITSEN, M. E. 1997. Novel inhibitors of cytokine-induced IkappaBalpha phosphorylation and endothelial cell adhesion molecule expression show anti-inflammatory effects in vivo. *J Biol Chem,* 272**,** 21096-103.

PINCUS, D., CHEVALIER, M. W., ARAGON, T., VAN ANKEN, E., VIDAL, S. E., EL-SAMAD, H. & WALTER, P. 2010. BiP binding to the ER-stress sensor Ire1 tunes the homeostatic behavior of the unfolded protein response. *PLoS Biol,* 8**,** e1000415.

PROMLEK, T., ISHIWATA-KIMATA, Y., SHIDO, M., SAKURAMOTO, M., KOHNO, K. & KIMATA, Y. 2011. Membrane aberrancy and unfolded proteins activate the endoplasmic reticulum stress sensor Ire1 in different ways. *Mol Biol Cell,* 22**,** 3520-32.

PROSTKO, C. R., DHOLAKIA, J. N., BROSTROM, M. A. & BROSTROM, C. O. 1995. Activation of the double-stranded RNA-regulated protein kinase by depletion of endoplasmic reticular calcium stores. *J Biol Chem,* 270**,** 6211-5.

PYTEL, D., SEYB, K., LIU, M., RAY, S. S., CONCANNON, J., HUANG, M., CUNY, G. D., DIEHL, J. A. & GLICKSMAN, M. A. 2014. Enzymatic Characterization of ER Stress-Dependent Kinase, PERK, and Development of a High-Throughput Assay for Identification of PERK Inhibitors. *J Biomol Screen,* 19**,** 1024-1034.

QUEITSCH, C., SANGSTER, T. A. & LINDQUIST, S. 2002. Hsp90 as a capacitor of phenotypic variation. *Nature,* 417**,** 618-24.

RAMIREZ, M., WEK, R. C. & HINNEBUSCH, A. G. 1991. Ribosome association of GCN2 protein kinase, a translational activator of the GCN4 gene of Saccharomyces cerevisiae. *Molecular and Cellular Biology,* 11**,** 3027-3036.

RANATUNGA, S., TANG, C. H., KANG, C. W., KRISS, C. L., KLOPPENBURG, B. J., HU, C. C. & DEL VALLE, J. R. 2014. Synthesis of novel tricyclic chromenone-based inhibitors of IRE-1 RNase activity. *J Med Chem,* 57**,** 4289-301.

RAVEN, J. F. & KOROMILAS, A. E. 2008. PERK and PKR: old kinases learn new tricks. *Cell Cycle,* 7**,** 1146-50.

RI, M., TASHIRO, E., OIKAWA, D., SHINJO, S., TOKUDA, M., YOKOUCHI, Y., NARITA, T., MASAKI, A., ITO, A., DING, J., KUSUMOTO, S., ISHIDA, T., KOMATSU, H., SHIOTSU, Y., UEDA, R., IWAWAKI, T., IMOTO, M. & IIDA, S. 2012. Identification of Toyocamycin, an agent cytotoxic for multiple myeloma cells, as a potent inhibitor of ER stress-induced XBP1 mRNA splicing. *Blood Cancer J,* 2**,** e79.

RODRIGUEZ, D. A., ZAMORANO, S., LISBONA, F., ROJAS-RIVERA, D., URRA, H., CUBILLOS-RUIZ, J. R., ARMISEN, R., HENRIQUEZ, D. R., CHENG, E. H., LETEK, M., VAISAR, T., IRRAZABAL, T., GONZALEZ-BILLAULT, C., LETAI, A., PIMENTEL-MUINOS, F. X., KROEMER, G. & HETZ, C. 2012. BH3-only proteins are part of a regulatory network that control the sustained signalling of the unfolded protein response sensor IRE1alpha. *EMBO J,* 31**,** 2322-35.

ROMERO-RAMIREZ, L., CAO, H., REGALADO, M. P., KAMBHAM, N., SIEMANN, D., KIM, J. J., LE, Q. T. & KOONG, A. C. 2009. X box-binding protein 1 regulates angiogenesis in human pancreatic adenocarcinomas. *Transl Oncol,* 2**,** 31-8.

RONG, J., CHEN, L., TOTH, J. I., TCHERPAKOV, M., PETROSKI, M. D. & REED, J. C. 2011. Bifunctional apoptosis regulator (BAR), an endoplasmic reticulum (ER)-associated E3 ubiquitin ligase, modulates BI-1 protein stability and function in ER Stress. *J Biol Chem,* 286**,** 1453-63.

RUEGSEGGER, U., LEBER, J. H. & WALTER, P. 2001. Block of HAC1 mRNA translation by long-range base pairing is released by cytoplasmic splicing upon induction of the unfolded protein response. *Cell,* 107**,** 103-14.

RUTKEVICH, L. A. & WILLIAMS, D. B. 2011. Participation of lectin chaperones and thiol oxidoreductases in protein folding within the endoplasmic reticulum. *Curr Opin Cell Biol,* 23**,** 157-66.

SABAPATHY, K. & WAGNER, E. F. 2004. JNK2: a negative regulator of cellular proliferation. *Cell Cycle,* 3**,** 1520-3.

SALVADÓ, L., PALOMER, X., BARROSO, E. & VÁZQUEZ-CARRERA, M. 2015. Targeting endoplasmic reticulum stress in insulin resistance. *Trends in Endocrinology & Metabolism*.

SANO, R. & REED, J. C. 2013. ER stress-induced cell death mechanisms. *Biochim Biophys Acta,* 1833**,** 3460-70.

SCHEUNER, D., SONG, B., MCEWEN, E., LIU, C., LAYBUTT, R., GILLESPIE, P., SAUNDERS, T., BONNER-WEIR, S. & KAUFMAN, R. J. 2001. Translational control is required for the unfolded protein response and in vivo glucose homeostasis. *Mol Cell,* 7**,** 1165-76.

SCHINDLER, A. J. & SCHEKMAN, R. 2009. In vitro reconstitution of ER-stress induced ATF6 transport in COPII vesicles. *Proc Natl Acad Sci U S A,* 106**,** 17775-80.

SCHRODER, M. 2008. Endoplasmic reticulum stress responses. *Cell Mol Life Sci,* 65**,** 862-94.

SHAMU, C. E. & WALTER, P. 1996. Oligomerization and phosphorylation of the Ire1p kinase during intracellular signaling from the endoplasmic reticulum to the nucleus. *EMBO J,* 15**,** 3028-39.

SHARROCKS, A. D., YANG, S. H. & GALANIS, A. 2000. Docking domains and substrate-specificity determination for MAP kinases. *Trends Biochem Sci,* 25**,** 448-53.

SHEN, J., CHEN, X., HENDERSHOT, L. & PRYWES, R. 2002. ER stress regulation of ATF6 localization by dissociation of BiP/GRP78 binding and unmasking of Golgi localization signals. *Dev Cell,* 3**,** 99-111.

SHEN, J. & PRYWES, R. 2004. Dependence of site-2 protease cleavage of ATF6 on prior site-1 protease digestion is determined by the size of the luminal domain of ATF6. *J Biol Chem,* 279**,** 43046-51.

SHEN, X., ELLIS, R. E., LEE, K., LIU, C. Y., YANG, K., SOLOMON, A., YOSHIDA, H., MORIMOTO, R., KURNIT, D. M., MORI, K. & KAUFMAN, R. J. 2001. Complementary signaling pathways regulate the unfolded protein response and are required for C. elegans development. *Cell,* 107**,** 893-903.

SHI, Y., VATTEM, K. M., SOOD, R., AN, J., LIANG, J., STRAMM, L. & WEK, R. C. 1998. Identification and Characterization of Pancreatic Eukaryotic Initiation Factor 2 α-Subunit Kinase, PEK, Involved in Translational Control. *Molecular and Cellular Biology,* 18**,** 7499-7509.

SIDRAUSKI, C. & WALTER, P. 1997. The transmembrane kinase Ire1p is a site-specific endonuclease that initiates mRNA splicing in the unfolded protein response. *Cell,* 90**,** 1031-9.

SMITH, M. H., PLOEGH, H. L. & WEISSMAN, J. S. 2011. Road to ruin: targeting proteins for degradation in the endoplasmic reticulum. *Science,* 334**,** 1086-90.

SMITH, M. I. & DESHMUKH, M. 2007. Endoplasmic reticulum stress-induced apoptosis requires bax for commitment and Apaf-1 for execution in primary neurons. *Cell Death Differ,* 14**,** 1011-1019.

SO, J. S., HUR, K. Y., TARRIO, M., RUDA, V., FRANK-KAMENETSKY, M., FITZGERALD, K., KOTELIANSKY, V., LICHTMAN, A. H., IWAWAKI, T., GLIMCHER, L. H. & LEE, A. H. 2012. Silencing of lipid metabolism genes through IRE1alpha-mediated mRNA decay lowers plasma lipids in mice. *Cell Metab,* 16**,** 487-99.

SONG, B., SCHEUNER, D., RON, D., PENNATHUR, S. & KAUFMAN, R. J. 2008. Chop deletion reduces oxidative stress, improves beta cell function, and promotes cell survival in multiple mouse models of diabetes. *J Clin Invest,* 118**,** 3378-89.

SPENCER, D., WANDLESS, T., SCHREIBER, S. & CRABTREE, G. 1993. Controlling signal transduction with synthetic ligands. *Science,* 262**,** 1019-1024.

SRIVASTAVA, S. P., DAVIES, M. V. & KAUFMAN, R. J. 1995. Calcium depletion from the endoplasmic reticulum activates the double-stranded RNA-dependent protein kinase (PKR) to inhibit protein synthesis. *J Biol Chem,* 270**,** 16619-24.

STEVENS, R. L., SCHWARTZ, L. B., AUSTEN, K. F., LOHMANDER, L. S. & KIMURA, J. H. 1982. Effect of tunicamycin on insulin binding and on proteoglycan synthesis and distribution in Swarm rat chondrosarcoma cell cultures. *Journal of Biological Chemistry,* 257**,** 5745-5750.

STOLLER, J. K. & ABOUSSOUAN, L. S. 2012. A review of alpha1-antitrypsin deficiency. *Am J Respir Crit Care Med,* 185**,** 246-59.

SUTCLIFFE, L. 2012. Univeristy of Durham.

SVENSSON, C., PART, K., KUNNIS-BERES, K., KALDMAE, M., FERNAEUS, S. Z. & LAND, T. 2011. Pro-survival effects of JNK and p38 MAPK pathways in LPS-induced activation of BV-2 cells. *Biochem Biophys Res Commun,* 406**,** 488-92.

TAKEUCHI, M., ROTHE, M. & GOEDDEL, D. V. 1996. Anatomy of TRAF2. Distinct domains for nuclear factor-kappaB activation and association with tumor necrosis factor signaling proteins. *J Biol Chem,* 271**,** 19935-42.

TAM, ARVIN B., KOONG, ALBERT C. & NIWA, M. 2014. Ire1 Has Distinct Catalytic Mechanisms for XBP1/HAC1 Splicing and RIDD. *Cell Reports,* 9**,** 850-858.

TAM, A. B., MERCADO, E. L., HOFFMANN, A. & NIWA, M. 2012. ER stress activates NF-kappaB by integrating functions of basal IKK activity, IRE1 and PERK. *PLoS One,* 7**,** e45078.

TASSI, E., BIESOVA, Z., DI FIORE, P. P., GUTKIND, J. S. & WONG, W. T. 1999. Human JIK, a novel member of the STE20 kinase family that inhibits JNK and is negatively regulated by epidermal growth factor. *J Biol Chem,* 274**,** 33287-95.

THASTRUP, O., CULLEN, P. J., DRØBAK, B. K., HANLEY, M. R. & DAWSON, A. P. 1990. Thapsigargin, a tumor promoter, discharges intracellular Ca2+ stores by specific inhibition of the endoplasmic reticulum Ca2(+)-ATPase. *Proceedings of the National Academy of Sciences of the United States of America,* 87**,** 2466-2470.

THUERAUF, D. J., MARCINKO, M., GUDE, N., RUBIO, M., SUSSMAN, M. A. & GLEMBOTSKI, C. C. 2006. Activation of the unfolded protein response in infarcted mouse heart and hypoxic cultured cardiac myocytes. *Circ Res,* 99**,** 275-82.

TIRASOPHON, W., LEE, K., CALLAGHAN, B., WELIHINDA, A. & KAUFMAN, R. J. 2000. The endoribonuclease activity of mammalian IRE1 autoregulates its mRNA and is required for the unfolded protein response. *Genes Dev,* 14**,** 2725-36.

TIRASOPHON, W., WELIHINDA, A. A. & KAUFMAN, R. J. 1998. A stress response pathway from the endoplasmic reticulum to the nucleus requires a novel bifunctional protein kinase/endoribonuclease (Ire1p) in mammalian cells. *Genes Dev,* 12**,** 1812-24.

TOBIUME, K., SAITOH, M. & ICHIJO, H. 2002. Activation of apoptosis signal-regulating kinase 1 by the stress-induced activating phosphorylation of pre-formed oligomer. *J Cell Physiol,* 191**,** 95-104.

TOURNIER, C., WHITMARSH, A. J., CAVANAGH, J., BARRETT, T. & DAVIS, R. J. 1997. Mitogen-activated protein kinase kinase 7 is an activator of the c-Jun NH2-terminal kinase. *Proc Natl Acad Sci U S A,* 94**,** 7337-42.

TOWBIN, H., STAEHELIN, T. & GORDON, J. 1979. Electrophoretic transfer of proteins from polyacrylamide gels to nitrocellulose sheets: procedure and some applications. *Proceedings of the National Academy of Sciences of the United States of America,* 76**,** 4350-4354.

TSITSIKOV, E. N., WRIGHT, D. A. & GEHA, R. S. 1997. CD30 induction of human immunodeficiency virus gene transcription is mediated by TRAF2. *Proc Natl Acad Sci U S A,* 94**,** 1390-5.

TSURU, A., FUJIMOTO, N., TAKAHASHI, S., SAITO, M., NAKAMURA, D., IWANO, M., IWAWAKI, T., KADOKURA, H., RON, D. & KOHNO, K. 2013. Negative feedback by IRE1beta optimizes mucin production in goblet cells. *Proc Natl Acad Sci U S A,* 110**,** 2864-9.

UEMURA, A., OKU, M., MORI, K. & YOSHIDA, H. 2009. Unconventional splicing of XBP1 mRNA occurs in the cytoplasm during the mammalian unfolded protein response. *J Cell Sci,* 122**,** 2877-86.

UPTON, J. P., WANG, L., HAN, D., WANG, E. S., HUSKEY, N. E., LIM, L., TRUITT, M., MCMANUS, M. T., RUGGERO, D., GOGA, A., PAPA, F. R. & OAKES, S. A. 2012. IRE1alpha cleaves select microRNAs during ER stress to derepress translation of proapoptotic Caspase-2. *Science,* 338**,** 818-22.

URANO, F., BERTOLOTTI, A. & RON, D. 2000a. IRE1 and efferent signaling from the endoplasmic reticulum. *J Cell Sci,* 113 Pt 21**,** 3697-702.

URANO, F., WANG, X., BERTOLOTTI, A., ZHANG, Y., CHUNG, P., HARDING, H. P. & RON, D. 2000b. Coupling of stress in the ER to activation of JNK protein kinases by transmembrane protein kinase IRE1. *Science,* 287**,** 664-6.

URRA, H., DUFEY, E., LISBONA, F., ROJAS-RIVERA, D. & HETZ, C. 2013. When ER stress reaches a dead end. *Biochim Biophys Acta,* 1833**,** 3507-17.

VANDEWYNCKEL, Y. P., LAUKENS, D., GEERTS, A., BOGAERTS, E., PARIDAENS, A., VERHELST, X., JANSSENS, S., HEINDRYCKX, F. & VAN VLIERBERGHE, H. 2013. The paradox of the unfolded protein response in cancer. *Anticancer Res,* 33**,** 4683-94.

VATTEM, K. M. & WEK, R. C. 2004. Reinitiation involving upstream ORFs regulates ATF4 mRNA translation in mammalian cells. *Proc Natl Acad Sci U S A,* 101**,** 11269-74.

VEKICH, J. A., BELMONT, P. J., THUERAUF, D. J. & GLEMBOTSKI, C. C. 2012. Protein disulfide isomerase-associated 6 is an ATF6-inducible ER stress response protein that protects cardiac myocytes from ischemia/reperfusion-mediated cell death. *J Mol Cell Cardiol,* 53**,** 259-67.

VOLKMANN, K., LUCAS, J. L., VUGA, D., WANG, X., BRUMM, D., STILES, C., KRIEBEL, D., DER-SARKISSIAN, A., KRISHNAN, K., SCHWEITZER, C., LIU, Z., MALYANKAR, U. M., CHIOVITTI, D., CANNY, M., DUROCHER, D., SICHERI, F. & PATTERSON, J. B. 2011. Potent and selective

inhibitors of the inositol-requiring enzyme 1 endoribonuclease. *J Biol Chem,* 286**,** 12743-55.
VOLMER, R., VAN DER PLOEG, K. & RON, D. 2013. Membrane lipid saturation activates endoplasmic reticulum unfolded protein response transducers through their transmembrane domains. *Proc Natl Acad Sci U S A,* 110**,** 4628-33.
VOYTAS, D. & KE, N. 2001. Detection and Quantitation of Radiolabeled Proteins and DNA in Gels and Blots. *Current Protocols in Immunology.* John Wiley & Sons, Inc.
WAJANT, H., HENKLER, F. & SCHEURICH, P. 2001. The TNF-receptor-associated factor family: scaffold molecules for cytokine receptors, kinases and their regulators. *Cell Signal,* 13**,** 389-400.
WALTER, P. & RON, D. 2011. The Unfolded Protein Response: From Stress Pathway to Homeostatic Regulation. *Science,* 334**,** 1081-1086.
WANG, Q., ZHANG, H., ZHAO, B. & FEI, H. 2008. IL-1β caused pancreatic β-cells apoptosis is mediated in part by endoplasmic reticulum stress via the induction of endoplasmic reticulum Ca2+ release through the c-Jun N-terminal kinase pathway. *Molecular and Cellular Biochemistry,* 324**,** 183-190.
WANG, X. Z., HARDING, H. P., ZHANG, Y., JOLICOEUR, E. M., KURODA, M. & RON, D. 1998. Cloning of mammalian Ire1 reveals diversity in the ER stress responses. *EMBO J,* 17**,** 5708-17.
WANG, Y., ALAM, G. N., NING, Y., VISIOLI, F., DONG, Z., NOR, J. E. & POLVERINI, P. J. 2012. The unfolded protein response induces the angiogenic switch in human tumor cells through the PERK/ATF4 pathway. *Cancer Res,* 72**,** 5396-406.
WANG, Y., SHEN, J., ARENZANA, N., TIRASOPHON, W., KAUFMAN, R. J. & PRYWES, R. 2000. Activation of ATF6 and an ATF6 DNA binding site by the endoplasmic reticulum stress response. *J Biol Chem,* 275**,** 27013-20.
WARBURG, O. A. W. C. 1945. Isolation and crystallization of enolase. *Biochem. Z.***,** 384-421.
WEK, R. C., JIANG, H. Y. & ANTHONY, T. G. 2006. Coping with stress: eIF2 kinases and translational control. *Biochem Soc Trans,* 34**,** 7-11.
WESTON, C. R. & DAVIS, R. J. 2002. The JNK signal transduction pathway. *Curr Opin Genet Dev,* 12**,** 14-21.
WESTON, C. R. & DAVIS, R. J. 2007. The JNK signal transduction pathway. *Curr Opin Cell Biol,* 19**,** 142-9.
WHITMARSH, A. J. 2006. The JIP family of MAPK scaffold proteins. *Biochem Soc Trans,* 34**,** 828-32.
WHITMARSH, A. J., CAVANAGH, J., TOURNIER, C., YASUDA, J. & DAVIS, R. J. 1998. A Mammalian Scaffold Complex That Selectively Mediates MAP Kinase Activation. *Science,* 281**,** 1671-1674.
WILLOUGHBY, E. A., PERKINS, G. R., COLLINS, M. K. & WHITMARSH, A. J. 2003. The JNK-interacting protein-1 scaffold protein targets MAPK phosphatase-7 to dephosphorylate JNK. *J Biol Chem,* 278**,** 10731-6.
WOEHLBIER, U. & HETZ, C. 2011. Modulating stress responses by the UPRosome: a matter of life and death. *Trends Biochem Sci,* 36**,** 329-37.
WOLFSON, J. J., MAY, K. L., THORPE, C. M., JANDHYALA, D. M., PATON, J. C. & PATON, A. W. 2008. Subtilase cytotoxin activates PERK, IRE1 and ATF6 endoplasmic reticulum stress-signalling pathways. *Cellular microbiology,* 10**,** 1775-1786.
WOOD, E. J. 1993. Gel electrophoresis of proteins by M J Dunn. pp 176. Bios Scientific, Oxford. 1993. £15 ISBN 1-872748-21-X. *Biochemical Education,* 21**,** 225-226.
WU, H., NG, B. S. & THIBAULT, G. 2014. Endoplasmic Reticulum Stress Response in Yeast and Humans. *Biosci Rep*.
WU, J., RUTKOWSKI, D. T., DUBOIS, M., SWATHIRAJAN, J., SAUNDERS, T., WANG, J., SONG, B., YAU, G. D. & KAUFMAN, R. J. 2007. ATF6alpha optimizes long-term endoplasmic reticulum function to protect cells from chronic stress. *Dev Cell,* 13**,** 351-64.
WU, S., TAN, M., HU, Y., WANG, J. L., SCHEUNER, D. & KAUFMAN, R. J. 2004. Ultraviolet light activates NFkappaB through translational inhibition of IkappaBalpha synthesis. *J Biol Chem,* 279**,** 34898-902.

WULCZYN, F. G., KRAPPMANN, D. & SCHEIDEREIT, C. 1998. Signal-dependent degradation of IκBα is mediated by an inducible destruction box that can be transferred to NF-κB, Bcl-3 or p53. *Nucleic Acids Research,* 26**,** 1724-1730.

YAMAGUCHI, H. & WANG, H. G. 2004. CHOP is involved in endoplasmic reticulum stress-induced apoptosis by enhancing DR5 expression in human carcinoma cells. *J Biol Chem,* 279**,** 45495-502.

YAMAMOTO, A., MIZUKAMI, Y. & SAKURAI, H. 2005. Identification of a novel class of target genes and a novel type of binding sequence of heat shock transcription factor in Saccharomyces cerevisiae. *J Biol Chem,* 280**,** 11911-9.

YAMAMOTO, K., SATO, T., MATSUI, T., SATO, M., OKADA, T., YOSHIDA, H., HARADA, A. & MORI, K. 2007. Transcriptional induction of mammalian ER quality control proteins is mediated by single or combined action of ATF6alpha and XBP1. *Dev Cell,* 13**,** 365-76.

YAMAZAKI, H., HIRAMATSU, N., HAYAKAWA, K., TAGAWA, Y., OKAMURA, M., OGATA, R., HUANG, T., NAKAJIMA, S., YAO, J., PATON, A. W., PATON, J. C. & KITAMURA, M. 2009. Activation of the Akt-NF-kappaB pathway by subtilase cytotoxin through the ATF6 branch of the unfolded protein response. *J Immunol,* 183**,** 1480-7.

YAN, W., FRANK, C. L., KORTH, M. J., SOPHER, B. L., NOVOA, I., RON, D. & KATZE, M. G. 2002. Control of PERK eIF2alpha kinase activity by the endoplasmic reticulum stress-induced molecular chaperone P58IPK. *Proc Natl Acad Sci U S A,* 99**,** 15920-5.

YANG, J. Y., DELLA-FERA, M. A., NELSON-DOOLEY, C. & BAILE, C. A. 2006a. Molecular mechanisms of apoptosis induced by ajoene in 3T3-L1 adipocytes. *Obesity (Silver Spring),* 14**,** 388-97.

YANG, Q., KIM, Y. S., LIN, Y., LEWIS, J., NECKERS, L. & LIU, Z. G. 2006b. Tumour necrosis factor receptor 1 mediates endoplasmic reticulum stress-induced activation of the MAP kinase JNK. *EMBO Rep,* 7**,** 622-7.

YANG, S. H., YATES, P. R., WHITMARSH, A. J., DAVIS, R. J. & SHARROCKS, A. D. 1998. The Elk-1 ETS-domain transcription factor contains a mitogen-activated protein kinase targeting motif. *Mol Cell Biol,* 18**,** 710-20.

YAO, F., SVENSJO, T., WINKLER, T., LU, M., ERIKSSON, C. & ERIKSSON, E. 1998. Tetracycline repressor, tetR, rather than the tetR-mammalian cell transcription factor fusion derivatives, regulates inducible gene expression in mammalian cells. *Hum Gene Ther,* 9**,** 1939-50.

YE, J., RAWSON, R. B., KOMURO, R., CHEN, X., DAVE, U. P., PRYWES, R., BROWN, M. S. & GOLDSTEIN, J. L. 2000. ER stress induces cleavage of membrane-bound ATF6 by the same proteases that process SREBPs. *Mol Cell,* 6**,** 1355-64.

YONEDA, T., IMAIZUMI, K., OONO, K., YUI, D., GOMI, F., KATAYAMA, T. & TOHYAMA, M. 2001. Activation of caspase-12, an endoplastic reticulum (ER) resident caspase, through tumor necrosis factor receptor-associated factor 2-dependent mechanism in response to the ER stress. *J Biol Chem,* 276**,** 13935-40.

YOSHIDA, H. 2007. ER stress and diseases. *Febs j,* 274**,** 630-58.

YOSHIDA, H., HAZE, K., YANAGI, H., YURA, T. & MORI, K. 1998. Identification of the cis-acting endoplasmic reticulum stress response element responsible for transcriptional induction of mammalian glucose-regulated proteins. Involvement of basic leucine zipper transcription factors. *J Biol Chem,* 273**,** 33741-9.

YOSHIDA, H., MATSUI, T., HOSOKAWA, N., KAUFMAN, R. J., NAGATA, K. & MORI, K. 2003. A Time-Dependent Phase Shift in the Mammalian Unfolded Protein Response. *Developmental Cell,* 4**,** 265-271.

YOSHIDA, H., MATSUI, T., YAMAMOTO, A., OKADA, T. & MORI, K. 2001. XBP1 mRNA is induced by ATF6 and spliced by IRE1 in response to ER stress to produce a highly active transcription factor. *Cell,* 107**,** 881-91.

YOSHIDA, H., OKADA, T., HAZE, K., YANAGI, H., YURA, T., NEGISHI, M. & MORI, K. 2000. ATF6 activated by proteolysis binds in the presence of NF-Y (CBF) directly to the cis-acting element responsible for the mammalian unfolded protein response. *Mol Cell Biol,* 20**,** 6755-67.

YU, C., MINEMOTO, Y., ZHANG, J., LIU, J., TANG, F., BUI, T. N., XIANG, J. & LIN, A. 2004. JNK suppresses apoptosis via phosphorylation of the proapoptotic Bcl-2 family protein BAD. *Mol Cell,* 13**,** 329-40.

YUAN, L., CAO, Y., OSWALD, F. & KNOCHEL, W. 2008. IRE1beta is required for mesoderm formation in Xenopus embryos. *Mech Dev,* 125**,** 207-22.

ZHANG, C., KAWAUCHI, J., ADACHI, M. T., HASHIMOTO, Y., OSHIRO, S., ASO, T. & KITAJIMA, S. 2001. Activation of JNK and Transcriptional Repressor ATF3/LRF1 through the IRE1/TRAF2 Pathway Is Implicated in Human Vascular Endothelial Cell Death by Homocysteine. *Biochemical and Biophysical Research Communications,* 289**,** 718-724.

ZHANG, C., KENSKI, D. M., PAULSON, J. L., BONSHTIEN, A., SESSA, G., CROSS, J. V., TEMPLETON, D. J. & SHOKAT, K. M. 2005. A second-site suppressor strategy for chemical genetic analysis of diverse protein kinases. *Nat Methods,* 2**,** 435-41.

ZHOU, J., LIU, C. Y., BACK, S. H., CLARK, R. L., PEISACH, D., XU, Z. & KAUFMAN, R. J. 2006. The crystal structure of human IRE1 luminal domain reveals a conserved dimerization interface required for activation of the unfolded protein response. *Proc Natl Acad Sci U S A,* 103**,** 14343-8.

ZINSZNER, H., KURODA, M., WANG, X., BATCHVAROVA, N., LIGHTFOOT, R. T., REMOTTI, H., STEVENS, J. L. & RON, D. 1998. CHOP is implicated in programmed cell death in response to impaired function of the endoplasmic reticulum. *Genes Dev,* 12**,** 982-95.

ZOU, H., LI, Y., LIU, X. & WANG, X. 1999. An APAF-1·Cytochrome c Multimeric Complex Is a Functional Apoptosome That Activates Procaspase-9. *Journal of Biological Chemistry,* 274**,** 11549-11556.